NOVEL CA^{2+} SIGNALLING PATHWAYS IN VASCULAR SMOOTH MUSCLE AND ENDOTHELIAL CELLS

Thesis submitted for the degree of

Doctor of Philosophy

in the

University of Oxford

Chloe S. S. Lim

Department of Pharmacology

Supervisors:

Professor Kim A. Dora

Professor Christopher J. Garland

Trinity Term 2014

“Ja, Kalzium, das ist alles!”

Otto Loewi, 1959

(1873-1961)

ABSTRACT

Novel Ca^{2+} signalling pathways in vascular smooth muscle and endothelial cells

Chloe S. S. Lim New College, University of Oxford

Doctor of Philosophy Trinity Term 2014

Novel Ca^{2+} signalling pathways in both endothelial cells and smooth muscle cells of rat small resistance arteries were investigated using a combination of confocal imaging, isometric tension recordings, and electrophysiology to study freshly isolated arteries and cells.

We first examined the hypothesis that hyperpolarization could alter endothelial cell Ca^{2+} events. Hyperpolarization evoked by direct opening of K_{ATP} channels in the smooth muscle with levcromakalim triggered an increase in the frequency of Ca^{2+} events in the endothelium of rat cremaster arterioles. These Ca^{2+} events were discrete in nature, requiring subcellular regions of interest to reliably identify them. Opening of K_{ATP} channels indirectly through β-adrenoceptor stimulation with isoprenaline, caused a similar increase in the frequency of endothelial cell Ca^{2+} events in rat mesenteric third order arteries. These events also had a similar, focal profile. Pharmacological investigation suggested that the response to isoprenaline was receptor-mediated, and dependent on Ca^{2+} influx and opening of K_{ATP} channels.

The presence of β-adrenoceptors on endothelial cells was confirmed using fluorescently-tagged β-adrenoceptor ligands, which showed punctate labelling in smooth muscle and endothelial cells of rat mesenteric arteries. Freshly isolated endothelial cells also showed Ca^{2+} increases to isoprenaline, although this was not consistently observed.

Following on from the observed endothelial cell Ca^{2+} response to hyperpolarization, we tested the hypothesized involvement of hyperpolarization-activated, cyclic nucleotide-gated (HCN) channels using the channel inhibitor, ZD7288. Pre-treatment with ZD7288 (1 μM) reduced both the endothelial cell Ca^{2+} response to isoprenaline (in mesenteric arteries) and levcromakalim (in cremaster arterioles). HCN channel subtypes were identified in cremaster arterioles through

immunolabelling. We also observed an interesting effect of higher concentrations of ZD7288 to potentially inhibit K^+ channels, including endothelial cell K_{Ca} channels, since hyperpolarization to isoprenaline, levcromakalim or acetylcholine (ACh) was reduced by 10 μM ZD7288, and relaxation to ACh was partially inhibited. ACh-mediated relaxation was also partially inhibited by the clinically used HCN channel blocker, ivabradine (0.3-30 μM).

Finally, we identified an interaction of the Ca^{2+}-releasing second messenger nicotinic acid adenine dinucleotide phosphate (NAADP) with BK_{Ca} channels in the smooth muscle. NAADP-mobilised Ca^{2+} has been reported to interact with ryanodine receptors hence we hypothesized an interaction with BK_{Ca} channels via Ca^{2+} sparks. We found that NAADP-AM relaxed and hyperpolarized rat mesenteric arteries, which was blocked by iberiotoxin (BK_{Ca} channel inhibitor) and high extracellular [K^+] (45 mM). Furthermore, NAADP increased paxilline-sensitive K^+ currents and the frequency and amplitude of spontaneous transient outward currents (STOCs) in freshly isolated vascular smooth muscle cells patched in the whole-cell configuration, further supporting an action at BK_{Ca} channels.

All together these data identify novel Ca^{2+} signalling pathways in resistance arteries that are both activated by and promote hyperpolarization, which is a key determinant of vascular tone.

ACKNOWLEDGEMENTS

Calcium may be everything, but sometimes it is not enough.

It has been an enormous privilege to learn and develop as a scientist under the unrivalled guidance of the vascular pharmacology group leaders, Professors Kim Dora and Christopher Garland. Their depth of knowledge and recall of detail is unmatched, but most impressive is their unrelenting drive to be leaders in their field. It has been inspiring to work in a world-class laboratory with world-class minds, and I am immensely grateful for this.

A world-leading laboratory must be filled with fantastic people, and those with whom I have had the pleasure of spending many long days are some of the best. The task of sustaining a DPhil student through her last few months has fallen to Alice, Chris, Esteban, Harrison, Pooneh, Ray and Steve. This is my opportunity to thank them all for the wisdom, laughs and metaphorical shoulder on which to cry. Many others who have since left the group provided invaluable advice and support, in particular Polly, Timi and Dynatra. Special thanks must also go to the Churchill and Galione laboratories which synthesized and generously donated NAADP-AM, and offered guidance for the experiments documented in Chapter 5.

Of all the techniques that I have learned, Dr Sergey Smirnov takes all the credit for one. Visiting Bath to learn to patch was one of the best experiences of my DPhil, and it was such a pleasure working together. I hope it is not the last time.

This section would not be complete without acknowledging Professor Arthur Weston, who filled a large part of that grey area between first and final year. As Arthur would say, “we had fun”.

Undergraduate lectures and my dissertation project with Dr Grant Churchill have made the Department of Pharmacology my home for the last six years. During that time I have received help and encouragement from many lovely people who have made this a wonderful department in which to work.

My DPhil work and travel to international conferences have been generously supported by the British Heart Foundation and New College and I am grateful for the experiences they have made possible.

I am indebted to my parents and family who instilled in me a strong work ethic and the drive necessary to succeed and achieve. I will always be thankful for all that you have done for me, which was so often far beyond the call of duty.

The final thank you goes to my fiancé, Matthew Powell. Your reward for getting me through - I will hopefully never be your Mrs, just Dr!

PUBLICATIONS FROM THE WORK IN THIS THESIS

KA Dora, TZ Beleznai, CS Lim, CJ Garland Hyperpolarization increases endothelial cell Ca^{2+} events. (*manuscript in preparation*)

CS Lim, CJ Garland, KA Dora β-adrenergic stimulation increases endothelial cell Ca^{2+} in resistance arteries. (*manuscript in preparation*)

CS Lim, SV Smirnov, A Galione, CJ Garland, KA Dora NAADP activates BK_{Ca} channels in vascular smooth muscle. (*manuscript in preparation*)

PRESENTATIONS OF THE WORK IN THIS THESIS

Poster Presentations

World Congress of Pharmacology 2014 Cape Town, South Africa (July 2014)

Chloe S.S. Lim, Chris J. Garland, Kim A. Dora *Activation of β-adrenoceptors increases endothelial cell calcium in isolated resistance arteries.*

3rd British Heart Foundation Fellows Meeting Cambridge, UK (September 2013)

Chloe S.S. Lim, Chris J. Garland, Kim A. Dora *β-adrenoceptor stimulation evokes endothelial cell Ca^{2+} events in rat mesenteric arteries.*

Experimental Biology 2013 Boston, USA (April 2013)

Chloe S.S. Lim, Sergey V. Smirnov, Grant C. Churchill, Antony Galione, Chris J. Garland, Kim A. Dora *A novel signalling role for NAADP in arterial smooth muscle cells.*

Microcirc 2012 Oxford, UK (July 2012)

Chloe S.S. Lim, Sergey V. Smirnov, Grant C. Churchill, Antony Galione, Chris J. Garland, Kim A. Dora *A novel signalling role for NAADP in vascular smooth muscle cells.*

Oral Presentations

BHF 4-Year PhD Student Symposium King's College London (March 2012)

Chloe S.S. Lim, Kim A. Dora *Novel Ca^{2+} signalling pathways in vascular smooth muscle and endothelial cells.*

Postgraduate Symposium University of Queensland School of Biomedical Sciences, Brisbane, Australia (September 2011)

Chloe S.S. Lim, Kim A. Dora *Role of NAADP in the vasculature.*

TABLE OF CONTENTS

TABLE OF FIGURES

ABBREVIATIONS

ACh	acetylcholine
Ap	apamin
BAEC	bovine aortic endothelial cell
Baf A1	bafilomycin A1
BK_{Ca} channel	large conductance Ca^{2+}-activated K^+ channel
BSA	bovine serum albumin
$[Ca^{2+}]_i$	intracellular Ca^{2+} concentration
cADPR	cyclic adenosine diphosphate ribose
cAMP	cyclic adenosine monophosphate
CICR	Ca^{2+}-induced Ca^{2+} release
COX	cyclooxygenase
CNBD	cyclic nucleotide binding domain
CNG channel	cyclic nucleotide-gated channel
Cx	connexin
DAG	diacylglycerol
DMSO	dimethylsulfoxide
DTT	dithiothreitol
EC	endothelial cell
EDH	endothelium-derived hyperpolarization
EDHF	endothelium-derived hyperpolarizing factor
eNOS	endothelial nitric oxide synthase
Epac	exchange protein activated by cAMP
ER	endoplasmic reticulum
FSK	forskolin
Glib	glibenclamide
GPCR	G protein-coupled receptor
GPN	glycyl-L-phenylalanine-β-naphthylamide
HCN channel	hyperpolarization-activated, cyclic nucleotide-gated channel
HEPES	4-(2-hydroxyethyl)piperazine-1-ethanesulfonic acid
IbTX	iberiotoxin
IEL	internal elastic lamina
IK_{Ca} channel	intermediate conductance Ca^{2+}-activated K^+ channel
iNOS	inducible nitric oxide synthase
IP_3	inositol-1,4,5-trisphosphate
IP_3R	inositol-1,4,5-trisphosphate receptor
Iso	isoprenaline
IV protocol	current-voltage protocol
K_{ATP} channel	ATP-sensitive K^+ channel
K_V channel	voltage-gated K^+ channel
L-NAME	N_ω-nitro-L-arginine methyl ester
LVK	levcromakalim
MEJ	myoendothelial junction
MEGJ	myoendothelial gap junction
MOPS	4-morpholinepropanesulfonic acid
NAADP	nicotinic acid adenine dinucleotide phosphate

nNOS	neuronal nitric oxide synthase
NO	nitric oxide
OGB-1	Oregon Green 488 BAPTA-1 AM
Pax	paxilline
PE	phenylephrine
PBS	phosphate-buffered saline
PFA	paraformaldehyde
PKA	protein kinase A
PI	propidium iodide
ROI	region of interest
RT-PCR	reverse transcription polymerase chain reaction
RyR	ryanodine receptor
sGC	soluble guanylyl cyclase
SERCA	sarcoplasmic / endoplasmic reticulum Ca^{2+} ATPase
SK_{Ca} channel	small conductance Ca^{2+}-activated K^+ channel
SMC	smooth muscle cell
SR	sarcoplasmic reticulum
STOC	spontaneous transient outward current
TPC	two-pore channel
TR, TRAM-34	1-[(2-chlorophenyl)diphenylmethyl]-1H-pyrazole
VGCC	voltage-gated Ca^{2+} channel
ZD7288	4-ethylphenylamino-1,2-dimethyl-6-methylaminopyrimidinium chloride

CHAPTER 1

INTRODUCTION

1.1 Structure of resistance arteries and arterioles

Comprising three layers: the intima, media and adventitia (**Figure 1.1.1**), small resistance arteries in the peripheral vasculature (Christensen & Mulvany, 2001) are the principle determinants of peripheral arterial resistance, and consequently blood pressure and tissue blood flow to match the metabolic demands of an organ (reviewed by Dora, 2001).

A monolayer of endothelial cells lines the lumen of arteries, arranged longitudinally such that one endothelial cell spreads across multiple smooth muscle cells arranged perpendicularly (**Figure 1.1.1**). Tight junctions between endothelial cells reduce the permeability of this monolayer (Lew *et al.*, 1989) (**Figure 1.1.2**), whilst homocellular gap junctions facilitate passage of small molecules between neighbouring cells. These gap junctions are comprised of three proteins: connexin (Cx) 37, 40 and 43 (Dhein, 1998; Yeh *et al.*, 1998; Looft-Wilson *et al.*, 2004). Homocellular gap junctions also exist between smooth muscle cells to facilitate passage of intracellular signals between neighbouring cells and thereby a coordinated, synchronized response to stimulus. In smaller arteries and arterioles, these gap junctions comprise Cx40, 45 and low levels of 43. Surrounding the smooth muscle layer(s) is the adventitia, composed of a number of different cell types, including nerves and connective tissue (reviewed by Stenmark *et al.*, 2013).

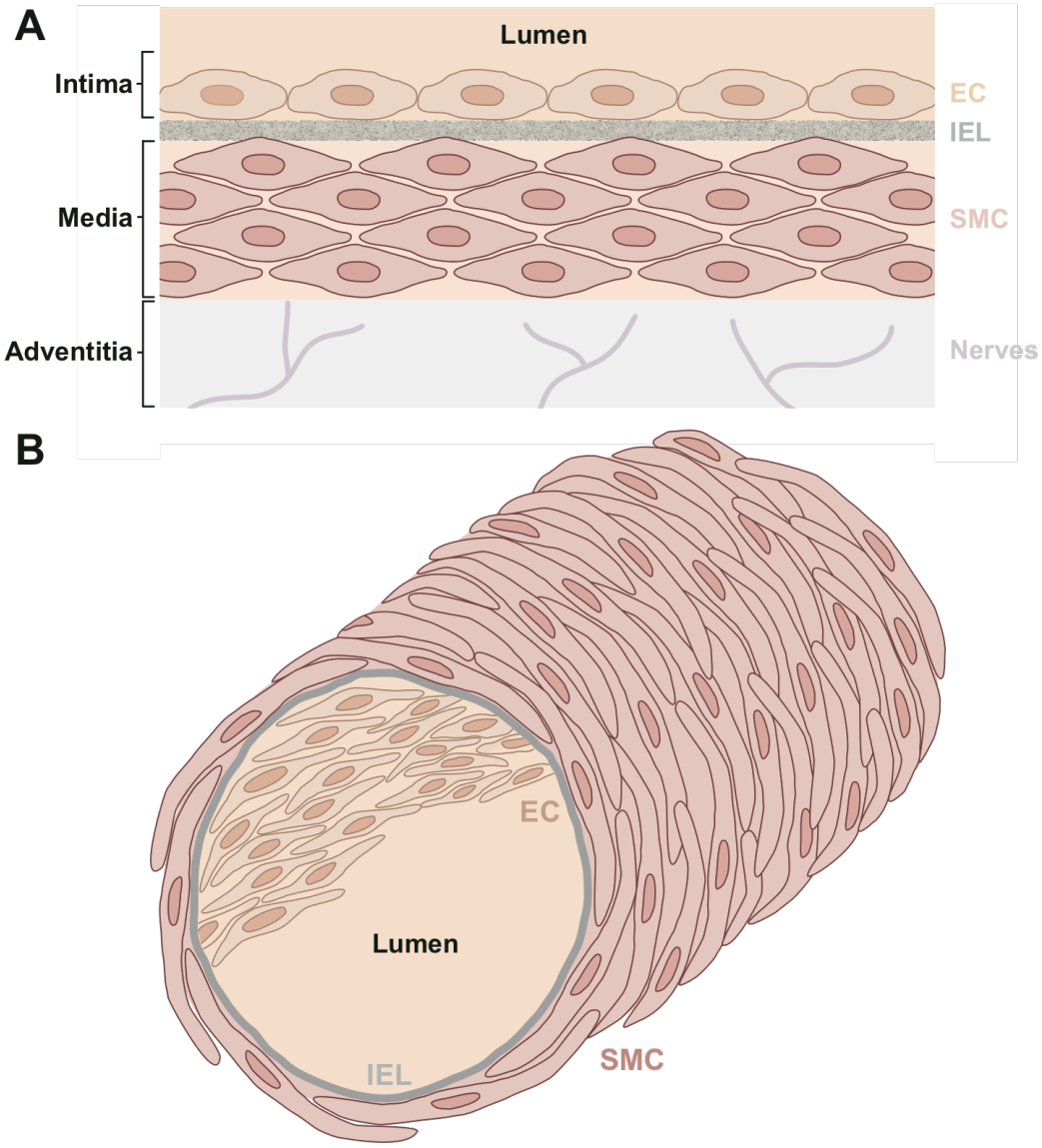

Figure 1.1.1 Layers of the resistance arterial wall
A Schematic illustrating the three layers of the arterial wall: the intima describes the monolayer of endothelial cells (EC); the media is composed of between one and several layers of smooth muscle cells (SMC) depending on the artery; and the adventitia comprises mainly elastin and collagen, as well as adrenergic nerves. The internal elastic lamina (IEL) separates the intima and media. Based on a figure from (Stenmark *et al.*, 2013). **B** Stylised schematic depicting the arrangement of cells in the intact artery: smooth muscle cells are long and wrap around the vessel, which is lined with the monolayer of endothelial cells arranged perpendicular to the media. The IEL (grey) separates the intima and media. Note that the rat mesenteric and cremaster arteries used in this dissertation have holes in the IEL, which are not shown here. This enables contact between endothelial and smooth muscle cells.

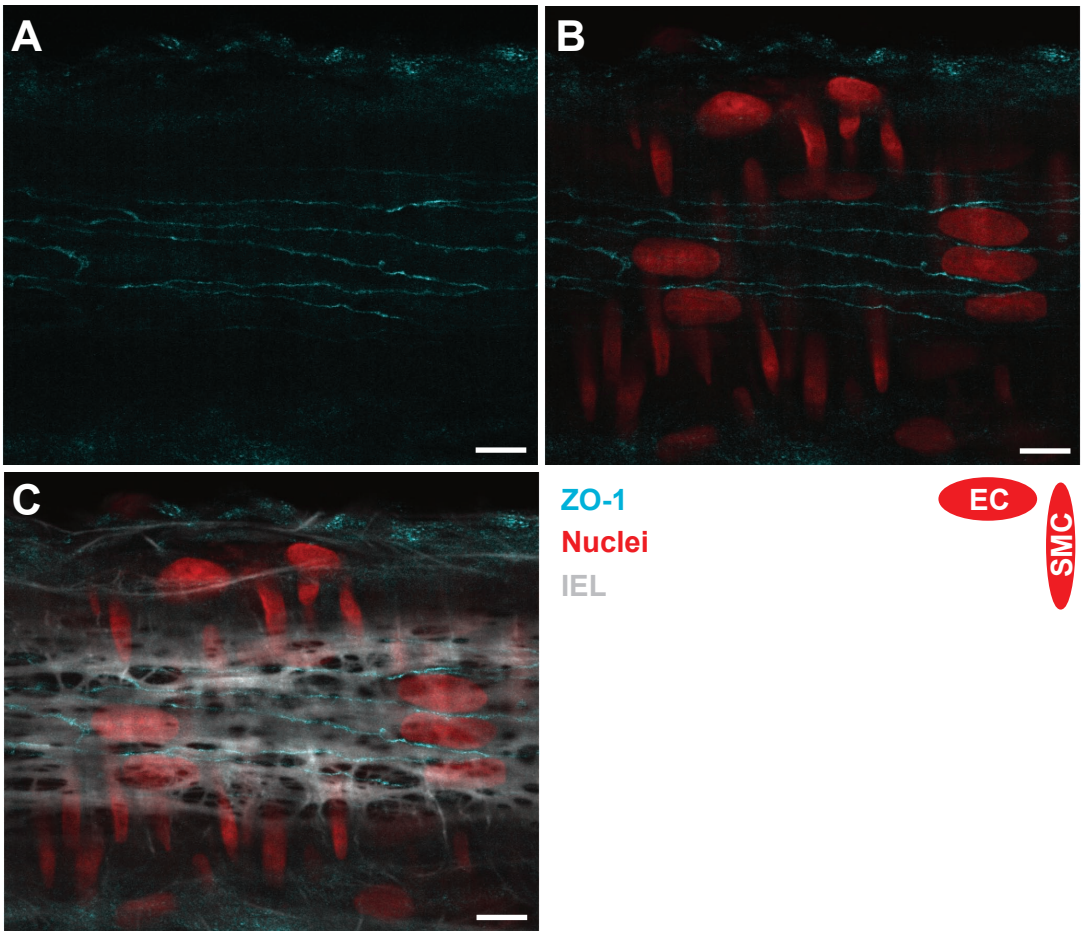

Figure 1.1.2 Expression of tight junction (zona occludens) in the endothelium of rat cremaster arterioles
A Tight junction protein zona occludens 1 (ZO-1, cyan) in pressurized rat cremaster arterioles is visible around the borders of endothelial cells where it forms a barrier to diffusion of substances from the blood. 1:200 mouse monoclonal primary antibody 339100 (Life Technologies, UK) + 1:200 chicken anti-mouse secondary antibody A-21200 (Life Technologies, UK). **B** Nuclei are stained with propidium iodide (45 μM, red). **C** Elastin is stained with Alexa Fluor 633 hydrazide (1 μM, grey), which identifies the internal elastic lamina (IEL) between endothelial and smooth muscle layers. Note the holes in the IEL. Scale bars = 10 μm.

1.1.i Myoendothelial junctions

Endothelial cells are separated from smooth muscle cells by the internal elastic lamina (IEL; **Figure 1.1.3**). This is a hydrophilic barrier, allowing free passage of water-soluble molecules through the vessel wall. Holes in the IEL allow projections of endothelial cells to adjoin neighbouring smooth muscle, forming so-called myoendothelial junctions (MEJs) (reviewed by Straub *et al.*, 2014). Within these MEJs, heterocellular myoendothelial gap junctions (MEGJs) are composed of Cx37, 40 and 43. They form a functional connection between the intima and sub-intimal layer of smooth muscle allowing passage of small molecules as well as current such that the membrane potential is shared across endothelial and smooth muscle cells. The earliest descriptions of these structures were first in 1957 (Moore & Ruska, 1957) and a decade later in 1967 (Rhodin, 1967) through use of electron microscopy in arterioles. Functional studies using fluorescent dyes demonstrated the coupling of endothelial cells to smooth muscle cells (Little *et al.*, 1995). More recent high-resolution electron microscopy images clearly illustrate the structure of myoendothelial projections protruding through the IEL and creating very close association with the nearest smooth muscle cell (Sandow *et al.*, 2002; McSherry *et al.*, 2006; Tran *et al.*, 2012; Straub *et al.*, 2014). MEJs can also form in the opposite direction and in human mesenteric arteries, ~40% of MEJs are proposed to originate from the smooth muscle (Chadha *et al.*, 2011), whilst in rat mesenteric arteries all are endothelial in origin (Sandow *et al.*, 2002). The incidence of MEJs is inversely correlated with diameter (Sandow & Hill, 2000; Sandow *et al.*, 2002), reflecting a greater role in the smallest resistance arteries and arterioles which is correlated with the greater importance of endothelium-derived hyperpolarization (EDH, discussed below) (Shimokawa *et al.*, 1996; reviewed by Garland *et al.*, 2011a).

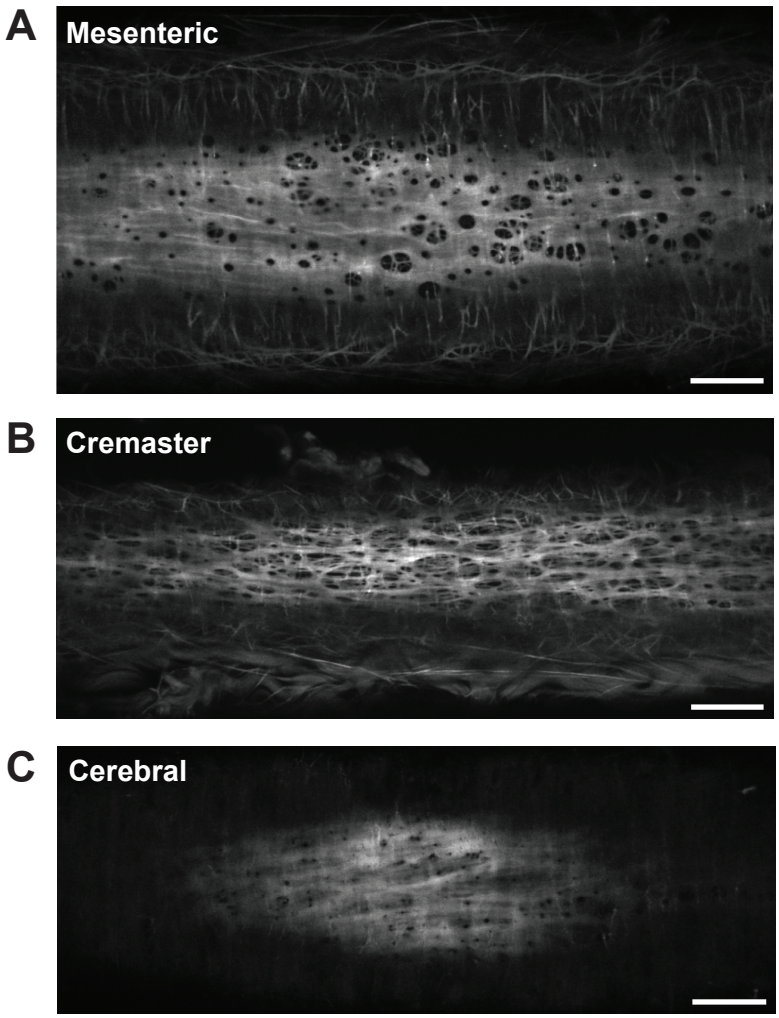

Figure 1.1.3 Internal elastic lamina (IEL) of resistance arteries / arterioles in different vascular beds

A The IEL of third order rat mesenteric arteries has an appearance often likened to 'Swiss cheese' with regular, circular holes. **B** The IEL of rat cremaster arterioles has a much more mesh-like appearance with a high proportion of space for potential myoendothelial junctions. **C** The IEL of rat middle cerebral arteries is more akin to mesenteric arteries but has far fewer holes, suggesting fewer myoendothelial junctions. In all cases the IEL is labelled with Alexa Fluor 633 hydrazide (1 μM, grey) and the arteries are pressurized to 20 mmHg. Scale bars = 30 μm.

1.2 Ca^{2+} signalling

The field of Ca^{2+} signalling began more than 120 years ago. In 1883, Ringer first observed the requirement of Ca^{2+} for the contraction of isolated rat hearts, noticing that hearts suspended in a medium using London tap water kept beating, whilst the beating ceased if the tap water was replaced with distilled water (Ringer, 1883). This early observation was followed up by a few reports in the first half of the 20th century mainly describing Ca^{2+} effects with respect to muscle fibres, such as Weber demonstrating that actomyosin was activated by Ca^{2+} binding to myofibrils (Weber, 1959). It was not until the second half of the 20th century that the field of Ca^{2+} signalling took off (reviewed by Carafoli, 2002) and now it is well established that changes in intracellular [Ca^{2+}] ($[Ca^{2+}]_i$) drive a plethora of intracellular signalling pathways in cells.

Changes in $[Ca^{2+}]_i$ are caused by movement of Ca^{2+} between intracellular stores, the cytoplasm and the extracellular space. Ca^{2+} release from intracellular stores can be spontaneous or initiated by agonists binding at receptors in the plasma membrane, which triggers an intracellular second messenger cascade. The majority of receptors are G protein-coupled receptors (GPCRs), of which there are three principal subtypes: $G_{q/11}$, G_s and G_i (**Figure 1.4.1**). While $G_{q/11}$ activates phospholipase C, an enzyme in the membrane, to trigger release of inositol-1,4,5-trisphosphate (IP_3) and diacylglycerol (DAG), G_s and G_i will increase or lower the intracellular levels of cyclic adenosine monophosphate (cAMP) through activation or inactivation (respectively) of adenylyl cyclase. cAMP has numerous cellular effects, principally mediated via protein kinase A (PKA).

1.2.i Ca^{2+}-mobilising second messengers

Inositol trisphosphate (IP_3) was the first second messenger characterised and has since been shown to release Ca^{2+} from the endoplasmic reticulum (ER) through IP_3 receptors (IP_3R) (Streb *et al.*, 1983; reviewed by Berridge, 1993). In more recent years cyclic adenosine diphosphate ribose (cADPR) has joined IP_3 as an established Ca^{2+}-mobilising second messenger, acting to modulate the Ca^{2+} sensitivity of ryanodine receptors (RyRs), also located on the ER membrane (reviewed by Berridge *et al.*, 2000). Both IP_3Rs and RyRs are Ca^{2+}-sensitive and both partake in Ca^{2+}-induced Ca^{2+} release. This feature enables a Ca^{2+} signal to be amplified along the length of a cell, often propagating as a 'Ca^{2+} wave' (Berridge *et al.*, 2000). Imaging experiments in cultured rat aortic smooth muscle cells using a calsequestrin-targeted Ca^{2+} indicator localised to the sarcoplasmic reticulum (SR) have monitored the pattern of [Ca^{2+}] changes within this Ca^{2+} store, which shows elevations of Ca^{2+} within the SR at the site of wave initiation and at the wave front, suggesting a role for SR Ca^{2+} in the wave initiation and propagation (Esfandiarei *et al.*, 2013). Nicotinic acid adenine dinucleotide phosphate (NAADP) is the most recently described second messenger, mobilising Ca^{2+} from lysosomal-type acidic stores via a receptor complex that contains the two-pore channel (TPC) (Calcraft *et al.*, 2009; reviewed by Patel & Docampo, 2010).

1.2.ii Ca^{2+}-binding proteins

In unstimulated cells, $[Ca^{2+}]_i$ is kept strictly within a range of 20-100 nM by numerous homeostatic mechanisms to avoid cytotoxic effects (reviewed by Berridge, 1997). As a consequence, Ca^{2+} has a very low diffusion distance within the cytosol. The major Ca^{2+}-binding protein in the vasculature is calmodulin. In smooth muscle cells, after

binding Ca^{2+}, the resulting Ca^{2+}-calmodulin complex triggers the contraction cascade by activating myosin light chain kinase.

1.2.iii Ca^{2+} influx

Ca^{2+} influx occurs via channels in the plasma membrane. In vascular smooth muscle, the principal Ca^{2+} influx channel is the L-type voltage-gated Ca^{2+} channel (VGCC). This is activated by depolarization of the membrane potential and provides the Ca^{2+} necessary for contraction (reviewed by Webb, 2003). Many other Ca^{2+}-permeable plasmalemmal channels have also been described, including several members of the TRP family of cation channels present in the endothelium. L-type VGCCs are absent from endothelial cells, which instead rely on Ca^{2+} leak which can be driven by membrane potential, but in the opposite direction to that in smooth muscle (reviewed by Dora & Garland, 2013), purinergic P2X receptors and cyclic nucleotide-gated (CNG) channels (Yao & Garland, 2005).

1.2.iv Ca^{2+} microdomains

The most recent period of research in the Ca^{2+} signalling field has focused on the study of Ca^{2+} microdomains. This is the concept that proteins are positioned within the cell so as to create small subcellular regions where $[Ca^{2+}]$ can rise to a level sufficient to activate its target (reviewed by Billaud *et al.*, 2014). Measurements of $[Ca^{2+}]$ in cells used to be achieved with chemicals based on aequorin, but the development of Ca^{2+}-sensitive fluorescent indicators around 25 years ago (Tsien, 1980) has allowed the study of more localised, transient Ca^{2+} events in Ca^{2+} microdomains. In the vasculature these include the measurement of single channel Ca^{2+} puffs (IP_3R), sparks (RyR), pulsars (IP_3R in the endothelium) and sparklets

(TRPV4 channels in the endothelium) (Wray *et al.*, 2005; Nausch *et al.*, 2012; Sonkusare *et al.*, 2012) (**Figure 1.4.1**). This spatiotemporal signalling forms part of the versatility of Ca^{2+} as a second messenger.

In the vascular wall, many pathways that alter diameter and tone rely on Ca^{2+} signalling. In smooth muscle cells, a rise in [Ca^{2+}] activates contractile machinery leading to vasoconstriction; conversely, an increase in endothelial cells usually results in vasodilation (with the exception of some endothelium-dependent vasoconstrictors) through a number of pathways.

1.3 Ca^{2+} signalling in vascular smooth muscle

The major stimulus for contraction is release of Ca^{2+} from intracellular stores and depolarization to activate L-type VGCC in the sarcolemma. In smooth muscle cells the SR is extensive and estimated using confocal microscopy to comprise 6% of total cell volume (Gordienko *et al.*, 2001). It has been suggested that the SR has different parts with distinct properties. The 'superficial' SR near the sarcolemma serves to restrict free Ca^{2+} fluxes; this limited diffusion permits high local [Ca^{2+}] near Ca^{2+}-regulated ion channels in the sarcolemma, so-called 'sub-sarcolemmal domains' (Wray *et al.*, 2005). The deeper SR is believed to provide Ca^{2+} predominately for binding to calmodulin and activating myofilaments for contraction (van Breemen *et al.*, 1995). Indeed, it is now thought that the SR forms 'nano-junctions' with the sarcolemma and multiple intracellular organelles to facilitate its numerous functions (van Breemen *et al.*, 2013).

1.3.i Ca^{2+} sparks

Ca^{2+} sparks from RyR in the SR were first described in cardiac myocytes (Cheng *et al.*, 1993) and later reported in smooth muscle (Nelson *et al.*, 1995). Miriel *et al* were the first to demonstrate Ca^{2+} sparks in intact vessels (Miriel *et al.*, 1999), which have since been shown to underlie the spontaneous transient outwards currents (STOCS; Benham & Bolton, 1986) evoked by transient opening of large conductance, Ca^{2+}-activated K^+ (BK_{Ca}) channels in the sarcolemma. Like endothelial Ca^{2+}-activated K^+ (K_{Ca}) channels, stimulated BK_{Ca} channels can have significant influence on membrane potential and therefore vascular tone. The absence of RyRs from endothelial cells (Burdyga *et al.*, 2003; Kansui *et al.*, 2008) precludes the presence of Ca^{2+} sparks in these cells.

1.4 Ca^{2+} signalling in the endothelium

1.4.i Characteristics of Ca^{2+} events in endothelial cells

Basal, spontaneous Ca^{2+} events in the endothelium of resistance arteries are typically discrete and focal in nature, when recorded *in vitro* (Kansui *et al.*, 2008; Bagher *et al.*, 2012), or *in vivo* (Duza & Sarelius, 2004). They seem to reflect release from IP_3Rs on the ER, since they were abolished by cyclopiazonic acid (CPA, sarcoplasmic / endoplasmic reticulum Ca^{2+} ATPase (SERCA) inhibitor) or U-73122 (phospholipase C (PLC) inhibitor). In rat mesenteric arteries (Kansui *et al.*, 2008), but not rat cremaster arterioles (Bagher *et al.*, 2012) they also rely on extracellular Ca^{2+}. In addition, the putative gap junction uncouplers carbenoxolone and 18α-glycyrrhetinic acid inhibited the spontaneous Ca^{2+} events, implying a signal from the smooth muscle via MEJs (Kansui *et al.*, 2008).

Although L-type VGCC are not present in endothelial cells (Johns *et al.*, 1987), Ca^{2+} increases in smooth muscle cells in response to depolarizing agonists can pass via MEGJs to cause a rise in endothelial cells. Dora, Duling and colleagues first demonstrated this in the hamster cheek pouch preparation in response to KCl and phenylephrine (PE, acting on smooth muscle α_1-adrenoceptors) (Dora *et al.*, 1997). Since then there has been much debate over the signal traversing the IEL to generate the secondary Ca^{2+} rise: the second messenger IP_3 has been proposed (Lamboley *et al.*, 2005); Ca^{2+} itself; or a combination of the two (Isakson *et al.*, 2007). The presence of the ER within the MEJ (Isakson *et al.*, 2007) facilitates a secondary amplification in the endothelium. IP_3Rs have also been identified on the ER in the vicinity of the MEJ (Ledoux *et al.*, 2008) and the Ca^{2+} release events termed 'Ca^{2+} pulsars'. These Ca^{2+} events were identified by use of the *en face* preparation of small resistance arteries taken from GCaMP2 mice. These are genetically encoded to express GCaMP2 exclusively in endothelial cells, removing the need for dye loading and potential simultaneous loading of smooth muscle cells. GCaMP2 is a fusion of calmodulin with enhanced green fluorescent protein (eGFP) such that it fluoresces upon Ca^{2+} binding. GCaMP2 genetically encoded mice have also facilitated examination of endothelial and smooth muscle Ca^{2+} activity *in vivo* (Mauban *et al.*, 2013). Arteries from these GCaMP2 mice in the same *en face* preparation have also been used to identify 'Ca^{2+} sparklets' which reflect influx through endothelial TRPV4 channels (Sonkusare *et al.*, 2012). TRPV4 channels have also been identified exclusively within the MEJ of rat cremaster arterioles (Bagher *et al.*, 2012).

The MEJ is therefore increasingly becoming a central signalling microdomain where the limited space can facilitate a high local concentration of Ca^{2+}, sufficient to cause activation of target proteins such as intermediate conductance, Ca^{2+}-activated K^+ (IK_{Ca}) channels located here (discussed below) (Bagher *et al.*, 2012).

1.4.ii Endothelial Ca^{2+}-dependent vasomodulatory pathways

The endothelium is a source of numerous tone-modulating signals, but until the 1970s it was still considered an inert barrier. The seminal Nobel Prize-winning bioassay experiments conducted by Furchgott and colleagues altered this perception with their discovery of endothelium-derived relaxing factor (EDRF) (Furchgott & Zawadzki, 1980; Furchgott, 1983). Prior to this, prostacyclin had been identified as a key vasodilator (Moncada *et al.*, 1976), later realised to originate from the endothelium as well (reviewed by Flower, 2006). Prostacyclin is produced by the enzyme cyclooxygenase (COX) and is an important anti-thrombotic and contributor to the inflammatory response. The vasodilatory properties of prostacyclin are more relevant in larger arteries, whilst inhibition of COX (with indomethacin) has little effect on endothelium-dependent relaxation in healthy rodent small arteries (Shimokawa *et al.*, 1996).

EDRF was soon realised to be nitric oxide (NO) (Ignarro *et al.*, 1987), which is made by the enzyme nitric oxide synthase (NOS). NOS has three isoforms: endothelial (eNOS), neuronal (nNOS) and inducible (iNOS). eNOS activity is principally regulated by phosphorylation and Ca^{2+}-calmodulin, and therefore an increase in endothelial Ca^{2+} has the potential to generate NO. NO released from the

endothelium will, amongst other targets, activate soluble guanylyl cyclase (sGC) in the smooth muscle to cause relaxation.

In conduit arteries, the vasorelaxant response to muscarinic stimulation with acetylcholine (ACh) causes release of intracellular Ca^{2+} via IP_3 and subsequent production of NO, whilst in the small resistance arteries, the endothelial Ca^{2+} increase to ACh predominately activates endothelium-derived hyperpolarization (EDH) (reviewed by Garland *et al.*, 2011a). Thus the relative importance of the three endothelial-derived relaxant pathways varies along the arterial tree.

1.4.iii Endothelium-derived hyperpolarization

The first observations leading to the discovery of EDH were in the 1970s where hyperpolarization was recorded in rabbit and guinea pig arteries in response to ACh (Kuriyama & Suzuki, 1978; reviewed by Garland *et al.*, 2011a). Combined with Furchgott's realisation that the endothelium was not simply inert, Bolton then proposed that the response to muscarinic stimulation originated in the endothelium with his studies of carbachol in guinea pig mesenteric arteries (Bolton *et al.*, 1984). EDH was unequivocally determined to be distinct from EDRF with sharp microelectrode studies of membrane potential, which demonstrated that the hyperpolarization to ACh, and ^{86}Rb efflux (marker of K^+), remained during inhibition of EDRF with methylene blue (NO scavenger and guanylyl cyclase inhibitor) and haemoglobin (another NO scavenger) (Chen *et al.*, 1988; reviewed by Garland *et al.*, 2011a). Hence the two pathways were independent. More recently the principal involvement of endothelial cell K_{Ca} channels was determined. After ruling out K_{ATP} (Garland & McPherson, 1992) and K_V (Adeagbo & Triggle, 1993) channels, the

importance of endothelial cell K_{Ca} channels was first realised when the hyperpolarization to ACh was partially inhibited by apamin (small conductance (S)K_{Ca} channel blocker) or charybdotoxin (IK_{Ca} and BK_{Ca} channel blocker), and fully blocked by a combination of the two (Waldron & Garland, 1994). Iberiotoxin (BK_{Ca} channel blocker) did not block the hyperpolarization (Zygmunt & Högestätt, 1996), eliminating BK_{Ca} channels (localised to the smooth muscle) and pinpointing the EDH response to SK_{Ca} and IK_{Ca} channels. K^+ was finally unequivocally determined an EDHF (Edwards *et al.*, 1998). SK_{Ca} and IK_{Ca} channels have a heterogenic distribution within endothelial cells, with IK_{Ca} channels concentrated at the MEJ and SK_{Ca} channels more uniformly distributed throughout the endothelial cell membrane (Sandow *et al.*, 2006; Dora *et al.*, 2008). This differential distribution corresponds with a differential role in EDH, whereby hyperpolarization, e.g. to ACh, from a resting membrane potential activates solely SK_{Ca} channels, whereas IK_{Ca} channels are recruited if the artery is in a depolarized state (Crane *et al.*, 2003). This is reportedly due to calcium-sensing receptor (CaSR)-mediated inhibition of IK_{Ca} channels in the myoendothelial space due to high resting extracellular [Ca^{2+}]; when myocytes depolarize and Ca^{2+} enters via VGCCs, lowered extracellular [Ca^{2+}] in the myoendothelial space releases the CaSR brake on IK_{Ca}, allowing it to be activated by the ACh-evoked elevated intracellular Ca^{2+} level (Dora *et al.*, 2008).

The membrane potential of arterial smooth muscle cells is a key determinant of arterial diameter and tone, particularly in the small resistance arteries (Nelson & Quayle, 1995). Since these factors hugely influence peripheral blood pressure and tissue blood flow, membrane hyperpolarization and EDH are therefore very powerful modulators of these important parameters.

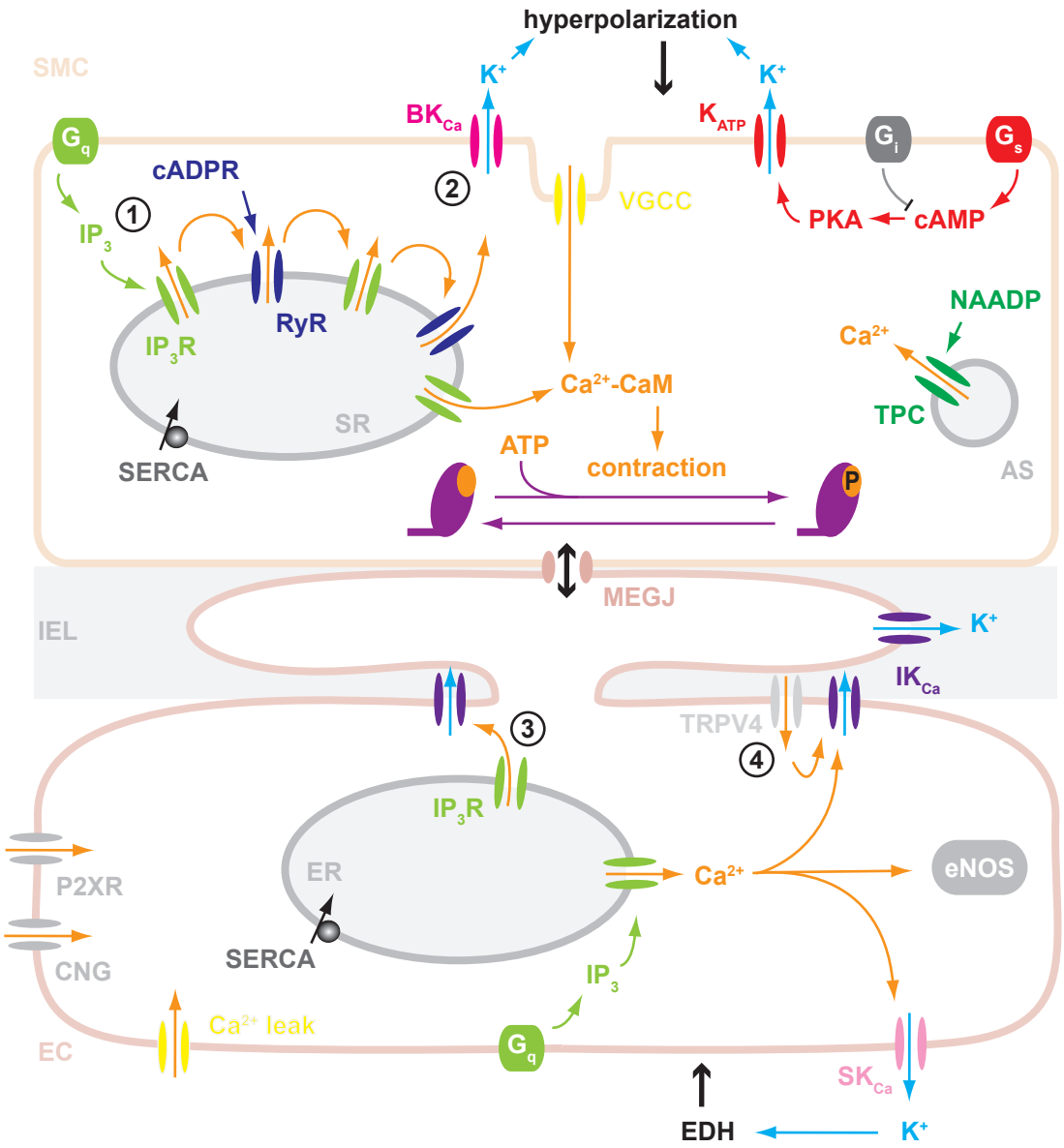
hyperpolarization
SMC
K+
K+
BKCa
KATP
Gq
Gi
Gs
cADPR
1
2
VGCC
IP3
PKA
cAMP
NAADP
Ca2+
RyR
IP3R
Ca2+-CaM
TPC
SR
ATP
contraction
SERCA
AS
P
MEGJ
IEL
K+
IKCa
TRPV4
3
4
IP3R
P2XR
ER
Ca2+
eNOS
SERCA
CNG
IP3
Ca2+ leak
EC
Gq
SKCa
EDH
K+

Figure 1.4.1 Ca^{2+} signalling pathways in vascular smooth muscle and endothelial cells
In vascular smooth muscle cells (SMC) $G_{q/11}$-coupled receptors (e.g. α-adrenoceptors) trigger phospholipase C-mediated production of the second messenger IP_3, which acts on IP_3 receptors (IP_3R) on the sarcoplasmic reticulum (SR) to release Ca^{2+}, 'Ca^{2+} puffs' (1). Ca^{2+} can also be mobilised from the SR via cADPR-mediated opening of ryanodine receptors (RyR), 'Ca^{2+} sparks' (2). These cause spontaneous transient outward currents, reflecting Ca^{2+}-triggered transient opening of large conductance, Ca^{2+}-activated K^+ (BK_{Ca}) channels in the sarcolemma. Ca^{2+} will also enter via voltage-gated Ca^{2+} channels (VGCC) upon depolarization, which may be localised in invaginations to deliver Ca^{2+} deep into the cell. When [Ca^{2+}] increases here it forms a complex with calmodulin to activate myosin light chain kinase, which will phosphorylate myosin and generate contraction. G_s-coupled receptors (e.g. β-adrenoceptors) activate adenylyl cyclase to increase levels of cyclic AMP (cAMP), which in turn will activate protein kinase A (PKA). This will lead to relaxation principally by opening K_{ATP} channels in the sarcolemma and permitting K^+ extrusion. Stimulation of BK_{Ca} channels by Ca^{2+} or depolarization will also generate robust hyperpolarization, which will spread via myoendothelial gap junctions (MEGJs) to neighbouring endothelial cells (ECs) through holes in the internal elastic laminar (IEL).

In ECs, IP_3R-originating Ca^{2+} events, 'Ca^{2+} pulsars' (3), can activate intermediate conductance, Ca^{2+}-activated K^+ (IK_{Ca}) channels in the myoendothelial junction (MEJ). 'Ca^{2+} sparklets' (4) representing influx via plasmalemmal TRPV4 channels also in the MEJ (opened by low pressure) can also activate IK_{Ca} channels. Ca^{2+} influx in ECs can also occur via cyclic nucleotide-gated (CNG) channels, purinergic P2X receptors (P2XR) and Ca^{2+} leak in response to hyperpolarization. A rise in EC [Ca^{2+}] can also activate small conductance, Ca^{2+}-activated K^+ (SK_{Ca}) channels, which together with IK_{Ca} channels, will evoke endothelium-derived hyperpolarization (EDH) that spreads to the SMC to limit constriction. Endothelial nitric oxide synthase (eNOS) is also Ca^{2+}-regulated.

The aim of the experiments in this thesis is to utilise a range of techniques for studying intact arteries *in vitro* to investigate the Ca^{2+} signalling pathways present in smooth muscle and endothelial cells that either regulate or are regulated by K^+ channels, and as such modulate vascular tone.

CHAPTER 2

METHODS & MATERIALS

2.1 Tissue isolation

2.1.i Rat mesenteric artery isolation

Male Wistar rats (220-250 g, Charles River, UK) were killed by cervical dislocation in accordance with Schedule 1 of the Animals (Scientific Procedures) Act 1986. The mesentery was removed from the animal and immediately placed in ice-cold MOPS-buffered solution (see **section 2.6** for composition) and brought to the laboratory. Tissue was transferred to fresh ice-cold MOPS-buffered solution within 30 min of removal from the animal. An arcade of mesenteric tissue was pinned in a dissection Petri dish coated with Sylgard (**Figure 2.1.1**). After use this dish was washed with ethanol and Milli-Q distilled water and re-used.

Third order branches of the superior mesenteric artery (300-380 μm outer diameter at 70 mmHg) were used in all experiments. These were dissected free from the neighbouring vein and adhering connective tissue (**Figure 2.1.1**) and cut into segments of final length ≥2 mm. For pressure myography experiments, care was taken to avoid small side branches in the segment. Tissue in the dissection dish was stored at 4°C for later use if necessary and the solution changed approximately every 2 h.

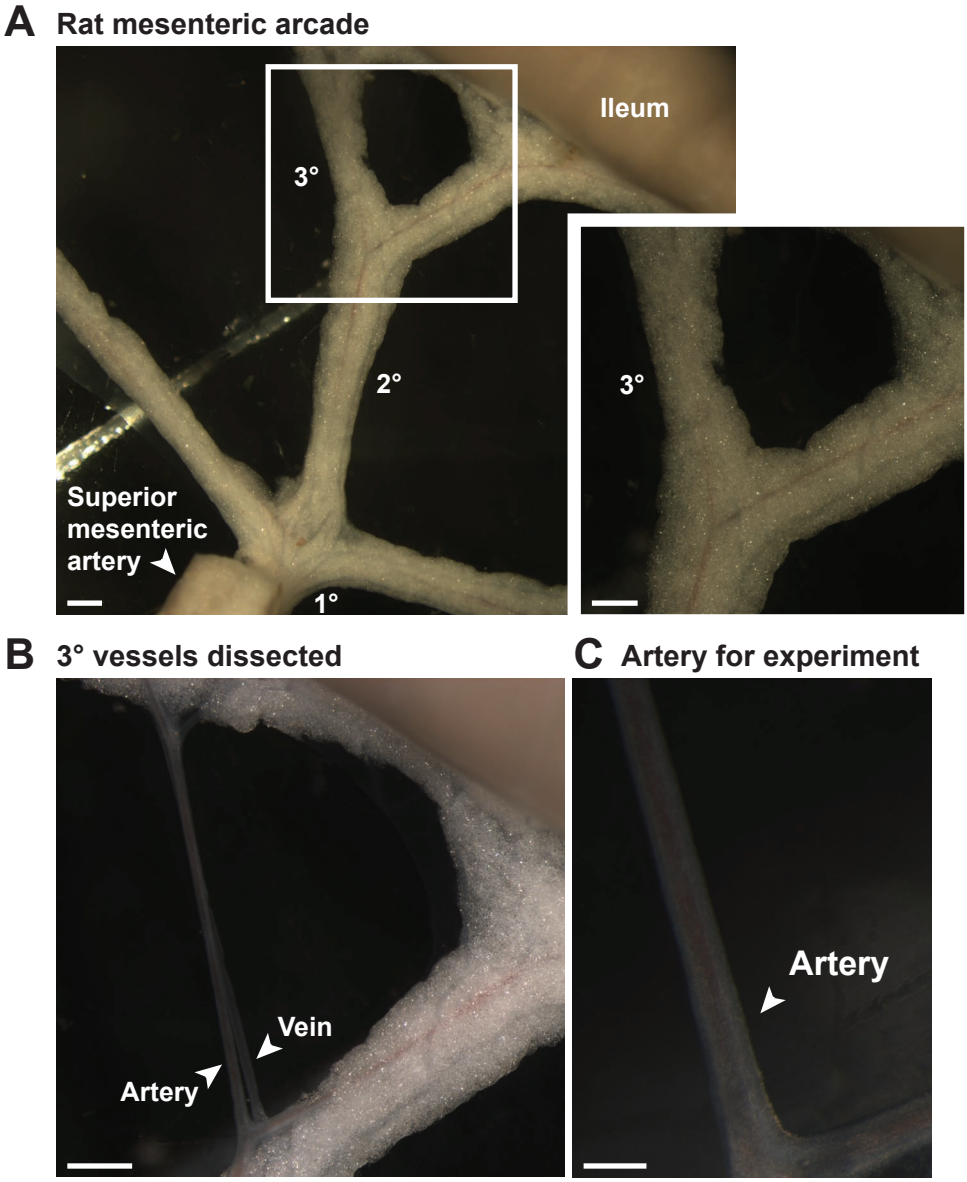

Figure 2.1.1 Dissection and isolation of rat mesenteric arteries
A Rat mesenteric arcade pinned into Sylgard-lined dissection dish. The superior mesenteric artery is visible, with first (1°), second (2°) and third (3°) order arteries as marked. **Inset** Third order artery for dissection. Scale bars = 1 mm. **B** Third order artery and vein (marked) have been dissected free from adhering fat and connective tissue. Scale bar = 1 mm. **C** Close-up of artery for experiment with the vein removed. Note that the lumen is still perfused with blood, giving a red colour. Scale bar = 250 μm.

2.1.ii Rat cremaster arteriole isolation

Male Wistar rats (240-270 g, Charles River, UK) were anaesthetized with urethane (2.8 g/kg intraperitoneally) in the animal housing facility, in accordance with the Animals (Scientific Procedures) Act 1986. The cremaster muscle was exteriorized, removed and immediately placed in ice-cold MOPS-buffered solution (see **section 2.6** for composition), after which the animals were killed by cervical dislocation in accordance with Schedule 1 of the Animals (Scientific Procedures) Act 1986. Tissue was brought back to the laboratory and transferred to fresh ice-cold MOPS-buffered solution within 30 min of removal from the animal. The cremaster muscle was pinned in a Sylgard-coated dissection Petri dish (**Figure 2.1.2**).

Segments of arterioles (150-180 μm maximum inner diameter at 80 mmHg) were dissected free from the neighbouring vein and adhering connective tissue (**Figure 2.1.2**). All experiments using cremaster arterioles involved pressure myography, therefore care was always taken to avoid small side branches in the dissected segment. Tissue in the dissection dish was stored at 4°C for later use if necessary and the solution changed approximately every 2 h.

Acknowledgement: P. Bagher and C. Stanley hold personal licences enabling them to anaesthetize rats. I am grateful for their assistance in collecting cremaster tissue for use in the experiments described in Chapters 3 and 4.

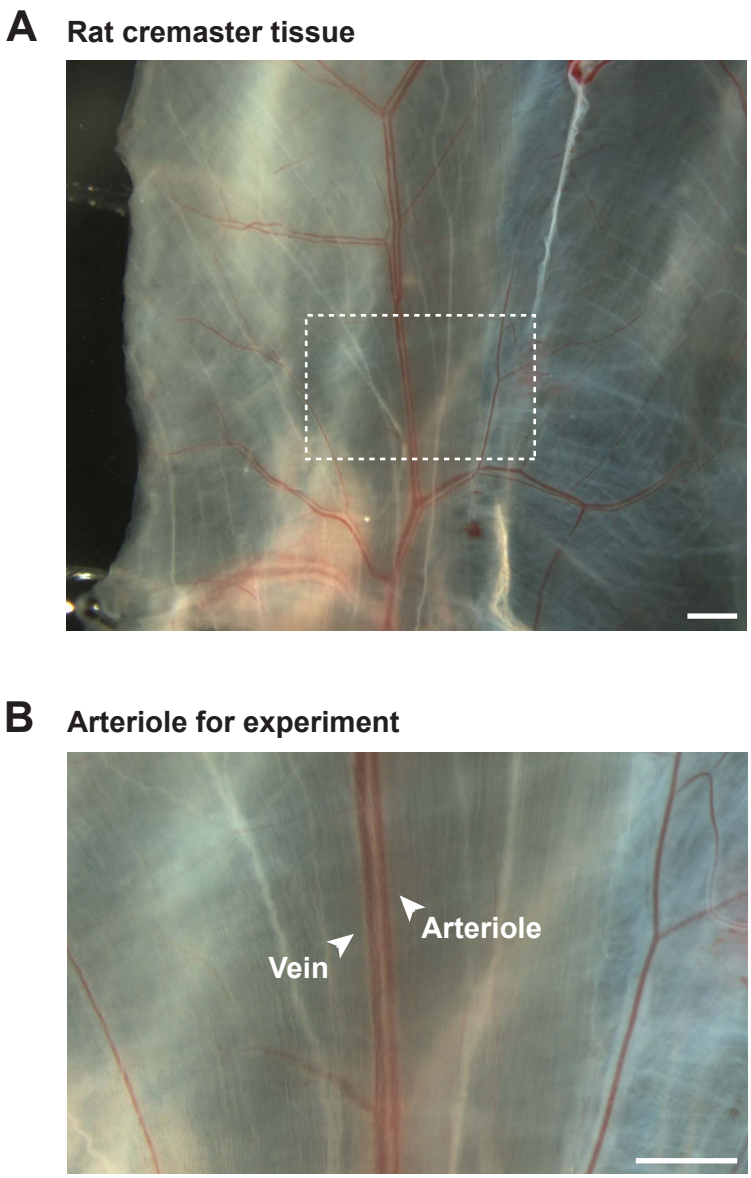

Figure 2.1.2 Dissection and isolation of rat cremaster arterioles
A Rat cremaster muscle tissue pinned into a dissection dish. Dashed box corresponds to close-up in B. **B** Close-up of arteriole for use in experiment; neighbouring vein is also marked. Scale bars = 1 mm.

2.2 Wire myography

This technique was originally invented by Bevan and Osher (Bevan & Osher, 1972) but later developed significantly by Mulvany and Halpern for the study of small resistance vessels (Mulvany & Halpern, 1977). The underlying principle is that arteries are mounted securely onto parallel metal supports using two luminal wires (**Figure 2.2.1**), such that artery walls do not move with changes in contraction, i.e. vessels are measured under isometric conditions. Vessels are stretched and the tension measurement at each distance between the wires are plotted, fitted to an exponential curve, and used to calculate the optimal resting tension equivalent to 0.8x the internal diameter at 70 mmHg (Mulvany & Halpern, 1977). 0.8x is chosen because Mulvany and Halpern showed that at tensions greater than this, the resting tension was 30-50% of the active tension value; they concluded precise measurement of active tension would therefore be masked. At 0.8x, the resting tension is 10-15% of active wall tension.

2.2.i Mounting arteries for wire myography

Segments of third order mesenteric artery (2 mm in length) were cleaned of adhering tissue and mounted, using two 25 μm diameter gold-plated tungsten wires positioned luminally, in a 5 mL chamber of a Mulvany-Halpern myograph (model 400A, DMT, Denmark) in cold MOPS-buffered solution. Following warming to 37ºC during an equilibration period of ~20 min, a resting tension-diameter curve was constructed as previously described (Mulvany & Halpern, 1977) and arteries were normalized. After 20 min equilibration at the optimum resting tension, the viability of the artery was assessed using the α_1-adrenergic vasoconstrictor, PE and the muscarinic M_3 receptor endothelium-dependent vasodilator, ACh. Only arteries with

functional smooth muscle (robust contraction to 3-10 μM PE) and endothelium (≥95% relaxation to 0.3 μM ACh) were subsequently used. In experiments where the endothelium was not required, endothelial cells were damaged / removed by luminal rubbing with a human hair after the initial function test. Following a second function test only arteries with unaltered vasoconstriction to PE (indicating undamaged smooth muscle) and ≤10% relaxation to 10 μM ACh (indicating damage to the endothelium) were considered successfully denuded. The bath temperature was maintained at 37°C throughout, therefore to avoid potential evaporation artefacts the bath solution was replaced every 20-30 min.

2.2.ii Analysis of wire myography data

Contraction is expressed as a % of the maximum level of tone achieved using 45 mM K^+ + 30 μM PE (applied at the end of the experiment), according to the following calculation:

$$\frac{\text{[recorded tension] - resting tension}}{\text{maximum tension - resting tension}} \times 100$$

Relaxation is expressed as a % of the level of pre-constriction using the following calculation:

$$\frac{\text{[recorded tension] - resting tension}}{\text{pre-constriction tension - resting tension}} \times 100$$

Where relaxation was assessed in arteries pre-constricted to an agent, the concentration of vasoconstrictor was adjusted to maintain a constant level of pre-constriction at ~70% maximum.

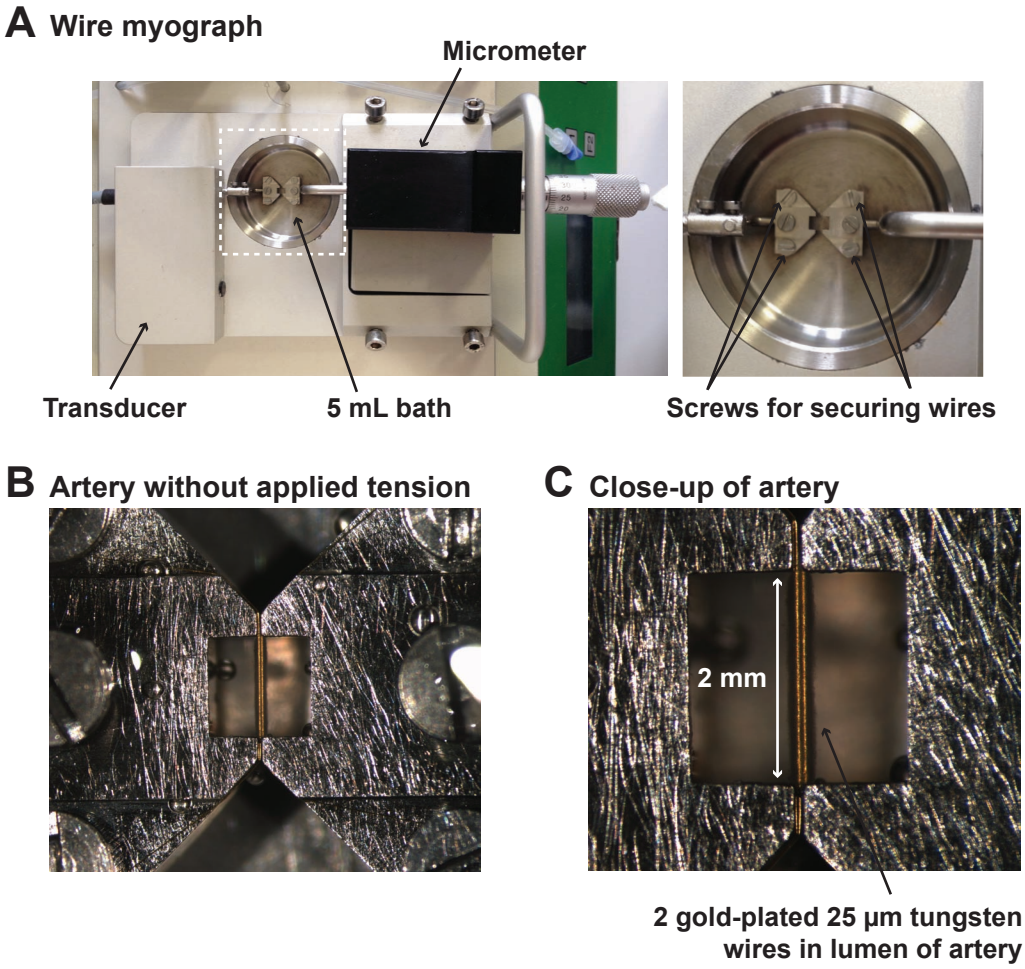

Figure 2.2.1 Wire myograph setup
A One myograph from the 400A DMT four chamber myograph, with transducer, micrometer and bath marked. Dashed box corresponds to close-up (right). **Right** Close-up of myograph bath and jaws, with the screws used for mounting the intraluminal wires identified. **B** A rat third order mesenteric artery secured in the chamber without any applied tension. The two jaws are visible, with a space in the middle for the artery. **C** Close-up of the artery (2 mm long) mounted on two 25 μm gold-plated tungsten wires.

2.3 Pressure myography

This technique was first developed for the study of resistance arteries and arterioles of the microcirculation by Duling and colleagues (Duling *et al.*, 1981) initially with a single cannula but later adding a second cannula to allow intraluminal perfusion (Duling & Rivers, 1986). It involves cannulating a freshly isolated small artery or arteriole connected to a gravity-fed pressurizing system, such that the intraluminal pressure can be controlled and arterial responses studied at physiological pressure. The intraluminal and extraluminal solutions can also be controlled, and the diameter and / or cells within the vessel wall visualised using brightfield or confocal microscopy for the study of responses to applied drugs or changes in pressure.

2.3.i Preparation of arteries

A segment of mesenteric artery or cremaster arteriole was cannulated at each end with polished glass pipettes and tied with sutures (Ethilon polyamide 10-0 or 11-0, Ethicon) to create a closed system. Different sizes of pipette were used depending on the artery type and internal diameter. For mesenteric arteries, pipettes had an external diameter of ~200 μm. For cremaster arterioles, pipettes had an external diameter of ~100 μm.

The artery was positioned in MOPS-buffered solution close to the base of a 2 mL temperature-controlled chamber (RC-27 chamber and PH-6 heating platform, Warner Instruments, USA; **Figure 2.3.1A**, **B**) seated on the stage of a laser scanning confocal microscope with FluoView software (Olympus, Japan). After heating to 37ºC (mesenteric arteries) or 34°C (cremaster arterioles) for ~15 min (flow rate 2 mL min^{-1}) the vessel was pressurized to physiological pressure of

70 mmHg (mesentery artery; **Figure 2.3.2A**; (Christensen & Mulvany, 1993; Fenger-Gron *et al*., 1995)) or 80 mmHg (cremaster arteriole; **Figure 2.3.1C**; (Hill *et al*., 1992)) and tested for leaks. A leak manifested as a decrease in arterial diameter when a three-way tap connecting to the pressure system was closed and indicated a small side branch was present in the arterial segment, or a loose suture. When this occurred, the artery was either retied or replaced with a new segment.

After confirming no leaks, the arteries were left to equilibrate at high pressure for ~15 min. During this period cremaster arterioles developed 40-50% myogenic tone within 5-15 min (**Figure 2.3.1C**). Intact endothelial function was assessed with ACh (0.1-1 μM). Only arterioles which developed myogenic tone at 80 mmHg, dilated maximally to ≤1 μM ACh, and recovered 40-50% myogenic tone following ACh washout, were subsequently used. Reactivity of mesenteric arteries was assessed by contraction to 1-3 μM PE followed by relaxation to 0.1-1 μM ACh (**Figure 2.3.2B**). Only vessels relaxing maximally to ≤1 μM ACh, reflecting undamaged endothelium, were subsequently used.

Drugs were typically applied to a static bath ('abluminally') and mixed using trituration with a pipettor set to 70 μL.

2.3.ii Measurement of changes in endothelial cell $[Ca^{2+}]_i$ levels

Pressurized arteries were luminally loaded with the Ca^{2+}-sensitive fluorescent dye Oregon Green 488 BAPTA-1 AM (OGB-1, 10 μM; dissolved in DMSO with 0.02% (w/v) Pluronic F-127) using a peristaltic pump, to enable selective loading of the dye into endothelial cells. The cells were exposed to the dye for 38 min at low pressure

before washing with MOPS-buffered solution for another 30 min to allow de-esterification at high pressure. OGB-1 was excited at 488 nm and the fluorescence emission intensity collected >505 nm using a laser scanning confocal microscope with confocal aperture 500 μm. Images were acquired at ~3 Hz using FluoView software (Olympus, Japan) with a 40x water immersion objective (NA 1.15, Olympus, Japan) to visualise endothelial cells situated at the bottom of the artery (**Figure 2.3.2C**). Images were stored for offline analysis using MetaMorph software (v6.1, Molecular Devices, USA).

2.3.iii Endothelial cell Ca^{2+} event detection and analysis

Endothelial cell Ca^{2+} imaging data were analysed offline using MetaMorph software (v6.1, Molecular Devices, USA). Several frames from the acquired time series run were averaged to create a clear image of the outlines of the endothelial cells. Regions were drawn around the cells, which were copied onto the time series run. These whole-cell regions were used to identify the borders of endothelial cells on the time series. Small, subcellular circular regions of interest (ROIs) were then placed manually at sites within each individual endothelial cell which appeared to show a Ca^{2+} event, seen as a peak in the average fluorescence trace over time. These potential events were then assessed by eye using movie playback and only events which were visible by eye were included. This ensured that changes in fluorescence intensity due to the movement of cells were avoided.

The total number of Ca^{2+} events was divided by the total number of whole cells in the field of view, providing a frequency of Ca^{2+} events expressed per minute, per cell.

2.3.iv Diameter measurements

For measurement of diameter changes, time series acquisitions were analysed offline using MetaMorph software (v6.1, Molecular Devices, USA). Outer diameters were tracked for mesenteric arteries as the inner wall was not clear during vasoconstriction (**Figure 2.3.2B**); for the smaller diameter cremaster arterioles the inner diameter could be tracked and was therefore measured.

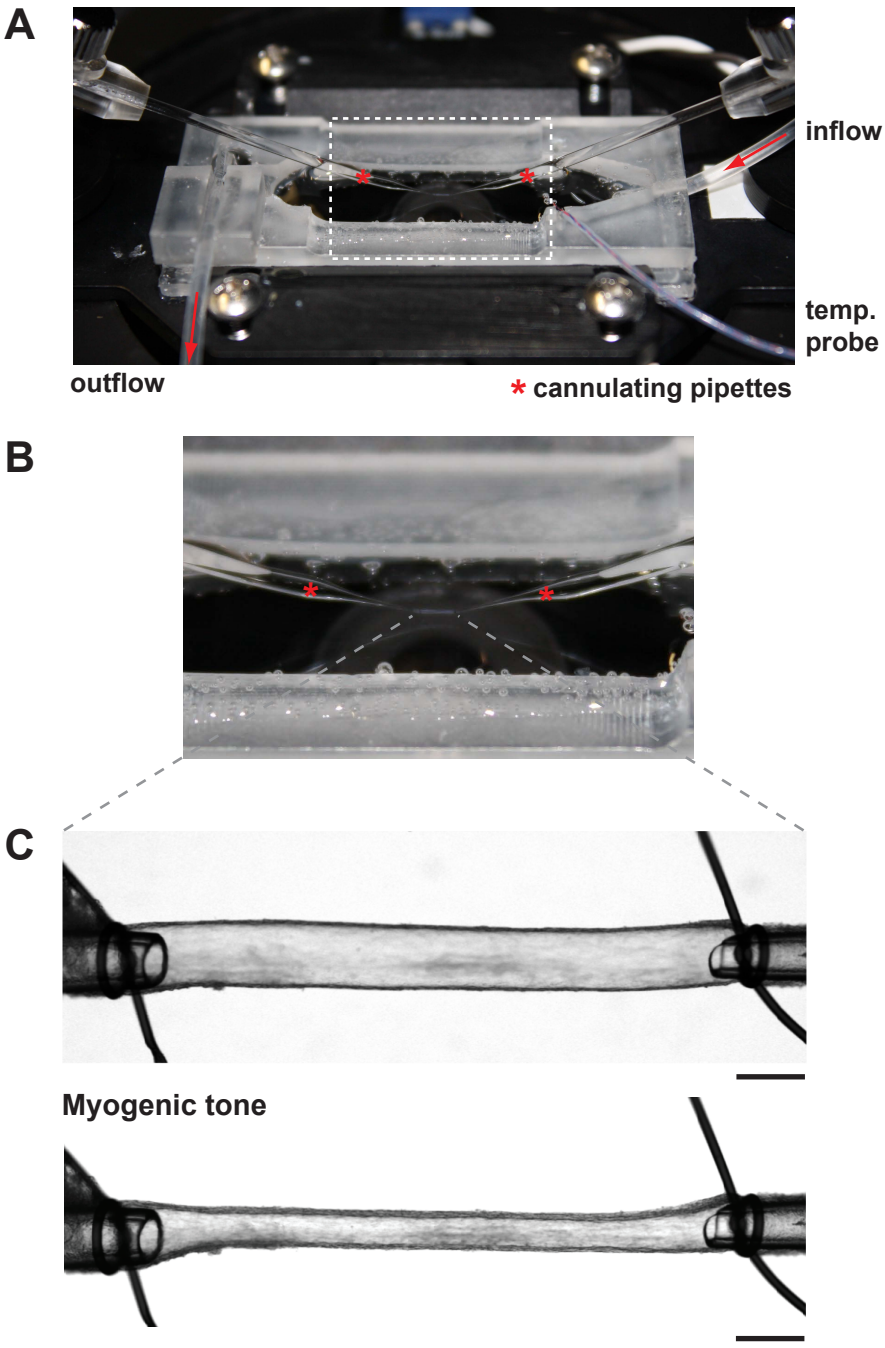

Figure 2.3.1 Pressure myography setup
A Photograph of the temperature-controlled chamber within the customized pressure myography setup, showing cannulating pipettes marked with *, inflow and outflow lines for bath exchange, and a temperature probe for constantly monitoring bath temperature. **B** Close-up of chamber showing an arteriole between the two cannulating pipettes. **C** Pressurized cremaster arteriole at physiological pressure (80 mmHg) visualised using confocal microscopy with a 4x objective and 2x digital zoom before (**top**) and after (**bottom**) development of 50% myogenic tone. Cannulating pipettes and sutures are visible at both ends of the arteriole. Scale bars = 100 μm.

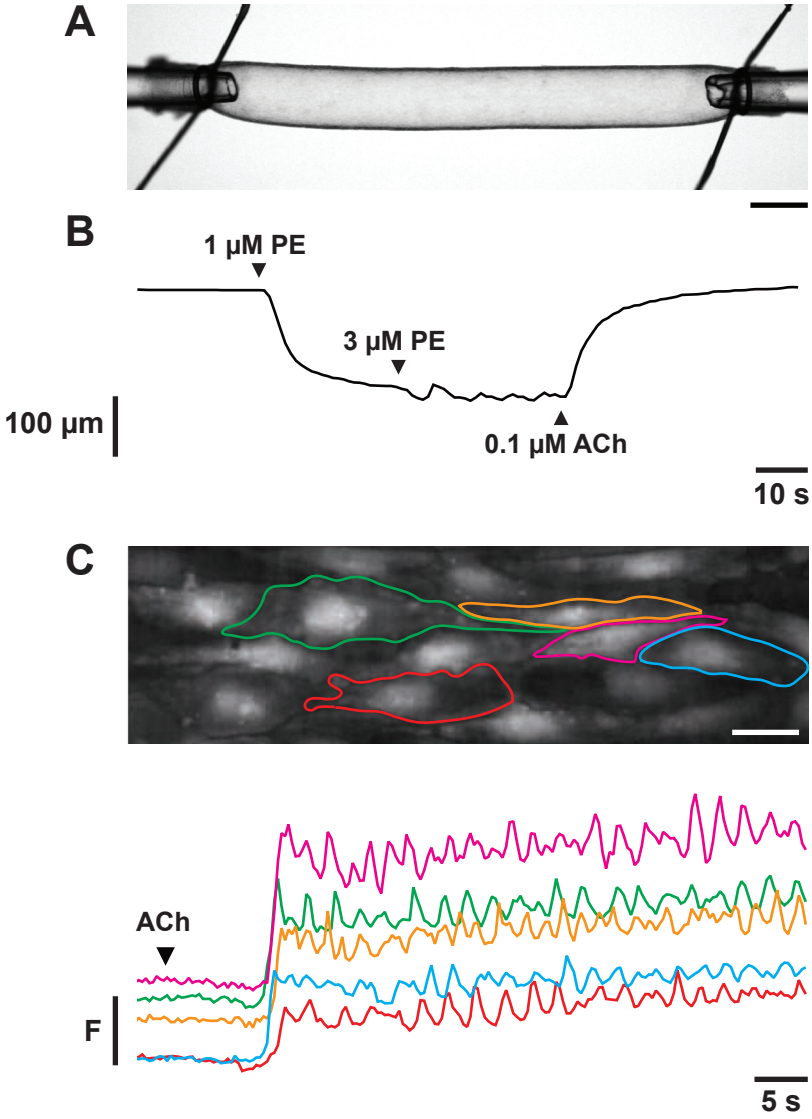

Figure 2.3.2 Pressurized mesenteric artery for endothelial cell Ca^{2+} imaging
A Cannulated third order rat mesenteric artery at physiological pressure (70 mmHg) visualised using confocal microscopy with a 4x objective, 1.5x digital zoom. Scale bar = 200 μm. The cannulating pipettes and sutures are visible at both ends. **B** Diameter measurement of the same artery showing the contraction to 1 μM and 3 μM phenylephrine (PE), which resulted in vasomotion, followed by 100% dilation to 0.1 μM acetylcholine (ACh); agonists were added at the time points marked. This function test was performed for every artery used. **C Top** The endothelial cells were loaded with Oregon Green 488 BAPTA-1 AM and visualised by focusing at the bottom of the vessel using confocal microscopy with a 40x objective (image shows an average of 100 frames acquired at 3 Hz). Scale bar = 50 μm. **Bottom** Average fluorescence traces showing the Ca^{2+} response to 0.3 μM ACh (addition marked by arrowhead). The whole-cell fluorescence intensity was averaged and the coloured traces correspond to the coloured regions in the image above. F (fluorescence intensity) = 200 a.u.

2.4 Immunohistochemistry

Third order mesenteric arteries or cremaster arterioles were pressurized as above and fixed in 2% paraformaldehyde (PFA) solution for 10 min at 37ºC, 70 mmHg (or 80 mmHg for cremaster arterioles), then washed with phosphate-buffered saline (PBS; 0.01 M, 3x 5 min, 37ºC, 70 / 80 mmHg). Arteries were then pre-incubated in blocking buffer (1% bovine serum albumin (BSA) and 0.1% Tween 20 in PBS), for 1 h at 37ºC, 15 mmHg, before incubating overnight at 4ºC (not pressurized) in primary antibody dissolved in blocking buffer at room temperature. Antibodies were generally applied luminally and abluminally, but when primary antibody was only applied luminally overnight to label endothelial cells, blocking buffer without antibody was applied in the bath. The next day, after washing with PBS, arteries were incubated for 2 h with secondary antibody dissolved in blocking buffer (1% BSA and 0.01% Tween 20 in PBS) applied luminally. Propidium iodide (45 μM) and Alexa Fluor 633 hydrazide (1 μM) were applied abluminally to stain nuclei and the internal elastic lamina (IEL) respectively. Fluorescence at the endothelial cell plane at the bottom of the vessel was excited at 488 nm, 543 nm and 633 nm and the emission at 505-550 nm, 560-620 nm and 655-755 nm was acquired sequentially through a 40x water immersion objective with 100 μm confocal aperture using confocal microscopy and FluoView software (Olympus, Japan). *z*-Stacks through the wall of the artery were obtained at 0.1-0.5 μm increments. After imaging the endothelial cell layer, secondary antibody in blocking buffer (as above) was applied abluminally for 2 h to label the smooth muscle cell layer, then imaged as above. Secondary antibodies applied luminally in cremaster arterioles were able to pass through the single smooth muscle layer and bind primary antibody in all layers, so abluminal

application of secondary antibody was not required. *z*-Stacks were reconstructed offline using Imaris software (Bitplane, Switzerland).

2.4.i Pinned immunohistochemistry

For pinned immunohistochemistry of the rat sino-atrial (SA) node, adult male Wistar rats were sacrificed by cervical dislocation and the heart immediately removed and placed in ice-cold MOPS-buffered solution. The heart was carefully dissected to reveal the region of the right atrium near the superior vena cava containing the SA node intact (**Figure 2.4.1**). This was cut into strips ~2 mm wide and pinned into a Sylgard-lined 24-well plate with the endocardium facing up such that SA node cells were accessible to antibodies.

The tissue was fixed with 2% PFA for 10 min at 37ºC. The strips were washed 3x 5 min in PBS at 37ºC, then pre-incubated in blocking buffer (1% BSA + 0.1% Tween 20 in PBS) before incubating overnight at 4ºC in primary antibody dissolved in blocking buffer applied at room temperature. After washing with PBS, tissue segments were incubated for 2 h with secondary antibody, propidium iodide (45 μM) and Alexa Fluor 633 hydrazide (1 μM) dissolved in blocking buffer (1% BSA and 0.01% Tween 20 in PBS). After washing with PBS, the segments were mounted on VectaShield Mounting Medium for Fluorescence H-1000 (Vector Laboratories Inc., USA) on microscope slides and sealed with colourless nail varnish under a 10 mm diameter glass coverslip.

Acknowledgement: I am grateful to Dr Rebecca Capel for instructing me on the correct technique for isolation of the SA node.

When using primary antibodies for the first time, pinned immunohistochemistry was performed on segments of artery using the protocol described above, with a range of dilutions of primary and secondary antibody, to find an optimal combination of concentrations to use in pressurized preparations.

2.4.ii Antibodies

Upon receipt, antibodies were reconstituted where necessary according to the product specification sheet, then vortexed, centrifuged and triturated before aliquoting in Protein Lo-bind Eppendorf tubes. Aliquots were stored at -20°C for up to 1 year. All primary and secondary antibodies used are described in **Table 2.4.1**.

2.4.iii Luminal application

An LKB peristaltic pump was used (~4 μL min^{-1}) to apply blocking buffer, PBS or antibodies in the lumen of the vessel where necessary.

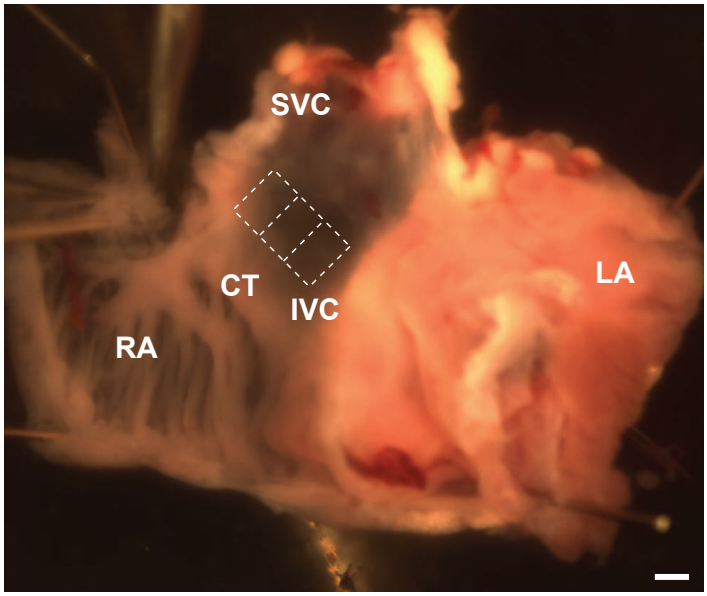

Figure 2.4.1 Sino-atrial node dissection
The heart was dissected such that the right atrium (RA, muscle fibres visible) was cut open to reveal the SA node region next to the crista terminalis (CT). This region was cut into three sections for pinned immunohistochemistry (dotted outlines mark the SA node region split into three sections). The left atrium (LA) remains intact. The superior vena cava (SVC) and inferior vena cava (IVC) have also been cut open and are marked. Ventricles have been removed. Scale bar = 1 mm.

Protein	Primary Antibody	Immunogen	Secondary Antibody
BK_{Ca}	• 1:100 • L6/60 • Mouse monoclonal • NeuroMab	Peptide corresponding with amino acid residues 690-1196 (99% homology with rat)	• 1:100 • A-21200 • Chicken anti-mouse
HCN1	• 1:200 • APC-056 • Rabbit polyclonal • Alomone	(C)KPNSASNSRDDGNSVYPS corresponding to amino acid residues 6-24 of rat HCN1	• 1:200 • A-11008 • Goat anti-rabbit
HCN2	• 1:200 • APC-030 • Rabbit polyclonal • Alomone	(C)EEAGPAGEPRGSQAS corresponding with amino acid residues 147-161 of human HCN2 (100% homology with rat)	• 1:200 • A-11008 • Goat anti-rabbit
HCN3	• 1:200 • ab94755 • Rabbit polyclonal • AbCam	Peptide sequence within the internal region 612-661 of human HCN3 (98% homology with rat)	• 1:200 • A-11008 • Goat anti-rabbit
HCN4	• 1:100 • APC-052 • Rabbit polyclonal • Alomone	HGHLHDSAEERRLIAEGDASPGEDRTPP GLAAEPERP corresponding to amino acid residues 119-155 of human HCN4 (95% homology with rat)	• 1:200 • A-11008 • Goat anti-rabbit
LAMP-2	• 1:200 • PA1-655 • Rabbit polyclonal • Thermo Scientific	CGLKRHHTGYEQF corresponding to amino acid residues 399-411 of rat LAMP-2	• 1:100 • A-11008 • Goat anti-rabbit

Table 2.4.1 Antibodies used for immunohistochemistry
Details of optimum primary and secondary antibody combinations used in all immunohistochemistry experiments. All secondary antibodies were purchased from Life Technologies (UK).

2.5 Whole-cell patch-clamp

Our understanding of the bioelectricity of cell membranes and methods for measuring them stem from the work famously conducted by Hodgkin and Huxley (Hodgkin *et al.*, 1952) who used a glass microelectrode to penetrate and measure the action potential of a squid giant axon, before much was really known of ion channels and conductance of charge. The concept of voltage-clamp was developed by Cole (Cole, 1949), which led to significant advances in the field of electrophysiology when combined with Hodgkin and Huxley's work. In 1976, Neher and Sakmann devised the variation of the voltage-clamp method known as 'patch-clamp'. For this the glass pipette has a relatively large opening (~1 μm) so that rather than penetrating through the membrane, it forms a tight seal with a 'patch' of the membrane (Neher & Sakmann, 1976).

The patch technique has since been refined and developed, mainly in terms of reducing the noise of the system by creating a higher resistance seal between the membrane and the pipette, known as a gigaseal (Hamill *et al.*, 1981). Many configurations of patch-clamp are also now possible; some of these make use of the adhesion between the glass pipette and membrane, which is actually stronger than the attraction between neighbouring phospholipids in the membrane, such that pulling away will break the membrane but leave the seal intact; this is known as inside-out patch-clamp (Molleman, 2002). In our experiments we used the whole-cell configuration to assess currents across the entire cell membrane (**Figure 5.2.1**). This involves sealing onto the cell and applying suction to rupture the membrane, which reseals around the glass pipette. The interior of the cell is consequently open to the pipette solution, which being a significantly larger volume than the cell, will

dialyse in over time. This has the advantage of allowing free access of any drugs in the pipette solution to the cytosol, but with the caveat that over time the interior of the cell will be altered.

2.5.i Preparation of cells

Six or seven third order branches of rat mesenteric arteries were dissected free of connective tissue and cut open longitudinally to disperse luminal red blood cells and improve access of the digestion enzymes. Care was taken to avoid damaging the endothelium during longitudinal cutting. Arteries were transferred from ice-cold Ca^{2+}-free HEPES-buffered solution into the same solution containing BSA (1 mg mL^{-1}) and digestive enzymes, papain (1 mg mL^{-1}) and DL-dithiotheitol (DTT; 1 mg mL^{-1}) and incubated at room temperature for 10 min, then at 37°C for 30 min. Arteries were washed twice in ice-cold Ca^{2+}-free HEPES-buffered solution and then manually triturated in a solution containing BSA (1 mg mL^{-1}) for 5 min using a wide-bore polished custom-made glass pipette. Cells were stored in this solution on ice for use during the day. Ca^{2+}-HEPES (1 mM) was added approximately every 2 hours to slowly increase [Ca^{2+}] in the cell suspension to 0.5 mM, to prevent cells being starved of Ca^{2+}.

2.5.ii Patch-clamp protocols

Details of the protocols used for whole-cell patch-clamp measurement of smooth muscle and endothelial cell currents are given in the Materials & Methods sections of the appropriate chapters.

The resistance of the patch pipettes measured 3-10 mΩ when filled. Electrophysiological data analysis was performed using Clampfit 9 (Molecular Devices, USA) and MiniAnalysis (Synaptosoft Inc., USA) software.

2.6 Solutions and drugs

All wire myography and pressure myography experiments were conducted in MOPS-buffered solution containing (mM): NaCl, 145.0; KCl, 4.7; $CaCl_2$ 2.0; $MgSO_4.7H_2O$ 1.17; MOPS, 2.0; NaH_2PO_4, 1.2; D-glucose, 5.0; pyruvate, 2.0; EDTA, 0.02; NaOH, 2.75; at 37ºC, pH = 7.40 ± 0.02 adjusted using 1M or 4M NaOH. All experiments involving isolated cells were conducted in HEPES-buffered solution containing (mM): NaCl, 130.0; KCl, 5.0; $MgCl_2$, 1.2; $CaCl_2$, 1.0; D-glucose, 10.0; HEPES, 10.0; at 37ºC, pH = 7.40 ± 0.02 adjusted using 1M or 4M NaOH. Nominally Ca^{2+}-free HEPES-buffered solution was used for cell isolation (1 mM $CaCl_2$ excluded from solution). For whole-cell patch-clamp recordings of isolated endothelial or smooth muscle cells, the pipette solution contained (mM): KCl, 140.0; $MgCl_2.6H_2O$, 0.5; EGTA, 0.1; Mg.ATP, 2.0; HEPES, 5.0; at 37ºC, pH 7.20 ± 0.02 adjusted with NaOH.

All salts were purchased from Sigma-Aldrich, UK. Details of suppliers of drugs and chemicals are given in **Table 2.6.1**.

Drug / Chemical	Product code	Supplier	Stock conc.	Stock solvent	Final conc.
Acetylcholine (ACh)	A6625	Sigma-Aldrich (UK)	10^{-2} M	Milli-Q	100 nM*
Apamin (Ap)	L8407	Latoxan (France)	10^{-2} M	Milli-Q	50 nM
Bafilomycin A1 (Baf A1)	1334	R&D Systems (UK)	10^{-1} M	DMSO	1 μM
Bovine serum albumin (BSA)	A7906	Sigma-Aldrich (UK)	NA	NA	*see text*
Calcein	C3100MP	Life Technologies (UK)	$2.5x10^{-1}$ M	DMSO	12.5 μM
Dithiothreitol (DTT)	D0632	Sigma-Aldrich (UK)	NA	NA	*see text*
Fluo-4 AM	F14201	Life Technologies (UK)	2 mM	DMSO	10 μM
Forskolin (FSK)	F3917	Sigma-Aldrich (UK)	10^{-2} M	DMSO	1 μM
Glibenclamide (Glib)	G0639	Sigma-Aldrich (UK)	10^{-2} M	DMSO	10 μM
Iberiotoxin (IbTX)	L8211	Latoxan (France)	$5x10^{-2}$ M	Milli-Q	100 nM
Isoprenaline (Iso)	I5627	Sigma-Aldrich (UK)	10^{-2} M	Milli-Q	1 μM*
Ivabradine	SML0281	Sigma-Aldrich (UK)	10^{-2} M	Milli-Q	0.3-30 μM
Hoechst trihydrochloride, trihydrate (10 mg mL^{-1} solution)	H3570	Life Technologies (UK)	16.2 mM	Distilled water	16.2 μM
Levcromakalim (LVK)	1378	R&D Systems (UK)	10^{-2} M	EtOH	3 μM
Lysotracker red DND-99	L7528	Life Technologies (UK)	10^{-4} M	Milli-Q	100 nM
NAADP	3905	R&D Systems (UK)	10^{-2} M	DMSO	*range*
NAADP-AM	*made in house*			DMSO (anhydrous)	0.1-0.5 μM
trans Ned-19	3954	R&D Systems (UK)	10^{-1} M	DMSO	10 μM
Nifedipine (Nif)	N7634	Sigma-Aldrich (UK)	10^{-2} M	EtOH	1 μM
Oregon Green 488 BAPTA-1 AM (OGB-1)	06807	Life Technologies (UK)	2 mM	DMSO	10 μM
Papain	P4762	Sigma-Aldrich (UK)	NA	NA	*see text*
Paraformaldehyde (PFA)	*custom-made*	Electron Microscopy Sciences (UK)	2%	Distilled water	2%
Paxilline (Pax)	P2928	Sigma-Aldrich (UK)	10^{-2} M	Milli-Q	1 μM
Phenylephrine (PE)	P6126	Sigma-Aldrich (UK)	10^{-2} M	Milli-Q	1 μM*
Pluronic F-127	P3000MP	Life Technologies (UK)	20% (w/v)	*supplied in DMSO*	0.05% (w/v)
Propidium iodide (PI)	P4170	Sigma-Aldrich (UK)	4.5 mM	Milli-Q	45 μM
TRAM-34 (TR)	2946	R&D Systems (UK)	10^{-2} M	DMSO	1 μM
U46619	16450	Cayman Chemical (USA)	10^{-2} M	DMSO	1 μM*
ZD7288	1000	R&D Systems (UK)	10^{-2} M	Milli-Q	1 μM*

Table 2.6.1 Details of drugs and chemicals used in this thesis
Chemicals are listed alphabetically and abbreviations given in brackets. Milli-Q is purified water; DMSO - dimethylsulfoxide; EtOH - 100% ethanol. All dilutions of stocks are made using the buffer solution. The final concentration given applies to experiments where a single concentration was applied. Some drugs were also applied over a range to create a concentration-response curve; these drugs are labelled with *.

2.7 Statistical analysis

All data are expressed as mean ± S.E.M. from *n* experiments, one *n* per animal unless stated otherwise and analysed using Microsoft Excel and GraphPad Prism 5.0 software for Mac. Two-way, one-way or repeated measures ANOVA was performed as appropriate for comparing multiple treatments, with a Bonferroni post-test to analyse specific sets as described in the figure legends. For single comparisons, a two-tailed Student's *t*-test was performed. $P<0.05$ was considered statistically significant.

CHAPTER 3

β-ADRENERGIC STIMULATION ACTIVATES ENDOTHELIAL CELL CA^{2+} EVENTS

3.1 Introduction

3.1.i Cardiovascular adrenoceptors

Two of the most significant modulators of the cardiovascular system are the endogenous catecholamines: noradrenaline and adrenaline, which are released from sympathetic nerves and the adrenal medulla respectively. The award of two Nobel Prizes in the area indicates the importance of sympathetic modulation in the cardiovascular system: to Sir James Black (Physiology or Medicine 1988) for his work on adrenoceptor-blocking drugs (those targeting β-adrenoceptors in the heart ('β-blockers') being one of the most widely prescribed drugs today); and more recently to Robert Lefkowitz and Brian Kobilka (Chemistry 2012) for pioneering studies of the structure and function of β-adrenoceptors (reviewed by Frishman, 2013).

The first observations of the differential effects of the sympathetic nervous system on the heart and peripheral circulatory system were principally described by Dale in the early 1900s (Dale, 1905). Dale observed that chrysotoxin slowed and augmented the heartbeat of a pithed cat, whilst there was widespread peripheral vasoconstriction. This peripheral pressor effect was reversed by prior injection of ergotoxine. Later in 1948, Ahlquist proposed two subtypes of adrenoceptors, α and β (Ahlquist, 1948). In the 1960-70s further pharmacological experiments identified additional subdivisions of these two categories; advances in molecular cloning technology and more selective drugs allowed characterisation of a total of nine adrenoceptor subtypes: α_{1A}, α_{1B}, α_{1C}, $\alpha_{2A/D}$, α_{2B}, α_{2C} and β_1, β_2, β_3 (Guimaraes & Moura, 2001).

Adrenoceptors are GPCRs. α_1-adrenoceptors are coupled to $G_{q/11}$: this activates phospholipase C, which triggers production of Ca^{2+}-mobilising second messengers, inositol trisphosphate (IP_3) and diacylglycerol (DAG). Additional intracellular signalling pathways have also been linked to α_1-adrenergic stimulation (Guimaraes & Moura, 2001) but the $G_{q/11}$ pathway is dominant in the resistance vasculature. α_2-Adrenoceptors are coupled to G_i, which inhibits adenylyl cyclase activity and consequently lowers intracellular cAMP levels.

β_1- and β_2-adrenoceptors were classically described by Lands *et al* (Lands *et al.*, 1967b; Lands *et al.*, 1967a), whilst the third subtype (β_3) was described later and does not share the same conventional pharmacology (lack of inhibition by β-adrenoceptor antagonists e.g. propranolol). A fourth β-adrenoceptor subtype (β_4) was proposed, but was later ascribed to a different conformational state of the β_1-adrenoceptor (Guimaraes & Moura, 2001). All β-adrenoceptors couple to the G_s-protein, which activates adenylyl cyclase and consequently increases cAMP levels. cAMP can then activate protein kinase A (PKA) which has multiple downstream targets.

In vascular smooth muscle cells this leads to relaxation via two main mechanisms: inhibition of myosin light chain kinase and opening of sarcolemmal K_{ATP} channels via phosphorylation (Nakashima & Vanhoutte, 1995). Opening of K_{ATP} channels will cause hyperpolarization, as has been demonstrated in rat mesenteric arteries (Takano *et al.*, 2004; Garland *et al.*, 2011b). K_{ATP} channels have been shown to reside exclusively on smooth muscle cells, since levcromakalim (K_{ATP} opener) is without effect on isolated endothelial cells (Takano *et al.*, 2004); however,

hyperpolarization of smooth muscle cells due to opening of K_{ATP} channels (directly with levcromakalim or indirectly via β-adrenoceptor stimulation) will transfer via heterocellular gap junctions to hyperpolarize the endothelium. This was measured in rat mesenteric arteries using sharp microelectrode electrophysiology directly impaling endothelial cells in an *en face* preparation, which showed hyperpolarization to levcromakalim (3 μM) of -25.1 ± 1.5 mV from a resting membrane potential of -52.6 ± 0.7 mV (bringing the membrane potential to ~-77.7 mV, which is ~E_k) (White & Hiley, 2000). The effect of levcromakalim was reversed with glibenclamide (K_{ATP} channel inhibitor, 10 μM); similar data were also reported by (Takano *et al.*, 2004).

Activation of cAMP can also activate a recently described target protein known as exchange protein activated by cAMP (Epac). Amongst other effects in vascular smooth muscle and endothelial cells, Epac has been shown to colocalise with K_{ATP} channels and using a cAMP analogue (8-pCPT-2'-O-Me-cAMP), to modulate their activity via a mechanism independent of PKA (Purves *et al.*, 2009).

3.1.ii β-Adrenoceptor subtypes in the vasculature

In the peripheral vasculature, β_1- and β_2-adrenoceptors are reported to participate in the vasodilatory effect to noradrenaline and adrenaline, first described over a century ago (Dale, 1913). Historically, it was thought that the β_1-adrenoceptors predominate centrally, whilst β_2-adrenoceptors mediated the main peripheral vasodilatory effect on vascular smooth muscle cells (Lands *et al.*, 1967b). Recently it has been shown through use of β_1- and β_2-adrenoceptor knockout mice that β_1-adrenoceptors are more widespread throughout the vasculature, whilst β_2-adrenoceptors are more restricted in their distribution (Chruscinski *et al.*, 2001). Indeed, there is debate as to which β-adrenoceptor(s) is / are present in the smaller resistance arteries. One recent direct examination of this in rat mesenteric arteries provides functional evidence for a predominance of the β_1 subtype of adrenoceptors. In a wire myograph setup, relaxation of PE (2-3 μM) pre-constricted arteries by isoprenaline (β_1- and β_2-adrenoceptor-selective agonist) was right-shifted by pre-incubation with atenolol (1 μM, β_1-adrenoceptor-selective antagonist) whilst ICI-118,551 (1 μM, β_2-adrenoceptor-selective antagonist) had little effect (Briones *et al.*, 2005). Interestingly, salbutamol (β_2-adrenoceptor-selective agonist) was seen to relax the arteries; however, when U46619 (0.1-1 μM, thromboxane mimetic) was used to pre-constrict the vessels instead of PE, salbutamol was ineffective. This suggests the observed relaxation was functional antagonism, rather than an action at β_2-adrenoceptors. In contrast, reports from our lab have demonstrated hyperpolarization to salbutamol in rat mesenteric arteries (-14.1 ± 1.5 mV from a resting membrane potential of -55.9 ± 1.1 mV), supporting a link to downstream opening of K_{ATP} channels (Garland *et al.*, 2011b). Briones *et al* also provided

evidence against β_3-adrenoceptors in the vasculature, finding α-adrenoceptor antagonist action of β_3-adrenoceptor-selective agonists (Briones *et al.*, 2005).

3.1.iii Endothelial cell β-adrenergic signalling pathways

Whilst the downstream pathways are well established in smooth muscle cells, more recently interest has developed in the pathways triggered by endothelial cell β-adrenoceptors. Briones *et al* show binding of BODIPY-TMR-CGP 12177, a fluorescent ligand of β_1-adrenoceptors, in the endothelium of fixed and permeabilised rat mesenteric arteries (Briones *et al.*, 2005). Stimulation of β-adrenoceptors on primary cultured bovine aortic endothelial cells (BAECs) with adrenaline (1 μM) reportedly causes Ca^{2+} influx via cyclic nucleotide-gated A2 (CNGA2) channels (Shen *et al.*, 2008). L-*cis*-diltiazem and LY-83583 (inhibitors of CNG channels) reduced the adrenaline-activated cation current and increases in Ca^{2+} in these cells. Of note, Ca^{2+} increases to adrenaline (1 μM) or isoprenaline (10 μM) were observed only if the cells were previously challenged with bradykinin (10 nM); the reason for this was unclear. ICI-118,551 (1 μM) blocked the increases to adrenaline and isoprenaline, which was taken as evidence that β_2-adrenoceptors were the likely target; however at the concentrations of isoprenaline and ICI-118,551 used, their actions may have been non-selective. Thapsigargin could also reduce the Ca^{2+} responses to adrenaline and isoprenaline. Furthermore, the same investigators showed in mouse aortic strips that endothelial cell Ca^{2+} levels increased in response to isoprenaline (10 μM) in the absence of pre-stimulation with bradykinin. The researchers proposed that there might be constitutive levels of Ca^{2+}-mobilising agonists in the tissue which are absent in isolated cells, hence exogenous addition was not necessary (Shen *et al.*, 2008). This was not

investigated further in the study, but is an interesting observation. An alternative interpretation could be that it reflects differential expression of proteins or a requirement for an intact connection with smooth muscle cells.

This observation in BAECs proposes a key role for β_2-adrenoceptors in endothelial cells for mediating a Ca^{2+} response to catecholamines. Our group previously published evidence in isolated rat mesenteric arteries that stimulation of β-adrenoceptors with isoprenaline, adrenaline or noradrenaline (the latter two in the presence of prazosin to prevent simultaneous smooth muscle α-adrenoceptor stimulation) caused inhibition of endothelial cell IK_{Ca} channels which reduced the EDH-type relaxation to ACh (Yarova *et al.*, 2013). The inhibition was sensitive to the β_1-adrenoceptor-selective antagonist atenolol (1 μM), but not ICI-118,551 (0.1 μM). Together with patch-clamp data from endothelial cell sheets, this provided evidence for functional β_1-adrenoceptors on the endothelium. The data further suggested that at least PKA was activated following stimulation of endothelial β_1-adrenoceptors as the effect against IK_{Ca} channels was mimicked by forskolin (adenylyl cyclase activator) and blocked by KT 5720 (PKA inhibitor). This extends the findings of Briones *et al* 2005 of endothelial β-adrenoceptor expression, demonstrating functionality and a role exclusively for β_1-adrenoceptors in mediating inhibition of IK_{Ca} channels. It remains to be determined whether β_2-adrenoceptors can facilitate an endothelial cell Ca^{2+} response in rat mesenteric arteries in parallel to this observed role for β_1-adrenoceptors, or whether there are species- and / or tissue-specific differences in β-adrenoceptor subtype localisation and function.

Whether endothelial β-adrenoceptor stimulation activates eNOS and NO production is controversial: it has been reported that β-adrenoceptor stimulation increases levels of NO *in vivo* (Figueroa *et al.*, 2009), whilst in experiments performed in rat mesenteric arteries in our group, L-NAME (eNOS inhibitor) was without effect on isoprenaline-induced relaxation or hyperpolarization (Garland *et al.*, 2011b).

3.1.iv Hyperpolarization-mediated increases in endothelial cell Ca^{2+} events

Increases in endothelial cell Ca^{2+} following hyperpolarization have previously been reported in cultured or freshly isolated cells (Lückhoff & Busse, 1990; Langheinrich *et al.*, 1998). However the mechanism remains elusive: since hyperpolarization increases the electrochemical gradient for Ca^{2+} entry, it has historically been attributed to influx via an undefined Ca^{2+} 'leak' channel (reviewed by Dora & Garland, 2013). This channel is yet to be defined. In cultured porcine aortic endothelial cells, stimulation with (lev)cromakalim to open K_{ATP} channels was associated with an increase in $[Ca^{2+}]_i$ from 60 nM to 110 nM (Lückhoff & Busse, 1990). Similarly, (lev)cromakalim increased $[Ca^{2+}]_i$ by ~50 nM in cultured bovine aortic endothelial cells. These observations were replicated in freshly isolated capillary endothelial cells, seeing a Ca^{2+} influx in 50% of cells hyperpolarized by K_{ATP} openers (Langheinrich *et al.*, 1998). Furthermore, there are numerous reports in endothelial cells that hyperpolarization, evoked secondary to an agonist-stimulated Ca^{2+} increase, can contribute to a sustained increase in Ca^{2+}. However, this may not be the case in small resistance arteries and arterioles, where block of K_{Ca} channels by charybdotoxin or apamin did not alter the plateau phase of the Ca^{2+}

response to methacholine (non-selective muscarinic agonist) (Cohen & Jackson, 2005).

The aim of the experiments in this chapter was to test the hypothesis that β-adrenergic stimulation of intact, pressurized arteries could increase endothelial cell Ca^{2+} potentially via a hyperpolarization-driven pathway, and use pharmacological tools to characterise the mechanism.

3.2 Methods & Materials

*Refer to **Chapter 2: Methods & Materials** for full details of the methods used in this chapter. Details relevant specifically to this chapter are given below.*

3.2.i Protocols for assessing endothelial cell Ca^{2+} in pressurized arteries

Rat third order mesenteric arteries were isolated, cannulated and pressurized as described (**Methods & Materials section 2.3.i**) and loaded with Ca^{2+}-sensitive dye, Oregon Green 488 BAPTA-1 AM (**Methods & Materials section 2.3.iii**). Basal, spontaneous Ca^{2+} activity was recorded for 90 s (270 frames acquired at 3 Hz) before addition of isoprenaline (1 μM) in the same acquisition run. The endothelial cell Ca^{2+} response to isoprenaline was recorded for an additional 150 s (450 frames), followed by washout for 25 min. Where drugs were applied to pre-treat the artery before a subsequent run, isoprenaline was washed out for 25 min before incubation with the drug for the specified time (see relevant figure legends).

In offline analysis (*refer to **section 2.3.iii***) Ca^{2+} events were sampled 30 s after addition of isoprenaline to the bath for 120 s. This time delay allows for the mixing of isoprenaline in the bath and is consistent with the time delay observed for hyperpolarization in sharp microelectrode electrophysiology experiments (**Figure 4.3.2**).

*Refer to **Methods & Materials section 2.3.iii** for details of Ca^{2+} event detection and analysis.*

3.2.ii Sharp microelectrode studies of membrane potential

Rat third order mesenteric arteries were mounted in an isometric wire myograph and normalised to resting tension as described (**Methods & Materials section 2.2.i**). A smooth muscle cell was impaled using a sharp microelectrode back-filled with 2 M KCl solution (tip resistance ~100 mΩ when filled) to measure the resting membrane potential (Em) and response to levcromakalim (3 μM) added to a static bath. Having acquired a stable recording, the microelectrode was removed to give a baseline value. The baseline value was calculated as an average of the recording pre- and post- impalement (although the two values did not differ markedly), and recorded values adjusted offline where the baseline value differed from 0 mV.

Acknowledgement: These experiments were set up by CS Lim and performed and analysed by KA Dora.

3.2.iii Imaging Ca^{2+} events in EC sheets

EC sheets were freshly isolated from rat third order mesenteric arteries using the digestion protocol described in **Methods & Materials section 2.5.i**. Cell suspension (500 μL) was added to a chamber and allowed to adhere for 10 min, before using a polished blunt glass pipette to pin the sheet (**Figure 3.3.12A**), as preliminary experiments found that EC sheets did not always robustly adhere to the chamber. HEPES-buffered solution (with 1 mM Ca^{2+}, 500 μL) containing the Ca^{2+}-indicator dye fluo-4 AM dissolved in DMSO with Pluronic F-127 (0.05%) was then added on top. The final concentration of fluo-4 AM in the 1 mL chamber was 10 μM. EC sheets were allowed to load for 15 min, before de-esterifying for an additional 15 min during superfusion (at 1 mL min^{-1}) with 1 mM Ca^{2+} HEPES-buffered solution. Drugs were

added into a static bath and mixed by trituration and washed out by superfusion for ≥20 min.

EC sheets were imaged at 3 Hz using a linescan confocal microscope supported by FluoView software (Olympus, Japan), excitation wavelength 488 nm, collecting light above 505 nm with 500 μm confocal aperture. All experiments were performed at room temperature.

3.2.iv Patch-clamp of EC sheets

EC sheets freshly isolated from rat third order mesenteric arteries as described (**Methods & Materials section 2.5.i**) were patched in the whole-cell configuration in current-clamp mode to monitor the membrane potential using an Axopatch 200B amplifier, Digidata 1200 interface and pCLAMP 8.0 software (Axon Instruments, USA) at sample rate 20 kHz, filter rate 1 kHz. Experiments were performed at room temperature, with continuous superfusion (1 mL min^{-1}) of HEPES-buffered solution (refer to **Methods & Materials section 2.6**). Pipettes measured 3-10 MΩ when filled (refer to **Methods & Materials section 2.6** for composition).

3.2.v Drugs and solutions

*Refer to **Methods & Materials Table 2.6.1**.*

Isoprenaline was dissolved in purified (MilliQ) water; glibenclamide and forskolin were dissolved in DMSO, and subsequent dilutions made in MOPS-buffered solution, such that the final dilution of DMSO into the chamber was 1:1000 or as indicated. Levcromakalim was dissolved in 100% EtOH and subsequent dilutions made in MOPS-buffered solution.

3.3 Results

As discussed in the Introduction (**section 3.1.iv**), there has been considerable speculation regarding Ca^{2+} entry into endothelial cells as a result of plasma membrane hyperpolarization. Previous work (unpublished) by other members of the group has demonstrated in rat intact cremaster arterioles that opening of K_{ATP} channels on the smooth muscle with levcromakalim (3 μM) causes an increase in the frequency of local Ca^{2+} events in endothelial cells (**Figure 3.3.1**). Levcromakalim (3 μM) is sufficient to cause -20.4 ± 5.2 mV (*n*=4) change in membrane potential of rat cremaster arterioles (**Figure 3.3.1C**), which from a resting membrane potential of -43.9 ± 2.2 mV (*n*=4), brings the membrane to -63.9 ± 6.0 mV, approaching ~E_K.

Since β-adrenergic stimulation classically leads to phosphorylation and opening of K_{ATP} channels via activation of PKA, we hypothesized that isoprenaline might provide a physiologically relevant correlate of the observation with levcromakalim. As such, isoprenaline (1 μM, which hyperpolarizes rat mesenteric arteries by ~-22 mV (Garland *et al.*, 2011b); **Figure 4.3.2C**) was added abluminally to a pressurized third order rat mesenteric artery whilst endothelial cell Ca^{2+} was imaged. An increase in the frequency of Ca^{2+} events was observed. Of note, these Ca^{2+} events were not generally visible when a whole-cell average is applied to a given endothelial cell; instead they are clearly visible when discrete regions of interest are positioned at sites within the cell (**Figure 3.3.2A**).

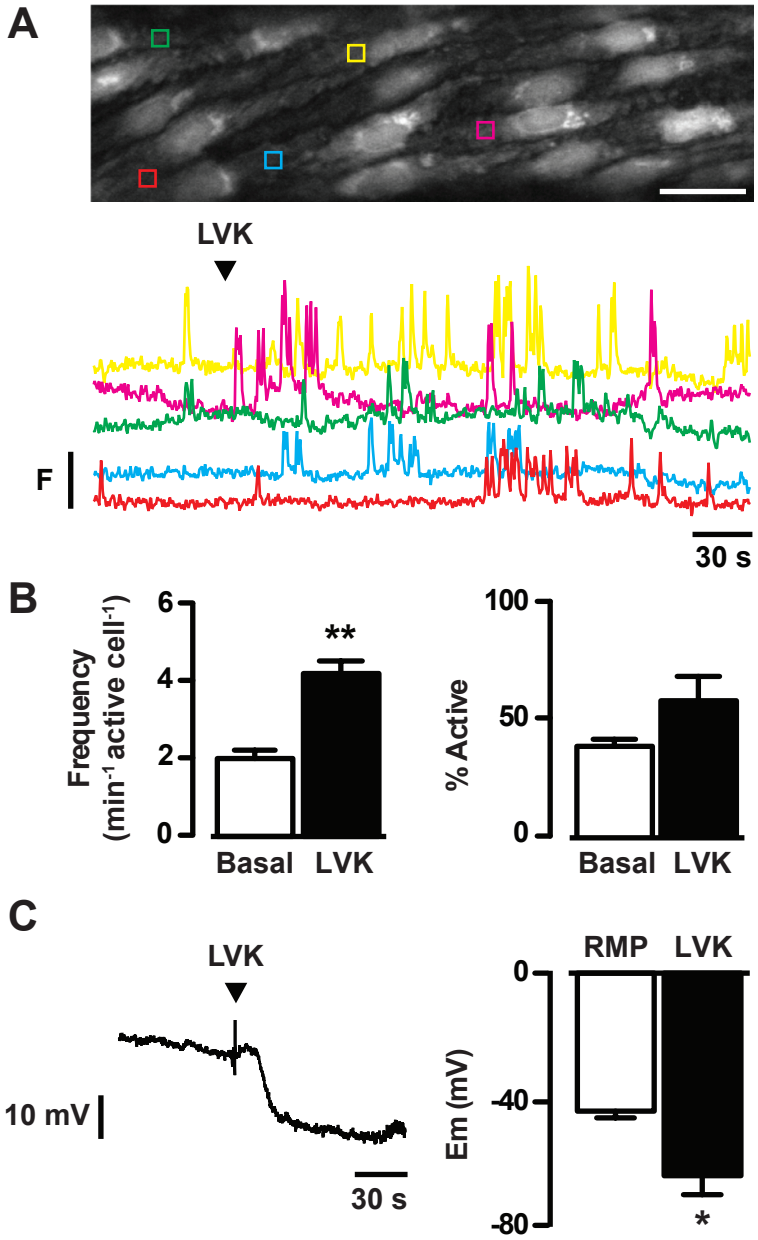

Figure 3.3.1 Opening of K_{ATP} channels increases endothelial cell Ca^{2+} in arterioles
A Top Endothelial cells in a rat pressurized cremaster arteriole loaded with a Ca^{2+}-sensitive dye, visualised using confocal microscopy with a 40x objective. Image is an average of 100 frames acquired at 3 Hz. Scale bar = 50 μm. Regions of interest (ROIs) correspond with raw fluorescence traces (**below**) illustrating the basal, spontaneous Ca^{2+} events as upward deflections, and the increase in frequency of events after addition of levcromakalim (K_{ATP} channel opener, LVK, arrowhead, 3 μM). F (fluorescence intensity) = 200 a.u. **B** Summary data showing the frequency of Ca^{2+} events per active cell (**left**) and the percentage of cells which responded (% active) within the field of view separately (**right**), illustrating a significant increase to opening of K_{ATP} channels with levcromakalim (LVK, 3 μM). Paired data, *n*=7, **P<0.01 by Student's *t*-test. **C** Levcromakalim (LVK, 3 μM) hyperpolarizes the resting membrane potential (RMP) of rat cremaster arterioles mounted under isometric tension in a wire myograph (for mean ± S.E.M. see text). **Left** Representative membrane potential trace; **right** summary data. Paired data, *n*=4, *P<0.05 by Student's *t*-test. **Acknowledgements:** KA Dora and TZ Beleznai performed and analysed the Ca^{2+} imaging experiments, and KA Dora performed and analysed the electrophysiology experiments.

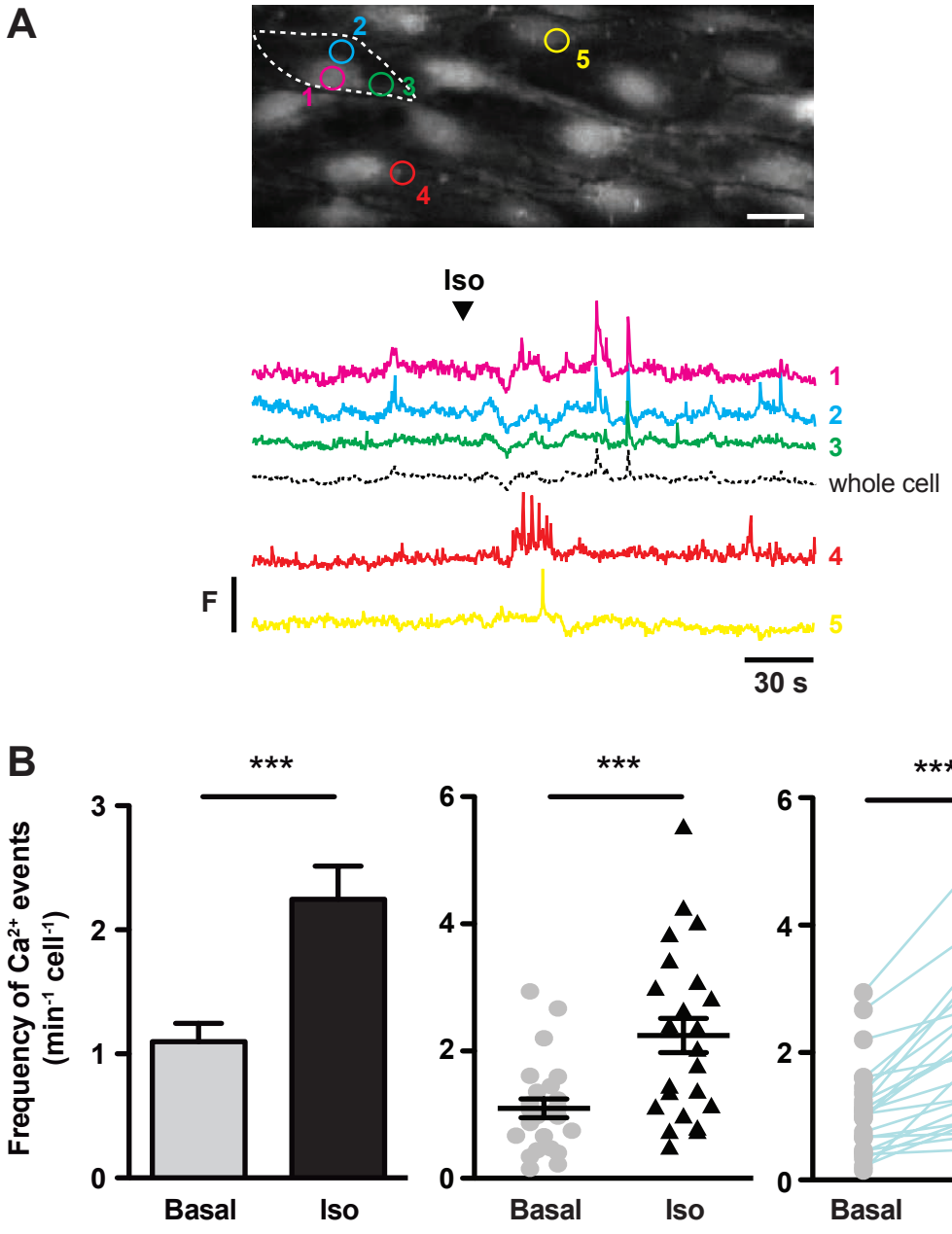

Figure 3.3.2 β-Adrenergic stimulation increases endothelial cell Ca^{2+} in resistance arteries

A Top Endothelial cells in a rat pressurized third order mesenteric artery loaded with a Ca^{2+}-sensitive dye, and visualised using confocal microscopy with a 40x objective. Subcellular ROIs from separate cells correspond with traces below. Note that subcellular ROIs are necessary to see Ca^{2+} events; whole-cell regions (dotted outline) mask some of these subcellular changes. Scale bar = 50 μm. **Bottom** Raw fluorescence intensity traces illustrating basal Ca^{2+} activity, which is increased after exposure to isoprenaline (arrowhead, 1 μM). F (fluorescence intensity) = 200 a.u. **B** Summary data as a histogram, dot-plot or before-after plot, showing the frequency of Ca^{2+} events averaged across all cells (~10) in the field of view per experiment, which is significantly increased from the level of activity at rest (Basal) by β-adrenoceptor stimulation with isoprenaline (Iso, 1 μM). Paired data, n=23, ***P<0.001 by Student's t-test.

To investigate the action of isoprenaline on endothelial cell Ca^{2+}, we first proposed to confirm that the response was receptor-mediated. As discussed in the Introduction (**section 3.1.iii**) there is some controversy regarding receptor subtypes in the resistance vasculature. We therefore first examined the relaxation response to isoprenaline in the presence of antagonists selective for different β-adrenoceptor subtypes, in rat third order mesenteric arteries mounted isometrically on a wire myograph. Arteries were pre-contracted with PE (α_1-adrenoceptor-selective agonist, 1 μM). L-NAME (100 μM) was present throughout to remove the basal release of nitric oxide that occurs with PE stimulation (Dora *et al.*, 1997) and produce a more stable level of vascular tone. Isoprenaline relaxation was right-shifted by pre-incubation with ICI-118,551 (0.1 μM, **Figure 3.3.3B**), a β_2-adrenoceptor-selective antagonist (543-fold selective over β_1-adrenoceptors, $\log IC_{50}$ = -9.3 (Baker, 2005)). The β_1-adrenoceptor-selective antagonist, bisoprolol (0.1-1 μM; $\log IC_{50}$ = -7.8 (Baker, 2005)) further right-shifted the isoprenaline relaxation, in a concentration-dependent manner (**Figure 3.3.3B**). This antagonist is much more selective for the β_1-adrenoceptor than the more commonly used atenolol (bisoprolol 13.5- vs. atenolol 4.7-fold selective over β_2-adrenoceptors (Baker, 2005)). It has not previously been used in rat mesenteric arteries; we therefore characterised its antagonist action in this tissue, constructing a Schild plot using three concentrations of bisoprolol (**Figure 3.3.3C**). The Schild analysis provided a pA_2 value of 7.5, consistent with the reported $\log IC_{50}$ for this compound (Baker, 2005). The linear regression provided a slope of 0.82 ± 0.1, supporting its action as a competitive antagonist.

Having established that both β_1- and β_2-adrenoceptors have a role in the response of this artery to isoprenaline, we used a combination of bisoprolol (1 μM) and ICI-118,551 (0.1 μM) to block β_1- and β_2-adrenoceptors respectively in our pressurized artery. This combined block prevented the endothelial cell Ca^{2+} response to isoprenaline (**Figure 3.3.4**). It is noteworthy that in control conditions, not every cell showed an increased Ca^{2+} event frequency to isoprenaline, which is apparent when the frequency for every cell from every experiment is displayed (**Figure 3.3.4A**). This was consistently observed in all data sets.

Treatment		**LogEC$_{50}$**
Control		-7.4 ± 0.08
ICI-118,551	0.1 μM	-6.7 ± 0.03
Bisoprolol	0.1 μM	-6.1 ± 0.07
	0.3 μM	-5.8 ± 0.03
	1 μM	-5.5 ± 0.05

Table 3.3.1 LogEC$_{50}$ values for isoprenaline relaxation
LogEC$_{50}$ values for the concentration-response curves of isoprenaline relaxation shown in **Figure 3.3.3** in control conditions and after treatment with β_2-adrenoceptor-selective antagonist, ICI-118,551 (0.1 μM) and β_1-adrenoceptor-selective antagonist, bisoprolol (0.1-1 μM).

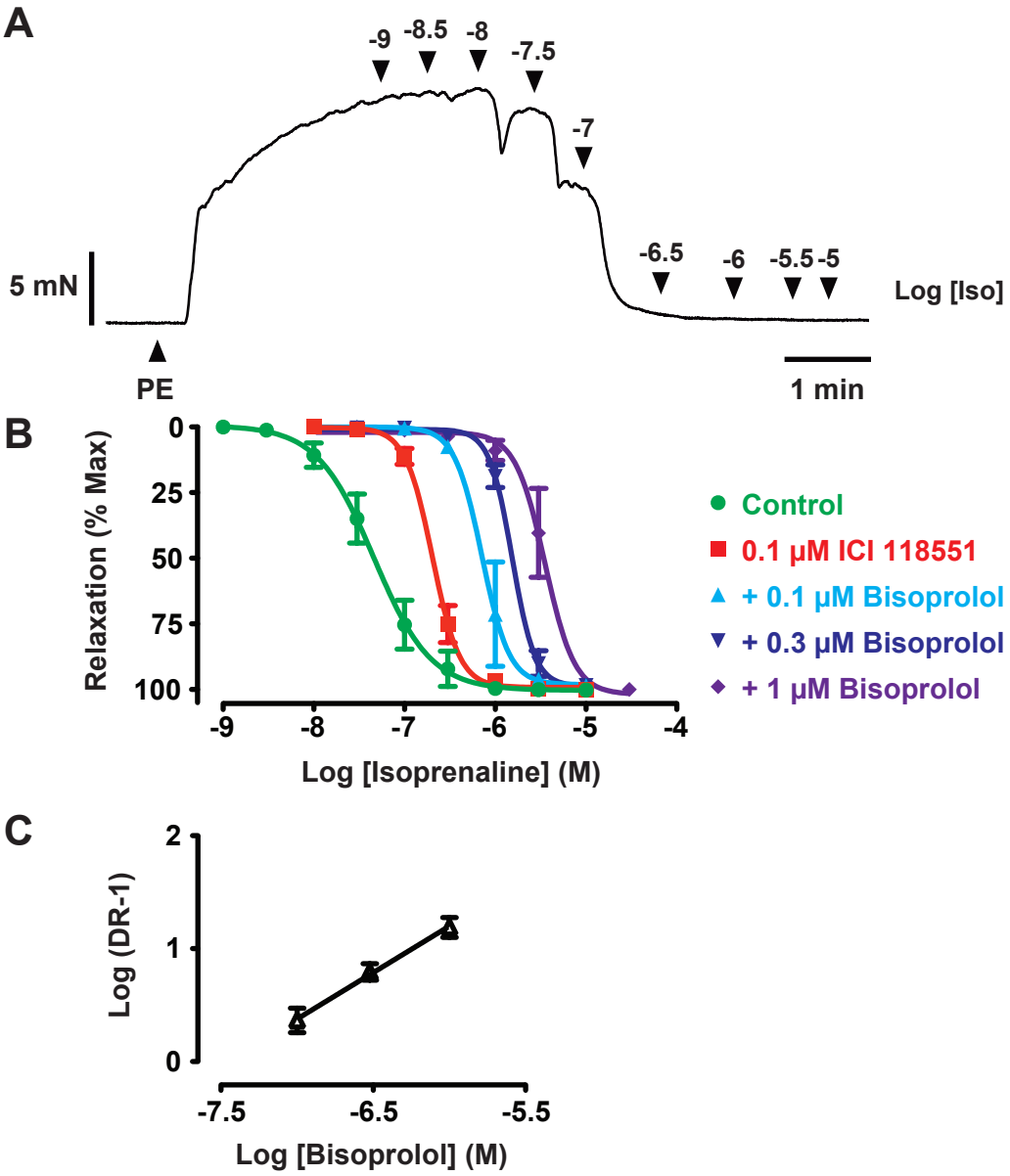

Figure 3.3.3 Characterisation of β-adrenergic relaxation of resistance arteries
A Representative trace showing concentration-dependent relaxation of a rat mesenteric artery pre-contracted with phenylephrine (α_1-adrenoceptor agonist, PE, 1 μM) by stimulation of β-adrenoceptors with isoprenaline (Iso, 1 nM - 10 μM). Log concentration additions of isoprenaline are indicated by arrowheads. L-NAME (100 μM) is present throughout. **B** Summary concentration-response curves showing relaxation by isoprenaline (Control, green circles; in the presence of L-NAME (eNOS inhibitor, 100 μM)), which is right-shifted by ICI-118,551 (red squares, β_2-adrenoceptor-selective inhibitor, 0.1 μM) and further by cumulative concentration-dependent inhibition of β_1-adrenoceptors by bisoprolol (blue / purple triangles / diamonds, β_1-adrenoceptor-selective inhibitor, 0.1-1 μM); n=4-11. $LogEC_{50}$ is calculated for each curve and used to construct the Schild plot in C. **C** Schild plot for bisoprolol antagonism of β-adrenoceptors in the presence of ICI-118,551 (0.1 μM); n=4. pA_2 = 7.5, slope = 0.82 ± 0.1, indicating the predicted competitive antagonism of bisoprolol.

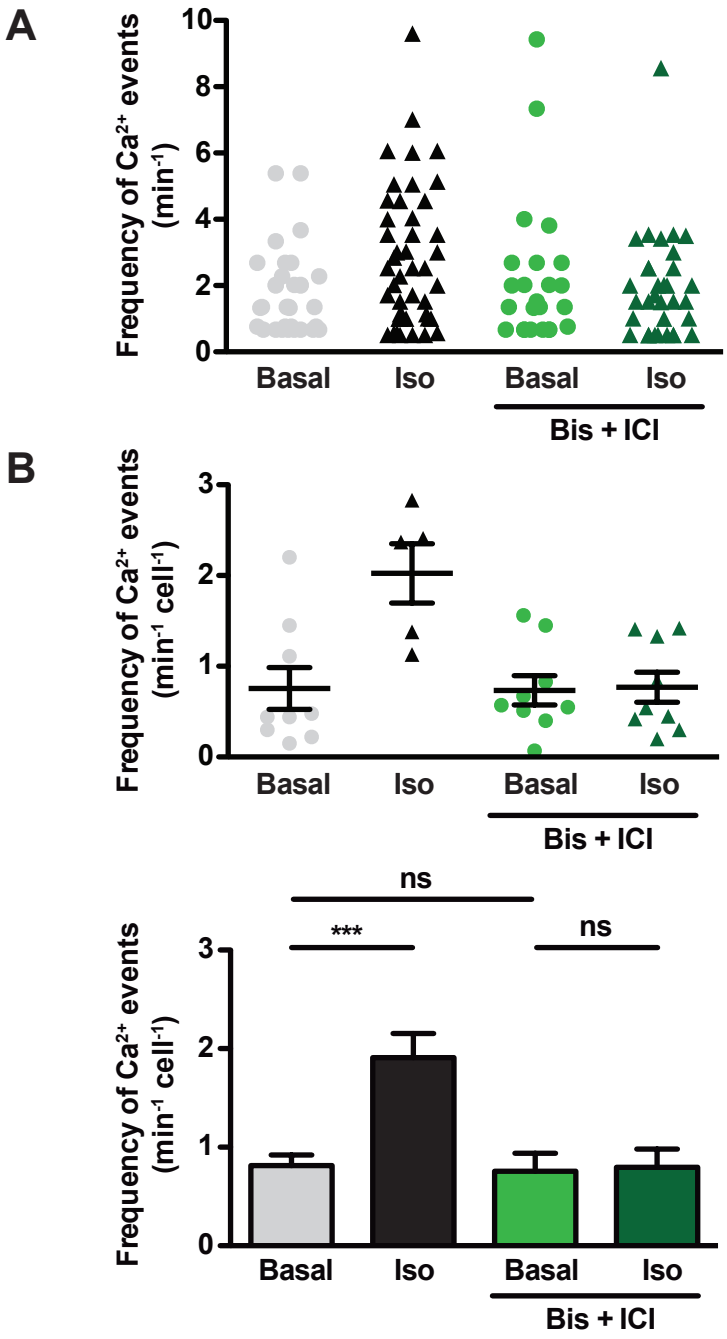

Figure 3.3.4 Increase in endothelial cell Ca^{2+} to β-adrenergic stimulation is receptor-mediated

Summary data showing the frequency of endothelial cell Ca^{2+} events from every cell (**A**) or averaged per artery (**B**) in rat pressurized mesenteric arteries in control conditions basally, and after stimulation of β-adrenoceptors with isoprenaline (Iso, 1 μM). Pre-incubation with bisoprolol (β_1-adrenoceptor-selective, 1 μM, 25 min) and ICI-118,551 (β_2-adrenoceptor-selective, 0.1 μM, 25 min) prevented the increase to isoprenaline (green bars). Data are pooled from two separate series of experiments: 1) Control basal + isoprenaline paired with β-blockers basal + isoprenaline n=5; 2) Control basal paired with β-blockers basal + isoprenaline n=4. Unpaired data, ***P<0.001 by one-way ANOVA with independent Bonferroni post-tests to compare selected data sets as indicated, ns = not significant.

Having established that the endothelial Ca^{2+} response to isoprenaline is receptor-mediated, we investigated the downstream mechanism. We first tested whether the endothelial Ca^{2+} increase was mediated by intracellular release, or extracellular influx of Ca^{2+}. Experiments in nominally Ca^{2+}-free extracellular solution indicated that an influx of Ca^{2+} was required (**Figure 3.3.5**), although this does not exclude a secondary involvement of intracellular Ca^{2+} stores via Ca^{2+}-induced Ca^{2+} release.

As described earlier, one of the major downstream effects of β-adrenoceptor stimulation is opening of K_{ATP} channels residing exclusively in the smooth muscle in rat mesenteric arteries. The characteristic blocker of K_{ATP} channels, glibenclamide (10 μM), seemed to prevent the endothelial Ca^{2+} increase to isoprenaline (**Figure 3.3.6**), supporting an involvement of K_{ATP} channel opening, and potentially of the subsequent hyperpolarization.

To further probe the intracellular pathway involved, we investigated the endothelial cell Ca^{2+} response to forskolin. Forskolin activates adenylyl cyclase to produce cAMP (Seamon *et al.*, 1981) and potentially augment all downstream targets of this second messenger. Forskolin added extraluminally to rat pressurized mesenteric arteries was seen to increase the frequency of endothelial cell Ca^{2+} events, with a profile similar to that of isoprenaline (**Figure 3.3.7**) whereby the Ca^{2+} events were not typically visible with a whole-cell average, but were usually discrete events identifiable with small subcellular regions of interest. This increase was concentration-dependent, with 1 μM forskolin producing a significant augmentation (**Figure 3.3.7B**). The increase to forskolin was also sensitive to inhibition of K_{ATP} channels with glibenclamide (10 μM, **Figure 3.3.8A**), supporting a critical

involvement of K_{ATP} channels in this response. Note that the effect of forskolin is irreversible, and was therefore only applied to the preparation once, hence our data set with glibenclamide treatment does not include a control forskolin response.

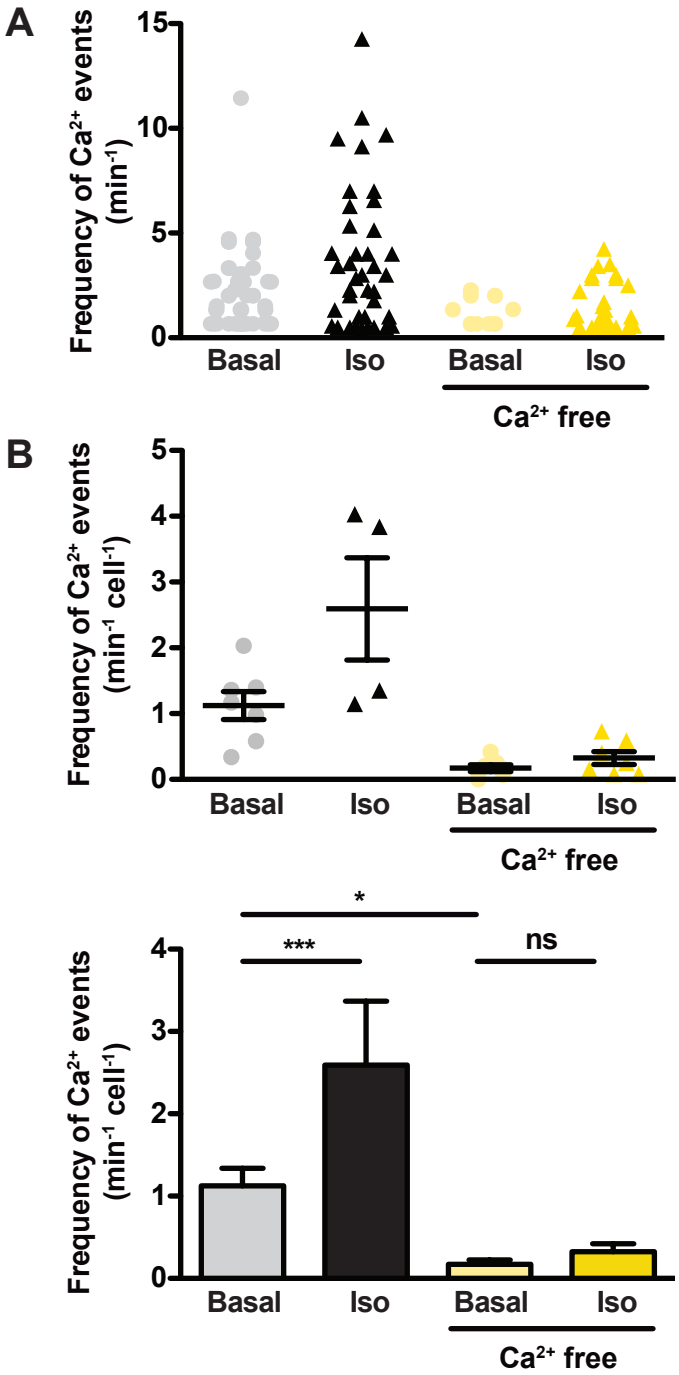

Figure 3.3.5 Increase in endothelial cell Ca^{2+} to β-adrenergic stimulation is dependent on Ca^{2+} entry

Summary data showing the frequency of endothelial cell Ca^{2+} events in every cell (**A**) or averaged per artery (**B**) in rat pressurized mesenteric arteries in control conditions basally, and after stimulation of β-adrenoceptors with isoprenaline (1 μM). This is prevented by removal of extracellular Ca^{2+} (30 min, yellow bars), which also reduces the basal, spontaneous activity. Pooled, unpaired data as in **Figure 3.3.4**, *n*=3-6 ***P<0.0001, *P<0.05 by one-way ANOVA with independent Bonferroni post-tests to compare selected data sets as indicated, ns = not significant.

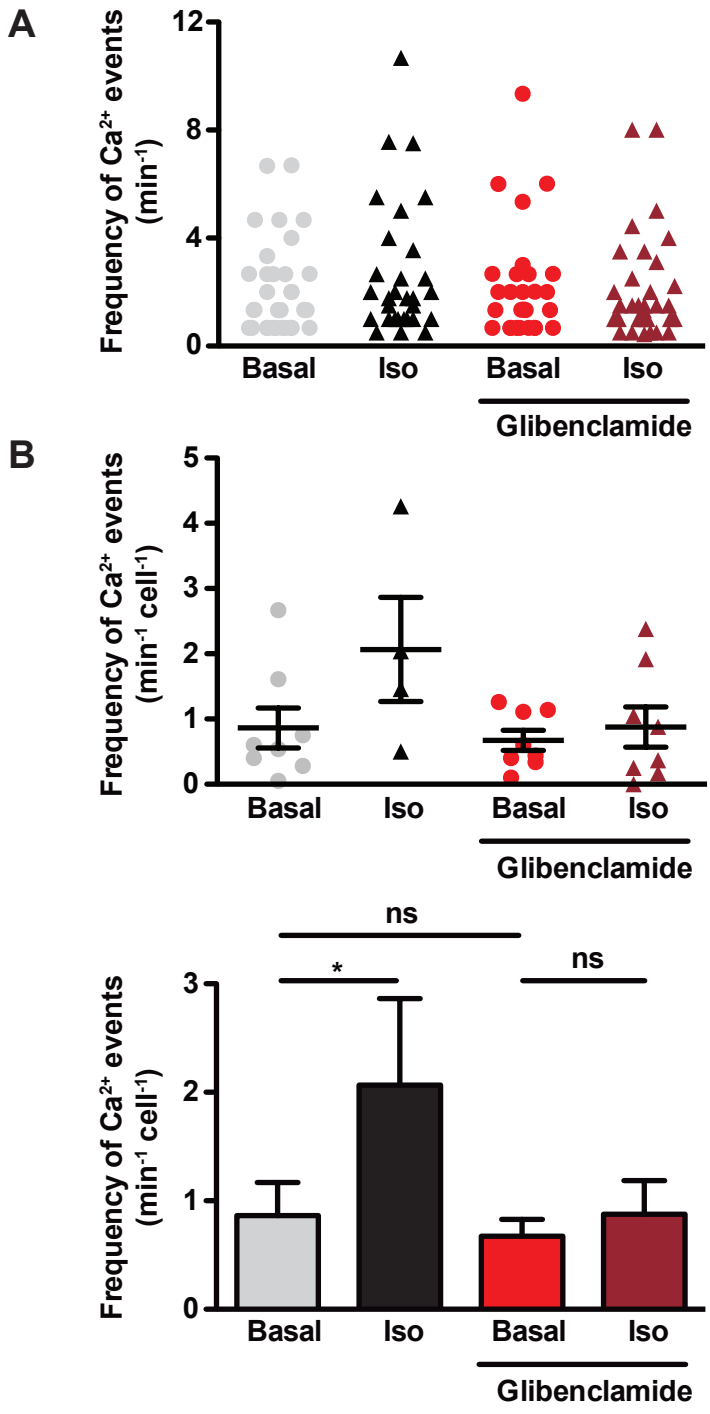

Figure 3.3.6 Increase in endothelial cell Ca^{2+} to β-adrenoceptor stimulation is prevented by inhibition of K_{ATP} channels

Summary data showing the frequency of endothelial cell Ca^{2+} events in rat pressurized mesenteric arteries in control conditions basally, and after stimulation of β-adrenoceptors with isoprenaline (1 μM). This is prevented by inhibition of K_{ATP} channels with glibenclamide (10 μM, 30 min, red bars). Pooled, unpaired data as in **Figure 3.3.4**, n=4-8, *P<0.05 by one-way ANOVA with independent Bonferroni post-tests to compare selected data sets as indicated, ns = not significant.

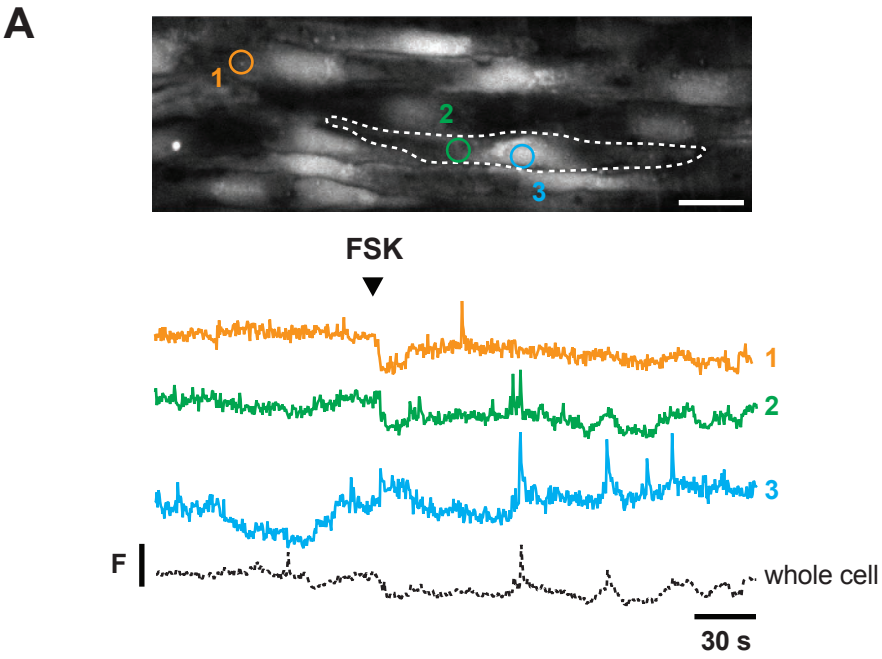
A
1
2
3
FSK
1
2
3
F
whole cell
30 s

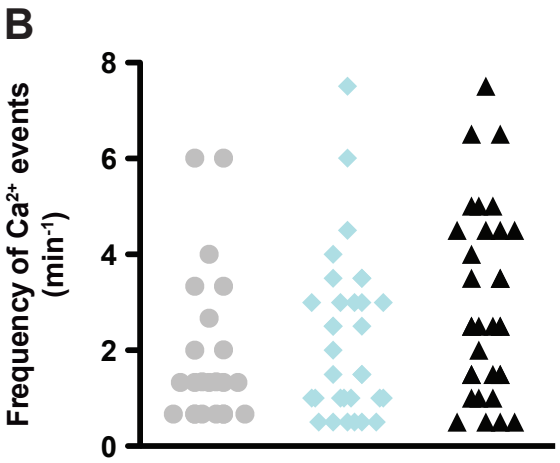
B
Frequency of Ca2+ events (min-1)
8
6
4
2
0

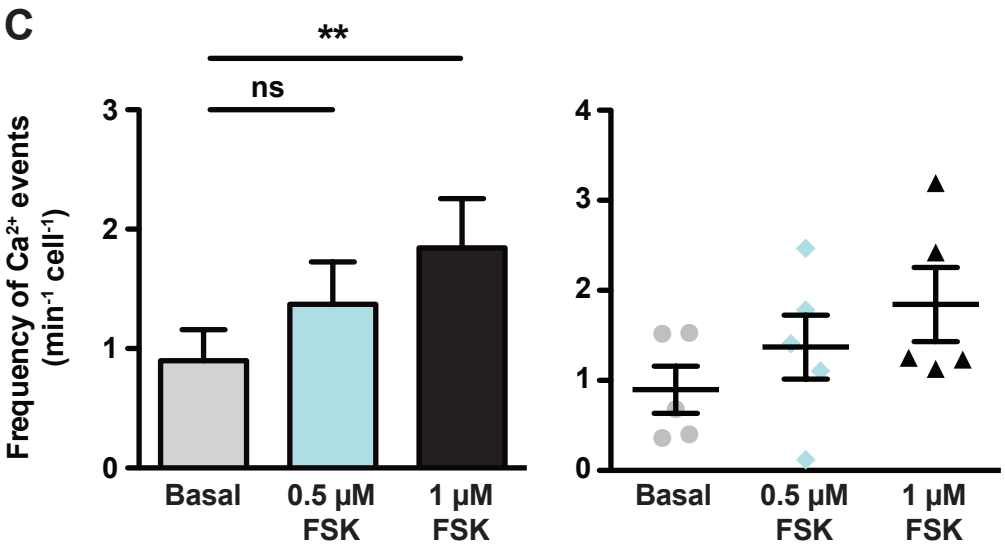
C
**
ns
Frequency of Ca2+ events (min-1 cell-1)
3
2
1
0
Basal
0.5 µM FSK
1 µM FSK
4
3
2
1
0
Basal
0.5 µM FSK
1 µM FSK

Figure 3.3.7 Activation of adenylyl cyclase also increases endothelial cell Ca^{2+} in resistance arteries

A Top Endothelial cells loaded with Ca^{2+}-sensitive dye in a rat pressurized mesenteric artery. Image is average of 100 frames acquired at 3 Hz. Regions of interest (ROIs) correspond with traces below. Scale bar = 50 μm. **Bottom** Raw fluorescence traces corresponding with subcellular ROIs in A, illustrating an increase in the frequency of discrete Ca^{2+} events to forskolin (1 μM). F (fluorescence intensity) = 200 a.u. **B** Summary histogram and dot plot demonstrating the increased frequency of Ca^{2+} events to forskolin (FSK) from all cells in all experiments, or averaged per experiment; note that 1 μM forskolin is necessary for a significant increase. Paired data, n=5, *P<0.05 by repeated measures ANOVA with independent Bonferroni post-tests to compare selected data sets as indicated.

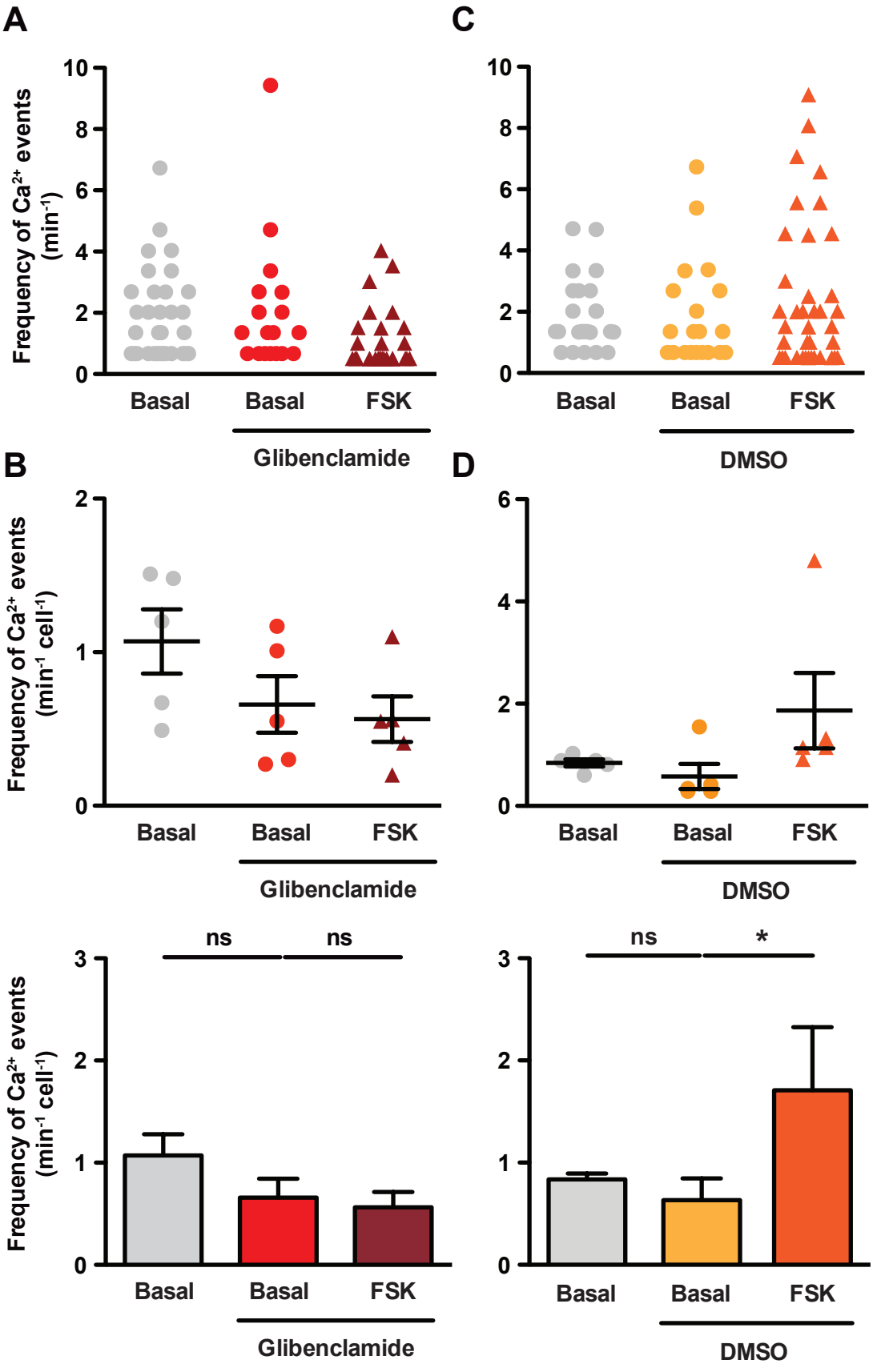
A
C
B
D
Frequency of Ca2+ events (min-1)
Frequency of Ca2+ events (min-1 cell-1)
Basal
Basal
FSK
Glibenclamide
DMSO
ns
ns
*

Figure 3.3.8 Increase in endothelial cell Ca^{2+} to forskolin is prevented by inhibition of K_{ATP} channels

A, **B** Summary histogram and dot plots showing inhibition of K_{ATP} channels with glibenclamide (10 μM, 30 min, red) prevents an increase in endothelial cell Ca^{2+} event frequency to forskolin (FSK, 1 μM); **A** - data from all cells in all experiments; **B** - average data from each experiment. Arteries were not pre-exposed to forskolin in control conditions because previous experiments found the effect of forskolin to be irreversible. **C**, **D** Summary histogram and dot plots demonstrating the increase in endothelial cell Ca^{2+} event frequency to forskolin is maintained in the presence of DMSO (glibenclamide vehicle). Forskolin is dissolved in DMSO, giving a final concentration after FSK addition of 1:500. Paired data, *n*=5 (**A, B**), *n*=6 (**C, D**), *P<0.05 by repeated measures ANOVA with independent Bonferroni post-tests to compare selected data sets as indicated, ns = not significant.

As discussed in the Introduction (**section 3.1.iii**) β-adrenoceptors have been reported to be present on endothelial cells of resistance arteries. Fluorescently-labelled β-adrenoceptor ligands (Baker *et al.*, 2011) have recently become commercially available and we proposed to use them to study the localisation of β-adrenoceptors in rat pressurized mesenteric arteries. In an attempt to validate the specificity of these fluorescent probes we first examined the relaxation response of rat mesenteric arteries mounted in an isometric wire myograph to fluorescent-salbutamol and compared it to non-fluorescent salbutamol (**Figure 3.3.9**). In agreement with our observed role for β_2-adrenoceptors in these arteries, salbutamol (1 μM; logEC_{50} = -6.1 (Baker, 2005)) caused robust relaxation of vessels pre-contracted with PE (1 μM, L-NAME (100 μM) present). Fluorescent-salbutamol also relaxed the arteries at the same concentration, although was slightly less potent (**Figure 3.3.9A**). The arteries exposed to fluorescent-salbutamol were carefully removed from the wire myograph and visualised on a coverslip using confocal microscopy. Focusing on the smooth muscle cell layer indicates clear punctate staining, presumably of β_2-adrenoceptors (**Figure 3.3.9B**). It was not possible to focus reliably on the endothelial cell plane.

To investigate the presence of endothelial cell β-adrenoceptors, we used fluorescent-propranolol (0.1 μM) in a rat pressurized mesenteric artery. Smooth muscle cell staining was clearly evident as expected (**Figure 3.3.10B**), as was staining in the nerves (**Figure 3.3.10A**). Punctate staining was also apparent in the endothelial cell plane (**Figure 3.3.10C**), which could be reliably identified by co-staining of nuclei with Hoechst dye, illustrating the horizontal orientation of the endothelial cells contrasting with the vertical orientation of smooth muscle cells.

Punctate fluorescent labelling in the endothelial cell plane was not uniform, and appeared restricted to certain endothelial cells (filled arrowheads, **Figure 3.3.10C**).

In an attempt to align the apparent sub-population of endothelial cells expressing the β-adrenoceptor with those which show robust Ca^{2+} responses to isoprenaline, the same artery was exposed to fluorescent propranolol after recording the Ca^{2+} response to isoprenaline (**Figure 3.3.11**). In this instance, the fluorescent propranolol staining appeared less punctate, although was brighter in some of the endothelial cells which responded to isoprenaline.

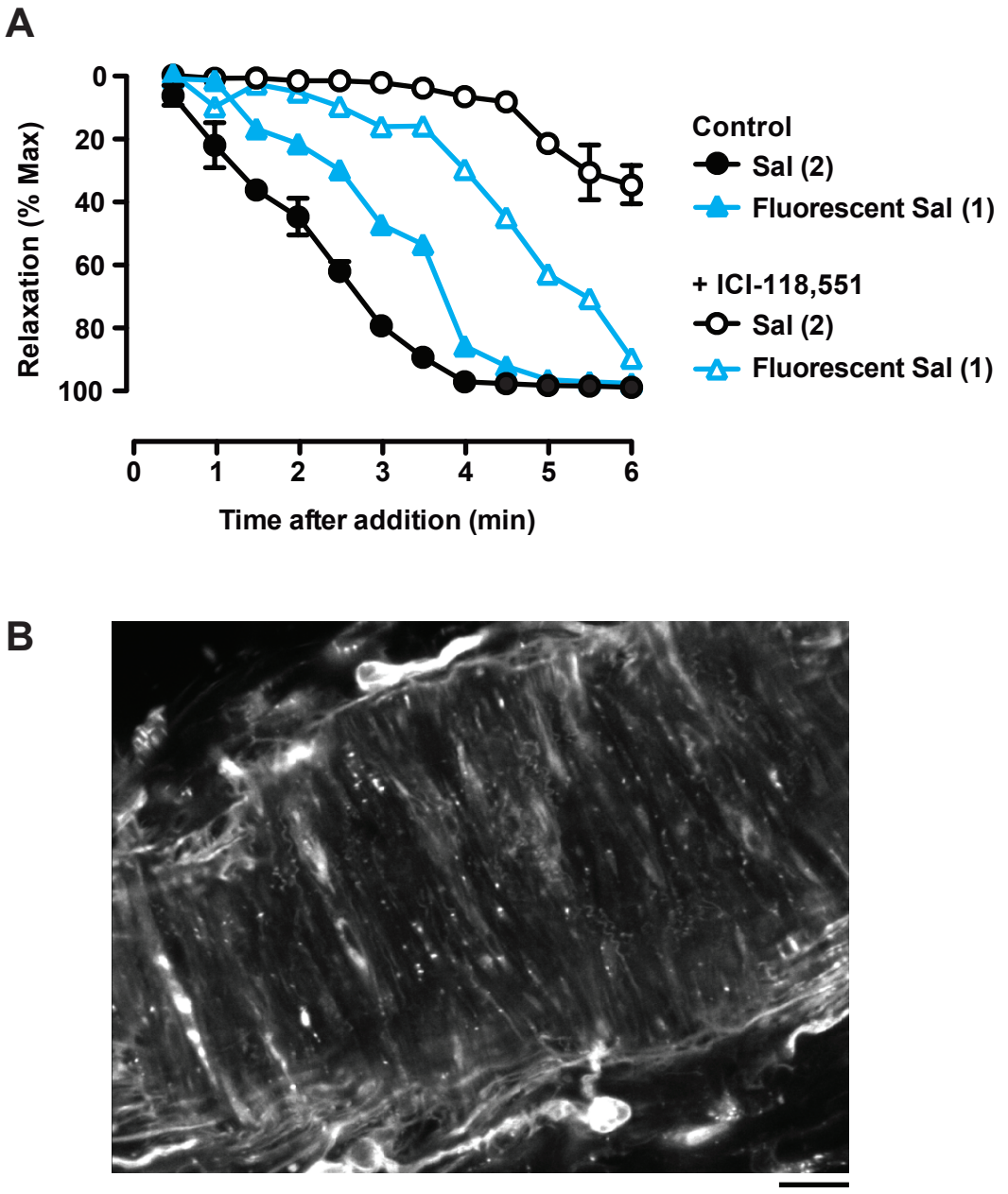

Figure 3.3.9 Fluorescent salbutamol labels smooth muscle cells and relaxes arteries with tone

A Comparison of the relaxation of rat third order mesenteric arteries to salbutamol (1 μM, black circles, *n*=2) with fluorescent salbutamol (1 μM, blue triangles, *n*=1). ICI-118,551 (β_2-adrenoceptor-selective antagonist, 0.1 μM, 20 min) prevented the relaxation to salbutamol (open black circle, *n*=2) but only delayed the relaxation to fluorescent salbutamol (open blue triangle, *n*=1). L-NAME (100 μM) was present throughout. **B** Artery exposed to fluorescent salbutamol appeared to label smooth muscle cells when visualised using confocal microscopy. Scale bar = 15 μm.

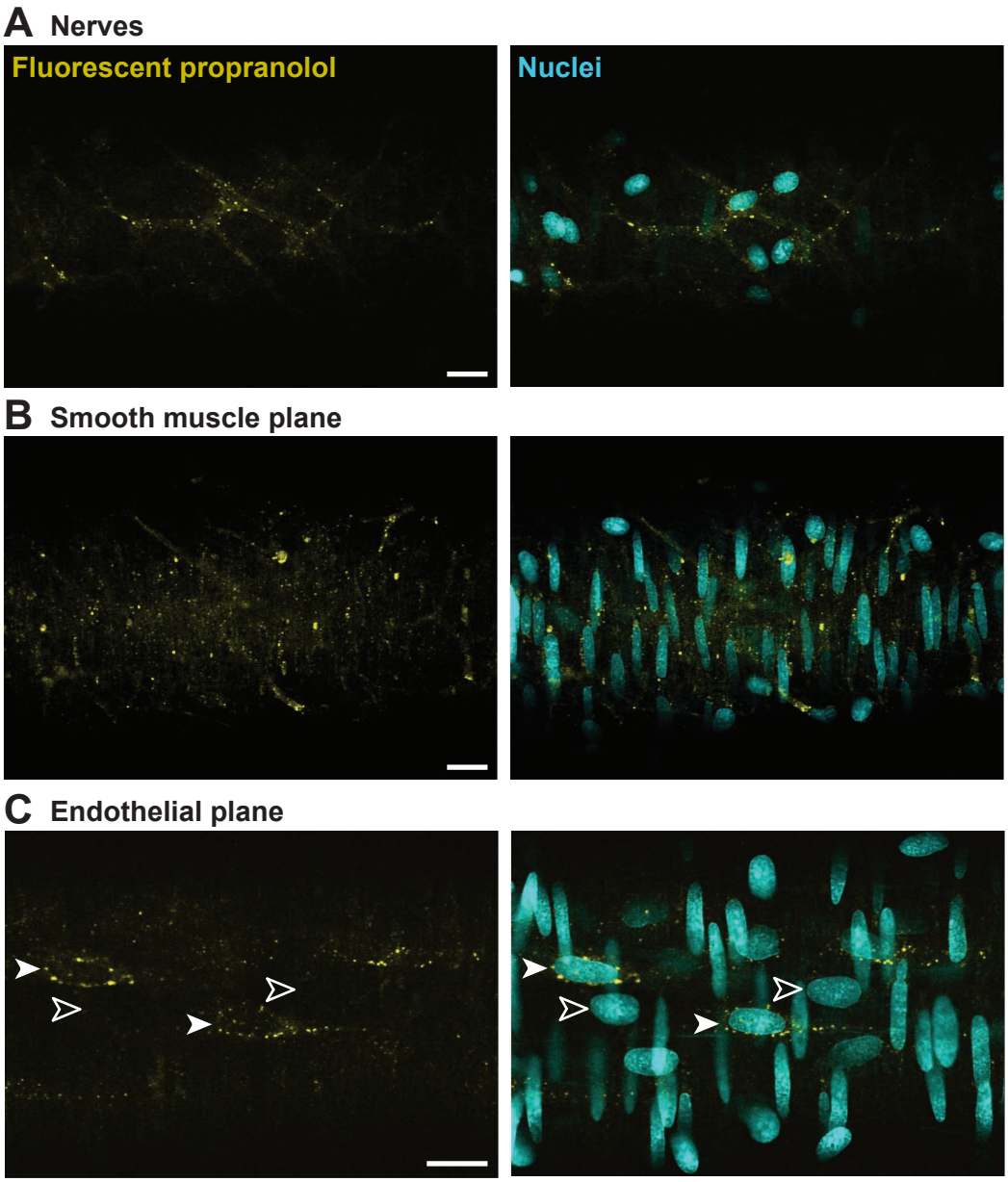

Figure 3.3.10 Fluorescent propranolol staining in rat mesenteric arteries
Fluorescent propranolol (0.1 μM, yellow, left column) stained the nerves (**A**) and smooth muscle cells (**B**) of a rat pressurized third order mesenteric artery. Staining was also clearly visible around a sub-population of endothelial cells (**C**, filled arrowheads). The endothelial cell plane was identified by the horizontal orientation of nuclei labelled with Hoechst dye (16.2 μM, cyan; **C, right**) contrasting with the vertical orientation of smooth muscle nuclei (**B, right**) Endothelial cells lacking fluorescent propranolol labelling are marked with unfilled arrowheads. Scale bars = 50 μm. Representative of n=2.

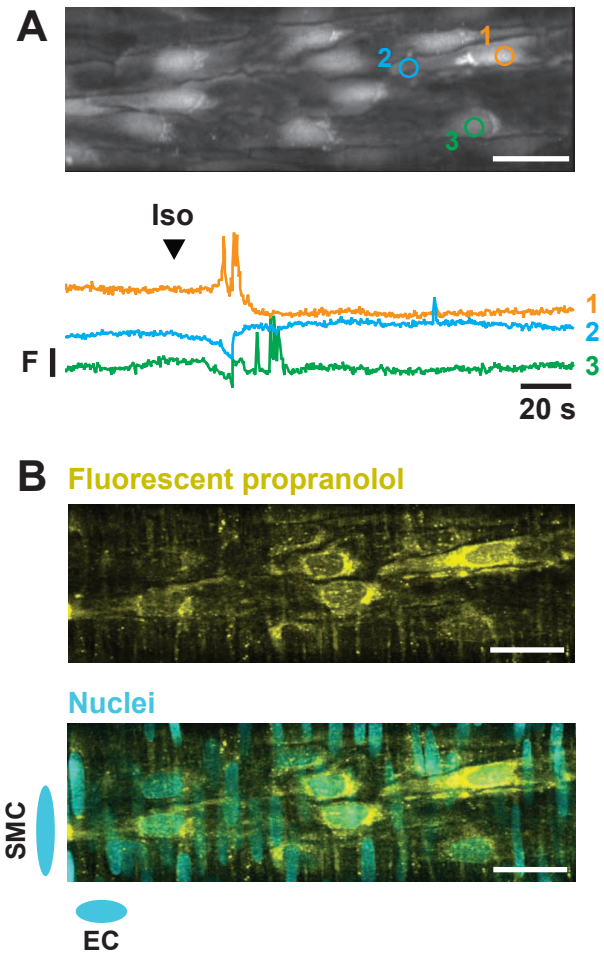

Figure 3.3.11 Fluorescent propranolol staining combined with Ca^{2+} imaging
A Top Endothelial cells loaded with OGB-1. Image is an average of 100 planes acquired at 3 Hz. Regions of interest correspond with the raw fluorescence traces (**bottom**). **B** Same endothelial cells after labelling with fluorescent propranolol (0.1 μM, yellow). Nuclei are labelled with Hoechst dye (16 μM, cyan). Some endothelial cells that respond most robustly to isoprenaline (1 μM, arrowhead) appear to have brighter labelling with fluorescent propranolol (Cell 1) whilst others do not (Cell 3). F (fluorescence intensity) = 200 a.u. Scale bars = 30 μm. Representative of n=2.

Since β-adrenoceptors appear to be present on endothelial cells in intact arteries, we investigated whether isoprenaline could elicit a Ca^{2+} response in freshly isolated endothelial cell sheets loaded with the Ca^{2+}-sensitive dye fluo-4 AM (10 μM; **Figure 3.3.12B**). These sheets consisted of ~20 endothelial cells and were identified by their intact connection with other cells and rounded morphology (**Figure 3.3.12A**). Isolated smooth muscle cells are typically long, spindle-shaped individual cells (see **Figure 5.2.2B** for comparison). In 9 out of 35 experiments, isoprenaline (3 μM) caused an increase in Ca^{2+} in some of the endothelial cells in the sheet (**Table 3.3.2**). The Ca^{2+} event was cell-wide and visible when fluorescence in the whole cell was averaged (**Figure 3.3.12B**). ACh was employed as a positive control for isolated endothelial cell viability, although in 4 EC sheets out of the 9 responding to isoprenaline, ACh (1 μM) did not appear to increase Ca^{2+}. The responses to ACh and isoprenaline are summarised for all experiments (**Table 3.3.2**).

Isoprenaline	ACh	*n*
✓	✓	2
✓	✗	4
✓	*not tested*	3
✗	✓	19
✗	✗	7

Table 3.3.2 Summary of all attempts to study Ca^{2+} responses in freshly isolated EC sheets
The responses of all EC sheets loaded with fluo-4 AM (10 μM) and challenged with isoprenaline (3 μM) or acetylcholine (ACh, 1 μM) are summarised.

In separate experiments using whole-cell patch-clamp in current-clamp mode we measured the resting membrane potential (Em) of EC sheets isolated using the same digestion protocol as used for the sheets in Ca^{2+} imaging experiments. Consistent with previous reports (Yarova *et al*., 2013), the membrane potential was depolarized compared to the usual resting membrane potential of these arteries (-11.35 ± 2.0 mV, *n*=7; **Figure 3.3.12C**).

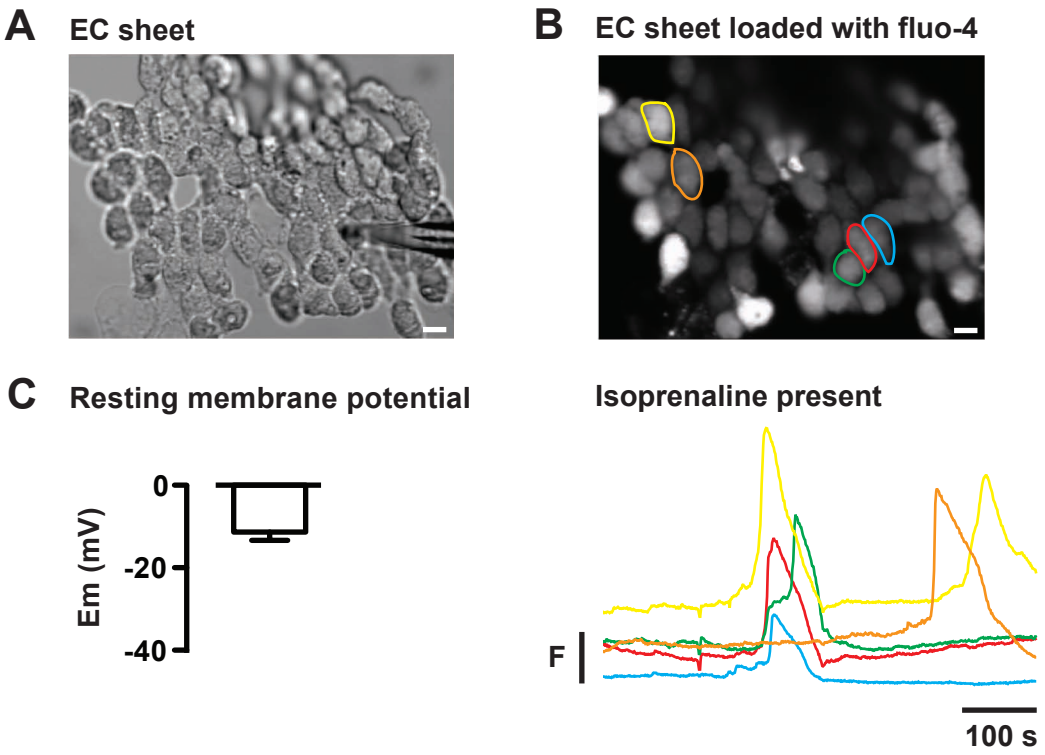

Figure 3.3.12 Isoprenaline can increase Ca^{2+} in EC sheets, which have a depolarized membrane potential

A Image of a representative EC sheet freshly isolated from rat third order mesenteric arteries. **B Top** Same EC sheet loaded with fluo-4 AM (10 μM). Scale bars = 50 μm. **Bottom** Raw fluorescence traces corresponding to regions of interest around whole endothelial cells above. Isoprenaline (3 μM, present throughout) produced cell-wide Ca^{2+} events in some endothelial cells. F (fluorescence intensity) = 500 a.u. Representative of *n*=9. **C** EC sheet membrane potential (RMP) measured using whole-cell patch-clamp in current-clamp mode. For mean ± SEM see text. *n*=7.

3.4 Discussion and Future Work

Data in this chapter indicate 1) that opening of K_{ATP} channels directly (with levcromakalim) or indirectly (by isoprenaline) results in an increase in endothelial cell Ca^{2+} events, which may reflect hyperpolarization-driven Ca^{2+} influx via an undetermined channel; 2) that β-adrenoceptors are present on endothelial cells and may be functionally relevant in this response, which appears to reflect heterogeneity in endothelial cell β-adrenoceptor expression.

3.4.i β-Adrenergic stimulation increases endothelial cell Ca^{2+} in intact arteries

Levcromakalim, a direct K_{ATP} channel opener, caused an increase in endothelial cell Ca^{2+} events in rat intact, pressurized cremaster arterioles (**Figure 3.3.1**). This led to the hypothesis that β-adrenergic stimulation, which opens K_{ATP} channels, might induce the same response. Isoprenaline did produce an increase in the frequency of Ca^{2+} events in rat intact, pressurized mesenteric arteries in a manner very similar to that of levcromakalim. Under both stimuli the nature of the Ca^{2+} events was similar, each producing an increase in discrete, spatially restricted Ca^{2+} events reliably identified only by small, subcellular ROIs rather than whole-cell averages. There also appeared to be heterogeneity in the responses whereby not all endothelial cells showed a robust increase in events. This suggested a mechanism common to both levcromakalim and isoprenaline.

The response to isoprenaline was sensitive to combined β_1- and β_2-adrenoceptor inhibitors (**Figure 3.3.4**), indicating that this was a receptor-mediated effect. It also appeared to be prevented by glibenclamide (K_{ATP} channel blocker, **Figure 3.3.5**)

consistent with a requirement for opening of K_{ATP} channels. Although the average graph data demonstrate a full inhibition by glibenclamide (**Figure 3.3.6B**), the graph portraying frequencies from all the endothelial cells (**Figure 3.3.6A**) suggests some cells *may* still respond to isoprenaline. An effect of isoprenaline was fully prevented by removal of extracellular Ca^{2+} (**Figure 3.3.5**), implicating Ca^{2+} entry as a probable component of the increased frequency of endothelial cell events. It should be noted that upon removal of extracellular Ca^{2+}, the basal Ca^{2+} activity was reduced (**Figure 3.3.5**). In cremaster arterioles, basal activity is reportedly unaffected by removal of extracellular Ca^{2+}; rather it appears reliant entirely on IP_3-mediated spontaneous intracellular release (Bagher *et al.*, 2012). In rat mesenteric arteries however, the reliance on extracellular Ca^{2+} observed in the present study has been previously reported (Kansui *et al.*, 2008) suggesting differing mechanisms determining basal, spontaneous Ca^{2+} activity in the two vascular beds.

In the response to isoprenaline (and levcromakalim), local Ca^{2+} events occasionally propagated and were observed as waves. This may reflect amplification due to Ca^{2+} released from intracellular stores, although this was not directly investigated. The response to isoprenaline was generally positively correlated with the level of basal activity (**Figure 3.3.2B right**), which further supports this notion. Regardless, influx of extracellular Ca^{2+} does appear to be required; whether secondary intracellular release occurs remains unknown. Additional experiments investigating the influence of block of IP_3 release (e.g. with xestospongin C) or emptying of endoplasmic reticulum Ca^{2+} stores (e.g. with thapsigargin or cyclopiazonic acid (CPA)) on the response to isoprenaline (and levcromakalim) might be informative in this regard. However, interpretation of the resulting data may be confounded by the increased

cytosolic [Ca^{2+}] as a consequence of SERCA inhibition. Elevated basal endothelial cell Ca^{2+} by CPA has been shown to activate SK_{Ca} channels (Crane *et al.*, 2003), and would be likely also to affect other Ca^{2+}-sensitive proteins in the endothelium.

Activation of adenylyl cyclase with forskolin appeared to mimic the response to isoprenaline, suggesting the mechanism is downstream of activation of adenylyl cyclase and presumably cAMP production. Since cAMP will activate PKA to phosphorylate K_{ATP} channels in smooth muscle cells it would be informative to use an inhibitor of PKA (e.g. with KT 5720 or Rp-cAMPs) to provide further support to this pathway.

All together the evidence from intact arteries supports an important role for opening of K_{ATP} channels and potentially the consequent hyperpolarization of the membrane potential.

3.4.ii Endothelial cells express β-adrenoceptors

As discussed in the Introduction (**section 3.1.iii**) there is evidence for endothelial cell expression of β-adrenoceptors (Briones *et al.*, 2005) and for functional effects of β-adrenoceptor stimulation in the endothelium (Yarova *et al.*, 2013). In this study we observed labelling of fluorescent salbutamol in the smooth muscle of intact arteries, and of fluorescent propranolol in pressurized arteries in the nerves, smooth muscle and the endothelium. The pattern of endothelial cell expression appeared to be heterogeneous, with a subpopulation of cells labelling with punctate staining of fluorescent propranolol (**Figure 3.3.10**).

Given this apparent heterogeneity in expression, and that only a sub-population of endothelial cells appeared to respond to β-adrenoceptor stimulation, we hypothesized that endothelial β-adrenoceptors might have a role in the response. We therefore attempted to align endothelial cells responding to isoprenaline with subsequent labelling with fluorescent propranolol. In this case the fluorescent propranolol did not have a punctate pattern, but instead was more uniform within the cell (**Figure 3.3.11**). There are two major differences compared with the experiments shown in **Figure 3.3.10**: first, the endothelial cells were loaded with OGB-1; second, they were pre-exposed to isoprenaline. The uniform staining within the cells may reflect internalisation of β-adrenoceptors following exposure to isoprenaline. However, fluorescent propranolol was added only after sufficient washout of isoprenaline (30 min at 2 mL min^{-1}), so if internalisation had occurred, we would expect the receptors to have been replaced at the membrane. This may have occurred, but was indistinguishable against the additional fluorescence of internalised receptors. It may also be possible that OGB-1 interacts somehow with the fluorescent propranolol and this may have altered the staining pattern. Indeed, staining in the smooth muscle planes (visible as vertical labelling at the top and bottom of the image in **Figure 3.3.11**) had remained punctate, even though receptors in these cells will also have been stimulated by isoprenaline, supporting the theory that OGB-1 confined to the endothelium could interact with the fluorescent propranolol. We were therefore unable successfully to compare endothelial cells expressing the β-adrenoceptors with those cells responding most to isoprenaline. Reliable primary antibodies for β-adrenoceptors are not commercially available, therefore we were also unable to utilise immunohistochemistry to probe the endothelial expression of subtypes of β-adrenoceptors. In an attempt to address

whether endothelial β-adrenoceptors have a functional role in the endothelial Ca^{2+} response to isoprenaline, we examined the Ca^{2+} responses in freshly isolated EC sheets.

3.4.iii β-Adrenergic stimulation can increase Ca^{2+} in freshly isolated EC sheets

In EC sheets isolated from rat third order mesenteric arteries as used in pressurized studies, isoprenaline caused a visible increase in endothelial cell Ca^{2+} (**Figure 3.3.12B** and **Table 3.3.2**); however, this was inconsistent and did not occur in every EC sheet challenged. On the one hand this suggests that isoprenaline acting directly on endothelial cells can cause a Ca^{2+} increase, independently of smooth muscle cells; on the other hand, the inconsistency might support the heterogeneity of Ca^{2+} response and β-adrenoceptor expression observed in intact arteries. The EC sheets also did not respond reliably to ACh. Muscarinic receptors are lost during culture of endothelial cells (Tracey & Peach, 1992) but previous work in our lab and others has shown freshly isolated EC sheets can respond reliably to ACh (McSherry *et al.*, 2005).

The Ca^{2+} responses observed in the EC sheets were very different from those observed in intact arteries. Any recordable responses were cell-wide Ca^{2+} elevations covering the entire cell, and were relatively slow (**Figure 3.3.12**), unlike the rapid, focal events observed in pressurized arteries. Spontaneous Ca^{2+} events were also rarely observed. There are various possible causes of this differing profile: the rounded, unstretched morphology of the endothelial cells in the isolated sheet (compared to the relatively flat, elongated cells in intact preparations) might mask

the subcellular Ca^{2+} events; alternatively the different morphology may physically disrupt and alter the arrangement of intracellular Ca^{2+} stores, affecting Ca^{2+} handling. The profile of Ca^{2+} events in isolated sheets we observed is consistent with a previous report from our group (McSherry *et al.*, 2005). There may also be an influence of the relatively depolarized resting membrane potential. In the non-myogenically active rat intact mesenteric artery, open K^+ channels in the smooth muscle markedly influence the resting membrane potential which is usually ~-55 mV both in intact arteries (White & Hiley, 2000; Garland *et al.*, 2011b) and isolated smooth muscle cells (Roberts *et al.*, 2013). The myoendothelial gap junctions allow the endothelial and smooth muscle cells to become isopotential. The strong influence from smooth muscle cells is evident from our measurements of endothelial cell membrane potential in EC sheets isolated using the same protocol (-11.0 ± 0.5 mV, *n*=7, **Figure 3.3.12C**). This is consistent with previously reported membrane potentials of EC sheets (e.g. -16.7 ± 2.4 mV, *n*=3) also from rat mesenteric arteries ((McSherry *et al.*, 2005) and (Yarova *et al.*, 2013)). Although the membrane potential was not measured in the Ca^{2+} imaging experiments, it seems reasonable to assume it would also be in a similar range. It would be feasible in future experiments to increase the resting membrane potential closer to that of an intact artery either through current injection (McSherry *et al.*, 2005) or opening of K_{Ca} channels with NS309 (Strøbæk *et al.*, 2004); the latter was achieved in preliminary patch-clamp experiments (**Figure 3.4.1**).

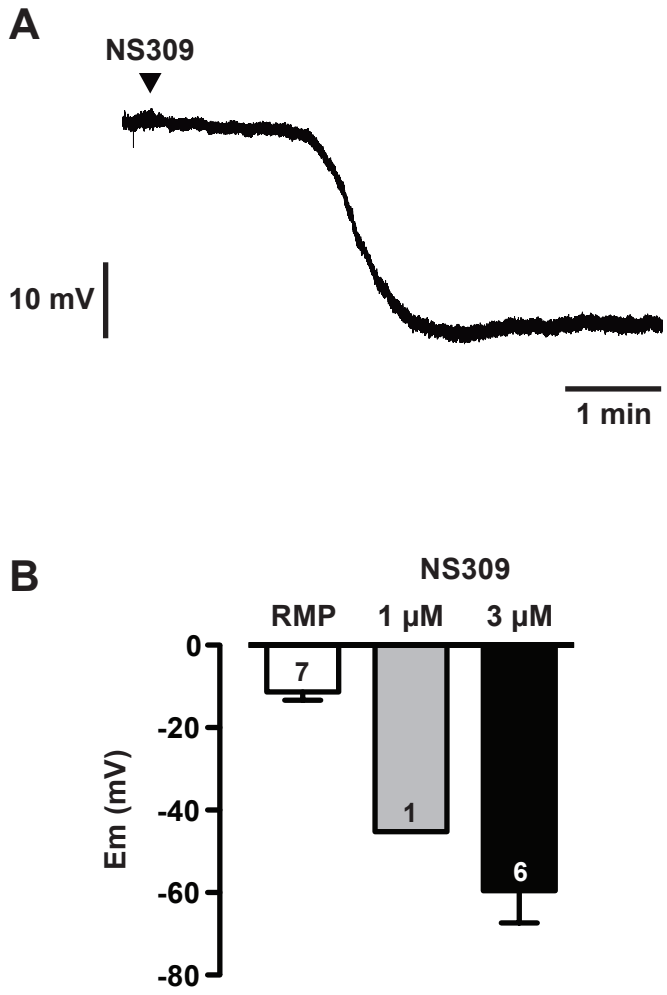

Figure 3.4.1 EC sheets can be hyperpolarized by NS309
A Representative trace of the hyperpolarization of the resting membrane potential of freshly isolated EC sheet to NS309 (3 μM). **B** Hyperpolarization of membrane potential by NS309 (1 μM, n=1; or 3 μM, n=6) in the same EC sheets.

To investigate the possible endothelial β-adrenoceptor response, but circumvent some of the aforementioned potential confounding issues of isolated EC sheets, it would be of interest to assess the response of isolated EC tubes (Cohen & Jackson, 2005; Socha *et al.*, 2011) to isoprenaline. These preparations are stretched by pinning pipettes which may result in the Ca^{2+} handling and responses being more akin to those in intact arteries. The morphology may also aid visualisation of subcellular Ca^{2+} events. EC tubes isolated from rat mesenteric arteries have not previously been reported, although preliminary attempts made in the laboratory have shown it is feasible.

It would also be interesting to further pharmacologically probe the importance of the β-adrenoceptor subtypes both in terms of mediating the endothelial Ca^{2+} response to isoprenaline, and whether both or only β_1- or β_2-adrenoceptors are expressed on endothelial cells.

3.5 Conclusion

Data in this chapter demonstrate that stimulation of β-adrenoceptors in small resistance arteries can cause an increase in endothelial Ca^{2+} events that reflects Ca^{2+} influx; furthermore, this is mimicked by direct opening of K_{ATP} channels with levcromakalim, and is likely to be caused by spread of hyperpolarization between smooth muscle and endothelial cells.

A dominant involvement of smooth muscle cells is likely to be due to the restricted localisation of K_{ATP} channels on this cell type; however, experiments in isolated EC sheets suggest that isoprenaline can also evoke a Ca^{2+} response in the endothelium. This is presumably via endothelial β-adrenoceptors, which were visible with a fluorescent β-adrenoceptor ligand.

The channel mediating Ca^{2+} influx to hyperpolarization is investigated in the following chapter.

CHAPTER 4

CHARACTERISING THE PATHWAY FOR HYPERPOLARIZATION-DRIVEN CA^{2+} INFLUX

4.1 Introduction

The simplest explanation for the observations described in Chapter 3 is the presence of a hyperpolarization-activated Ca^{2+} influx channel in the endothelium. As reviewed already in the preceding chapter (**section 3.1.iv**), the possibility of hyperpolarization-driven Ca^{2+} influx in the endothelium is a pre-existing notion, due to the increased driving force for Ca^{2+} entry at high membrane potentials, but surprisingly the identity of the leak channel has never been established. One possibility is the classic example of hyperpolarization-activated channels, the hyperpolarization-activated, cyclic nucleotide-gated (HCN) channels, which have recently been demonstrated to conduct Ca^{2+}.

4.1.i Hyperpolarization-activated, cyclic nucleotide-regulated (HCN) channels

From the superfamily of voltage-gated cation channels, HCN channels are responsible for the control of heart rate and constitute the 'funny' I_f current in the sino-atrial (SA) node. They also have an important role in neuronal excitability. They conduct a mixed Na^+, K^+ (and potentially Ca^{2+}, discussed below) depolarizing cation current with a permeability ratio of 1:4 Na^+:K^+. In the SA node the majority of the current is carried by Na^+ since the resting membrane potential is ~-70 mV, close to the reversal potential for K^+ (E_k). There are four subtypes HCN1-4, each with different characteristics (**Table 4.1.1**) and expression. Subtypes share the same general structure with ~60% sequence homology (Biel *et al.*, 2009). Since the structure of HCN channels was determined, HCN channelopathies have also been investigated, identifying at least four mutations in human *HCN4* gene causing

bradycardic and arrhythmic heart conditions (Nof *et al.*, 2007; Baruscotti *et al.*, 2010).

4.1.ii Structure of HCN channels

HCN channels share their structure with close relatives, the cyclic nucleotide-gated (CNG) channels. The structure of the CNG channel was solved first, cloned from bovine retinal rod cells (Cook *et al.*, 1987). From this the molecular structure and function were realised. They form tetramers, which can be homomeric or heteromeric, offering multiple configurations. Each subunit comprises six transmembrane α-helix subunits, with the ion-selective loop domain in the pore region between S5 and S6 (**Figure 4.1.1**). The S4 helix contains between three and nine positively-charged arginine or lysine residues every three amino acids. This voltage-sensing domain is common to all voltage-sensitive channels. In HCN channels, movement of this domain opens the channel; in depolarization-gated channels such as K_v channels, the inward movement of S4 charges closes the channel. In CNG channels, the importance of this region is currently unsolved (Biel, 2009).

HCN channel activity is regulated by cyclic nucleotides such that binding will facilitate opening of the channel by right-shifting the voltage dependence for activation (Wainger *et al.*, 2001). They can bind both cAMP and cGMP, although HCN channels have a greater affinity for cAMP. Cyclic nucleotides bind in the cyclic nucleotide-binding domain (CNBD) situated in the C terminus, attached to the sixth transmembrane α-helix (S6) via the 80 amino acid C-linker peptide (**Figure 4.1.1**). The CNBD-C-linker autoinhibits the channel: binding of cAMP releases the

autoinhibition, facilitating the voltage-dependent opening of the channel. The crystal structure for the CNBD has been solved for HCN2, which identified an eight-stranded antiparallel β-roll between two α-helices. The cyclic nucleotide binds to a cleft in the β-roll (Zagotta *et al.*, 2003). HCN channel subtypes have different sensitivities for cyclic nucleotides, summarized in **Table 4.1.1**, which is determined by the amino acids present in the CNBD. For example, the high sensitivity for cAMP of HCN2 channels is due to amino acid residues, R632, R635, I636 and K638 (Wahl-Schott & Biel, 2009).

HCN channels may also be regulated by additional factors, the most extensively researched being phosphatidylinositol-4,5-bisphosphate ($PI(4,5)P_2$). Increase in $PI(4,5)P_2$ levels by agonists coupled to phospholipase C shifted the activation of HCN channels to more positive voltages in HCN1- and HCN2-transfected *Xenopus* oocytes, or in native SA node cells (Pian *et al.*, 2007). The potential shift by $PI(4,5)P_2$ is ~20 mV independent of the shift by cyclic nucleotides (Wahl-Schott & Biel, 2009).

Subtype	Sensitivity to cyclic nucleotides	Activation kinetics
HCN1	Low	Fast
HCN2	High (+10-25 mV)	Intermediate
HCN3	None	Slow
HCN4	High (+10-25 mV)	Slow

Table 4.1.1 Summary of the characteristics of HCN channel subtypes
Summary of the different sensitivities to cyclic nucleotides and the activation kinetics of each of the four HCN channel subtypes.

4.1.iii HCN channel conductance

HCN channels have recently been shown to conduct Ca^{2+} in addition to Na^{+} and K^{+}. This was first proposed in 2004 in dorsal root ganglion neurons (Yu *et al.*, 2004) and later in rat ventricular myocytes (Yu *et al.*, 2007) using a combination of whole-cell patch-clamp of HEK293 cells expressing HCN4, or native HCN currents, with fluorescence imaging of Ca^{2+} transients using fura-2. A hyperpolarization-induced Ca^{2+} current was inhibited by Cs^{+} (2 mM) or ZD7288 (30 μM), blockers of HCN channels. Most recently a single-channel patch-clamp study using HCN2 expressed in CHO-K1 cells, or native HCN channels in rat or human myocytes, aimed to directly demonstrate and characterise the Ca^{2+} conductance (Michels *et al.*, 2008). They clearly showed a Ca^{2+} conductance of ~9 pS at 2 mM extracellular [Ca^{2+}] in the absence of any other ions, which was augmented by cAMP (10 μM) and inhibited by ivabradine (HCN channel blocker, 10 μM). HCN could also conduct Ca^{2+} in the presence of Na^{+} (128 mM) and K^{+} (4 mM), where the single-channel conductance with 2 mM Ca^{2+} was 10.9 ± 0.59 pS.

Only HCN2 and HCN4 have been specifically studied with respect to Ca^{2+} conductance, although it is likely that all HCN channel subtypes would behave analogously due to the structural similarities in the pore-forming region. Interestingly, HCN2 and HCN4 are also the subtypes most affected by cAMP. One might speculate that there could be a relationship between Ca^{2+} conductance and cAMP sensitivity, and a functional relevance of this link.

4.1.iv HCN channel pharmacology

The two most commonly used blockers of HCN channels are ZD7288 (Marshall *et al.*, 1993) and ivabradine (known as S 16257 during development; (Thollon *et al.*, 1994)), both of which are non-selective for HCN channel subtype. Additional 'bradines' also exist, and are derived from verapamil. HCN channels can also be inhibited by Cs^+.

Ivabradine is currently the only HCN channel blocker in clinical use and is prescribed for the treatment of angina and heart failure. Two clinical trials tested its heart-rate reducing benefit in the outcome of patients with coronary artery disease (BEAUTIFUL trial, (Fox *et al.*, 2008)), or chronic heart failure (SHIFT study, (Swedberg *et al.*, 2010)). Ivabradine (and similar molecules, e.g. zatebradine) binds the channel from the intracellular side after crossing the plasma membrane. The amino acid residues within the channel pore responsible for binding ivabradine have recently been identified in HCN4 channels through systematic mutation as Y506, F509 and I510, which were shown to line a cavity where ivabradine binds below the channel pore. Furthermore, in the open state the smallest diameter of the cavity is 11 Å, whereas during closed state the smallest diameter is 4-5 Å, preventing ivabradine from entering; hence blockers can work only in the open state and become 'trapped' in the closed state. Block is also reportedly current-dependent, relying on flow of cations through the pore (Bucchi *et al.*, 2013).

Trapping of ZD7288 in murine HCN2 channels has also been described, but in contrast to ivabradine, the block of ZD7288 may not be current-dependent (Bucchi *et al.*, 2002). ZD7288 block of HCN channels is characteristically slow, perhaps

reflecting that it cannot cross the plasma membrane very easily (Stieber *et al.*, 2005). The IC_{50} for ZD7288 is not dependent on subtype; however, native I_f is reportedly blocked more potently than heterologously expressed HCN (Cheng *et al.*, 2007). Values calculated from human HCN transfected into HEK293 cells are as follows: 20, 41, 34 and 21 μM for hHCN1, 2, 3 and 4 respectively (Stieber *et al.*, 2005), whilst ZD7288 inhibits I_f in freshly isolated SA node cells with an IC_{50} of ~0.3 μM (BoSmith *et al.*, 1993). The IC_{50} of ivabradine is 1.5-4.5 μM (Postea & Biel, 2011). Both ivabradine and ZD7288 are also functionally irreversible due to trapping in the pore.

There has been a lot of recent interest in developing HCN-targeting drugs, potentially subtype-specific, for treatment of arrhythmias or pain (Roubille & Tardif, 2013). Reportedly the main limitation at present is a lack of high-resolution structure of the transmembrane core, since this is where most ligands interact (Postea & Biel, 2011).

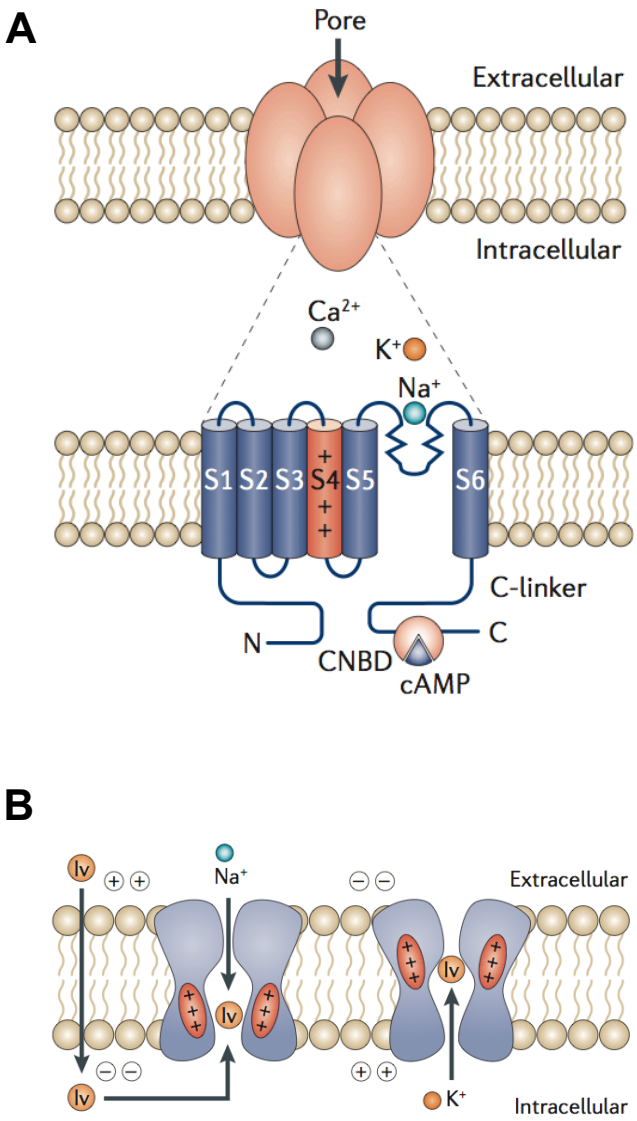

Figure 4.1.1 HCN channel structure and pharmacological binding sites
A Top Schematic illustrating the tetrameric structure of HCN channels, showing the composition of each of the four subunits (**bottom**) with the cyclic nucleotide-binding domain (CNBD) in the C terminus connected to the sixth transmembrane α-helix (S6) via the C-linker. The fourth transmembrane subunit (S4) is positively charged, and functions as the voltage sensor of the channel. The loop domain between S5 and S6 in the channel pore determines the cation conductance of Na^+, K^+ and Ca^{2+}. **B** Ivabradine crosses the plasma membrane and binds in the open HCN channel pore from the intracellular side. The movement of the S4 α-helix is indicated. Both schematics taken from (Postea & Biel, 2011).

4.1.v HCN channel expression

HCN channels are predominately expressed in the heart and brain. HCN4 is the main subtype present in the SA node, at least in humans and mice (Herrmann *et al.*, 2011). In HCN4-knockout mice, the I_f was reduced by 70-80% *versus* wild-type nodal cells (Stieber *et al.*, 2003). HCN2 reportedly comprises 20%, although immunohistochemistry studies of mouse heart tissue slices found a strong presence of HCN1 in the SA node as well (Herrmann *et al.*, 2011). The study also found high levels of HCN2 in mouse ventricular tissue, indeed several recent reports have also begun investigating the expression and function of HCN channels elsewhere in non-pacemaking regions of the heart. HCN2 appears to be ubiquitous throughout atrial and ventricular myocytes, whilst HCN1, 3 and 4 transcripts have also been detected in cardiac muscle. The expression of HCN channels in the heart can also be reportedly upregulated in cardiac hypertrophy and heart failure (Wahl-Schott & Biel, 2009).

HCN channels have also been proposed to perform a pacemaker function in the smooth muscle of rabbit portal veins, which generate rhythmic spontaneous oscillations. Reverse transcription polymerase chain reaction (RT-PCR) identified subtypes HCN2-4, whilst ZD7288 (10 μM) produced a characteristic slow-block of hyperpolarization-activated cation currents in portal vein myocytes patched in the whole-cell configuration (Greenwood & Prestwich, 2002). HCN channels were also implicated in rat bladder detrusor smooth muscle cells, which display spontaneous contraction, since ZD7288 (10-100 μM) inhibited an inwardly-rectifying current (I_{IR}) with similar activation and conductance properties to I_f (Green *et al.*, 1996).

4.1.vi β-Adrenoceptors and HCN channels

There is a large body of literature supporting a close relationship between β-adrenoceptors and the pacemaking HCN channels in the heart, which is underpinned by the sensitivity of HCN channels to cAMP. Sympathetic stimulation of β-adrenoceptors in cardiac myocytes increases the activation of HCN channels by left-shifting the activation curve. Whilst β_1-adrenoceptors raise global cAMP levels, β_2-Adrenoceptors cause cAMP elevation which is restricted in space (compartmentation in cardiac myocytes reviewed by Steinberg & Brunton, 2001). β_2-adrenoceptors have recently been shown to colocalise with HCN4 in caveolae; furthermore, the β_2-adrenoceptor appears to bind to the N-terminus of HCN4, which is proposed to be critical for its chronotropic effect on I_f (Greene *et al.*, 2012).

The aim of the experiments in this chapter was to investigate the hypothesis that HCN channels mediate the increase in endothelial cell Ca^{2+} events to hyperpolarizing agents, including a β-adrenoceptor agonist, using a combination of pharmacological tools and immunohistochemistry of intact, pressurized arteries.

4.2 Methods & Materials

*Refer to **Chapter 2: Methods & Materials** for full details of the methods used in this chapter. Details relevant specifically to this chapter are given below.*

4.2.i Protocols for assessing endothelial cell Ca^{2+} events

*Refer to **Chapter 3 sections 3.2.i and 3.2.ii** for full details of pressurized arteries for Ca^{2+} imaging and offline Ca^{2+} event analysis.*

Rat third order mesenteric arteries were isolated, cannulated and pressurized as described (**Methods & Materials section 2.3.i**) and loaded with OGB-1 (**Methods & Materials section 2.3.iii**). Basal, spontaneous Ca^{2+} activity was recorded for 90 s (270 frames acquired at 3 Hz) before addition of isoprenaline (1 μM) in the same acquisition run. The endothelial Ca^{2+} response to isoprenaline was recorded for an additional 150 s (450 frames), followed by washout for 25 min. ZD7288 was applied for 30 min or 60 min as indicated (see figure legends) in the superfusion after washout of isoprenaline for 25 min. Preliminary Ca^{2+} imaging experiments in rat cremaster arterioles conducted by TZ Beleznai found an increase in basal, spontaneous endothelial Ca^{2+} events in the presence of ZD7288, which could be inhibited by nifedipine. It was thus assumed that ZD7288 might directly or indirectly activate L-type VGCC in the smooth muscle. We therefore included the VGCC blocker, nifedipine (1 μM, 20 min at low pressure) in all our Ca^{2+} imaging experiments with ZD7288. Nifedipine does not alter basal Ca^{2+} event frequency (Bagher *et al.*, 2012); nor did it alter the frequency of events to isoprenaline (**Figure 4.2.1**) or levcromakalim.

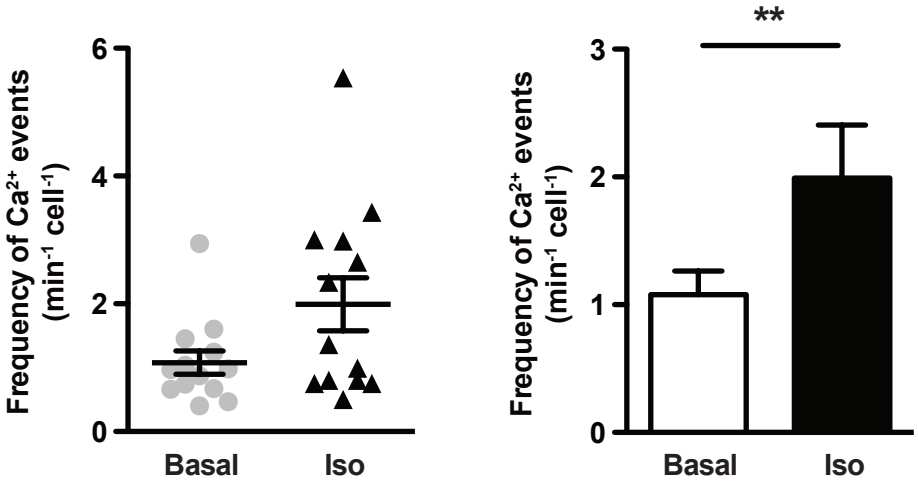

Figure 4.2.1 Inhibition of L-type VGCC does not affect spontaneous or isoprenaline-evoked endothelial cell Ca^{2+} events

Summary data showing the frequency of endothelial cell spontaneous Ca^{2+} events basally and in response to isoprenaline (1 μM) stimulation, in the presence of nifedipine (L-type VGCC blocker, 1 μM) in rat pressurized mesenteric arteries. **Left** Individual data points shown on a scatter graph; **right** histogram of the same data. Paired data, n=13, **P<0.01 by Student's t-test.

4.2.ii Isometric tension recordings of ACh relaxation

Refer to ***Chapter 2: Methods & Materials section 2.2.i*** *for full details of wire myography setup.*

For assessing the ACh-mediated relaxation of third order mesenteric arteries, vessels were pre-constricted with a sub-maximal concentration of PE. Where drugs were applied in the static bath for 60 min (ZD7288, ivabradine or apamin), the solution was changed after 30 min to prevent evaporation artefacts. L-NAME (100 μM) was present throughout to remove the basal or PE-induced release of nitric oxide, so as to obtain a more stable level of tone.

4.2.iii Sharp microelectrode studies of membrane potential

Rat third order mesenteric arteries were mounted on an isometric wire myograph and normalised to resting tension as described (**Methods & Materials section 2.2.i**). A smooth muscle cell was impaled using a sharp microelectrode back-filled with 2 M KCl solution to measure the resting membrane potential (Em). Having acquired a stable recording, drugs were carefully applied to the static bath and mixed by bubbling, whilst the smooth muscle cell remained impaled and the response recorded. After the response had plateaued, the electrode was pulled out. The recording was adjusted offline where the baseline value differed from 0 mV, and an average taken pre- and post-impalement (although the two values did not differ markedly). For treatment with ZD7288, the drug was added to the static bath for a total of 60 min, changing solution after 30 min to prevent potential evaporation artefacts.

Acknowledgement: These experiments were set up by CS Lim and conducted and analysed by KA Dora.

4.2.iv Immunohistochemistry

*Refer to **Chapter 2: Methods & Materials section 2.4.i** for details of the pinned protocol for immunohistochemistry on the sino-atrial node.*

In preliminary experiments investigating labelling of HCN channel primary antibodies, staining was observed consistently within the holes in the internal elastic lamina (IEL) (not shown). This pattern was also observed in the control experiments, where only the secondary antibody was applied to the artery (**Figure 4.2.2**). Following troubleshooting of the immunohistochemistry protocol, the secondary alone control showed no staining in any plane of the artery wall (**Figure 4.3.10**), and labelling with the HCN channel primary antibodies shown in **Figures 4.3.8 and 4.3.9** followed this protocol, which is described in **Methods & Materials section 2.4**.

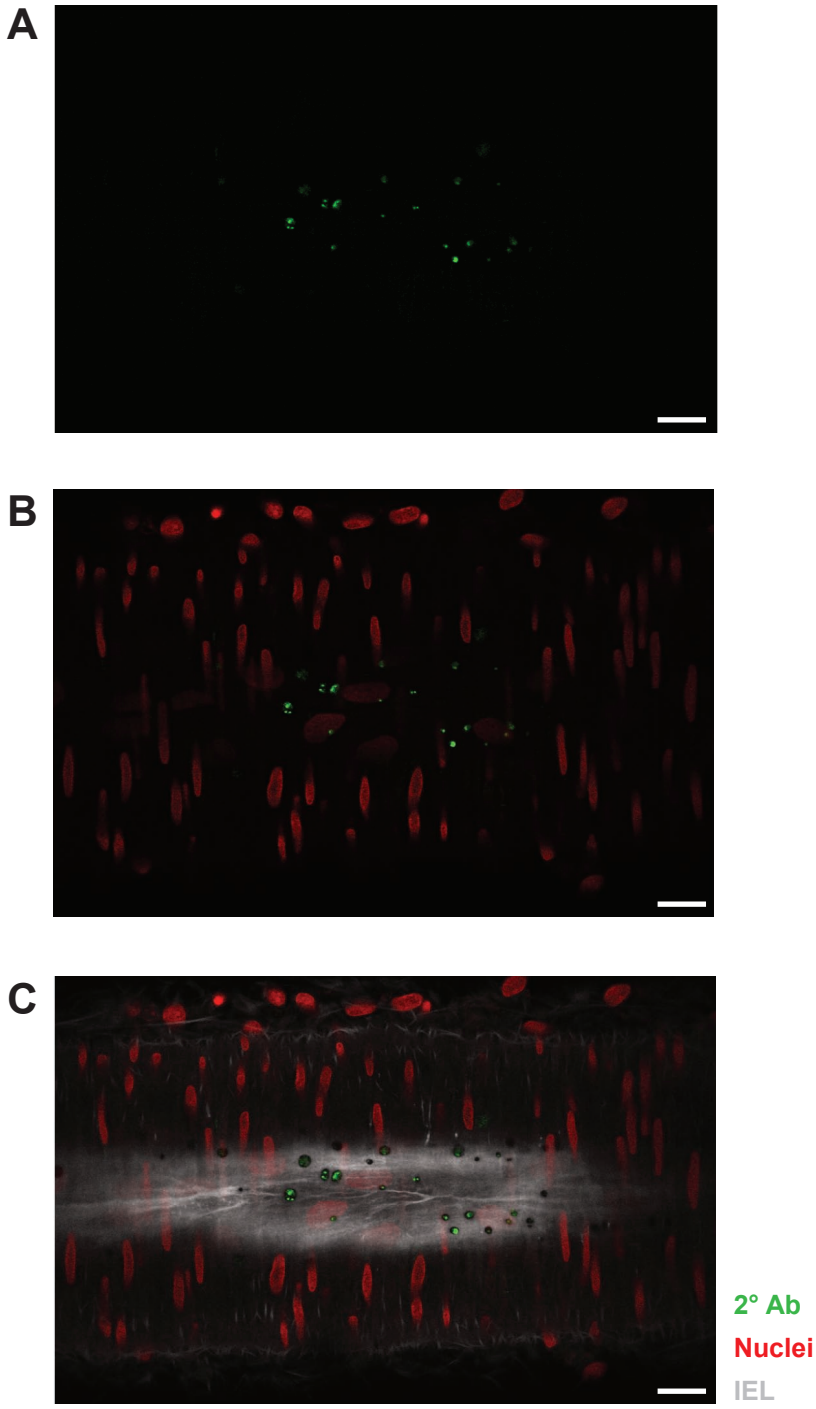

Figure 4.2.2 Secondary antibody alone in preliminary experiments
In rat pressurized cremaster arterioles, the secondary antibody (2° Ab) was applied alone in the absence of the primary antibody (**A**). Staining (green) was not visible in the adventitia, or smooth muscle planes, but was visible in the endothelium; in particular the staining aligned with holes in the internal elastic laminar (IEL, grey, **C**). This staining was replicated in preliminary experiments with HCN2 channel primary antibody present. Nuclei are stained with propidium iodide (45 μM, red). Scale bars = 20 μm.

4.3 Results

We proposed to test the possible involvement of HCN channels in our observed hyperpolarization-driven Ca^{2+} influx in rat mesenteric arteries using the HCN blocker, ZD7288. Treatment with ZD7288 (10 μM, 30 min) inhibited the increase in endothelial cell Ca^{2+} events to β-adrenergic stimulation with isoprenaline (1 μM; **Figure 4.3.1**).

Since HCN channels appeared to be present and functional in rat mesenteric arteries, we proposed to investigate any potential contribution of HCN channels to the resting membrane potential. In arteries mounted under isometric tension, ZD7288 (1-10 μM) did not significantly affect the resting membrane potential (**Figure 4.3.2A**). 10 μM ZD7288 (60 min) did, however, reduce the hyperpolarization to isoprenaline (1 μM, 3 μM; **Figure 4.3.2C**). 10 μM ZD7288 also reduced the hyperpolarization to levcromakalim (3 μM; **Figure 4.3.2B**) and ACh (0.1-1 μM; **Figure 4.3.2D**), suggesting a common mechanism. Although the nature of this mechanism is currently unknown, it introduces the possibility that our observed inhibition of isoprenaline-activated endothelial cell Ca^{2+} might be a result of reduced hyperpolarization rather than direct block of the HCN channels. In the electrophysiological recordings 1 μM ZD7288 appeared to have much less effect on hyperpolarization to isoprenaline and ACh (**Figure 4.3.2C**, **D**), hence we repeated our endothelial cell Ca^{2+} experiments using 1 μM instead of 10 μM (**Figure 4.3.3**). In this case ZD7288 was seen to reduce, but not fully prevent, an increase in endothelial cell Ca^{2+} to isoprenaline.

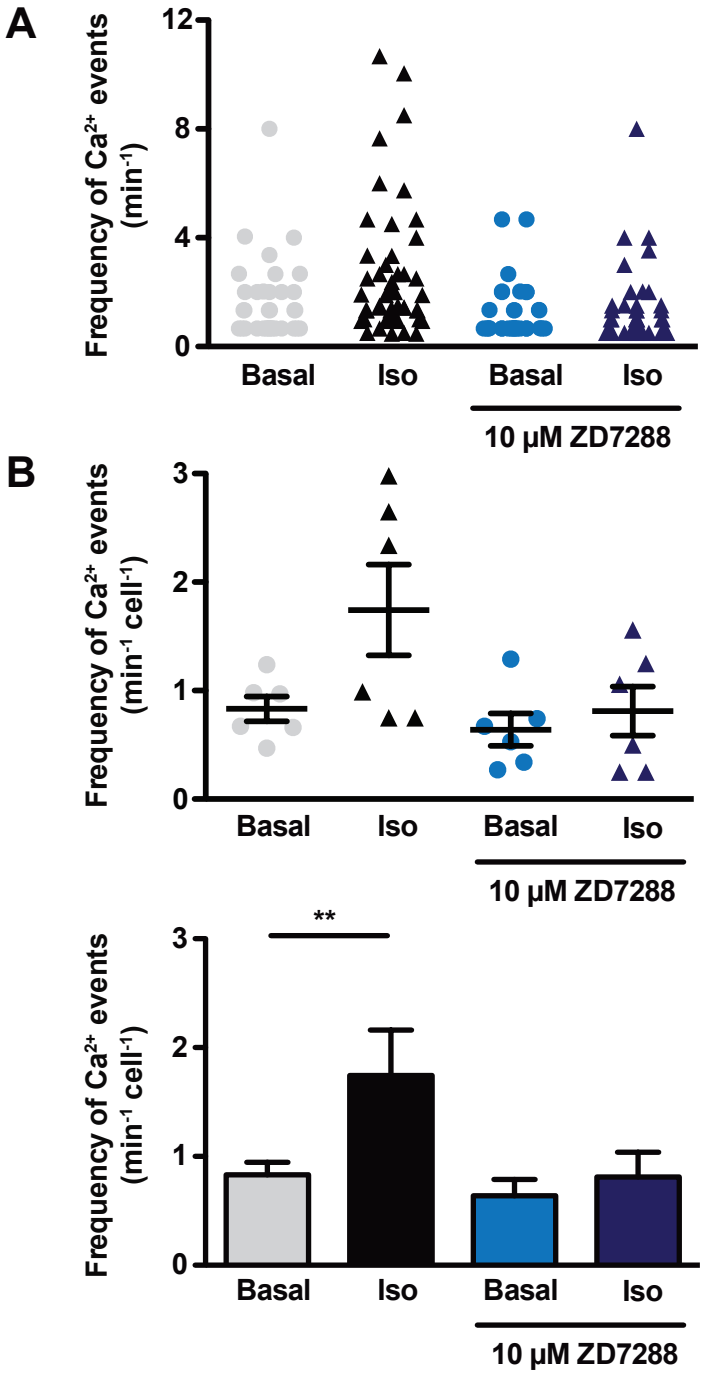

Figure 4.3.1 Increase in endothelial cell Ca^{2+} to β-adrenoceptor stimulation is prevented by inhibition of HCN channels
Summary data of Ca^{2+} event frequency from individual cells (**A**) or averaged per experiment (**B**) showing block of hyperpolarization-activated, cyclic nucleotide-gated (HCN) channels with ZD7288 (10 μM, 30 min) inhibits the response to isoprenaline (Iso, 1 μM) in rat pressurized mesenteric arteries. Paired experiments, n=5, *P<0.05 by repeated measures ANOVA with Bonferroni post-tests to compare selected data sets as indicated.

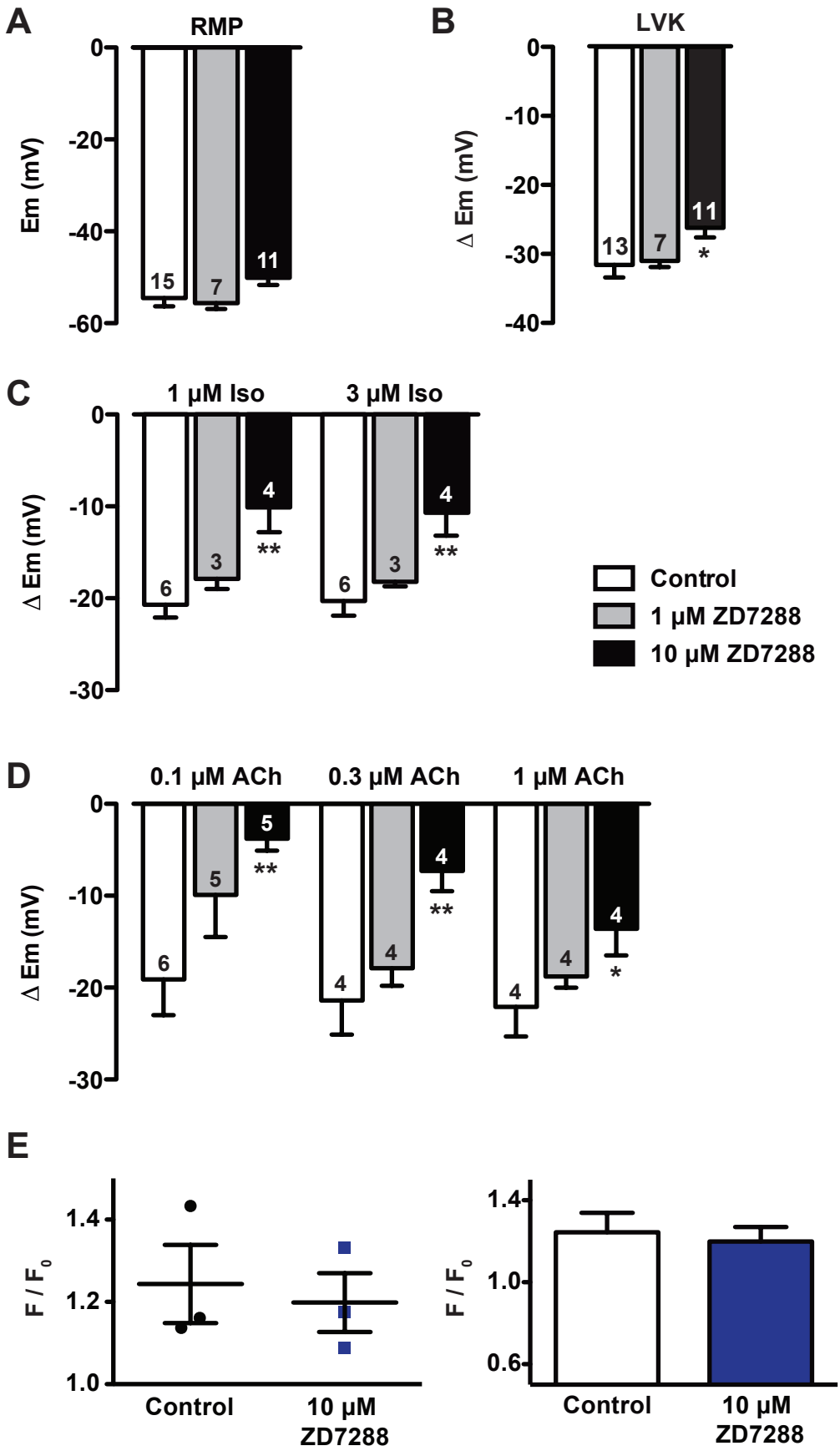
A
RMP
Em (mV)
0
-20
-40
-60
15
7
11
B
LVK
Δ Em (mV)
0
-10
-20
-30
-40
13
7
11
*
C
1 μM Iso
3 μM Iso
Δ Em (mV)
0
-10
-20
-30
6
3
4
**
6
3
4
**
Control
1 μM ZD7288
10 μM ZD7288
D
0.1 μM ACh
0.3 μM ACh
1 μM ACh
Δ Em (mV)
0
-10
-20
-30
6
5
5
**
4
4
4
**
4
4
4
*
E
F / F0
1.4
1.2
1.0
Control
10 μM ZD7288
F / F0
1.4
1.0
0.6
Control
10 μM ZD7288

Figure 4.3.2 Hyperpolarization to β-adrenergic stimulation, levcromakalim or ACh is inhibited by ZD7288

A Resting membrane potential (Em) of rat mesenteric arteries mounted isometrically in a wire myograph is unchanged by 1 μM ZD7288 (60 min, grey bars) but slightly depolarized by 10 μM ZD7288 (60 min, black bars). *n* numbers as indicated within bars. Hyperpolarization to levcromakalim (**B**; LVK, 3 μM), isoprenaline (**C**; Iso, 1-3 μM) and acetylcholine (**D**; ACh, 0.1-1 μM) is slightly reduced by 1 μM ZD7288 (grey bars) and significantly inhibited by 10 μM ZD7288 (black bars). Data are a mix of paired and unpaired, *n* numbers as indicated within bars, *P<0.05, **P<0.01 by one-way ANOVA with independent Bonferroni post-tests vs. Control. **E** The increase in endothelial cell Ca^{2+} to ACh (0.3 μM) in pressurized rat mesenteric arteries is unaffected by ZD7288 (10 μM, 30 min). Paired data, *n*=3.

Acknowledgements: KA Dora performed and analysed the experiments, which were set up by CS Lim. Ca^{2+} imaging experiments were performed and analysed by CS Lim.

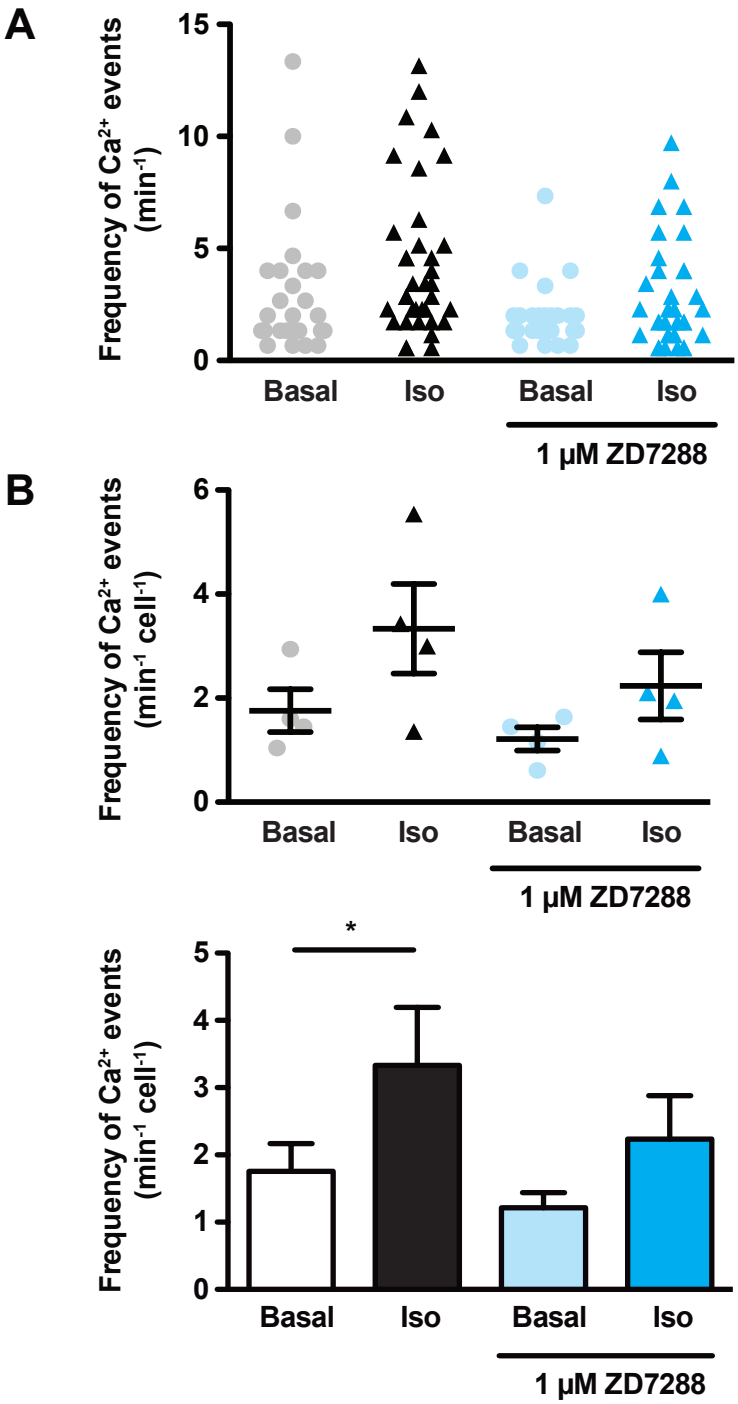

Figure 4.3.3 β-Adrenergic stimulation of endothelial cell Ca^{2+} events is reduced by ZD7288 (1 μM)

Summary data of Ca^{2+} event frequency from individual cells (**A**) or averaged per experiment (**B**) showing that ZD7288 (1 μM, 60 min) reduces the endothelial cell Ca^{2+} response to isoprenaline (Iso, 1 μM). Paired experiments, n=4, *P<0.05 by repeated measures ANOVA with Bonferroni post-tests to compare selected data sets as indicated.

In rat cremaster arterioles, the increase in endothelial cell Ca^{2+} events to levcromakalim (3 μM) as previously observed (**Figure 3.3.1**) was blocked by ZD7288 (1 μM and 10 μM; **Figure 4.3.4**). ZD7288 (10 μM) did not, however, alter the endothelial cell Ca^{2+} response to ACh (0.3 μM; **Figure 4.3.2E**), which reflects release of intracellular Ca^{2+} from the endoplasmic reticulum via IP_3. The effect of ZD7288 is therefore likely to be direct against the channels mediating the hyperpolarization. To investigate this further, the effect of ZD7288 (0.1-10 μM, 60 min) on ACh-mediated relaxation of rat mesenteric arteries was assessed. ZD7288 concentration-dependently inhibited the relaxation to ACh of arteries pre-constricted to sub-maximal tone with PE (**Figure 4.3.5**, **Table 4.3.1**). The clinically used HCN channel blocker, ivabradine, also concentration-dependently inhibited the relaxation to ACh (**Figure 4.3.6**, **Table 4.3.1**).

[ZD7288]	**Control**	**+ ZD7288**	**+ Apamin**
Time control	-7.44	-7.33	-6.61#
0.1 μM	-7.38	-7.27	-6.69#
1 μM	-7.40	-7.17*	-6.96#
10 μM	-7.29	-6.95*	-6.40#
[Ivabradine]	**Control**	**+ Ivabradine**	**+ Apamin**
Time control	-7.40	-7.08	-6.52#
0.3 μM	-7.33	-7.47	-6.51#
3 μM	-7.48	-6.88*	-6.22#
30 μM	-7.40	-6.17*	-5.42#

Table 4.3.1 $LogEC_{50}$ values for ACh relaxation in the presence of ZD7288 or ivabradine, and apamin
Values correspond to concentration-response curves displayed in **Figures 4.3.5** and **4.3.6**. *P<0.001 by one-way ANOVA with Bonferroni post-test to compare HCN channel blocker treatment $logEC_{50}$ to Control $logEC_{50}$; #P<0.001 by one-way ANOVA with Bonferroni post-test to compare Apamin treatment $logEC_{50}$ to HCN channel blocker treatment $logEC_{50}$.

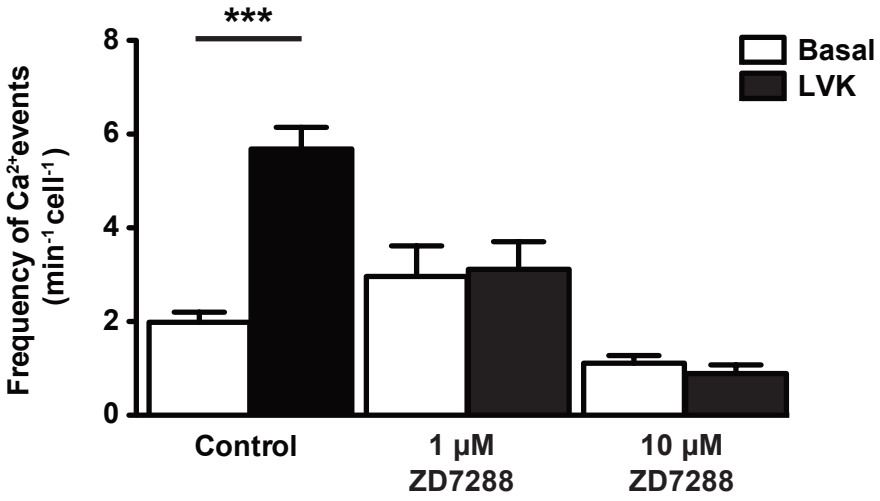

Figure 4.3.4 Levcromakalim-evoked endothelial cell Ca^{2+} events are blocked by ZD7288

Summary data showing that ZD7288 (1 μM, 60 min or 10 μM, 30 min) inhibited the endothelial cell Ca^{2+} increase to levcromakalim (LVK, 3 μM, black bars). Unpaired data, *n*=4-15, ***P<0.001 by one-way ANOVA with Bonferroni post-tests to compare selected data sets as indicated. **Acknowledgements:** KA Dora and TZ Beleznai performed these experiments; KA Dora analysed the data; CS Lim set up some of these experiments.

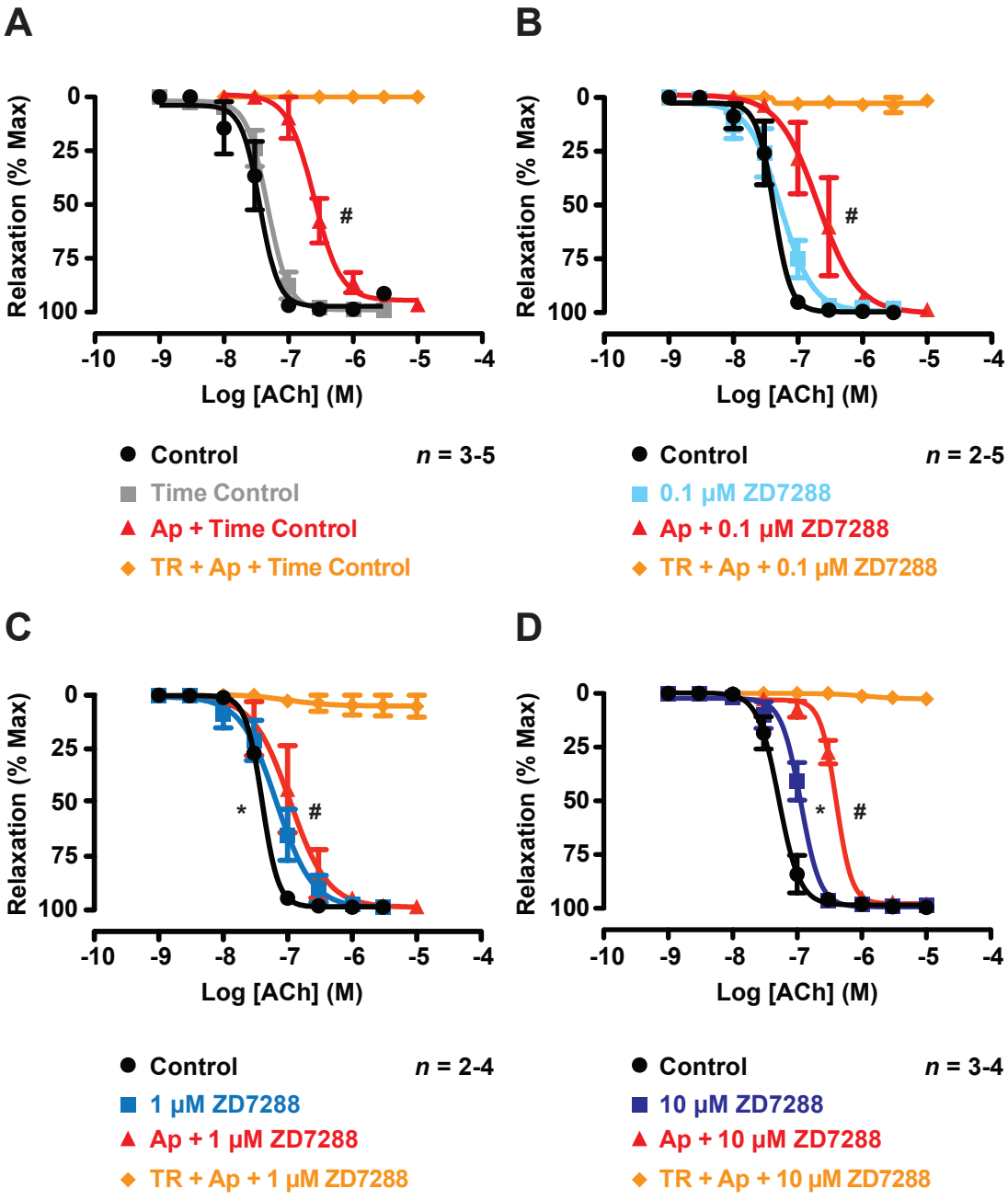

Figure 4.3.5 ZD7288 partially inhibits ACh-mediated relaxation
Rat mesenteric arteries were pre-constricted to a sub-maximal level of tone with PE. Relaxation to ACh is unaltered over time (**A**) or in the presence of 0.1 μM ZD7288 (**B**, 60 min, blue square), but is significantly inhibited by 1 μM (**C**) or 10 μM (**D**) ZD7288 (60 min, blue square). Apamin (Ap; 50 nM, 60 min, red triangle) further right-shifted the concentration-response curves, and the relaxation to ACh was fully blocked by additional application of TRAM-34 (TR; 1 μM, 30 min, orange diamond). L-NAME (100 μM) was present throughout. Paired experiments throughout, *n* numbers as indicated, *P<0.001 by one-way ANOVA with Bonferroni post-test to compare ZD7288 treatment logEC_{50} to Control logEC_{50}; #P<0.001 by one-way ANOVA with Bonferroni post-test to compare Apamin treatment logEC_{50} to ZD7288 treatment logEC_{50}.

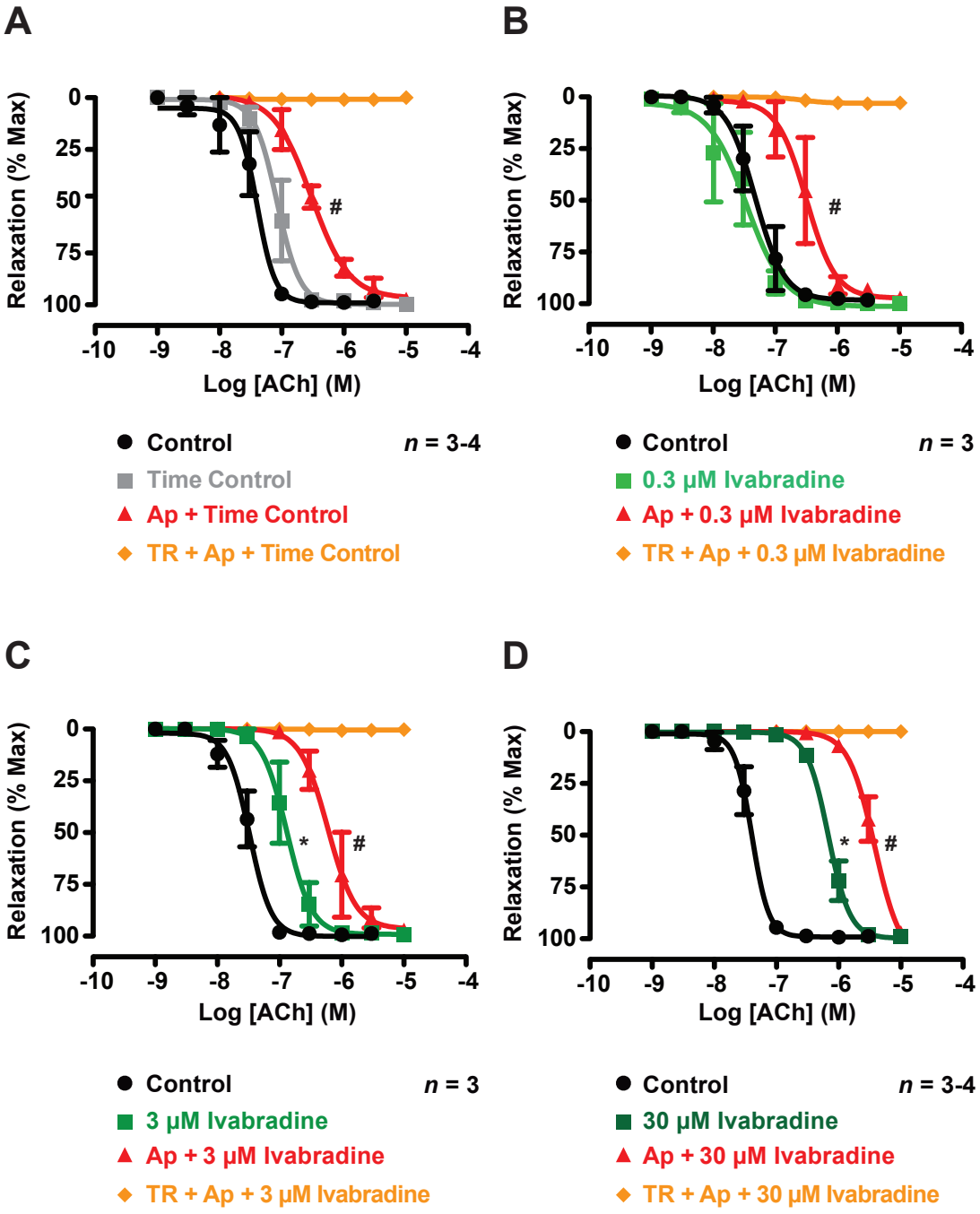

Figure 4.3.6 Ivabradine inhibits ACh-mediated relaxation
Rat mesenteric arteries were pre-constricted to a sub-maximal level of tone with PE. Relaxation to ACh is unaltered over time (**A**) but is significantly inhibited by 0.3 μM (**B**) 3 μM (**C**) or 30 μM (**D**) ivabradine (60 min, green square). Apamin (Ap; 50 nM, 60 min, red triangle) further right-shifted the concentration-response curves, and the relaxation to ACh was fully blocked by additional application of TRAM-34 (TR; 1 μM, 30 min, orange diamond). L-NAME (100 μM) was present throughout. Paired experiments throughout; *n* numbers as indicated, *P<0.001 by one-way ANOVA with Bonferroni post-test to compare Ivabradine treatment $logEC_{50}$ to Control $logEC_{50}$; #P<0.001 by one-way ANOVA with Bonferroni post-test to compare Apamin treatment $logEC_{50}$ to Ivabradine treatment $logEC_{50}$.

To investigate the presence of HCN channels in the resistance vasculature immunohistochemistry was performed on pressurized, fixed arteries using primary antibodies against each of the four subtypes of HCN channels (Herrmann *et al.*, 2011). As a positive control the primary antibodies were first used on sections of the rat sino-atrial node region in the right atrium, which showed staining for all four subtypes (**Figure 4.3.7**). In rat fixed, pressurized cremaster arterioles, punctate staining was visible in the smooth muscle layer for HCN1, 2 and 3 (**Figure 4.3.8A, B; Figure 4.3.9A**). There was also HCN3 staining visible in the endothelium in 2 out of 5 arterioles (**Figure 4.3.9**). HCN4 was not present in rat cremaster arterioles (**Figure 4.3.8C**).

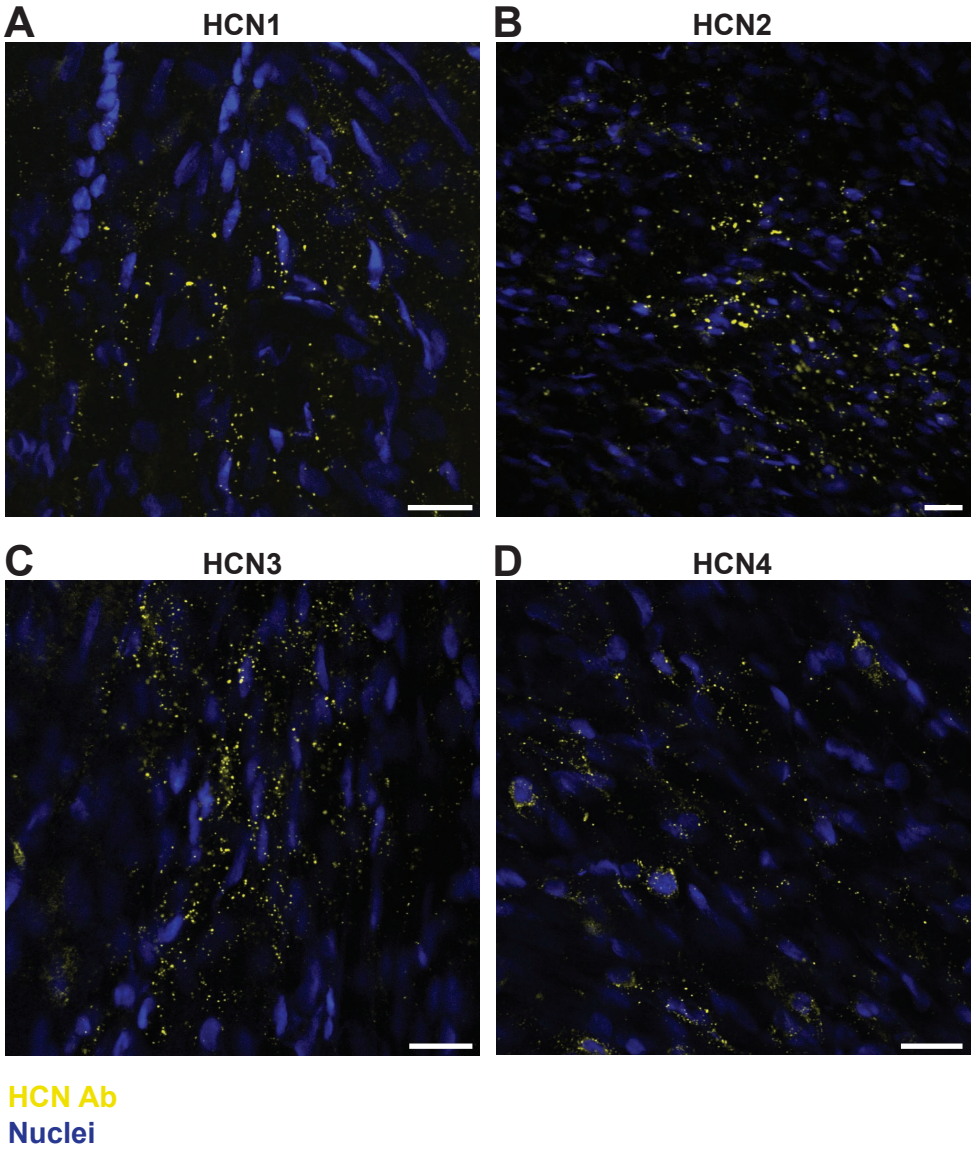

Figure 4.3.7 HCN expression in sino-atrial node
Staining was visible for all four subtypes of HCN channel (yellow) in the rat sino-atrial node region. **A** HCN1 (*n*=2), **B** HCN2 (*n*=2), **C** HCN3 (*n*=2), **D** HCN4 (*n*=1). Nuclei are stained with propidium iodide (45 μM, blue). Scale bars = 20 μm.

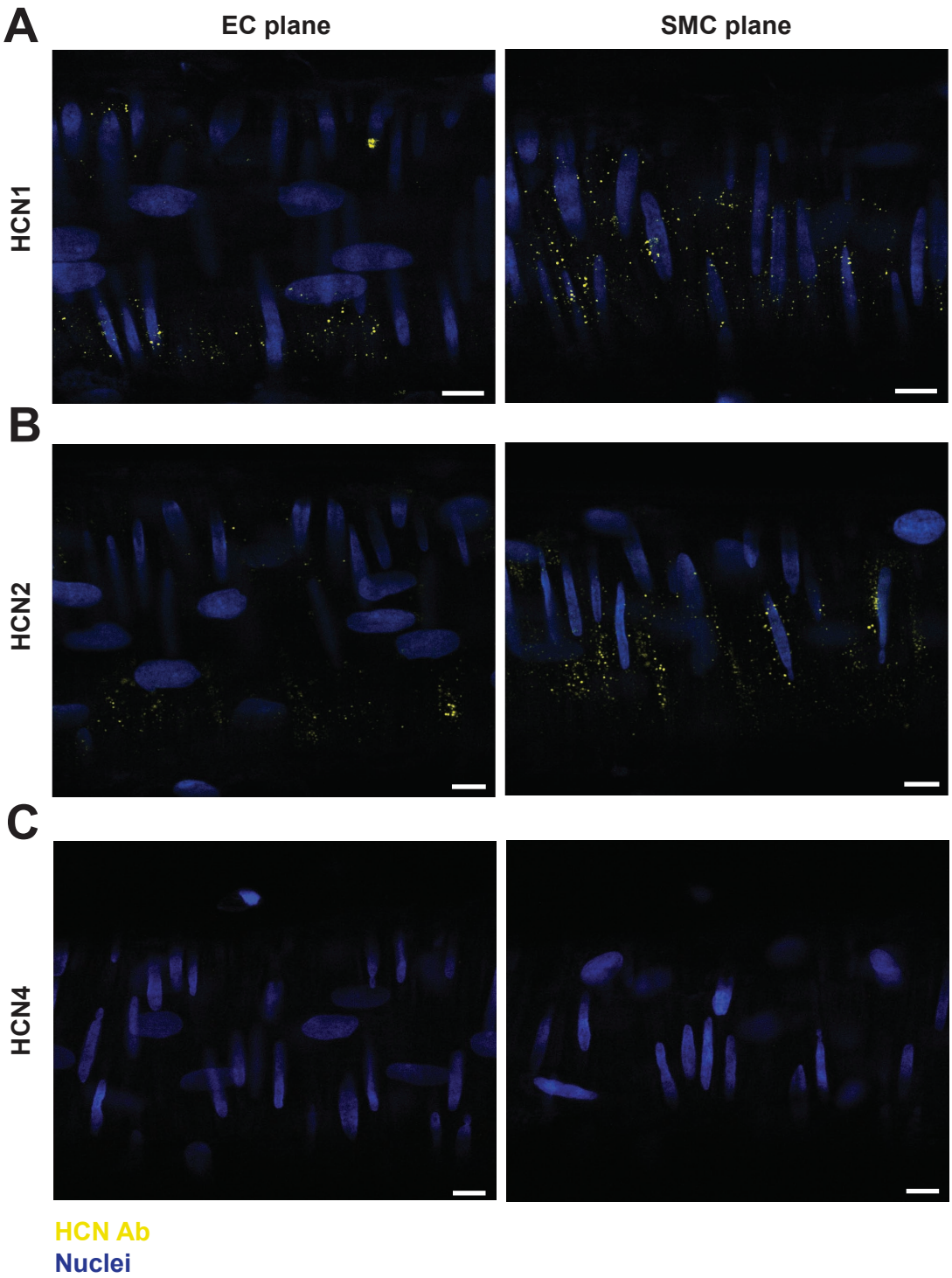

Figure 4.3.8 HCN channel expression in rat cremaster arterioles
Immunolabelling (yellow) for HCN channel subtypes 1 (**A**) and 2 (**B**) was visible in the smooth muscle (**right**) of rat pressurized cremaster arterioles. HCN4 was not present in either the endothelial (EC) or smooth muscle cell (SMC) layers in these arterioles (**C**). Nuclei are stained with propidium iodide (45 μM, blue). Images are representative of n=1-5. Scale bars = 10 μm.

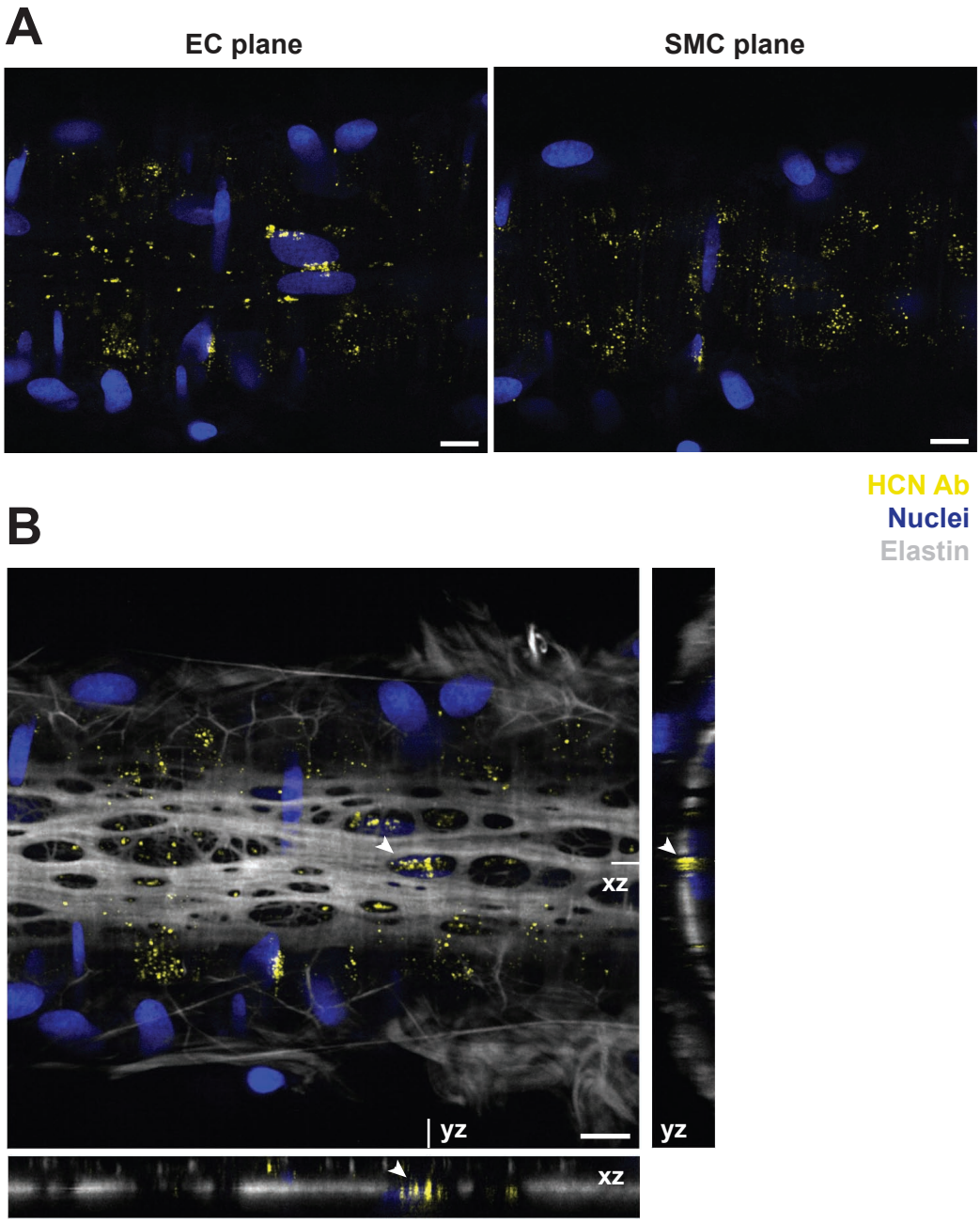

Figure 4.3.9 HCN3 channel expression in rat cremaster arterioles
A Immunolabelling (yellow) for HCN3 shows staining in both smooth muscle cell (SMC, **right**) and endothelial cell (EC, **left**) cell layers of rat pressurized cremaster arterioles. **B** HCN3 is visible in holes in the IEL (grey, labelled with Alexa Fluor 633 hydrazide (1 μM)) in xz and yz cross-sections (arrowhead). Nuclei are stained with propidium iodide (45 μM, blue). Images are representative of n=5. Scale bars = 10 μm.

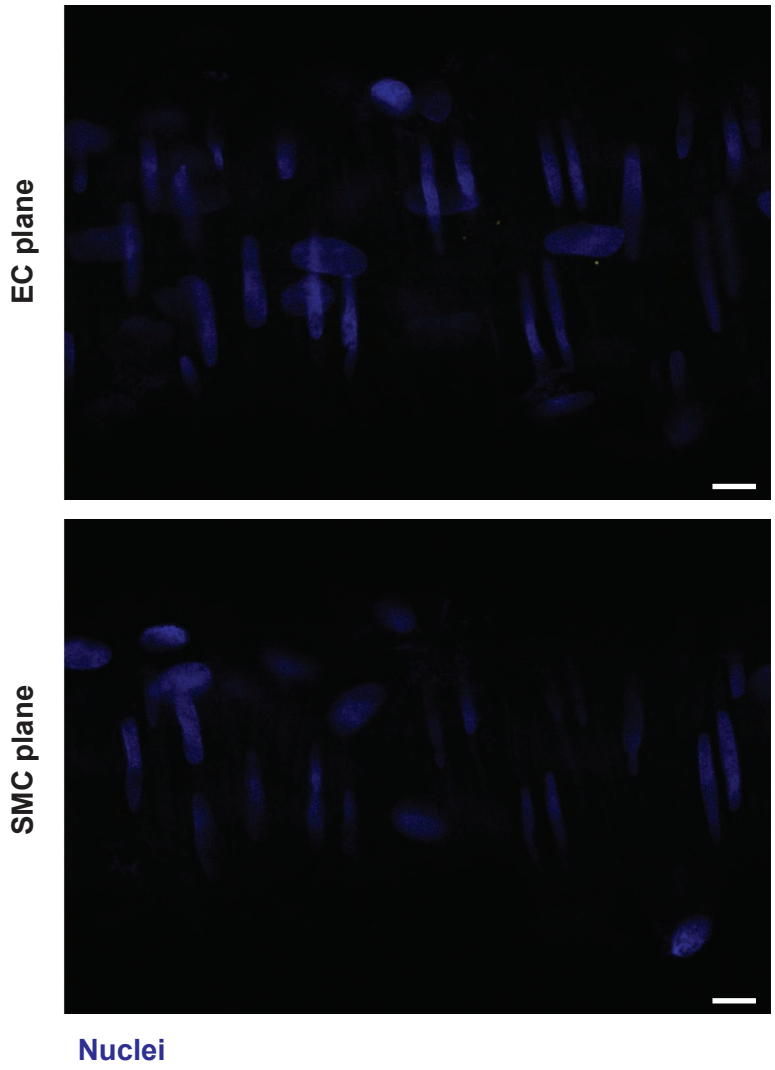

Figure 4.3.10 Lack of staining with secondary antibody alone
In the absence of primary antibody, the secondary antibody applied alone did not produce any fluorescent staining in the endothelium (EC, **top**) or smooth muscle (SMC, **bottom**) imaging planes of rat pressurized cremaster arterioles. Nuclei are stained with propidium iodide (45 μm, blue). n=1. Scale bars = 10 μm.

4.4 Discussion and Future Work

The data in this chapter suggest that HCN channels might contribute to hyperpolarization-driven Ca^{2+} influx in resistance arteries and show that these channels are present in these arteries. Of note the hyperpolarization-dependent mechanism appears to be conserved between at least two vascular beds in the rat: the mesenteric and cremaster, and it is interesting to speculate that perhaps this is a conserved pathway to aid the control of vascular tone and blood flow in the resistance vessels. In addition, potential off-target effects of ZD7288 and ivabradine have been observed, which appear to reflect partial inhibition of endothelial SK_{Ca} and IK_{Ca} channels.

4.4.i HCN channels and β-adrenoceptors

We have shown that stimulation of β-adrenoceptors with isoprenaline causes an increase in endothelial Ca^{2+} event frequency, which was inhibited by 10 μM ZD7288 (**Figure 4.3.1**) and reduced by 1 μM ZD7288 (**Figure 4.3.3**). Whether the partial inhibition of the isoprenaline response with 1 μM ZD7288 reflects partial inhibition of the HCN channel, or partial involvement of HCN channels in the response, cannot be differentiated due to the confounding effects of ZD7288 to reduce hyperpolarization to isoprenaline (**Figure 4.3.2**; discussed in **section 4.4.iv**).

If the former, it is interesting to speculate on a potential interaction between β-adrenoceptors and HCN channels in the vasculature, as has been reported in the heart by multiple studies (discussed in **section 4.1.vi**). With the commercial availability of reliable β-adrenoceptor (subtype-specific) antibodies, immunohistochemistry would facilitate colocalisation studies of β-adrenoceptors with

HCN3 channels in the endothelial cells of intact arteries. Preliminary attempts to align fluorescent propranolol labelling of live arteries with HCN channel immunolabelling were unsuccessful: the fluorescent ligand did not remain after fixation and permeabilization.

4.4.ii HCN channel expression

HCN subtypes 1, 2, 3 and 4 were identified in sections of the SA node region of the rat right atrium (**Figure 4.3.7**). The exact location of the channel was not directly assessed; therefore it is possible that some of this expression was within atrial myocytes or neuronal innervation rather than pacemaking nodal cells. Co-immunohistochemistry with markers of SA node cells e.g. Cx45, or of atrial myocytes e.g. Cx43 or atrial natriuretic peptide (as employed by Liu *et al.*, 2007 for this purpose), would help to differentiate the cell types.

In rat cremaster arterioles, using the same combinations of primary and secondary antibodies, HCN subtypes 1, 2 and 3 were visible in the smooth muscle layer (**Figure 4.3.8**). HCN3 was also inconsistently observed in the endothelium (**Figure 4.3.8C**). This inconsistency is likely to reflect non-uniform expression of the channel, rather than an artefact of the protocol, since the expression pattern in the smooth muscle, which had been treated in the same manner, was consistent. Indeed, non-uniform expression of the HCN channel in the endothelium would fit with the pattern of Ca^{2+} responses observed to levcromakalim in this vessel (and to isoprenaline in mesenteric arteries) whereby not every cell showed an increase in Ca^{2+} events. Perhaps a responding endothelial cell has HCN channels present facilitating Ca^{2+} influx to the hyperpolarizing agent. Alignment of Ca^{2+} responses with

immunohistochemistry for proteins of interest is feasible and has previously been reported (Bagher *et al.*, 2012); this was not attempted in this study but would certainly be of value to address this theory. It would also be of value to perform immunohistochemistry on rat pressurized mesenteric arteries to determine if the subtype expression pattern mimics that observed in cremaster arterioles.

4.4.iii HCN channel function in resistance arteries

The function of HCN1, 2 and 3 channels in the smooth muscle of rat cremaster arterioles was not investigated. It is possible that hyperpolarization-driven opening of HCN channels could raise Ca^{2+} in the smooth muscle. This would presumably represent a discrete increase in Ca^{2+}, since a global increase would theoretically result in contraction. This discrete increase might be sufficient to communicate through MEJs to endothelial cells, which is well known to occur for example following α-adrenoceptor activation (Dora *et al.*, 2000). Although smooth muscle Ca^{2+} events evoked by hyperpolarization were not monitored in this study, the expression of HCN channels observed in the smooth muscle cells is not consistent with this hypothesis, which would presumably rely on smooth muscle HCN channels focused at the MEJ - the pattern was more uniform across the cells. How these channels operate in concert with the major Ca^{2+} signalling mechanism in vascular smooth muscle cells, that of *depolarization*-induced VGCC Ca^{2+} influx is unknown. In excitable smooth muscle, HCN channels have been proposed to perform a pacemaker role similar to that in the sino-atrial node (as discussed in **section 4.1.v**) (Green *et al.*, 1996; Greenwood & Prestwich, 2002). The function of HCN channels in 'quiescent' smooth muscle cells remains to be determined.

There is some controversy over the activation range and kinetics of HCN channels. Whole-cell patch-clamp experiments propose a half-maximal activation potential ($V_{0.5}$) of -70 mV to -100 mV (Biel *et al.*, 2009), whereas a study of the single-channel properties of I_f in human atrial myocytes calculated $V_{0.5}$ of -72.9 ± 3.7 mV, which was right-shifted by forskolin to -55.87 ± 1.7 mV (Michels *et al.*, 2005). Similarly, single-channel patch-clamp of HCN1, 2 or 4 expressed in CHO-K1 cells found $V_{0.5}$ values of -51.2 ± 6.8 mV, -58.5 ± 4.8 mV, and -74.2 ± 5.2 mV respectively (Michels *et al.*, 2005). It is therefore plausible that HCN1, 2 or 3 channels in resistance arteries might be open at resting membrane potential (~-55 mV). Indeed, the observed inhibition by ZD7288 of hyperpolarization-evoked endothelial cell Ca^{2+} events is consistent with HCN channels being open at resting membrane potential, since ZD7288 requires an open state to work. Furthermore, it is feasible that these channels will be activated by hyperpolarization evoked by opening of smooth muscle K_{ATP} channels. In addition, HCN channels *in situ* in the vasculature will conceivably possess different activation characteristics to those reported for cardiac I_f since these channels are regulated principally by cAMP, but also by other factors such as levels of $PI(4,5)P_2$ (reviewed by Wahl-Schott & Biel, 2009).

4.4.iv Potential off-target effects of HCN channel blockers in resistance arteries

In sharp microelectrode experiments conducted on rat mesenteric arteries mounted under isometric tension, ZD7288 (10 μM) reduced the hyperpolarization from resting membrane potential to levcromakalim (**Figure 4.3.2B**), isoprenaline (**Figure 4.3.2C**) and ACh (**Figure 4.3.2D**). 1 μM ZD7288 did not significantly inhibit the hyperpolarization in all cases. Although not an original aim of this chapter, we

therefore sought to extend these observations by investigating the potential off-target actions of ZD7288 and ivabradine in rat mesenteric arteries. In arteries sub-maximally pre-contracted with PE, we found evidence that both ZD7288 and ivabradine concentration-dependently right-shifted the relaxation to ACh (**Figure 4.3.5** and **4.3.6**).

There are a number of possible explanations for this. ZD7288 did not appear to affect the endothelial cell Ca^{2+} response to ACh (**Figure 4.3.2E**) suggesting an influence downstream of the muscarinic M_3 receptor-mediated intracellular Ca^{2+} release via the $G_{q/11}$-IP_3-triggered pathway. The increase in endothelial cell Ca^{2+} activates eNOS and production of NO, as well as endothelial cell K_{Ca} channels, SK_{Ca} and IK_{Ca}. In our experiments, we included L-NAME to inhibit eNOS; therefore the K_{Ca} channels are the only other feasible target. From the resting state, ACh-evoked hyperpolarization is solely mediated by SK_{Ca} channels (Crane *et al.*, 2003). Therefore an effect of ZD7288 on hyperpolarization from rest (**Figure 4.3.2D**) suggests an effect against SK_{Ca} channels. From the depolarized state, as in our tension experiments, IK_{Ca} channels are also activated. In these experiments, apamin still further right-shifted the response curve after 10 μM ZD7288, indicating that if ZD7288 did inhibit SK_{Ca} channels, it was only partial (at least at this concentration). Interestingly, in the presence of ZD7288 the IK_{Ca} channel blocker TRAM-34 still had a large effect, suggesting that ZD7288 was more effective at blocking SK_{Ca} channels.

To better assess these proposed actions of ZD7288 or ivabradine directly on K_{Ca} channels, it would be informative to conduct single-channel patch-clamp of these

channels on isolated EC sheets or EC tubes, perhaps against the opening of these channels by NS309, an SK_{Ca} / IK_{Ca} opener with greater selectivity for the former (Strøbæk *et al.*, 2004). In our freshly isolated EC sheets, which have a depolarized resting membrane potential compared to the intact non-myogenically active artery (**Figure 3.3.12C**), NS309 (3 μM) hyperpolarized the membrane potential to -48.69 ± 7.2, *n*=6 (**Figure 3.4.1**). Inhibition of this response by ZD7288 or ivabradine would point towards a direct action against these channels.

In preliminary experiments we also observed an increase in basal endothelial cell Ca^{2+} activity to ZD7288 consistent with (direct or indirect) activation of VGCC in the smooth muscle, since the effect could be prevented by pre-treatment with nifedipine (1 μM). A study investigating the inwardly-rectifying cation current in rat bladder detrusor smooth muscle found ZD7288 (0.3-100 μM) increased the force of spontaneous contractions in this tissue; this would be consistent with opening of VGCC though was not investigated further in this study (Green *et al.*, 1996). ZD7288 has also been reported to inhibit T-type VGCC. In spermatocytes ZD7288 blocked native T-type currents with an IC_{50} of ~100 μM (Felix *et al.*, 2003); in pyramidal neurons it blocked T-type currents with an IC_{50} of ~41 μM (Sánchez-Alonso *et al.*, 2008). T-type VGCC have been reported in numerous vascular beds including mesenteric and cerebral (McNeish *et al.*, 2010); T-type currents have also been recorded from endothelial cells (Kuo *et al.*, 2011). However, it seems unlikely that T-type currents are relevant in our responses given the literature would propose a block of the channel, whilst we see apparent activation of VGCC.

From a clinical perspective these off-target effects of ivabradine, which is widely prescribed to treat angina and chronic heart failure, are concerning. Disturbance of normal endothelial K_{Ca} channel function has the potential to be highly detrimental since EDH, which operates principally via these channels, is so crucial in regulating tone in these small resistance arteries that determine tissue blood flow and pressure.

4.5 Conclusion

Data in this chapter support the presence and function of HCN channels within the resistance vasculature. They also highlight some potential off-target effects of commonly used blockers of HCN channels, indicating a need for careful interpretation of data relying on these compounds, particularly in the presence of K_{Ca} channels, which appear to be affected.

Together with data presented in **Chapter 3**, we propose that HCN channels in the vasculature can be activated to increase endothelial cell Ca^{2+} events by hyperpolarization evoked via activation of K_{ATP} channels by levcromakalim or (indirectly by) isoprenaline. This supports a unified mechanism, although the importance of this pathway requires future direct investigation.

CHAPTER 5

INVESTIGATING NAADP-MEDIATED CA^{2+} SIGNALLING IN VASCULAR SMOOTH MUSCLE

5.1 Introduction

Nicotinic acid adenine dinucleotide phosphate (NAADP) is the most recently described and potent second messenger (Lee, 1997). NAADP was originally discovered by Lee and colleagues as a contaminant of commercially available $NADP^+$ (Clapper *et al.*, 1987; Lee & Aarhus, 1995). Initial studies crucially identified that NAADP released Ca^{2+} from stores distinct from those targeted by IP_3 through use of Percoll density gradient centrifugation (Lee & Aarhus, 1995). These stores were thapsigargin-insensitive (Genazzani & Galione, 1996) and were subsequently identified as lysosomal-like stores: the organelles stained with a label of acidic stores (Lysotracker Red) and were also sensitive to glycyl-L-phenylalanine-β-naphthylamide (GPN, Churchill *et al.*, 2002). GPN lyses the acidic organelles, disrupting the Ca^{2+} store (Haller *et al.*, 1996).

5.1.i Acidic organelles as Ca^{2+} stores

Historically, the major function of the endo-lysosomal pathway is protein degradation, be it endocytosed proteins or intracellular proteins engulfed through autophagy. During endocytosis transport vesicles bud from the plasma membrane containing engulfed material; these transport vesicles become endosomes. The early endosome is mildly acidic and invaginates its own membrane to internalize membrane proteins for digestion, forming intraluminal vesicles (ILVs). Early endosomes are characterised by a high proportion of transferrin, which is lost during maturation into late endosomes; late endosomes are characterised by a much higher number of ILVs. Late endosomes eventually fuse with lysosomes, emptying their contents before recycling back to the plasma membrane. Lysosomes contain

many hydrolytic enzymes and are the most acidic component (pH = 4-5 vs. endosomes pH = 6) (Patel & Docampo, 2010).

The lysosomal membrane has a characteristic composition of cholesterol, phospholipids and a high level of carbohydrates; glycosylation is important for stability in the membrane. Lysosomal membrane proteins are responsible for acidification of the lumen, transport of macromolecules resulting from the hydrolytic degradation, and are involved in fusion of lysosomes with themselves and with endosomes, phagosomes and the plasma membrane. Several highly glycosylated proteins have been identified, e.g. lysosome associated membrane protein (LAMP) -1 and -2, first described in 1985 (Chen *et al.*, 1985). LAMPs are major components of lysosomal and late endosomal membranes, constituting approximately 50% of total membrane proteins. LAMP-1 and LAMP-2 share 37% sequence homology. The high glycosylation helps to maintain a tight barrier between the highly acidic intralysosomal environment of hydrolases and the cytosol. The generation of knockout mice has suggested functions in addition to structural integrity. LAMP-1 knockout mice are viable and fertile, with very little observable difference in phenotype to that of wild-type mice (Andrejewski *et al.*, 1999); however, LAMP-2 knockout mice show a pronounced phenotype with 50% of litter dying aged 20-40 days. Electron microscopy showed this was due to massive accumulation of autophagic vacuoles in many tissues (Tanaka *et al.*, 2000). This points to an important role for LAMP-2 in maturation of autophagosomes. LAMP-1 / LAMP-2 double knockout is embryonically lethal (Eskelinen *et al.*, 2004). LAMP proteins have a short cytosolic tail responsible for targeting the protein to the lysosome; this tail has also been recognised as important for directing proteins with a KFERQ motif

for degradation via a specific chaperone-mediated autophagy (CMA) pathway. It also appears to be required for lysosomal movement within the cell since a lack of LAMP proteins causes lysosomes to accumulate at the cell periphery (Schwake *et al.*, 2013).

Since the 1970s it has been known that the endosomal pathway organelles are also stores of Ca^{2+}, observed using electron microscopy and histochemical techniques (Patel & Docampo, 2010). Endosomal [Ca^{2+}] has also been difficult to measure, with contradictory reports. One suggests endosomes lose the Ca^{2+} they engulf with invagination of the plasma membrane as they acidify; the other suggests a concentration of approximately 40 μM (Patel & Muallem, 2011). Using internalized fluorescent indicators, intra-lysosomal free [Ca^{2+}] is estimated to be approximately 500 μM, a similar concentration to that in the endoplasmic reticulum (Patel & Docampo, 2010). It is thought that the large proton gradient across the specialized endolysosomal membrane is utilized for mediating Ca^{2+} entry. Whilst Ca^{2+}/H^{+} exchangers have been observed in plant and yeast vacuoles, these may be absent in mammals (Shigaki & Hirschi, 2006); rather, it is postulated that proton pumps combine with Na^{+}/H^{+} exchangers coupled to Na^{+}/Ca^{2+} exchangers. Regardless, the lysosomal accumulation of Ca^{2+} depends on a proton gradient.

Traditionally thought to be required for trafficking and fusion events, an additional role for endolysosomal Ca^{2+} stores in signalling pathways involving NAADP has now emerged.

5.1.ii The NAADP receptor

Much controversy exists regarding the molecular identity of the NAADP receptor. In 2009 Calcraft *et al* and others independently converged on two-pore channels (TPCs) as a target for NAADP (Brailoiu *et al.*, 2009; Calcraft *et al.*, 2009; Zong *et al.*, 2009).

TPCs were originally cloned from rat in 2000 (Ishibashi *et al.*, 2000). These channels are members of the superfamily of voltage-gated ion channels and three isoforms (TPC1-3) exist with significant sequence similarity to voltage-gated Ca^{2+} and Na^{+} channels. Only TPC1 and TPC2 are present in mice, rats and humans, and appear to be differentially distributed with TPC1 reportedly endosomal and lysosomal, whilst TPC2 appears restricted to lysosomes (Brailoiu *et al.*, 2009; Calcraft *et al.*, 2009). Multiple lines of evidence made a convincing case for the TPC to be the true NAADP receptor. In HEK293 cells, HA-tagged TPC overlapped with staining for the LAMP-2 and surrounded intracellular stores that stained with Lysotracker Red. A radioactive binding assay using [^{32}P]NAADP suggested NAADP binds TPC with high affinity (Calcraft *et al.*, 2009). This was consistent with single-channel measurements using lipid bilayers which show TPC is highly selective for Ca^{2+} and dependent on intralysosomal pH and [Ca^{2+}]. It has also been shown that very low levels of NAADP can open the channel, which supports the notion that NAADP is the most potent second messenger (Lee & Aarhus, 1995; Pitt *et al.*, 2010; Schieder *et al.*, 2010). Furthermore, electrophysiological measurements of TPC directed to the plasma membrane instead of the lysosomal membrane, which uncoupled NAADP-evoked Ca^{2+} release from the subsequent global Ca^{2+} rise, clearly demonstrated sensitivity of TPC to NAADP (Brailoiu *et al.*, 2010a).

Unexpectedly however, photoaffinity labelling of NAADP using a probe based on 5-azido-NAADP showed no staining of endogenous or overexpressed TPC (Lin-Moshier *et al.*, 2012) despite exhibiting robust binding and characteristic Ca^{2+} release from sea urchin egg homogenate (Walseth *et al.*, 2012). Instead, NAADP was seen to bind cytosolic proteins, although these are yet to be characterised. This led to the alternative suggestion that TPC may be the Ca^{2+} channel but that it is part of a larger receptor complex that NAADP binds; indeed, it has been hypothesized that NAADP binds cytosolic proteins, which then bind the Ca^{2+} release channel (TPC or others, see below) (Guse, 2013). NAADP has been shown to withstand 5′ substitution (Jain *et al.*, 2010) and this technique has been used successfully to demonstrate agonist-receptor binding for other proteins, e.g. 8-azido-ATP binding to K_{ATP} channels (Tanabe *et al.*, 1999).

Most recently it has been proposed that TPC1 and TPC2 are actually Na^{+} channels, rather than Ca^{2+} channels, and sensitive to PIP_2 rather than NAADP (Wang *et al.*, 2012; Cang *et al.*, 2013). However, these studies used artificially enlarged endolysosomes (to allow a direct whole-cell patch of the endolysosomal membrane proteins) and in some cases tagged TPC with GFP at the N-terminus. It has since been demonstrated that N-terminal tagging of TPC removes its NAADP sensitivity (Churamani *et al.*, 2013), which may be a reason for the reported negative result. It has also been proposed that TPC subtypes have different properties, and human TPC1 reconstituted in lipid bilayers has most recently been shown to pass protons and monovalent cations preferentially over Ca^{2+} (Pitt *et al.*, 2014). Furthermore it

was shown that PIP_2 did not alter TPC open probability, but did shift the relative permeability to Na^+, going someway to resolving the Na^+ channel reports.

Other channels have also been suggested as targets for NAADP-mediated Ca^{2+} release. TRPML1 was so-named after the mutated gene was identified as the cause of lysosomal storage disease mucolipidosis type IV. These channels have a well-established role in ion homeostasis and membrane trafficking in the endosomal pathway, so are certainly present and functional in acidic stores. TRPML channels are non-selective cation channel permeable to Na^+, K^+ and Ca^{2+}, and reportedly regulated by pH and Na^+ (Yamaguchi *et al.*, 2011). TRPML1 has also been suggested to transport Fe^{2+} (Dong *et al.*, 2008). One group has used siRNA and blocking antibodies for TRPML1 in coronary arterial myocytes to propose a role for this channel in the NAADP response (Zhang & Li, 2007; Zhang *et al.*, 2009; Zhang *et al.*, 2011). In contrast, a direct comparison of TRPML1 and TPC function in response to NAADP stimulation showed a lack of effect of a dominant negative TRPML1 construct on the endogenous NAADP response, whilst overexpression of TPC enhanced the response (Yamaguchi *et al.*, 2011). The two proteins both appear to reside on the acidic stores, and it has been suggested that TRPML1 might have a regulatory role for TPC rather than being a direct target for NAADP (Abe & Puertollano, 2011).

Ryanodine receptors have also been proposed as the NAADP receptor (Gerasimenko *et al.*, 2003), but again evidence to the contrary has also been reported (Copello *et al.*, 2001). This is complicated by frequent reports from multiple cell types of channel 'chatter' and signalling between lysosomes and the

endoplasmic reticulum (ER) due to Ca^{2+}-induced Ca^{2+} release (Boittin *et al.*, 2002; Kinnear *et al.*, 2004; Kinnear *et al.*, 2008) and lysosomes have been visualised to make close contact with the ER (Kilpatrick *et al.*, 2013). Most recently it has been proposed that Ca^{2+} released from the ER could trigger endolysosomal Ca^{2+} release, through indirect measurement of lysosomal Ca^{2+} store pH, which alkalinises following NAADP-induced Ca^{2+} release (Morgan *et al.*, 2013). Furthermore, lysosomal stores may sequester ER Ca^{2+} and shape an IP_3-mediated response since bafilomycin A1 (by inhibiting the H^+-ATPase is an indirect inhibitor of lysosomal Ca^{2+} uptake) increased the Ca^{2+} transient to the G_q-coupled muscarinic receptor agonist, carbachol (López-Sanjurjo *et al.*, 2013).

5.1.iii NAADP receptor pharmacology

An unusual property of the NAADP receptor has been observed since the discovery of NAADP as a second messenger: NAADP has a bell-shaped concentration-response curve, such that low or high concentrations of NAADP will inactivate the receptor (Genazzani *et al.*, 1996; Lee, 1997). This property has often been utilised to inhibit NAADP-mediated Ca^{2+} release (Macgregor *et al.*, 2007). Ned-19 was discovered using high-throughput screening of the ZINC database for compounds with similar three-dimensional structure and electrostatic properties to that of NAADP (Naylor *et al.*, 2009). It is therefore believed to share the binding site for NAADP. Using analogues of Ned-19, two binding sites have been shown to exist on the receptor: one low-affinity opening site and one high-affinity locking site (Rosen *et al.*, 2009). Of note, Ned-19 has since been shown to act as a partial agonist at nanomolar concentrations, whilst being an effective inhibitor at micromolar

concentrations (Pitt *et al.*, 2010). To date it is the only proposed NAADP receptor antagonist.

Other pharmacological tools commonly used to investigate NAADP signalling are compounds that disrupt the acidic Ca^{2+} store. GPN has already been mentioned as an early commonly used tool. It is a cell-permeable di-peptide substrate for the lysosomal acid hydrolase cathepsin C. It causes osmotic permeabilisation of the organelle, which releases lysosomal proteases and protons as well as disrupting the Ca^{2+} store (Haller *et al.*, 1996). A major caveat of disrupting acidic organelles is the simultaneous release of protons and proteases into the cytosol of the cell with unknown effects, making it unfavourable to use in physiological systems although still employed in some cell studies (López-Sanjurjo *et al.*, 2013). Bafilomycin A1 has already been mentioned and is an inhibitor of the H^+-ATPase (proton pump) residing on the endolysosomal membrane. This pump facilitates accumulation of Ca^{2+}; therefore, by inhibiting the pump, further Ca^{2+} accumulation is prevented. Since bafilomycin A1 does not directly cause release of Ca^{2+}, the level of constitutive activity of Ca^{2+} release from the acidic store will determine how quickly it empties: sometimes it is necessary to stimulate lysosomal Ca^{2+} release to ensure the store is empty.

NAADP responses are also inhibited by blockers of L-type Ca^{2+} channels e.g. diltiazem, nifedipine, at least in sea urchin eggs and some other mammalian tissues. In sea urchin eggs, both blockers inhibited the alkalinisation of acidic organelles in response to uncaging NAADP (Morgan *et al.*, 2013). PPADS, a nucleotide mimetic

and inhibitor of P2 receptors, has also been used to inhibit NAADP responses (Billington & Genazzani, 2007; Morgan *et al.*, 2013).

5.1.iv The role of NAADP-mobilised Ca^{2+} in the cardiovascular system

Although originally studied in sea urchin eggs (Clapper *et al.*, 1987), the functional importance of NAADP as a Ca^{2+}-mobilising second messenger is emerging in many mammalian systems, including the cardiovascular system. In cardiac atrial myocytes, photo-release of caged NAADP, or application of cell-permeant NAADP-AM, induces a transient rise in Ca^{2+} that is sensitive to bafilomycin A1, ryanodine and thapsigargin (Collins *et al.*, 2011). It was proposed that NAADP-released Ca^{2+} might be taken up by the sarcoplasmic / endoplasmic reticulum Ca^{2+}-ATPase (SERCA) thereby increasing SR Ca^{2+} load. In support, isoprenaline (β-adrenoceptor agonist) induced a Ca^{2+} transient in these cells, which was sensitive to bafilomycin A1 and GPN (Collins *et al.*, 2011). Furthermore, measurement of NAADP and cADPR levels in response to β-adrenergic activation showed a transient increase in NAADP, with a more sustained increase in its sister compound, cADPR (Lewis *et al.*, 2012).

Evidence supporting an endogenous role for NAADP extends to the vasculature. Imaging studies of isolated rat pulmonary artery smooth muscle cells show a NAADP-triggered 'Ca^{2+} burst' at the periphery of the cell, resulting in a global Ca^{2+} wave and contraction in 80% of cells (Boittin *et al.*, 2002). Notably, generation of the Ca^{2+} wave was necessary for contraction, hence the investigators propose a threshold for initiation of the Ca^{2+} wave. To date, this has not been characterised. Thapsigargin (a SERCA inhibitor) and ryanodine receptor (RyR) inhibitors prevented

generation of the Ca^{2+} wave, but not the initial Ca^{2+} burst, supporting the concept of a 'trigger hypothesis' in which Ca^{2+} released from lysosomal stores by NAADP triggers Ca^{2+} release from the sarcoplasmic reticulum (SR) through RyR in a Ca^{2+}-induced Ca^{2+} release (CICR) mechanism. In pulmonary arterial smooth muscle cells, Ca^{2+} imaging combined with immunocytochemistry shows co-localisation of clusters of lysosomes with RyRs on the SR, specifically RyR subtype 3 (Kinnear *et al.*, 2004; Kinnear *et al.*, 2008). Their proposal of a lysosomal-sarcoplasmic reticulum junction is consistent with the trigger hypothesis concept outlined above, as well as bidirectional communication recently proposed (Morgan *et al.*, 2013) and may provide a reason for a number of conflicting reports implicating RyR as the alternative target for NAADP (Gerasimenko *et al.*, 2003; Dammermann *et al.*, 2009). Another group has investigated NAADP signalling in coronary arterial myocytes, where Ca^{2+} released by NAADP has been linked to Fas activation (Zhang *et al.*, 2006; Zhang *et al.*, 2010).

There have been two reports to date describing a role for NAADP in the endothelium. In human cultured umbilical vein endothelial cells, NAADP was implicated as a crucial second messenger for the Ca^{2+}-mediated secretion of von Willebrand factor following histamine H1 receptor activation, using either Ned-19 (50 μM) or siRNA knockdown of TPC1 and TPC2. Also in these cells, Ned-19 staining was seen to overlap with that of Lysotracker Red (Esposito *et al.*, 2011). In addition, Brailoiu and colleagues have provided evidence that NAADP-mediated Ca^{2+} release is involved in aortic tone-modulating pathways. Cell-permeant NAADP-AM concentration-dependently evoked Ca^{2+} transients in human aortic endothelial cells cultured *in vitro*, which were attenuated by ryanodine and inhibited by Ned-19 (1 μM)

or bafilomycin A1, consistent with the idea that NAADP-released Ca^{2+} from acidic stores triggers CICR from the ER through RyRs. Use of a NO indicator (DAF-FM) showed NAADP-AM-induced Ca^{2+} transients couple to NO release, whilst use of a voltage-sensitive dye, ($DiBAC_4$) and K_{Ca} channel blockers, apamin (SK_{Ca} channel-selective) and charybdotoxin (IK_{Ca} channel- and BK_{Ca} channel-selective) suggest NAADP-released Ca^{2+} can activate the EDHF pathway (Brailoiu *et al.*, 2010b). In conflict with these data obtained in cultured endothelial cells, there is no evidence for a role for RyR in the endothelium of intact arteries, either in spontaneous Ca^{2+} events or in agonist-mediated Ca^{2+} responses (Kansui *et al.*, 2008). Thus, it is possible that the findings in cultured cells may not reflect those in intact arteries.

NAADP-mediated Ca^{2+} release has therefore been implicated in major tone-modulating pathways in both cell types in the vascular wall, prompting further investigation at a cellular and perhaps more importantly, at a functional level in intact vessels.

5.1.v Ca^{2+} spark modulation of STOCs

Since the initial studies identifying Ca^{2+} sparks originating from RyR in vascular smooth muscle there have been several reports characterising their parameters – amplitude, duration and spatial spread (Nelson *et al.*, 1995; Pérez *et al.*, 1999). It has also been proposed in some tissues that RyRs may distribute on the SR membrane into regions of higher density where sparks are more commonly initiated. These have been described as 'frequent discharge sites' in rabbit portal vein myocytes (Gordienko *et al.*, 2001; Wray *et al.*, 2005).

It is now well established that spontaneous Ca^{2+} sparks from RyR activate large conductance Ca^{2+}-activated K^+ (BK_{Ca}) channels in the sarcolemma. The resulting small outward K^+ current is termed a spontaneous transient outward current (STOC), first described by Benham and Bolton (Benham & Bolton, 1986). In cerebral artery myocytes held at -40 mV, almost all detected Ca^{2+} sparks were associated with a STOC and were correlated in amplitude (Pérez *et al.*, 1999). Thus in smooth muscle, unlike cardiac and skeletal muscle where Ca^{2+} sparks contribute positively to contraction, Ca^{2+} sparks serve to hyperpolarize the myocytes and limit muscle contraction. Indeed a single STOC has been shown to elicit a significant hyperpolarization (>20 mV; Ganitkevich & Isenberg, 1990).

To date much of the evidence linking Ca^{2+} sparks with STOCs has been pharmacological, using ryanodine or SERCA inhibitors (CPA or thapsigargin) to inhibit Ca^{2+} sparks, and using iberiotoxin or tetraethylammonium (TEA) to block STOCs. The resulting vasoconstriction and depolarization after block of BK_{Ca} channels with iberiotoxin illustrates the critical importance of this tone-modulating Ca^{2+} pathway (Brenner *et al.*, 2000). BK_{Ca} channels are also sensitive to paxilline (Sanchez & McManus, 1996; Li & Cheung, 1999).

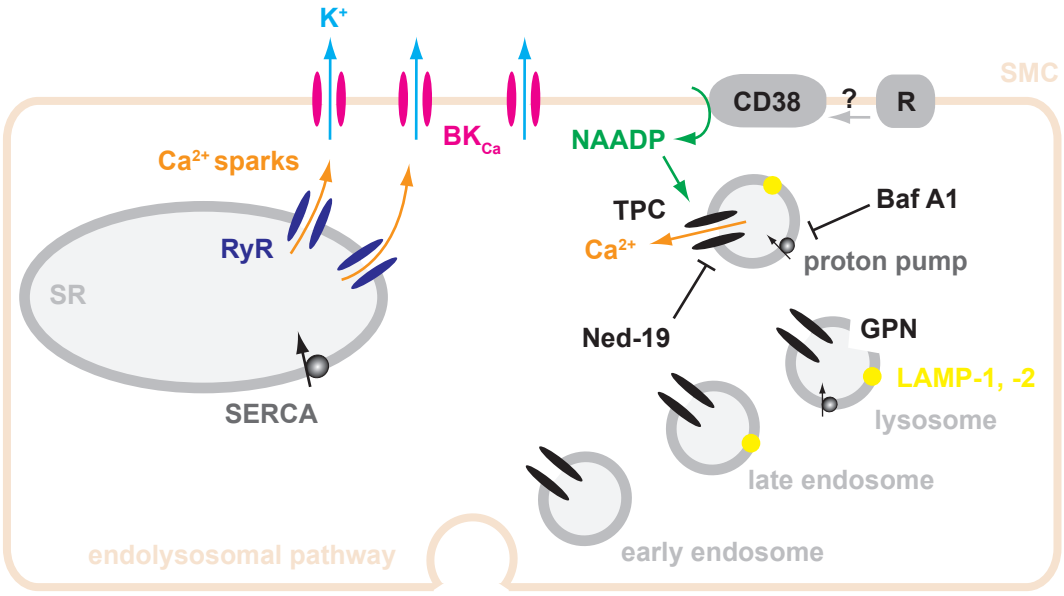

Figure 5.1.1 Proposed NAADP signalling pathway in the vasculature
Schematic illustrating the proposed Ca^{2+}-mobilising signalling pathway in vascular smooth muscle. Abbreviations: Baf A1 - bafilomycin A1; BK_{Ca} - large conductance Ca^{2+}-activated K^+ channel; CD38 - CD38 ectoenzyme believed to be responsible for NAADP synthesis; GPN - glycyl-L-phenylalanine-β-naphthylamide; LAMP - lysosome associated membrane protein; NAADP - nicotinic acid adenine dinucleotide phosphate; R - receptor; RyR - ryanodine receptor; SERCA - sarcoplasmic / endoplasmic reticulum Ca^{2+} ATPase; SMC - smooth muscle cell; SR - sarcoplasmic reticulum; TPC - two-pore channel.

The aim of the experiments in this chapter was therefore to explore the potential role of NAADP in vascular smooth muscle cells and establish whether it modulates vascular tone.

5.2 Methods & Materials

*Refer to **Chapter 2: Methods & Materials** for full details of the methods used in this chapter. Details relevant specifically to this chapter are given below.*

5.2.i Wire myography

*Refer to **Methods & Materials section 2.2** for full details of the method for mounting arteries under isometric tension in wire myography experiments.*

For experiments studying the relaxing effect of NAADP-AM, rat third order mesenteric arteries were pre-constricted with 1 μM U46619. U46619 was used rather than PE (as used in the initial function tests) because U46619 produces a more sustained contraction. We hypothesize this could be due to the additional activation of the Ca^{2+} sensitisation pathway via $G_{12/13}$ and Rho kinase. 1 μM U46619 was determined in preliminary experiments to be a sub-maximal concentration that gave a sustained contraction (**Figure 5.2.1**).

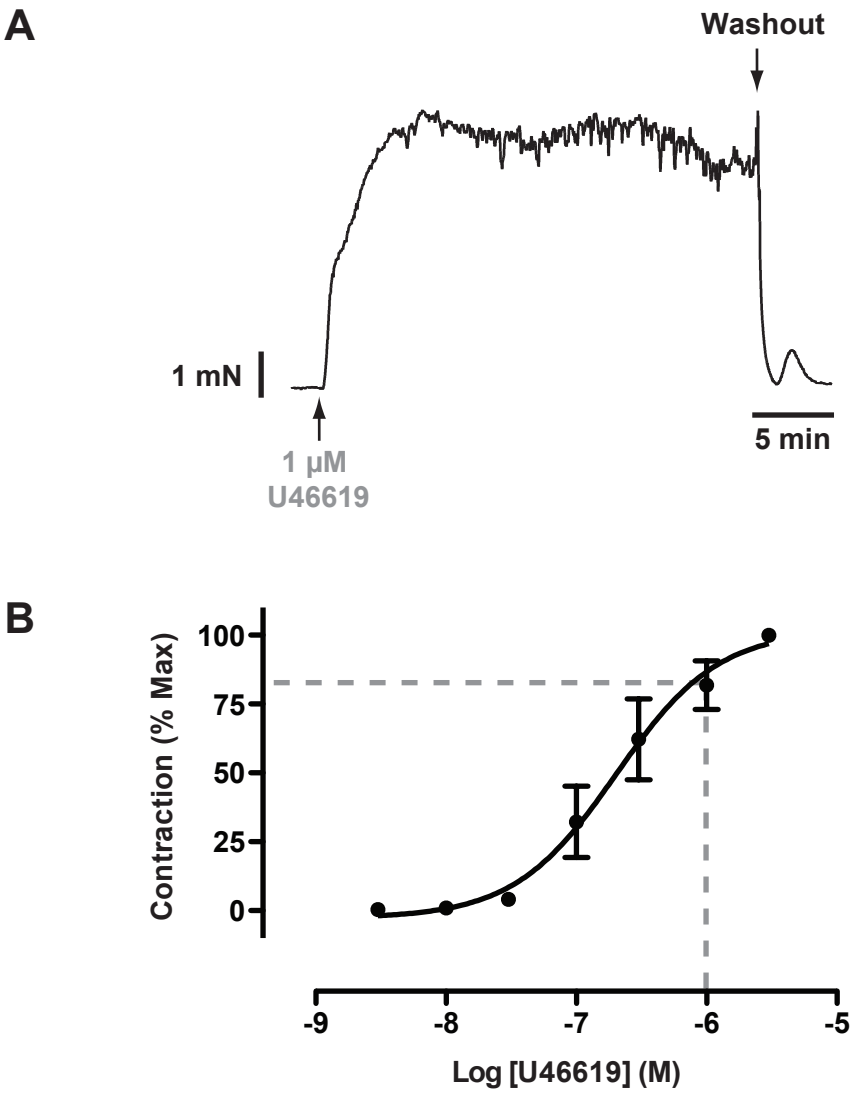

Figure 5.2.1 The thromboxane mimetic U46619 is used to generate sustained contraction

A Representative trace of sustained contraction of rat mesenteric arteries after addition of 1 μM U46619 to the tissue bath, followed by washout. **B** U46619 concentration-response curve demonstrating 1 μM is a sub-maximal concentration. LogEC_{50} = -6.7, *n*=6. Contraction is expressed as a percentage of the maximal contraction achieved by 3 μM.

5.2.ii Immunohistochemistry

Rat third order mesenteric arteries were cannulated, pressurized to 70 mmHg and tested for viability as described in **Methods & Materials section 2.3**. Vessels were fixed and blocked on Day 1, and imaged on Day 2 as described in **Methods & Materials section 2.4**.

5.2.iii Pressure myography

Rat third order mesenteric arteries were cannulated, pressurized to 70 mmHg and tested for viability as described in **Methods & Materials section 2.3**.

In experiments investigating live cell staining, Ned-19 (10 μM) was added directly to the bath (abluminally). Staining was visible within 30 min using confocal microscopy at 405 nm with a confocal aperture of 200 μm. Lysotracker Red (0.1 μM) was applied abluminally on top of Ned-19, and was visible within 5 min with excitation wavelength 543 nm. There was no crossover of the dyes, so Ned-19 staining could be acquired in parallel with Lysotracker Red staining using sequential scanning mode. Calcein AM (12.5 μM) was also added abluminally to illustrate the location and orientation of the smooth muscle cells.

5.2.iv Patch-clamp studies of freshly isolated smooth muscle cells

Cells were prepared as described in **Methods & Materials section 2.5.i**. For analysis of K^+ currents, smooth muscle cells were patched in the whole-cell configuration in voltage-clamp mode, using an Axopatch 200B amplifier, Digidata 1200 interface and pCLAMP 8.0 software (Axon Instruments, USA) at sample rate 10 kHz, filter rate 2 kHz. Experiments were conducted at room temperature, with

continuous superfusion (1 mL min^{-1}) of HEPES-buffered solution (*refer to* ***Methods & Materials section 2.6***). Patch pipettes were pulled from borosilicate glass capillaries (OD 1.2 mm x ID 0.69 mm, Harvard Apparatus, USA) using a horizontal micropipette puller (Model P-87, Sutter Instruments, USA). When filled, pipette resistance measured 3-10 MΩ. For each cell patched, the cell membrane capacitance (Cm) was assessed immediately after breaking through the cell membrane. The capacitance was then calculated by integrating the area under the capacitance artefact elicited by a 10 mV hyperpolarizing step, filter rate 10 kHz (**Figure 5.2.2C**). The capacitance of a cell is an indication of the size of the cell membrane, and therefore was used to normalize cell currents to the size of the cell (current density = current / cell capacitance (pA/pF)). Cell capacitance was 5.83 ± 0.7 pF (*n*=8) across all smooth muscle cells successfully patched. From 30 s after breakthrough, K^+ currents were monitored using a voltage step protocol, which used a holding potential of -60 mV, stepping to +60 mV for 300 ms every 10 s (**Figure 5.2.2D**). At 5 min, 10 min, 20 min, 30 min, 40 min an IV protocol was performed in order to assess the current-voltage relationship over time with dialysis of the pipette solution. This protocol used a holding potential of -70 mV, stepping between -80 mV and +60 mV in 10 mV increments every 200 ms (**Figure 5.2.2E**). In experiments studying the effect of NAADP, 0.1-10 μM NAADP was added to the pipette solution just prior to patching. Paxilline (1 μM) was delivered to the patched cells via the superfusion and an IV protocol performed after the short delay (~2 min) in reaching the cell. Arrival of paxilline was evident from the currents in the Step protocol, and the IV protocol for the presence of paxilline was performed after this point.

To study the effect of NAADP on the spontaneous transient outward currents (STOCs), cells were patched in continuous mode to monitor the K^+ currents continually. After breakthrough and recording of cell capacitance (as above), cells were held at -40 mV for 30 s; STOCs were occasionally, but not generally, observed at this potential. The membrane potential was then stepped to -20 mV for ~10 min where STOCs were routinely observed. For analysis, STOCs were sampled in the interval 1.5-6.5 min after breakthrough.

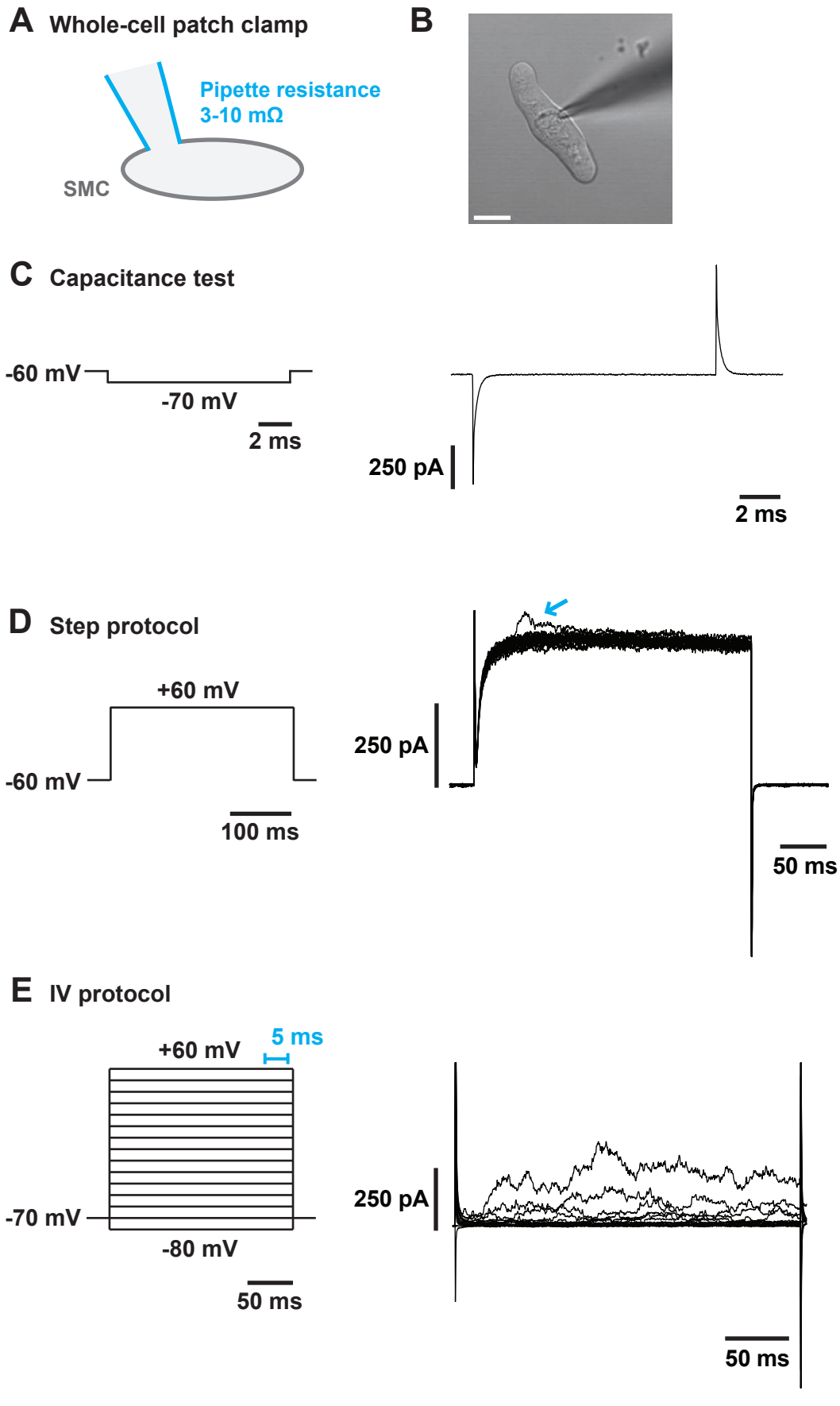
A Whole-cell patch clamp
Pipette resistance
3-10 mΩ
SMC
B
C Capacitance test
-60 mV
-70 mV
2 ms
250 pA
2 ms
D Step protocol
+60 mV
-60 mV
100 ms
250 pA
50 ms
E IV protocol
+60 mV
5 ms
-70 mV
-80 mV
50 ms
250 pA
50 ms

Figure 5.2.2 Whole-cell patch-clamp of vascular smooth muscle cells
A Simplified schematic illustrating the whole-cell configuration of the patch-clamp technique used to assess K^+ currents across the entire cell membrane of freshly isolated smooth muscle cells (SMC) from rat mesenteric arteries. Over time the pipette solution dialyses with the cell cytosol. **B** Representative image of patched SMC (scale bar = 10 μm). **C** Protocol for measuring the cell capacitance (pF), with a representative trace. This protocol was performed immediately after achieving breakthrough of the membrane. The integral of the capacitance artefact is used as a measure of the cell size, and was used to normalise the currents to current density. **D** Step protocol for monitoring K^+ currents during dialysis of the pipette solution, with a representative trace from control conditions (**right**). The membrane potential was held at -60 mV and stepped to +60 mV for 300 ms to activate K^+ currents. Arrow indicates additional spontaneous transient outward current (STOC) activity on top of the outward K^+ current through BK_{Ca} and K_v channels. **E** IV protocol for measuring the current-voltage relationship over time, with a representative trace from control conditions (**right**). This protocol was performed at 5 min, 10 min, 20 min, 30 min and 40 min (where the patch lasted this long). The membrane potential was held at -70 mV, and stepped from -80 mV through to +60 mV in 10 mV increments, for 200 ms at each potential.

5.2.v Solutions and drugs

For all experiments except patching experiments, MOPS-buffered solution was used (refer to **Methods & Materials section 2.6** for composition). For patching experiments, HEPES-buffered solution was used extracellularly (refer to **Methods & Materials section 2.6** for composition). The pipette solution for whole-cell voltage-clamp patching experiments studying K^+ currents contained (mM): KCl, 140.0; $MgCl_2.6H_2O$, 0.5; EGTA, 0.1; Mg.ATP, 2.0; HEPES, 5.0; at 37ºC, pH 7.20 ± 0.02 adjusted with NaOH. The pipette solution for whole-cell voltage-clamp patching experiments studying STOC activity contained (mM): KCl, 140.0; $MgCl_2.H_2O$, 0.5; EGTA, 1.0; Mg.ATP, 2.0; HEPES, 5.0; $CaCl_2.2H_2O$, 0.35; at 37ºC, pH 7.20 ± 0.02 adjusted with NaOH. In this solution 1 mM EGTA + 0.35 mM Ca^{2+} gave a free [Ca^{2+}] of 0.92 μM.

*Refer to **Table 2.6.1** for full details of the drugs and chemicals used in this chapter.*

5.2.vi Statistical analysis

Refer to ***Methods & Materials section 2.7***.

For analysis of whole-cell K^+ currents, Clampfit 9 (Molecular Devices, USA) software was used to analyse the current-voltage relationship during control and treatments.

For analysis of STOCs, Clampfit 9 software was used to select the interval 1.5-6.5 min after breakthrough. Mini Analysis (Synaptosoft Inc., USA) software was then used to assess the characteristics of the STOCs within this time frame. STOC 'events' were automatically found using the following search parameters:

Threshold	8 pA
Period to search for a local maximum	50,000 μs
Time before a peak for baseline	50,000 μs
Period to search a decay time	20,000 μs
Fraction of peak to find a decay time	0.333
Period to average a baseline	20,000 μs
Area threshold	0
Peak direction	Positive

These automatically selected events were then checked manually by eye. 8 pA was defined as the threshold for recording a STOC as this represents ~3 times the unitary current of a BK_{Ca} channel (Pérez *et al.*, 1999).

5.3 Results

In this chapter we sought to characterise a role for NAADP in vascular smooth muscle. As discussed in **section 5.1**, NAADP is believed to target lysosomal-like acidic stores of Ca^{2+}. Thus, to initially demonstrate the presence of such stores in vascular smooth muscle, we fixed pressurized rat mesenteric arteries and performed immunohistochemistry to establish the expression pattern of the endolysosomal membrane protein, LAMP-2. As shown in **Figure 5.3.1**, punctate staining of this vesicular marker is clearly visible in all layers of smooth muscle and uniformly throughout all cells in the field of view; indeed this was observed across the length of the artery. LAMP-2 staining is also visible in the endothelial cell layer and of note, sometimes appears to congregate in areas aligning with holes in the IEL (**Figure 5.3.2**). Endothelial cell projections pass through these holes to make contact with smooth muscle cells. Known as myoendothelial junctions, these are highly significant signalling microdomains for heterocellular communication and regulation of vascular tone (see **Chapter 1 section 1.3**).

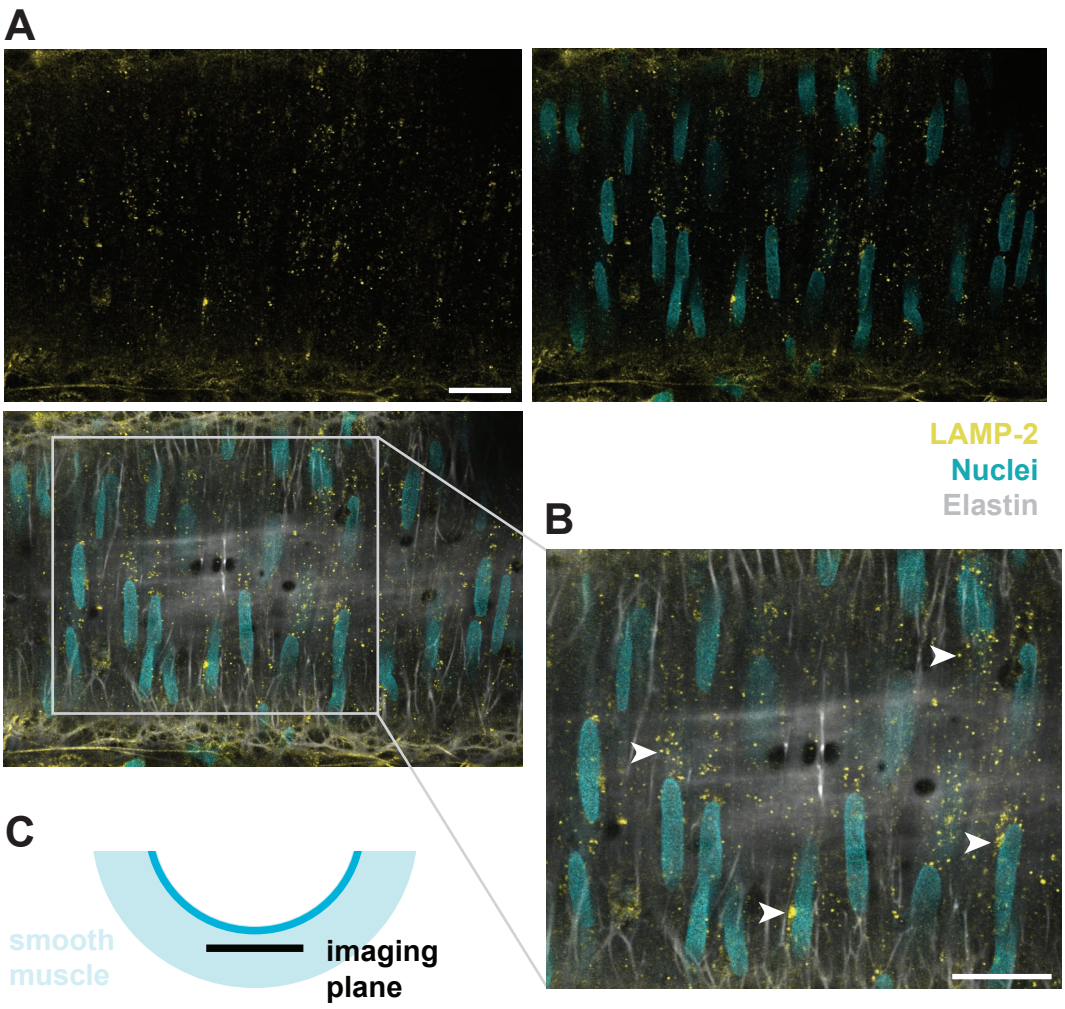

Figure 5.3.1 Acidic organelles containing LAMP-2 are present in vascular smooth muscle cells
A LAMP-2 fluorescence is visible as punctate, uniformly distributed staining (**top left**, yellow) in all layers of the smooth muscle of rat pressurized mesenteric arteries. Scale bar = 20 μm, applicable to all images. **Right** Nuclei stained with propidium iodide (45 μM, cyan) illustrate the vertical orientation of the smooth muscle cells. **Bottom left** Alexa 633 hydrazide (1 μM, grey) stains the elastin in between smooth muscle cells and the internal elastic lamina (visible beneath the inner smooth muscle layer). **B** Insert shows LAMP-2 staining is uniform across all smooth muscle cells (arrowheads). Scale bar = 20 μm. **C** Schematic to illustrate the focal plane for acquisition of images within the smooth muscle cell layers. Images are representative of *n*=3.

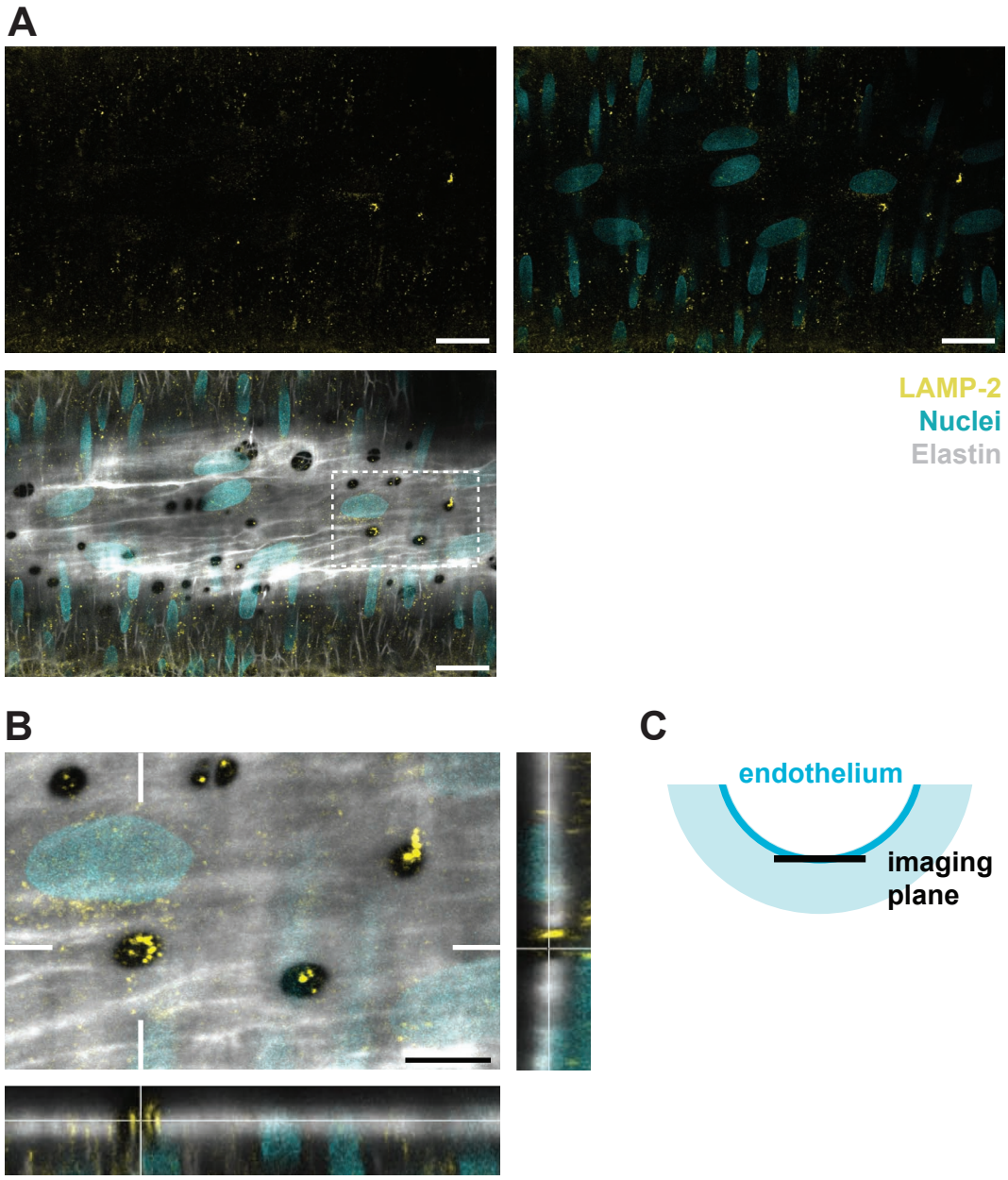

Figure 5.3.2 Acidic organelles containing LAMP-2 are present in endothelial cells
A LAMP-2 fluorescence (yellow) is visible in the endothelial cell layer (**top left**) of rat pressurized mesenteric arteries. Scale bar = 20 μm, applicable to all images. Endothelial cell orientation is illustrated by nuclei staining with propidium iodide (45 μM, cyan, **right**) showing cells aligned horizontally, with the inner smooth muscle cell nuclei arranged vertically, visible at the top and bottom of the image. On occasion, endothelial cell LAMP-2 expression aligned with holes in the internal elastic lamina, which was stained with Alexa 633 hydrazide (1 μM, grey, **bottom left**). **B** Higher magnification image with 3D reconstruction of the z-plane in the x- (right) and y- (bottom) axes to support the alignment of LAMP-2 staining in some IEL holes. Scale bar = 20 μm. **C** Schematic to illustrate the focal plane for acquisition of images within the endothelial cell layer. Images are representative of n=3.

To link the presence of lysosomal-type acidic organelles to NAADP signalling, we utilized the fluorescent property of the NAADP receptor antagonist, Ned-19 (Naylor *et al.*, 2009; Esposito *et al.*, 2011). Ned-19 (10 μM) was applied abluminally to a pressurized artery. After the fluorescence of Ned-19 became visible, the acidic organelle dye Lysotracker Red (0.1 μM) was also applied. Ned-19 fluorescence emission is collected in the 450-480 nm channel, whilst Lysotracker Red fluorescence is visible in the 560-660 nm channel. We therefore imaged both simultaneously at different wavelengths and observed punctate staining in the smooth muscle (**Figure 5.3.3**). The pattern of staining is similar to that of LAMP-2: punctate and uniform within and across all cells. It appeared that a small sub-population of organelles that stained with Lysotracker Red did not stain with Ned-19. Finally, calcein AM (12.5 μM) was applied to stain actin and illustrate the orientation and location of the smooth muscle cells (**Figure 5.3.3**).

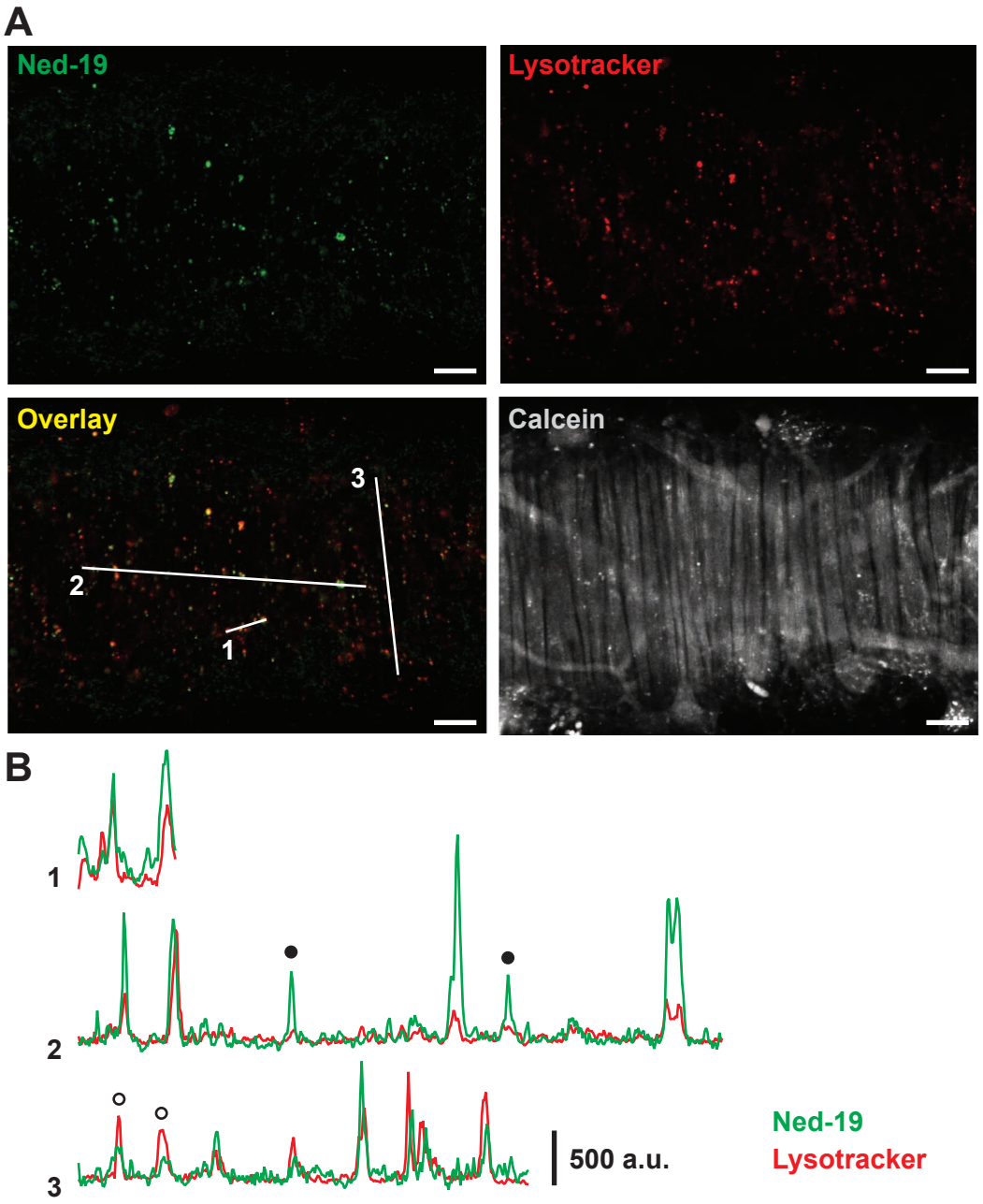

Figure 5.3.3 Acidic organelles overlap with staining for the NAADP receptor
A Ned-19 (NAADP receptor antagonist, 10 μM, green) fluorescence was punctate and uniformly distributed in the smooth muscle cells of pressurized rat mesenteric arteries. Lysotracker Red (0.1 μM, red) staining of acidic organelles showed a similar pattern of staining to Ned-19. Overlay of Ned-19 and Lysotracker Red staining showed co-localisation of the two dyes (yellow). Calcein AM (12.5 μM) illustrates the vertical orientation of the smooth muscle cells (grey). Images are representative of n=3 experiments. Scale bar = 50 μm. **B** Raw fluorescence traces correspond with linescan regions in Overlay image, demonstrating that the majority of Ned-19 staining (green lines) overlaps with Lysotracker staining for acidic organelles (red lines).

Having established that acidic organelles are present in vascular smooth muscle cells, and that at least a high proportion of these stain with the NAADP receptor antagonist, we investigated the functional effects of NAADP in an intact vessel preparation. We used wire myography to measure changes in isometric tension in response to cell-permeable NAADP-AM added to the bath from resting tension. It is assumed that NAADP-AM will cross the cell membranes to enter both the smooth muscle and endothelial cells of the artery and become de-esterified to release active NAADP (Brailoiu *et al.*, 2010b; Collins *et al.*, 2011). NAADP-AM (100 nM - 3 μM) had no observable effect on tone when applied from resting tension (data not shown); however, 100 nM NAADP-AM incubated for 20 min caused a right-shift in the PE concentration-response (**Figure 5.3.4**; Control pEC_{50} = 6.06; 100 nM NAADP pEC_{50} = 5.52). This suggested NAADP inhibited contraction, which could be partially reversed upon wash out.

Therefore the ability of NAADP-AM to stimulate relaxation was established in arteries with sub-maximal tone. U46619 (a thromboxane mimetic) was used to pre-constrict the arteries as it typically produces stable tone (PE tone often fades). This may be attributable to the activation of a Rho kinase / Ca^{2+} sensitisation pathway in smooth muscle cells by U46619, in addition to the well established IP_3-mediated Ca^{2+} release pathway (Shaw *et al.*, 2004). In these experiments, NAADP-AM stimulated reproducible relaxation which was rapid, relaxing fully within 5 min, and concentration-dependent (100-500 nM, **Figure 5.3.5B**). The relaxation was fully sensitive to 45 mM [K^+] (*n*=4) and iberiotoxin (100 nM, *n*=3), implicating a role for BK_{Ca} channels (**Figure 5.3.6**). The relaxation was also partially sensitive to ryanodine (10 μM, *n*=1) (**Figure 5.3.6**), suggesting signalling via ryanodine

receptors may also be involved. Of particular interest, the same profile was observed in endothelium-denuded preparations (**Figure 5.3.6B**), suggesting that NAADP is mediating its effect in smooth muscle cells. It should be noted that we tried to inhibit the NAADP-mediated relaxation with Ned-19 over a range of concentrations, but that Ned-19 did not prevent the relaxation (**Table 5.3.1**). We also tried bafilomycin A1, the proton pump inhibitor, but found no effect (**Table 5.3.1**). It is also of note that Ned-19 (10 μM) inhibited PE contraction (consistent with previous observations by Dr. Francesc Jimenez-Altayo in our laboratory), hence we opted to use U46619 to generate tone.

[Ned-19]	*n*	[Baf. A1]	*n*
1 µM	1	100 nM	4
3 µM	1	300 nM	1
10 µM	6		
20 µM	1		
30 µM	4		
50 µM	2		
60 µM	1		
100 µM	2		

Table 5.3.1 Attempts to inhibit NAADP-AM-mediated relaxation with Ned-19 and bafilomycin A1
Summary of attempts to inhibit relaxation of rat mesenteric arteries pre-constricted with U46619 (1 μM) under isometric tension. The concentrations of Ned-19 and bafilomycin A1 that were used are shown in the left-hand columns, with the number of attempts in the right-hand columns. For all treatments, the inhibitors were applied for 20 min before pre-contracting the artery. At the concentrations of Ned-19 shaded in grey (30-100 μM) the vehicle (DMSO) concentration was higher than the usual limit for intact arteries (1:500 dilution).

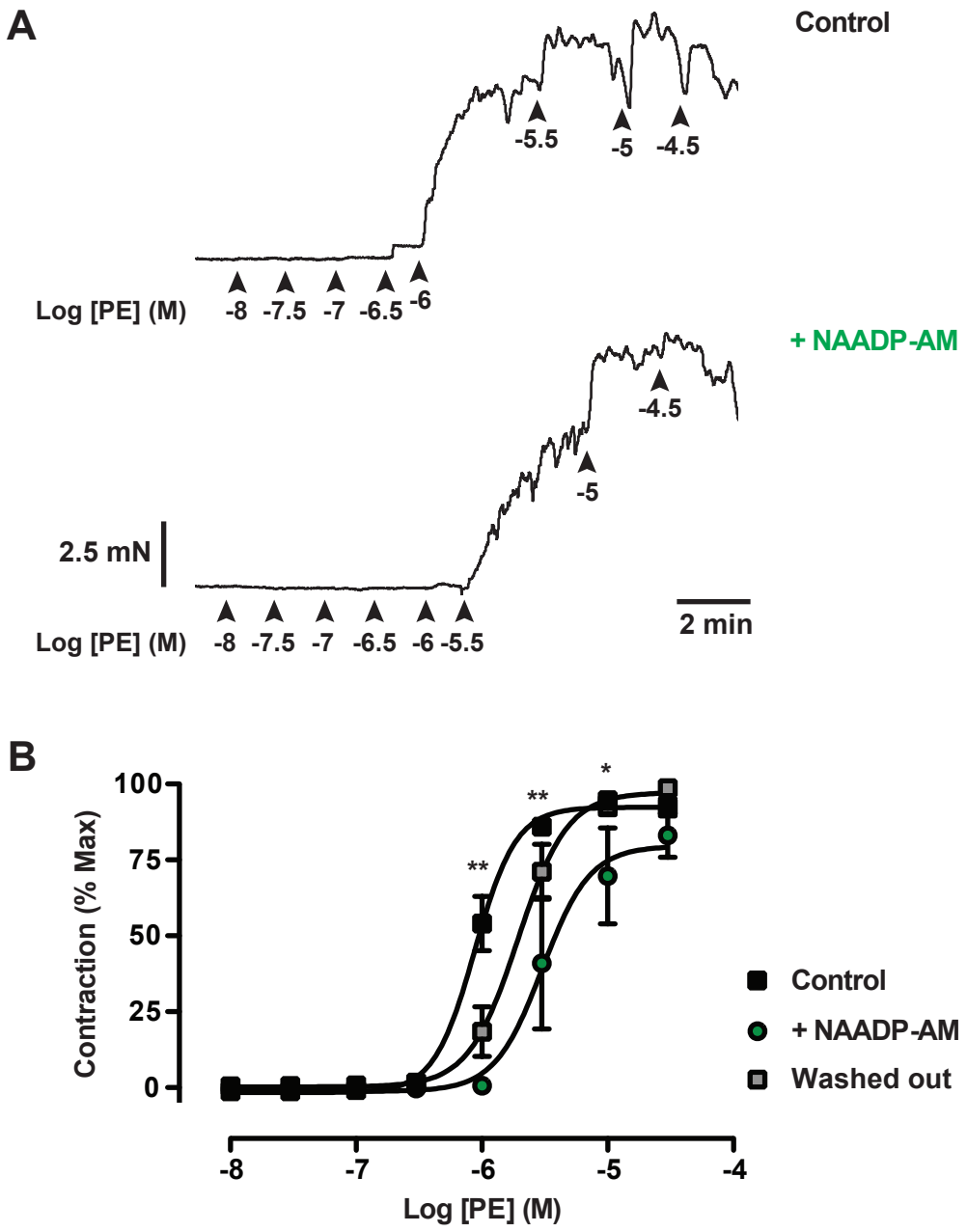

Figure 5.3.4 NAADP-AM inhibits PE contraction
A Representative traces showing phenylephrine (PE)-induced isometric vasoconstriction of rat mesenteric arteries over the concentration range 0.01-30 μM in control conditions (**top**) and after pre-incubation with NAADP-AM (100 nM, **bottom**). **B** Summary data showing NAADP-AM-mediated inhibition of PE contraction (100 nM, green circles, *n*=3), which is illustrated by a rightward shift of the control PE concentration-response curve (black squares, *n*=3); the inhibition could be partially reversed by washout (grey squares, *n*=3). *P<0.05, **P<0.01 using two-way ANOVA with Bonferroni post-test NAADP-AM vs. Control. L-NAME (100 μM) is present throughout.

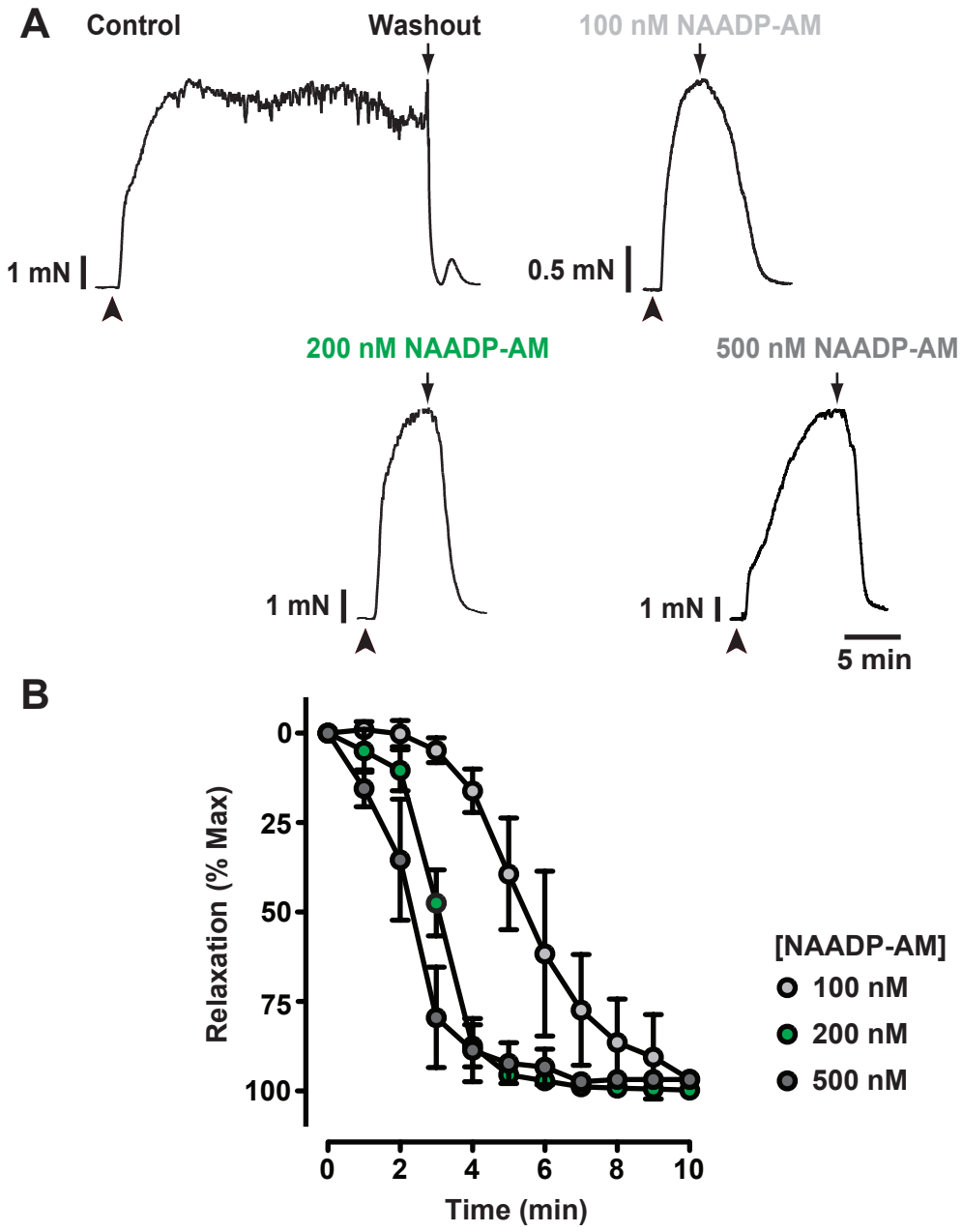

Figure 5.3.5 NAADP-AM concentration-dependently relaxes pre-constricted arteries
A Representative traces showing isometric pre-constriction of rat mesenteric arteries to U46619 (1 μM, arrowhead) in Control conditions (no treatment, **top left**), and relaxation to the concentrations of NAADP-AM (100 nM, **top right**; 200 nM, **bottom left**; 500 nM, **bottom right**). The time scale is applicable to all traces; tension measurements differ due to variation in size of the arteries. **B** Summary data showing NAADP-AM-mediated relaxation is concentration-dependent (100-500 nM, *n*=3-4). 200 nM NAADP-AM (green circles) was subsequently used in tension measurement recordings.

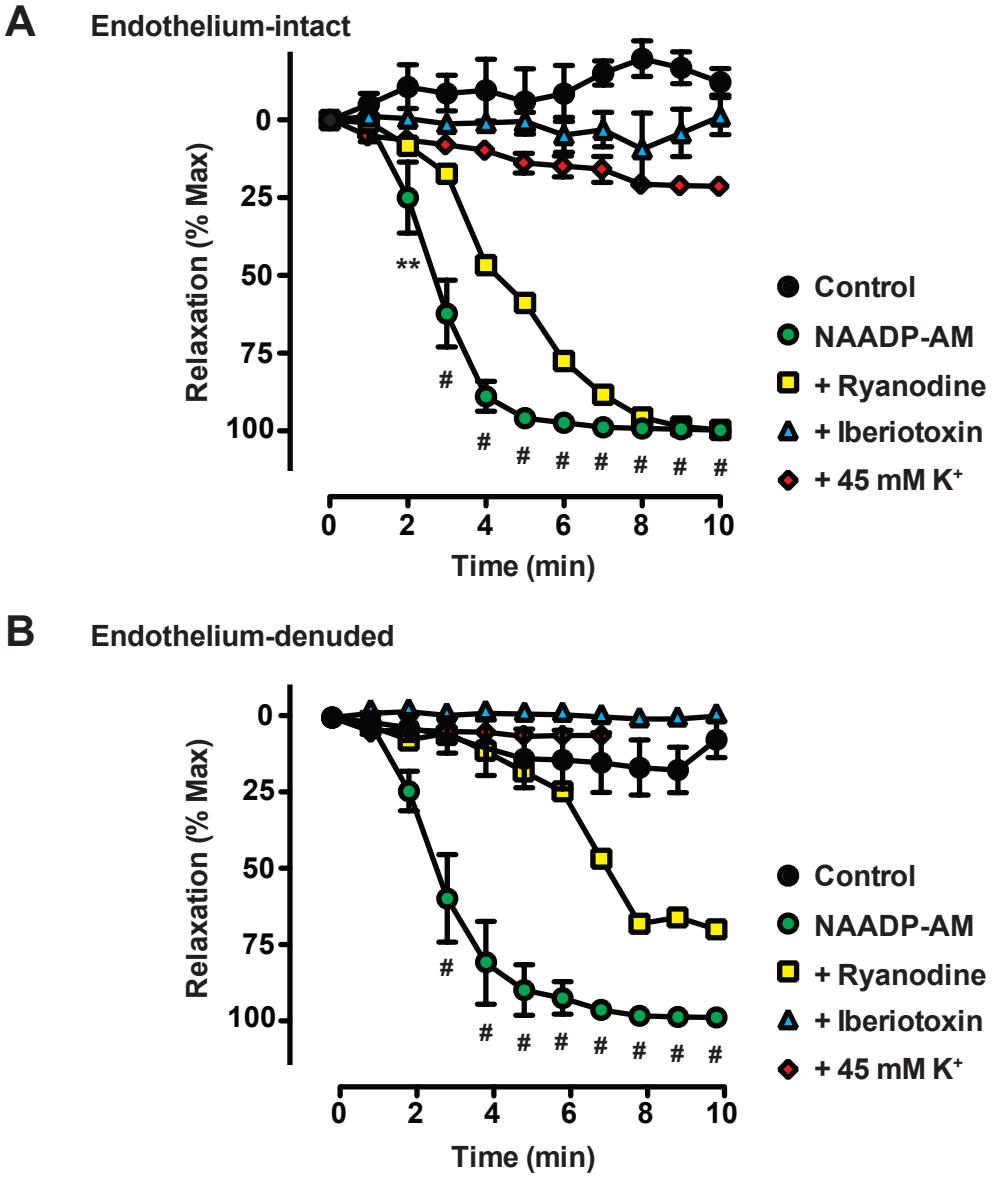

Figure 5.3.6 NAADP-AM-mediated relaxation is inhibited by K^+ channel blockers
A Summary data showing relaxation triggered by NAADP-AM (200 nM, green circle, *n*=5) is sensitive to iberiotoxin (100 nM, blue triangle, *n*=3) and high K^+ (45 mM, red diamond, *n*=4) in endothelium-intact arteries. Relaxation appears to be partially sensitive to ryanodine (10 μM, yellow square, *n*=1). Control arteries not exposed to NAADP-AM remain constricted for the duration of the NAADP-mediated relaxation response (black circle, *n*=7). Rat mesenteric arteries were pre-constricted with U46619 (1 μM) under isometric tension. **B** A similar pharmacological profile is observed in endothelium-denuded arteries (Control *n*=7, NAADP-AM *n*=4, Iberiotoxin *n*=1, Ryanodine *n*=1, K^+ *n*=1). **P<0.01, #P<0.001 by two-way ANOVA with Bonferroni post-test NAADP-AM vs. Control.

To study the apparent involvement of BK_{Ca} channels more directly, we proposed to measure the BK_{Ca} channel outward K^+ currents and thus employed whole-cell patch-clamp of freshly isolated smooth muscle cells from rat mesenteric arteries. The whole-cell configuration was necessary to enable dialysis of NAADP, which has a strong negative charge preventing it crossing the cell membrane. **Figures 5.3.7** and **5.3.8** show representative traces and summary current density-voltage relationships from control conditions and in the presence of NAADP (300 nM). Current density was compared at 0 mV as this is the most depolarized the membrane potential is likely to reach physiologically in mesenteric smooth muscle cells. Whilst over 40 min K^+ currents were unchanged in cells in control conditions (**Figure 5.3.7B**,**C**), the K^+ currents in cells exposed to NAADP appeared to increase significantly with time (**Figure 5.3.8B**,**C**). The increase was sensitive to block of BK_{Ca} channels with paxilline (1 μM; **Figure 5.3.8B**,**C**).

This recorded increase in whole-cell K^+ currents was not consistently observed across all cells exposed to 300 nM NAADP. This may be due to inconsistent rates of dialysis of the pipette solution within the cytosol over the 40 min period and may also disrupt the normal intracellular signalling mechanisms. Additionally the protocol sampled K^+ channel activity every 10 s, thus potentially missing a more rapid, acute effect of the NAADP in the pipette. We therefore proposed to investigate the potential effect of NAADP on spontaneous transient outward current (STOC) activity. Cells were again patched in the whole-cell configuration in voltage-clamp mode, but activity was monitored continuously from 30 s after breakthrough. STOCs were occasionally observed at a holding potential of -40 mV, but consistently when stepped to -20 mV (**Figure 5.3.9A**). In control conditions, over the 5 min sampling

period, STOCs had an average current amplitude of 18.87 pA ± 2.0 (*n*=4) and an average frequency of 57.3 ± 21.5 min^{-1} (*n*=4). In contrast, 30 μM NAADP produced larger, more frequent STOCs with an average current amplitude of 33.03 pA ± 6.4 (*n*=3) and an average frequency of 127.9 ± 58.4 min^{-1} (*n*=3) (**Figure 5.3.9B**).

To confirm the presence of BK_{Ca} channels in our arteries, we conducted immunohistochemistry of rat fixed, pressurized third order mesenteric arteries. Punctate labelling demonstrated clear expression of BK_{Ca} channels uniformly throughout the smooth muscle cells (**Figure 5.3.10**).

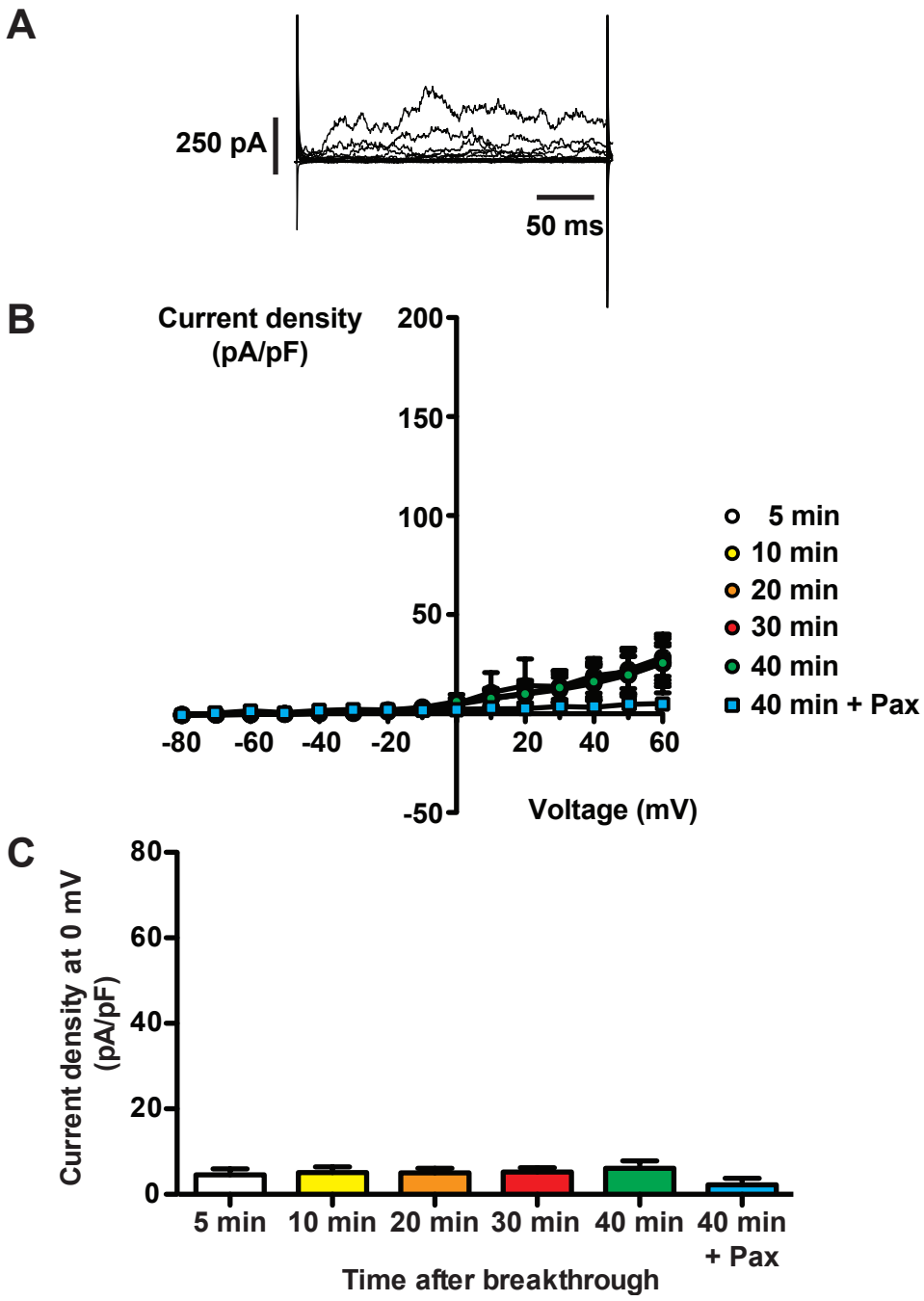

Figure 5.3.7 Whole-cell K^+ currents in control conditions
A Representative trace of outward K^+ currents in rat isolated mesenteric artery smooth muscle cells during the IV protocol (-80 mV to +60 mV) under control conditions after a 40 min continuous patch. **B** Summary current density-voltage relationship sampled at intervals as indicated over 40 min (*n*=4-5) showed no increase with time. Addition of paxilline (BK_{Ca} channel inhibitor, blue circles, 1 μM; *n*=2) markedly reduced the current density. **C** Bar graph showing the average current density measured at 0 mV at time intervals over 40 min, and after addition of paxilline. The current density did not alter significantly over the time period, a portion of which was sensitive to paxilline. The average cell capacitance for cells patched in control conditions was 5.82 ± 1.2 pF (*n*=5).

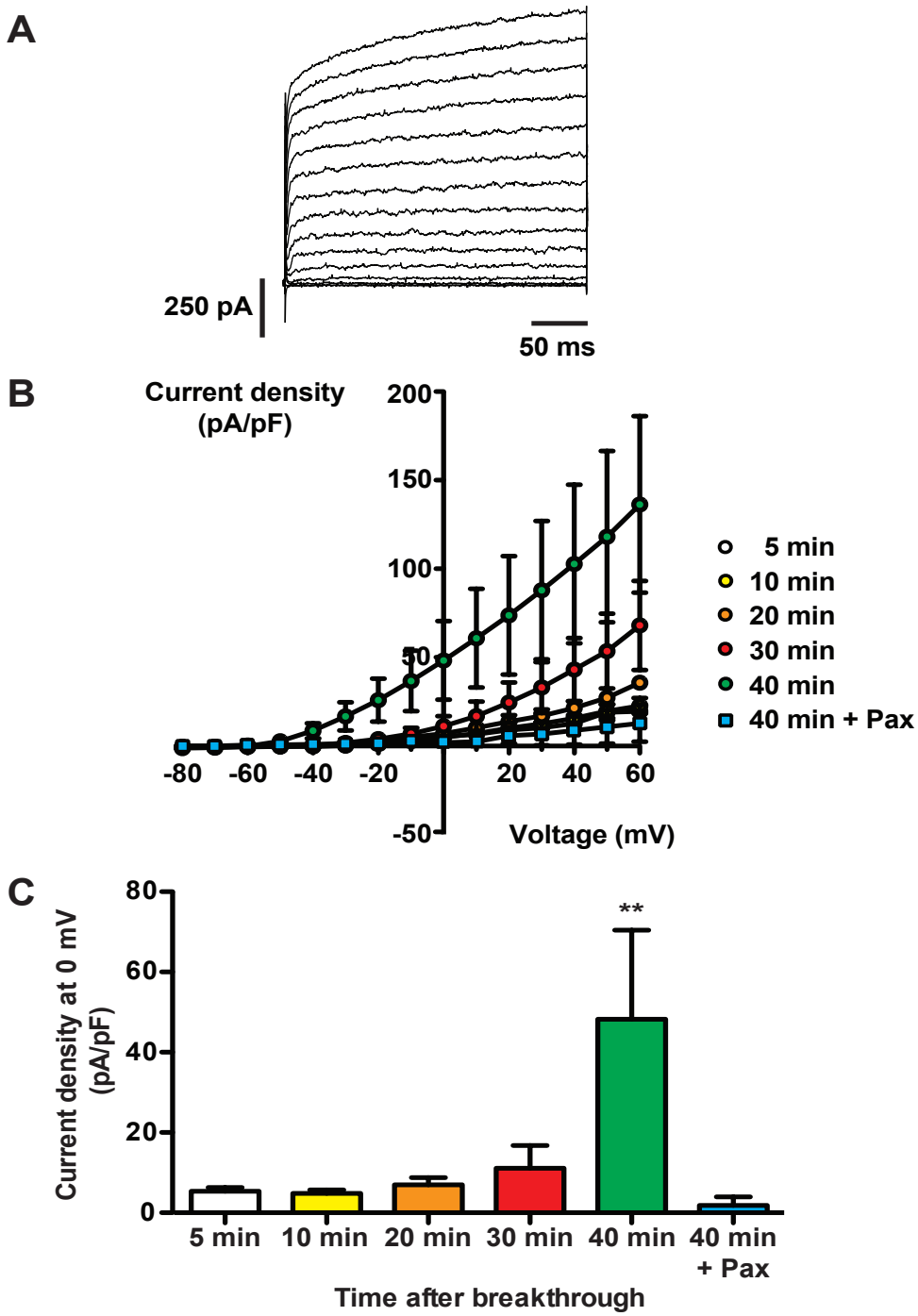

Figure 5.3.8 NAADP increases whole-cell K^+ currents
A Representative trace of K^+ currents in rat isolated mesenteric artery smooth muscle cells after 40 min continuous dialysis of NAADP (300 nM; *n*=3). Summary current density-voltage relationship sampled at intervals over 40 min, showing a large increase in current density over time with dialysis of NAADP. The increase to NAADP was fully reversed by application of paxilline (blue circles, 1 μM; *n*=3). **C** Histogram of current density at 0 mV measured over time, showing a significant increase by 40 min, which was inhibited by paxilline. $^{**}P<0.01$ by one-way repeated measures ANOVA with a Bonferroni post-test vs. 40 min + paxilline. The average cell capacitance for cells patched with NAADP conditions was 5.85 ± 0.7 pF (*n*=3).

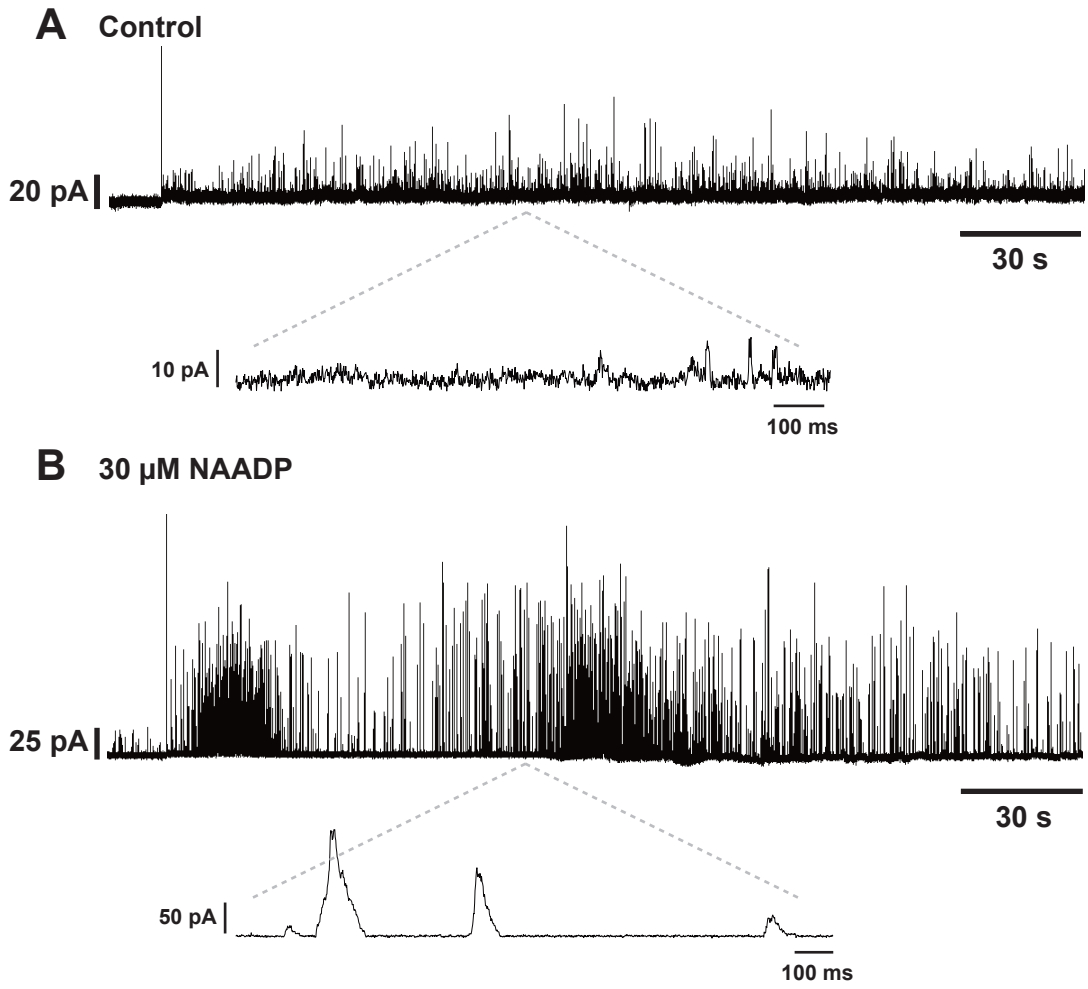
A
Control
20 pA
30 s
10 pA
100 ms
B
30 µM NAADP
25 pA
30 s
50 pA
100 ms

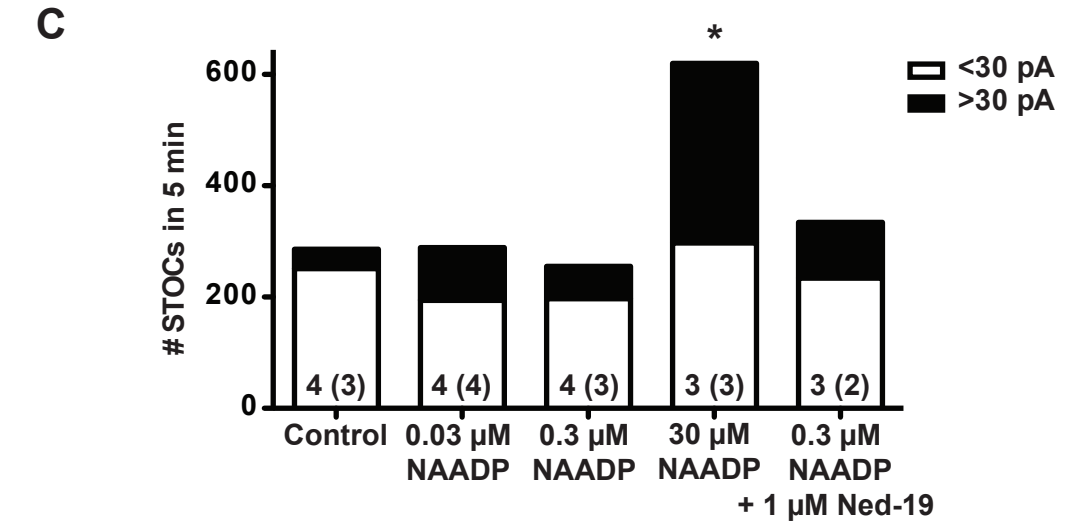
C
*
<30 pA
>30 pA
STOCs in 5 min
600
400
200
0
4 (3)
4 (4)
4 (3)
3 (3)
3 (2)
Control
0.03 µM NAADP
0.3 µM NAADP
30 µM NAADP
0.3 µM NAADP + 1 µM Ned-19

Figure 5.3.9 NAADP increases the amplitude and frequency of STOCs
A Representative trace of STOC activity in rat isolated mesenteric artery smooth muscle cells under control conditions. The arrow indicates stepping the holding potential from -40 mV to -20 mV. **B** Representative trace of STOC activity in the presence of NAADP (30 μM) showing that STOC events appeared more frequently and were greater in amplitude. **C** Summary data illustrating the average number of STOCs counted in a 5 min interval 1.5-6.5 min after breakthrough under different treatments, showing that 30 μM NAADP produces significantly more STOCs of amplitude >30 pA. The events are grouped by amplitude: white bars indicate the number of events of magnitude <30 pA; the black bars indicate the number with an amplitude >30 pA. Numbers shown within bars indicate the number of cells from which the average was calculated; numbers in brackets indicate the number of animals from which these cells came. *P<0.05 by one-way ANOVA with Bonferroni post-test >30 pA 30 μM NAADP vs. >30 pA Control.

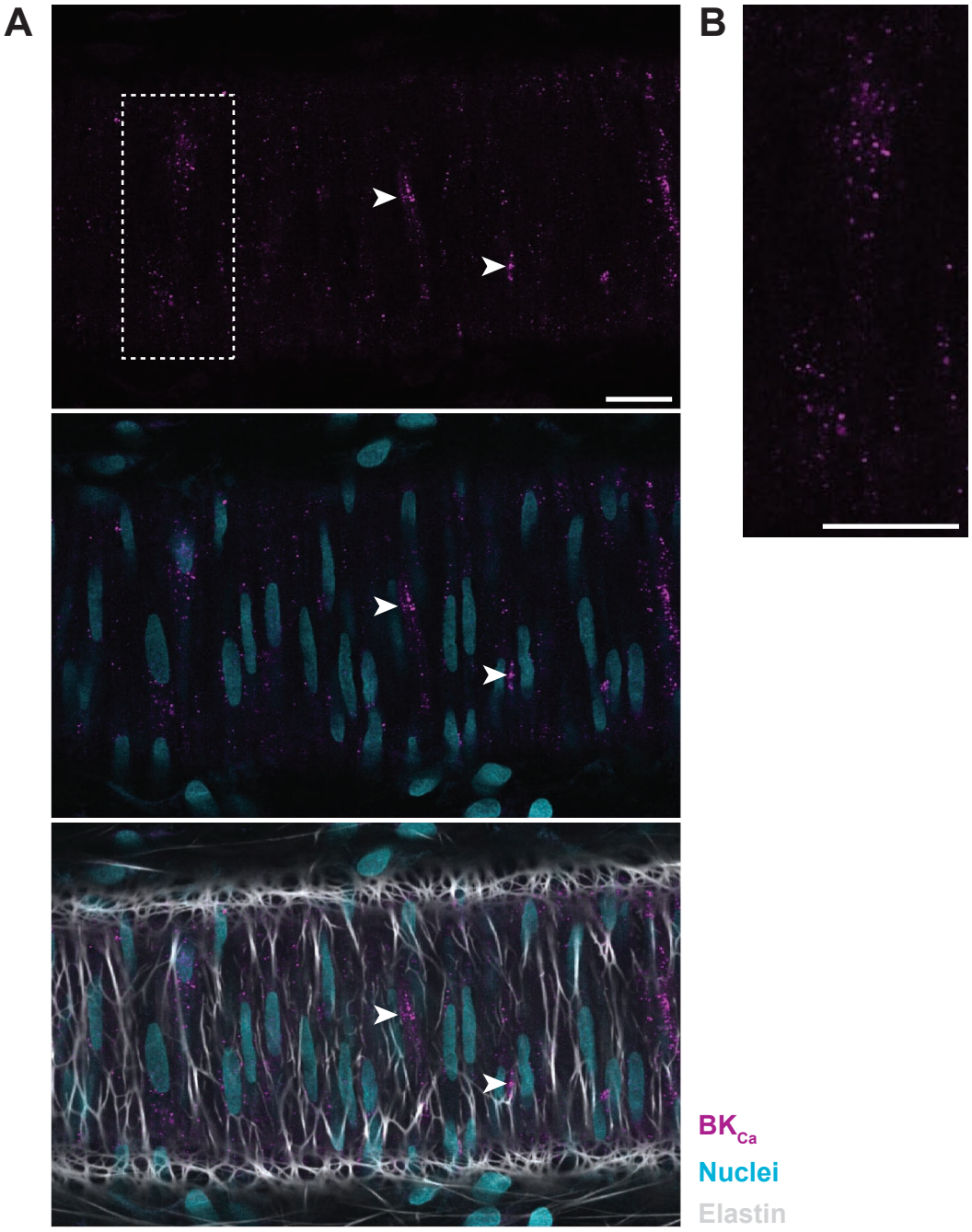

Figure 5.3.10 BK_{Ca} channels are present in vascular smooth muscle cells
A BK_{Ca} staining (magenta, **top**) is visible as a punctate, uniformly distributed pattern in smooth muscle cells of a rat pressurized mesenteric artery. The staining pattern is also consistent with the vertical orientation of smooth muscle nuclei in the same focal plane identified with propidium iodide (45 μM, cyan, **middle**). The elastin between smooth muscle cells is visualised with Alexa 633 hydrazide (1 μM, grey, **bottom**). **B** BK_{Ca} staining identified by the box outline in **A** shown at higher magnification clearly shows the uniform, punctate distribution of this channel. Images are representative of n=3. Scale bar = 20 μm throughout.

5.4 Discussion and Future Work

We sought to determine the role of NAADP in small resistance arteries, using the rat mesenteric artery as a model. In this chapter we have presented evidence supporting the theory that NAADP-targetable stores are present in the smooth muscle cells of this tissue and that functionally this can lead to opening of BK_{Ca} channels on the sarcolemma presumably via Ca^{2+} release.

5.4.i NAADP-targetable stores are present in smooth muscle

Figure 5.3.1 illustrates a pattern of staining of the lysosomal membrane protein, LAMP-2 that might be predicted for a protein on intracellular organelles. In particular, the pattern of staining is consistent with the pattern seen in live arteries stained with the NAADP receptor antagonist, Ned-19 and the acidic store label, Lysotracker Red (**Figure 5.3.3**). Collectively, these data from fixed and live cells not only indicate that acidic organelles are present in the smooth muscle cells, but the observation that Ned-19 staining overlaps with that of Lysotracker Red strongly suggests that the NAADP receptor is present on these organelles.

It is worth noting that LAMP-2 staining is sometimes of higher density in areas aligning with holes in the IEL. It is through these holes that projections of endothelial cells make contact with smooth muscle cells, so-called 'myoendothelial junctions' (MEJs); furthermore, it is predominately via gap junctions at these contact sites (myoendothelial gap junctions; MEGJs) that communication between the two cell types occurs. As such, several components of important tone-modulating pathways have been shown to localise to this signalling microdomain e.g. IK_{Ca} channels, IP_3R Ca^{2+} 'pulsars' and Hbα (Ledoux *et al.*, 2008; Straub *et al.*, 2012). It is interesting to

speculate what functional role the restricted location of these LAMP-2-staining stores serves. It has been frequently observed that agonists acting at either smooth muscle- or endothelial-specific receptors can cause a secondary rise in Ca^{2+} in the neighbouring cell type. Therefore it is conceivable that release of Ca^{2+} from acidic stores could directly, or secondarily via activation of IP_3Rs, activate IK_{Ca} channels to evoke endothelial and smooth muscle cell hyperpolarization, and hence relaxation. In this way both endothelial and smooth muscle cell pathways lead to relaxation. Although this was not pursued further in the current study, we propose to investigate this potential parallel pathway upon future availability of NAADP-AM.

If we assume in the context of this chapter that the stores labelled with LAMP-2 are Ca^{2+} stores targetable by NAADP, we might then hypothesize that NAADP-released Ca^{2+} may be capable of transferring between the two cell layers of the vessel. It is difficult to ascertain from the acquisition voxel size and offline 3D reconstruction of our immunohistochemistry in which cell type the accumulation of LAMP-2 resides. This could be achieved using immunogold labelling at the electron microscope level, or alternatively through use of confocal imaging at the mid-plane of the vessel (Bagher *et al.*, 2012). Here it can be possible to resolve the IEL in cross-section rather than reconstructing offline. This has been achieved in the cremaster arteriole which is ~180 μm in outer diameter; mesenteric arteries are larger at ~360 μm outer diameter, but it would still be feasible despite the limited working distance of the objective.

5.4.ii NAADP relaxes pre-constricted arteries

Looking at the functional effects of NAADP in arteries mounted on the wire myograph, we could not observe any evidence for a role in vasoconstriction when NAADP-AM was added from resting tension over a range of 100 nM to 3 μM (data not shown). There are alternative interpretations we could make from this: either the effective concentration of NAADP after de-esterification was not optimal to see an effect, or NAADP does not contribute to vasoconstriction, at least not in an unstimulated artery.

When considering effective concentrations of NAADP after de-esterification, we can reason that at least in arteries with tone, the available concentration of NAADP from 200 nM NAADP-AM was certainly sufficient to induce relaxation (**Figure 5.3.5**). However, it is important to note that with pre-constriction, the levels of intracellular [Ca^{2+}] and arrangement of intracellular proteins are likely to be different from those in the resting state. Exactly how pre-constriction might alter NAADP effects in the smooth muscle (and endothelium) is unknown, although recent reports have suggested that Ca^{2+} released from the endoplasmic reticulum can be sequestered by lysosomes, and consequently augment the response to NAADP (López-Sanjurjo *et al.*, 2013; Morgan *et al.*, 2013). It therefore remains possible that the optimal concentration of NAADP after de-esterification is different when the vessel is at rest.

One can imagine that the NAADP-mobilised Ca^{2+} from acidic organelles in smooth muscle cells might have local actions, perhaps near the sarcolemma, and that the levels of Ca^{2+} released solely from these are insufficient to trigger contraction. Indeed it has been proposed that the SR has sub-sarcolemmal regions where Ca^{2+}

is released into restricted microdomains to activate sarcolemmal channels, whilst deeper sections of the SR contribute to activation of contractile elements (Wray *et al.*, 2005).

In further support of the concentration of NAADP-AM being sufficient to elicit an effect, pre-treatment with NAADP-AM (100 nM) was able partially to inhibit PE contraction (**Figure 5.3.4**). This also points towards a role for NAADP in limiting, rather than aiding vasoconstriction.

5.4.iii NAADP-mobilised Ca^{2+} opens BK_{Ca} channels

The data shown in **Figures 5.3.5** and **5.3.6** clearly demonstrate that NAADP-AM induces relaxation of pre-contracted arteries. This was concentration-dependent (**Figure 5.3.5**) and similar in both endothelium-intact and endothelium-denuded arteries (**Figure 5.3.6**). We conclude from these data that NAADP is having its effect, at least predominately, in the smooth muscle. Consistent with this, sharp microelectrode measurements of smooth muscle membrane potential by Dr. Hiromichi Takano recorded hyperpolarization (~-20 mV) to NAADP-AM (100-200 nM) added to a vessel under resting tension (**Figure 5.4.1**). This hyperpolarization was maintained, consistent with the maintained relaxation observed in **Figure 5.3.6**. Furthermore it was also prevented by pre-treatment with 45 mM K^+ to depolarize the resting membrane potential.

It is possible that the predominant smooth muscle effect of NAADP-AM reflects limited access of the compound to the endothelial layer, where the final concentration may be lower. Alternatively it is also feasible that NAADP-AM is

having effects in endothelial cells, perhaps parallel hyperpolarization through activation of endothelial K_{Ca} channels, but that the action in the smooth muscle is dominant and masks these effects. Experimentally it is possible to add a compound directly to the endothelium via the lumen in a pressurized myography setup; this is not feasible in a wire myography setup.

Taken together, we propose that NAADP induces hyperpolarization to cause the observed relaxation; furthermore, the pharmacology suggests that opening BK_{Ca} channels in the sarcolemma is involved (**Figure 5.3.6**). 45 mM K^+ was used to alter the equilibrium of ions and depolarize the resting membrane potential, effectively preventing outward movement of K^+ ions when BK_{Ca} channels were opened. Together with the block with iberiotoxin (Galvez *et al.*, 1990), the data strongly support an action of NAADP to open smooth muscle cell BK_{Ca} channels and stimulate relaxation.

At this point our studies were limited by supply of NAADP-AM, which is synthesized in-house. Future availability of this compound will enable additional pharmacological investigation of the effects of NAADP-AM, particularly using the characteristic inhibitors of the NAADP pathway: bafilomycin A1 and Ned-19. Attempts were made to use these inhibitors in the isometric tension experiments (**Table 5.3.1**). With regard to bafilomycin A1, concentrations of 0.1 and 0.3 μM were used; however some studies use up to ten-fold more (Macgregor *et al.*, 2007) which may be necessary in our system. With regard to Ned-19, we made the assumption that if Ned-19 fluorescence were visible in the smooth muscle, Ned-19 was functionally inhibiting the NAADP receptor. Preliminary experiments conducted in human

umbilical vein endothelial cells (HUVECs) suggest this may not be the case: whilst 50 μM was sufficient to observe fluorescence, 100 μM Ned-19 (30 min) was necessary to achieve functional inhibition of Ca^{2+} release. Due to the solubility limit of Ned-19, we are unable to use Ned-19 at 100 μM without causing vehicle effects in our arteries of the high quantity of DMSO (which includes an increase in endothelial Ca^{2+}). It may therefore be difficult to proceed in an intact artery, although use of Ned-19 at this concentration may still be feasible in isolated smooth muscle cells.

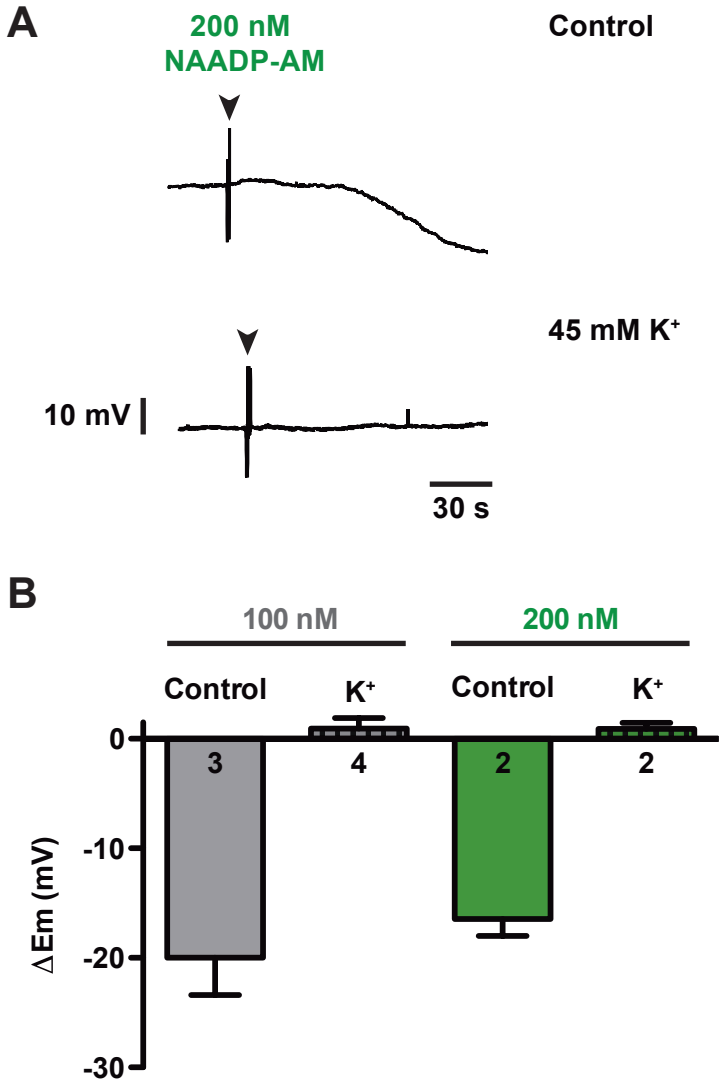

Figure 5.4.1 NAADP-AM hyperpolarizes resting membrane potential
A Representative trace of smooth muscle membrane potential in a rat mesenteric artery showing hyperpolarization to NAADP-AM (200 nM, arrowhead) in control conditions (**top**), which is prevented by pre-treatment with 45 mM K^+ (**bottom**). Scale is applicable to both traces. **B** Summary data showing the negative change in membrane potential (indicating hyperpolarization) to 100 nM (grey) and 200 nM (green) NAADP-AM (Control), which is blocked by pre-treatment with 45 mM K^+ (K^+). *n* numbers as shown.

In order to proceed further and continue to investigate the effects of NAADP on ion channel activity and membrane potential in smooth muscle cells, we moved to a more direct approach using NAADP. Our electrophysiological studies using whole-cell patch-clamp of freshly isolated smooth muscle cells were conducted under the guidance of Dr Sergey Smirnov at the University of Bath. Our data (**Figures 5.3.7-5.3.9**) might go towards supporting our hypothesis that NAADP activates BK_{Ca} channels. In the measurement of whole-cell K^+ currents, NAADP (300 nM) was often able to increase the amplitude of the currents significantly when compared with control; furthermore this increase was sensitive to paxilline. However, this was not consistently observed, and as discussed in **section 5.3** we proposed to investigate activity of the BK_{Ca} channel through analysis of STOC activity since the potential effect of NAADP could be monitored continuously during dialysis from the patch pipette. In this regard we observed significant amplification of both the magnitude and frequency of STOCs by NAADP (30 μM). In all conditions (control and in the presence of NAADP) we observed a range of amplitudes of STOCs, which is consistent with previous reports (Pérez *et al.*, 1999). Our frequency measured in control conditions is consistent with published data (~1 Hz), although the artery type, holding potential and pipette solution differ (Pérez *et al.*, 1999). It would have been highly informative to have continued these experiments with pharmacological manipulation (Ned-19, bafilomycin, ryanodine), and potentially to have combined them with simultaneous measurement of the underlying Ca^{2+} activity. In particular, it would have been interesting to determine whether NAADP-released Ca^{2+} could activate a STOC independently of RyR and the SR. We might also speculate that in our whole-cell K^+ measurements, 30 μM NAADP may have produced a notable increase earlier than observed for 300 nM (**Figure 5.3.8**). An effect of NAADP on

BK_{Ca} channels may be more readily resolved by patching in the presence of an inhibitor of K_v channels (e.g. 4-aminopyridine); as K_V channels are present in smooth muscle cells of this artery, and generate significant currents when activated by voltage (Smirnov & Aaronson, 1992; Zhang *et al.*, 2005).

Our current working hypothesis is that Ca^{2+} released by NAADP from acidic organelles (that stain with Ned-19) might open BK_{Ca} channels in the plasma membrane directly or via the SR (**Figure 5.4.1**). It remains to be determined if and how the two Ca^{2+} stores interact: whether this involves NAADP-mediated loading of the SR (as in (Collins *et al.*, 2011)) or a more direct trigger of Ca^{2+} sparks from RyRs (as in (Kinnear *et al.*, 2004). Based on our experimental data thus far, both may be true in the smooth muscle of resistance arteries and could account for our observed activation of BK_{Ca} channels. It will therefore be imperative in the future to ascertain whether the NAADP-mediated relaxation is sensitive to ryanodine. On the basis of our data thus far we also cannot rule out the possibility that NAADP opens BK_{Ca} channels directly. Indeed, the BK_{Ca} channel opener, NS1619 (40 μM), has been shown to hyperpolarize the resting membrane potential in these arteries by ~-22 mV (Crane & Garland, 2004), which is similar to the hyperpolarization we observed to NAADP-AM (**Figure 5.4.1**).

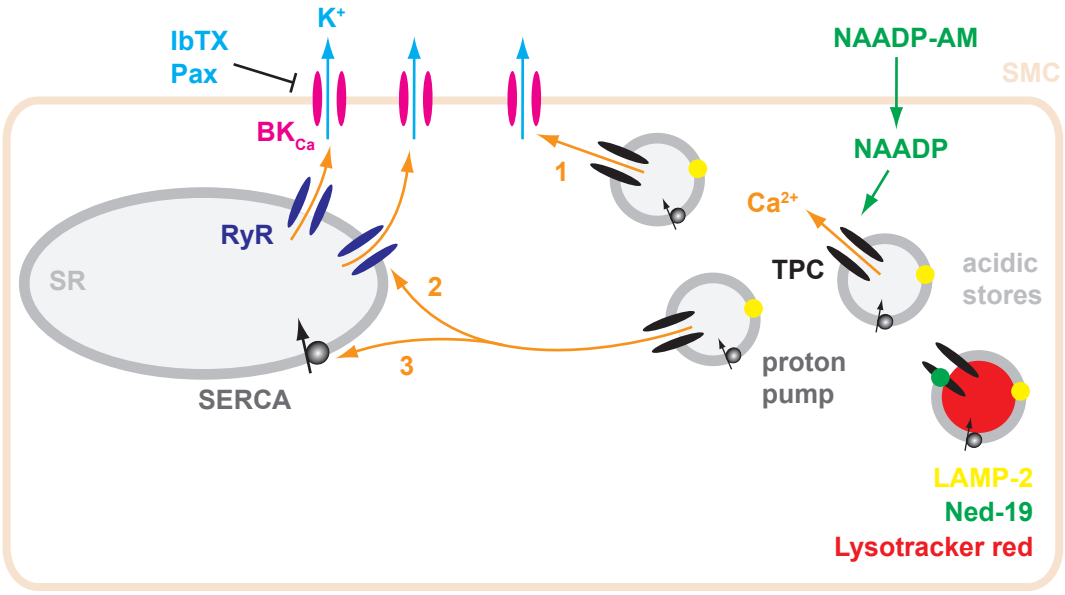

Figure 5.4.2 Proposed NAADP signalling pathway mediating opening of BK_{Ca} channels in vascular smooth muscle cells

Schematic illustrating the hypothesized action of NAADP in the smooth muscle cells of rat mesenteric arteries. NAADP-AM, once de-esterified within the cell, opens two-pore channels (TPC, black) situated on the membrane of lysosomal-type acidic stores, which label with lysotracker red (red) in live tissue and antibodies to LAMP-2 (yellow) in fixed, permeabilized arteries. In live arteries Ned-19 (green, NAADP receptor antagonist) presumably labels the TPCs. Ca^{2+} released by NAADP from acidic stores facilitates opening of plasmalemmal BK_{Ca} channels (pink) to allow K^+ efflux (cyan) via three possible pathways: 1 - direct action of Ca^{2+} from acidic stores (presumably situated close to the plasmalemma) on BK_{Ca} channels, 2 - triggering Ca^{2+}-induced Ca^{2+} release via ryanodine receptors (RyR, purple) on the sarcoplasmic reticulum (SR), or 3 - increasing the SR Ca^{2+} load due to Ca^{2+} uptake via the sarcoplasmic / endoplasmic reticulum Ca^{2+} ATPase (SERCA). K^+ efflux via BK_{Ca} channels could be inhibited in our experiments by iberiotoxin (IbTX) or paxilline (Pax).

5.4.iv Additional functional implications for an interaction between NAADP and BK_{Ca} channels in resistance arteries

Our experiments have studied rat mesenteric third order arteries as a model of resistance arteries. Resistance arteries in some other vascular beds generate myogenic tone, spontaneous tone evoked by increases in intraluminal pressure; this is typically observed and studied in skeletal muscle or cerebral arteries. The exact mechanisms underlying the development of myogenic tone remain unresolved, and are likely to be complex and may vary with tissue. It appears to be associated with increased $[Ca^{2+}]_i$ and changes in membrane potential (Kotecha & Hill, 2005). Given the potential relationship between NAADP-mobilised Ca^{2+} and opening of BK_{Ca} channels, we might hypothesize that NAADP signalling has a role in reducing the development of myogenic tone.

It is also well established *in vitro* and *in vivo* that vasodilators such as ACh can mediate dilation of small arteries at greater distances than can be accounted for by physical diffusion of the agonist. Conducted vasodilation is an important phenomenon in the microcirculation for control of tissue blood flow. Work from several groups and this laboratory in particular, has characterised how conducted vasodilation is associated with conducted hyperpolarization (Takano *et al.*, 2004). Through use of specific inhibitors it has been demonstrated that this hyperpolarization is basally attenuated by open BK_{Ca} and voltage-gated K^+ channels (Beleznai *et al.*, 2011). Following on from our hypothesized signalling microdomain, it would be interesting to see whether basal NAADP-mediated Ca^{2+} release is involved in opening these channels, and whether application of Ned-19 could serve to augment the spread of dilation by reducing opening of these channels.

5.5 Conclusion

In summary, the data in this chapter are suggestive of a novel action of NAADP-mobilised Ca^{2+} (presumably from acidic stores close to the plasma membrane) to facilitate opening of BK_{Ca} channels, causing hyperpolarization and leading to relaxation of pre-constricted intact arteries. The relationship between RyR Ca^{2+} release, STOCs and control of BK_{Ca} activity is well studied, and is a major tone-modulating pathway in the resistance vasculature. It is therefore very interesting that NAADP might participate in this control and will be of great interest in future investigations in this tissue as well as in arteries which develop myogenic tone.

CHAPTER 6

FUTURE DIRECTIONS

We have investigated novel intracellular Ca^{2+} signalling pathways both driven by hyperpolarization, and generating hyperpolarization through interactions with K^+ channels. The outcomes encompass major mechanisms controlling tone and pathways originating in both the smooth muscle and the endothelium of small resistance arteries and arterioles, studied using *in vitro* preparations of the rat mesenteric and cremaster models respectively.

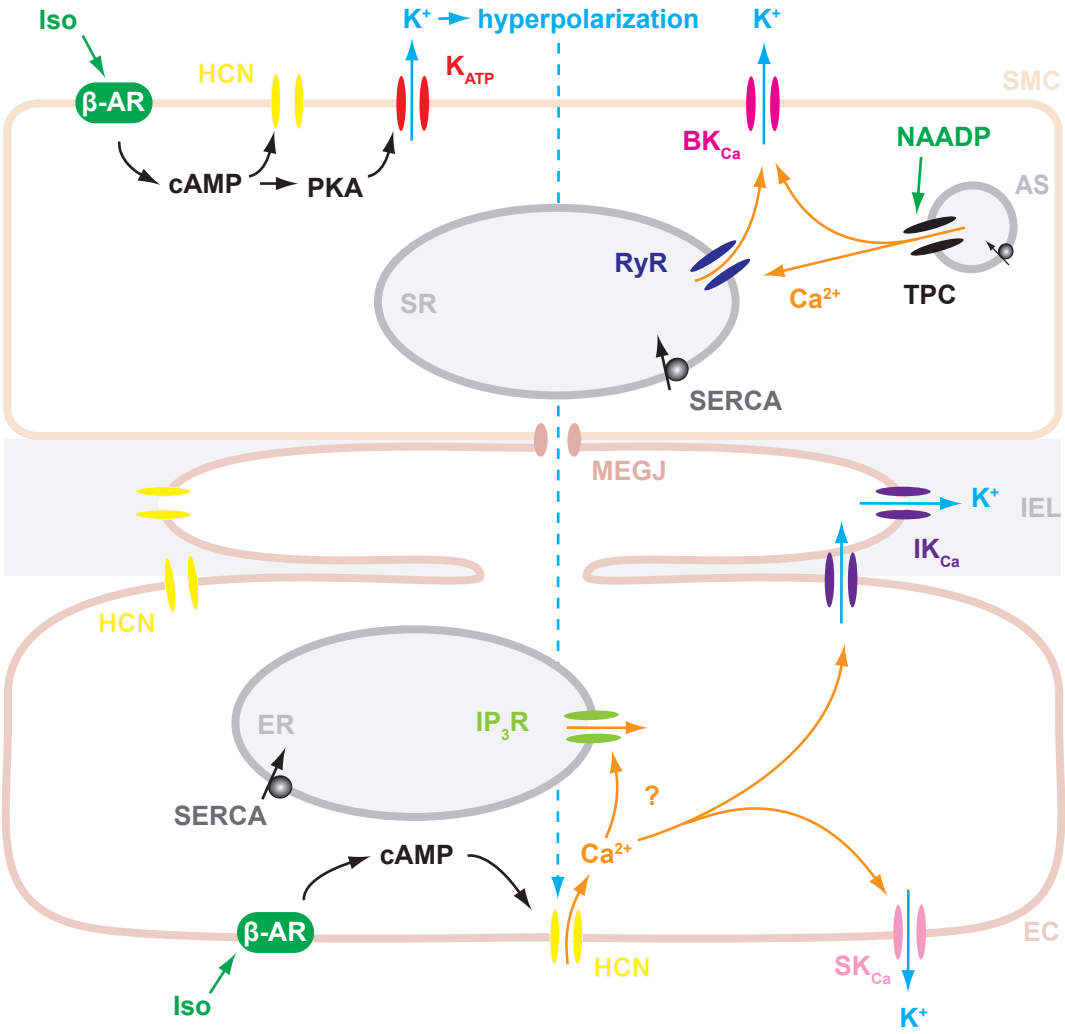

Figure 6.1.1 Schematic illustrating the novel Ca^{2+} signalling pathways in vascular smooth muscle and endothelial cells proposed as a result of the data in this thesis
In vascular smooth muscle cells (SMC) stimulation of β-adrenoceptors (β-AR) with isoprenaline (Iso) elevates intracellular cAMP levels. This may activate HCN channels situated on the sarcolemma. cAMP activates PKA, which in turn phosphorylates K_{ATP} channels in the sarcolemma; this generates robust hyperpolarization, which can spread via myoendothelial gap junctions (MEGJs) to the neighbouring endothelial cells (EC) to open HCN channels here, which are sometimes also present in the myoendothelial projections. Ca^{2+} influx may trigger secondary intracellular release from IP_3 receptors (IP_3R) on the endoplasmic reticulum (ER). Ca^{2+} increase in the endothelium may activate SK_{Ca} and IK_{Ca} channels to amplify hyperpolarization and contribute to conducted vasodilation (see **section 6.1.i**). Endothelial β-adrenergic signalling may contribute to activation of endothelial cell HCN channels. In the SMC, NAADP acting on the putative NAADP receptor, two-pore channels (TPC) on lysosomal-type acidic stores (AS) can also generate hyperpolarization via Ca^{2+}-mediated activation of BK_{Ca} channels in the sarcolemma, directly or indirectly via ryanodine receptors (RyR) or via increasing Ca^{2+} load through the sarcoplasmic / endoplasmic reticulum Ca^{2+} ATPase (SERCA) on the sarcoplasmic reticulum (SR). The internal elastic lamina (IEL) separates the two cell types.

6.1 Novel Ca^{2+} events evoked by hyperpolarization

We have observed an increase in endothelial cell Ca^{2+} events to hyperpolarization or β-adrenoceptor stimulation in small resistance arteries; however, this study has not investigated the functional importance of this mechanism. One possibility is a role in conducted vasodilation.

6.1.i Conducted dilation

Conducted vasodilation is an important phenomenon in the microcirculation for control of tissue blood flow, originally observed and described in skeletal muscle more than 50 years ago (Hilton, 1959) and later in the microcirculation of the hamster cheek pouch (Duling & Berne, 1970). Conducted vasodilation relies on an intact endothelium (Emerson & Segal, 2000b) and is underpinned by spread of hyperpolarization through homocellular gap junctions between endothelial cells (Segal & Duling, 1986; Emerson & Segal, 2000a; Takano *et al.*, 2004). Heterocellular myoendothelial gap junctions (MEGJs) between endothelial cells and the surrounding smooth muscle (**section 1.3**; (Emerson & Segal, 2000a; McSherry *et al.*, 2006)) mean that the two cell types are also electrically coupled. Consequently hyperpolarization originating in the endothelium will spread radially to the surrounding smooth muscle (Emerson & Segal, 2000a). In the context of conducted vasodilation, this means that the spreading hyperpolarization will decay over distance as the signal dissipates to the adjoining smooth muscle cells, as well as through open plasmalemmal ion channels in endothelial or smooth muscle cells.

Endothelium-dependent vasodilators such as ACh generate conducted dilation in addition to local dilation due to activation of endothelial Ca^{2+}-activated K^+ channels

and the endothelium-derived hyperpolarization (EDH) response (Segal & Duling, 1986; Edwards *et al.*, 1998; Dora *et al.*, 2003; Winter & Dora, 2007). Additionally, any agonists which directly evoke hyperpolarization e.g. opening of K_{ATP} channels by levcromakalim, also induce local and conducted vasodilatation in rat mesenteric arteries (Takano *et al.*, 2004; Garland *et al.*, 2011b). Indeed, any agonist that can hyperpolarize the vessel has the potential to initiate conducted vasodilation. β-Adrenergic stimulation with isoprenaline also evokes conducted vasodilation due to opening of K_{ATP} channels. Physiologically, sympathetic stimulation will also activate smooth muscle α-adrenoceptors, which trigger vasoconstriction. A recent study from our group examining this paradox found that even in the absence of an α-adrenoceptor blocker such as prazosin, the endogenous catecholamines adrenaline and noradrenaline both evoked local vasoconstriction (as expected) but conducted vasodilation (Garland *et al.*, 2011b).

While conducted vasodilation is not reliant on changes in endothelial cell Ca^{2+} *per se* (Takano *et al.*, 2004), an increase in Ca^{2+} in the endothelium would have the potential to open endothelial cell K_{Ca} channels, facilitate longitudinal spread of hyperpolarization, and thereby amplify the conducted response. One might therefore speculate that the Ca^{2+} entering HCN channels could activate these K_{Ca} channels, to further potentiate hyperpolarization.

Interestingly, in rat pressurized cremaster arterioles with ACh applied during superfusion by picospritzing downstream onto the artery (**Figure 6.1.2A**), an increase in discrete endothelial cell Ca^{2+} events is seen upstream at sites not directly exposed to ACh, but which are (presumably) hyperpolarized (**Figure**

6.1.2C). This supports the theory that hyperpolarization itself is sufficient to induce an elevation in endothelial cell Ca^{2+}. The frequency of Ca^{2+} events upstream is also similar to the frequency in response to levcromakalim stimulation, again potentially reflecting a common mechanism. Furthermore, the upstream increase in Ca^{2+} event frequency was prevented by pre-treatment with ZD7288 (1 μM; **Figure 6.1.2C**), implicating HCN channels in mediating the Ca^{2+} increase. Following on from this, it would be highly informative to assess the effect of ZD7288 on the conducted dilation to hyperpolarizing agents such as levcromakalim.

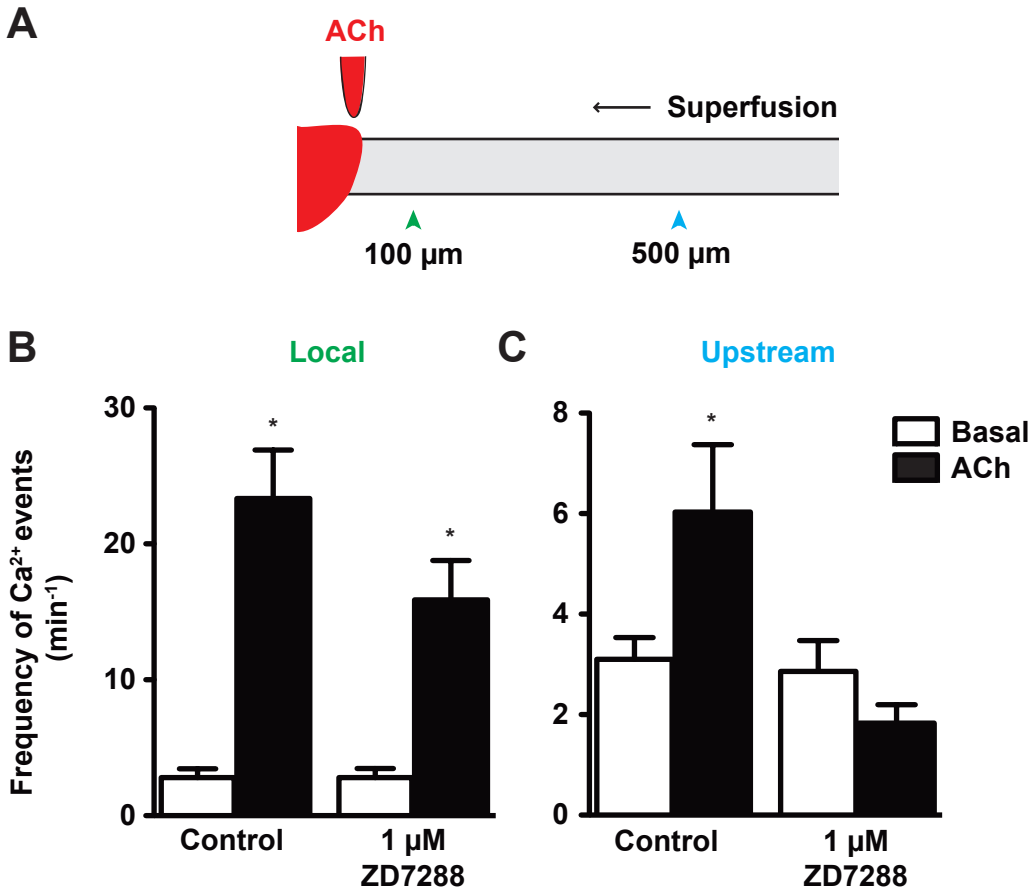

Figure 6.1.2 Increase in endothelial Ca^{2+} events at local and upstream sites in response to ACh

A Schematic illustrating the focal application of acetylcholine (ACh) to the outside of the rat pressurized cremaster arteriole, using pressure-pulse ejection (picospritzing, 5-10 psi). ACh (10 μM) is picospritzed for ≤60 s during continuous superfusion to restrict the exposure of ACh to the artery as illustrated. The part of the vessel exposed to ACh is visualised using sulforhodamine 101 (3 μM) included in the pipette solution (illustrated by red colour). Sulforhodamine 101 is fluorescent when excited at 543 nm (emission >560 nm). Sulforhodamine 101 and OGB-1 were imaged simultaneously using a 20x objective (0.7 NA, Olympus) (0.45 s/scan) to monitor ACh delivery with Ca^{2+} events. The site 0-100 μm from exposure to ACh (equivalent to one endothelial cell length) and the site 500 μm upstream (not directly exposed to ACh) are indicated on the diagram. These are referred to as the 'Local' and 'Upstream' response sites. **B** Summary data showing an increase in frequency of Ca^{2+} events to ACh at the Local site, which is reduced but not inhibited by ZD7288 (1 μM, 60 min), and an increase at the Upstream site, which is fully prevented by ZD7288. Nifedipine (1 μM) is present throughout. Paired data, n=4, *P<0.05 by repeated measures ANOVA with independent Bonferroni post-tests to compare selected data sets as indicated.

Acknowledgement: KA Dora performed and analysed these experiments, which were set up by CS Lim.

6.1.ii Additional channels involved in the isoprenaline response

In examining the effect of the HCN channel blocker, ZD7288 on endothelial cell Ca^{2+} increases, we found that 1 μM was sufficient to inhibit the response to levcromakalim (**Figure 4.3.4**) but at this concentration it did not fully inhibit the endothelial Ca^{2+} response to isoprenaline. This introduces the possibility that an additional pathway might be involved in the response to β-adrenergic stimulation. The latter involves production of cAMP, and since removal of extracellular Ca^{2+} prevented this response, we might hypothesize that a Ca^{2+} influx channel that is regulated by cAMP might also be involved, such as cyclic nucleotide-gated (CNG) channels.

CNG channels are cation channels permeable to Na^+, K^+, Ca^{2+} and Mg^{2+}. Ca^{2+} binds tightly to the channel pore, limiting the single-channel conductance and effectively creating selectivity of the channel for Ca^{2+} over other cations (Brown *et al.*, 2006). CNG channels conduct 10-80% Ca^{2+} in 2.5 mM external Ca^{2+} (Biel, 2009).

Despite the importance of CNG channels in sensory signal transduction, there remains a lack of a specific pharmacological inhibitor. The most frequently employed and best-characterised blocker of this family of channels is L-*cis*-diltiazem, first reported in bovine rod outer segment vesicles (Koch & Kaupp, 1985). It is membrane-permeable and blocks at micromolar concentrations from the cytoplasmic side of the channel, with different affinities depending on the subunit composition of the CNG channel. D-*cis*-diltiazem is much less effective at blocking CNG channels and also blocks L-type VGCC. The L-*cis*-isomer does also block L-type VGCC, albeit with ten-fold lower affinity (Brown *et al.*, 2006). Another

commonly used blocker is LY83583, a soluble guanylyl cyclase (sGC) inhibitor with an IC_{50} of 20 μM. Dichloro-benzamil is a derivative of amiloride (epithelial sodium channel blocker) and another non-specific blocker of CNG channels.

Preliminary endothelial cell Ca^{2+} imaging experiments with β-adrenergic stimulation found inconsistent effects of L-*cis*-diltiazem and LY83583; however, if HCN and CNG channels are both activated, a combination of blockers might produce full inhibition of the response. CNG channels have been proposed to act as Ca^{2+} influx channels in endothelial cells by one group through use of L-*cis*-diltiazem and LY83583, reporting an involvement in response to multiple physiological stimuli such as ATP (Cheng *et al.*, 2008) and adrenaline (Shen *et al.*, 2008).

6.2 Novel Ca^{2+} signalling pathway evoking hyperpolarization

In rat mesenteric arteries, NAADP appears to elicit opening of BK_{Ca} channels in the smooth muscle, presumably via release of Ca^{2+} from acidic stores. Probing this mechanism further in intact arteries and isolated cells has already been discussed in the previous chapter (**section 5.4**), but additional future directions are considered below.

6.2.i Smooth muscle NAADP-mediated Ca^{2+} signalling

In our experiments NAADP-mediated mobilisation of Ca^{2+} in smooth muscle cells was not directly assessed, but inferred from the observed activation of BK_{Ca} channels (which are Ca^{2+}-activated). It is feasible to study smooth muscle Ca^{2+} in intact arteries, but it may be difficult to resolve the release of Ca^{2+} from acidic stores close to BK_{Ca} channels, which is presumably a focal event. In this regard it may be

more consistent to examine the responses in isolated cells loaded with Ca^{2+}-sensitive dye. NAADP may be applied by patch pipette, or using cell-permeant NAADP-AM if it is available; alternatively caged NAADP might provide the most reliable effective final concentration in the cell. It would be of further interest to combine imaging of the Ca^{2+} response to NAADP with simultaneous patch-clamp analysis of STOCs.

6.2.ii Endothelial NAADP-mediated Ca^{2+} signalling

Our experiments identified a dominant role for the smooth muscle in arteries mounted under isometric tension. It is conceivable that NAADP would have an effect in the endothelium, but was masked by the substantial hyperpolarization evoked by opening BK_{Ca} channels or was minimal due to limited access of NAADP-AM to the endothelium in the wire myograph preparation. Indeed, two reports of a role in endothelial signalling using cultured cells or conduit vessels have been published supporting a possible action in our small arteries (Brailoiu *et al.*, 2010b; Esposito *et al.*, 2011).

An influence of NAADP on endothelial Ca^{2+} signalling would ideally be assessed using confocal imaging of endothelial cells loaded with a Ca^{2+}-sensitive dye, as we have used in the experiments described in **Chapters 3** and **4**. NAADP-AM could be applied abluminally (in the bath) or directly into the lumen using a syringe pump, during continuous imaging at physiological pressure. The latter would circumvent a potential diffusion limitation of the -AM form through the smooth muscle layer where it is presumably de-esterified. Preliminary experiments adding NAADP-AM abluminally suggest that it might increase Ca^{2+} and with availability of NAADP-AM

synthesized in-house, this can be pursued. It would be particularly exciting to investigate whether a Ca^{2+} increase is linked to opening of endothelial IK_{Ca} or SK_{Ca} channels, in a microdomain mimicking that which we propose in the smooth muscle.

6.2.iii The NAADP receptor

The target protein for NAADP in our experiments in rat mesenteric arteries and isolated smooth muscle cells was not investigated. Two-pore channel (TPC) knockout mice are available and would be of invaluable use, not least in assessing NAADP signalling in a different animal model, but predominately for probing the involvement of TPC as the NAADP receptor in our observations and which subtype is important. Additionally, endothelial Ca^{2+} signalling could be assessed in knockout mice. Loading of Ca^{2+}-sensitive dyes is notoriously difficult in mouse arteries, although it would be theoretically feasible to use mice with a Ca^{2+} sensor genetically-encoded (Tallini *et al.*, 2007).

CHAPTER 7

REFERENCES

Abe K, Puertollano R (2011). Role of TRP channels in the regulation of the endosomal pathway. *Physiology* 26**:** 14-22.

Adeagbo AS, Triggle CR (1993). Varying extracellular [K^+]: a functional approach to separating EDHF- and EDNO-related mechanisms in perfused rat mesenteric arterial bed. *J Cardiovasc Pharmacol* 21**:** 423-429.

Ahlquist RP (1948). A study of the adrenotropic receptors. *Am J Physiol* 153**:** 586-600.

Andrejewski N, Punnonen EL, Guhde G, Tanaka Y, Lüllmann-Rauch R, Hartmann D*, et al.* (1999). Normal lysosomal morphology and function in LAMP-1-deficient mice. *J Biol Chem* 274**:** 12692-12701.

Bagher P, Beleznai T, Kansui Y, Mitchell R, Garland CJ, Dora KA (2012). Low intravascular pressure activates endothelial cell TRPV4 channels, local Ca^{2+} events, and IK_{Ca} channels, reducing arteriolar tone. *Proc Natl Acad Sci U S A* 109**:** 18174-18179.

Baker JG (2005). The selectivity of β-adrenoceptor antagonists at the human β_1, β_2 and β_3 adrenoceptors. *Br J Pharmacol* 144**:** 317-322.

Baker JG, Adams LA, Salchow K, Mistry SN, Middleton RJ, Hill SJ*, et al.* (2011). Synthesis and characterization of high-affinity 4,4-difluoro-4-bora-3a,4a-diaza-s-indacene-labeled fluorescent ligands for human β-adrenoceptors. *J Med Chem* 54**:** 6874-6887.

Baruscotti M, Bottelli G, Milanesi R, DiFrancesco JC, DiFrancesco D (2010). HCN-related channelopathies. *Pflugers Arch* 460**:** 405-415.

Beleznai TZ, Yarova PL, Yuill KH, Dora KA (2011). Smooth muscle Ca^{2+}-activated and voltage-gated K^+ channels modulate conducted dilation in rat isolated small mesenteric arteries. *Microcirculation* 18**:** 487-500.

Benham CD, Bolton TB (1986). Spontaneous transient outward currents in single visceral and vascular smooth muscle cells of the rabbit. *J Physiol* 381**:** 385-406.

Berridge MJ (1993). Inositol trisphosphate and calcium signalling. *Nature* 361**:** 315-325.

Berridge MJ (1997). Elementary and global aspects of calcium signalling. *J Exp Biol* 200**:** 315-319.

Berridge MJ, Lipp P, Bootman MD (2000). The versatility and universality of calcium signalling. *Nat Rev Mol Cell Biol* 1**:** 11-21.

Bevan JA, Osher JV (1972). A direct method for recording tension changes in the wall of small blood vessels in vitro. *Agents Actions* 2**:** 257-260.

Biel M (2009). Cyclic nucleotide-regulated cation channels. *J Biol Chem* 284**:** 9017-9021.

Biel M, Wahl-Schott C, Michalakis S, Zong X (2009). Hyperpolarization-activated cation channels: from genes to function. *Physiol Rev* 89**:** 847-885.

Billaud M, Lohman AW, Johnstone SR, Biwer LA, Mutchler S, Isakson BE (2014). Regulation of cellular communication by signaling microdomains in the blood vessel wall. *Pharmacol Rev* 66**:** 513-569.

Billington RA, Genazzani AA (2007). PPADS is a reversible competitive antagonist of the NAADP receptor. *Cell Calcium* 41**:** 505-511.

Boittin FX, Galione A, Evans AM (2002). Nicotinic acid adenine dinucleotide phosphate mediates Ca^{2+} signals and contraction in arterial smooth muscle via a two-pool mechanism. *Circ Res* 91**:** 1168-1175.

Bolton TB, Lang RJ, Takewaki T (1984). Mechanisms of action of noradrenaline and carbachol on smooth muscle of guinea-pig anterior mesenteric artery. *J Physiol* 351**:** 549-572.

BoSmith RE, Briggs I, Sturgess NC (1993). Inhibitory actions of ZENECA ZD7288 on whole-cell hyperpolarization activated inward current (I_f) in guinea-pig dissociated sinoatrial node cells. *Br J Pharmacol* 110**:** 343-349.

Brailoiu E, Rahman T, Churamani D, Prole DL, Brailoiu GC, Hooper R*, et al.* (2010a). An NAADP-gated two-pore channel targeted to the plasma membrane uncouples triggering from amplifying Ca^{2+} signals. *J Biol Chem* 285**:** 38511-38516.

Brailoiu E, Churamani D, Cai X, Schrlau MG, Brailoiu GC, Gao X*, et al.* (2009). Essential requirement for two-pore channel 1 in NAADP-mediated calcium signaling. *J Cell Biol* 186**:** 201-209.

Brailoiu GC, Gurzu B, Gao X, Parkesh R, Aley PK, Trifa DI*, et al.* (2010b). Acidic NAADP-sensitive calcium stores in the endothelium: agonist-specific recruitment and role in regulating blood pressure. *J Biol Chem* 285**:** 37133-37137.

Brenner R, Peréz GJ, Bonev AD, Eckman DM, Kosek JC, Wiler SW*, et al.* (2000). Vasoregulation by the β1 subunit of the calcium-activated potassium channel. *Nature* 407**:** 870-876.

Briones AM, Daly CJ, Jimenez-Altayo F, Martinez-Revelles S, Gonzalez JM, McGrath JC*, et al.* (2005). Direct demonstration of β_1- and evidence against β_2- and β_3-adrenoceptors, in smooth muscle cells of rat small mesenteric arteries. *Br J Pharmacol* 146**:** 679-691.

Brown RL, Strassmaier T, Brady JD, Karpen JW (2006). The pharmacology of cyclic nucleotide-gated channels: emerging from the darkness. *Curr Pharm Des* 12**:** 3597-3613.

Bucchi A, Baruscotti M, DiFrancesco D (2002). Current-dependent block of rabbit sino-atrial node I_f channels by ivabradine. *J Gen Physiol* 120**:** 1-13.

Bucchi A, Baruscotti M, Nardini M, Barbuti A, Micheloni S, Bolognesi M*, et al.* (2013). Identification of the molecular site of ivabradine binding to HCN4 channels. *PLoS One* 8**:** e53132.

Burdyga T, Shmygol A, Eisner DA, Wray S (2003). A new technique for simultaneous and in situ measurements of Ca^{2+} signals in arteriolar smooth muscle and endothelial cells. *Cell Calcium* 34**:** 27-33.

Calcraft PJ, Ruas M, Pan Z, Cheng X, Arredouani A, Hao X*, et al.* (2009). NAADP mobilizes calcium from acidic organelles through two-pore channels. *Nature* 459**:** 596-600.

Cang C, Zhou Y, Navarro B, Seo YJ, Aranda K, Shi L*, et al.* (2013). mTOR regulates lysosomal ATP-sensitive two-pore Na^+ channels to adapt to metabolic state. *Cell* 152**:** 778-790.

Carafoli E (2002). Calcium signaling: a tale for all seasons. *Proc Natl Acad Sci U S A* 99**:** 1115-1122.

Chadha PS, Liu L, Rikard-Bell M, Senadheera S, Howitt L, Bertrand RL*, et al.* (2011). Endothelium-dependent vasodilation in human mesenteric artery is primarily mediated by myoendothelial gap junctions intermediate conductance calcium-activated K^+ channel and nitric oxide. *J Pharmacol Exp Ther* 336**:** 701-708.

Chen G, Suzuki H, Weston AH (1988). Acetylcholine releases endothelium-derived hyperpolarizing factor and EDRF from rat blood vessels. *Br J Pharmacol* 95**:** 1165-1174.

Chen JW, Murphy TL, Willingham MC, Pastan I, August JT (1985). Identification of two lysosomal membrane glycoproteins. *J Cell Biol* 101**:** 85-95.

Cheng H, Lederer WJ, Cannell MB (1993). Calcium sparks: elementary events underlying excitation-contraction coupling in heart muscle. *Science* 262**:** 740-744.

Cheng KT, Leung YK, Shen B, Kwok YC, Wong CO, Kwan HY*, et al.* (2008). CNGA2 channels mediate adenosine-induced Ca^{2+} influx in vascular endothelial cells. *Arterioscler Thromb Vasc Biol* 28**:** 913-918.

Cheng L, Kinard K, Rajamani R, Sanguinetti MC (2007). Molecular mapping of the binding site for a blocker of hyperpolarization-activated, cyclic nucleotide-modulated pacemaker channels. *J Pharmacol Exp Ther* 322**:** 931-939.

Christensen KL, Mulvany MJ (1993). Mesenteric arcade arteries contribute substantially to vascular resistance in conscious rats. *J Vasc Res* 30**:** 73-79.

Christensen KL, Mulvany MJ (2001). Location of resistance arteries. *J Vasc Res* 38**:** 1-12.

Chruscinski A, Brede ME, Meinel L, Lohse MJ, Kobilka BK, Hein L (2001). Differential distribution of β-adrenergic receptor subtypes in blood vessels of knockout mice lacking β_1- or β_2-adrenergic receptors. *Mol Pharmacol* 60**:** 955-962.

Churamani D, Hooper R, Rahman T, Brailoiu E, Patel S (2013). The N-terminal region of two-pore channel 1 regulates trafficking and activation by NAADP. *Biochem J* 453**:** 147-151.

Churchill GC, Okada Y, Thomas JM, Genazzani AA, Patel S, Galione A (2002). NAADP mobilizes Ca^{2+} from reserve granules, lysosome-related organelles, in sea urchin eggs. *Cell* 111**:** 703-708.

Clapper DL, Walseth TF, Dargie PJ, Lee HC (1987). Pyridine nucleotide metabolites stimulate calcium release from sea urchin egg microsomes desensitized to inositol trisphosphate. *J Biol Chem* 262**:** 9561-9568.

Cohen KD, Jackson WF (2005). Membrane hyperpolarization is not required for sustained muscarinic agonist-induced increases in intracellular Ca^{2+} in arteriolar endothelial cells. *Microcirculation* 12**:** 169-182.

Cole KS (1949). Dynamic electrical characteristics of the squid axon membrane. *Arch Sci Physiol* 3**:** 253-258.

Collins TP, Bayliss R, Churchill GC, Galione A, Terrar DA (2011). NAADP influences excitation-contraction coupling by releasing calcium from lysosomes in atrial myocytes. *Cell Calcium* 50**:** 449-458.

Cook NJ, Hanke W, Kaupp UB (1987). Identification, purification, and functional reconstitution of the cyclic GMP-dependent channel from rod photoreceptors. *Proc Natl Acad Sci U S A* 84**:** 585-589.

Copello JA, Qi Y, Jeyakumar LH, Ogunbunmi E, Fleischer S (2001). Lack of effect of cADP-ribose and NAADP on the activity of skeletal muscle and heart ryanodine receptors. *Cell Calcium* 30**:** 269-284.

Crane GJ, Garland CJ (2004). Thromboxane receptor stimulation associated with loss of SK_{Ca} activity and reduced EDHF responses in the rat isolated mesenteric artery. *Br J Pharmacol* 142**:** 43-50.

Crane GJ, Gallagher N, Dora KA, Garland CJ (2003). Small- and intermediate-conductance calcium-activated K^+ channels provide different facets of endothelium-dependent hyperpolarization in rat mesenteric artery. *J Physiol* 553**:** 183-189.

Dale HH (1905). On some physiological actions of ergot. *J Physiol* 34**:** 163-206.

Dale HH (1913). On the action of ergotoxine; with special reference to the existence of sympathetic vasodilators. *J Physiol* 46**:** 291-300.

Dammermann W, Zhang B, Nebel M, Cordiglieri C, Odoardi F, Kirchberger T*, et al.* (2009). NAADP-mediated Ca^{2+} signaling via type 1 ryanodine receptor in T cells revealed by a synthetic NAADP antagonist. *Proc Natl Acad Sci U S A* 106**:** 10678-10683.

Dhein S (1998). Gap junction channels in the cardiovascular system: pharmacological and physiological modulation. *Trends Pharmacol Sci* 19**:** 229-241.

Dong XP, Cheng X, Mills E, Delling M, Wang F, Kurz T*, et al.* (2008). The type IV mucolipidosis-associated protein TRPML1 is an endolysosomal iron release channel. *Nature* 455**:** 992-996.

Dora KA (2001). Cell-cell communication in the vessel wall. *Vasc Med* 6**:** 43-50.

Dora KA, Garland CJ (2013). Linking hyperpolarization to endothelial cell calcium events in arterioles. *Microcirculation* 20**:** 248-256.

Dora KA, Doyle MP, Duling BR (1997). Elevation of intracellular calcium in smooth muscle causes endothelial cell generation of NO in arterioles. *Proc Natl Acad Sci U S A* 94**:** 6529-6534.

Dora KA, Xia J, Duling BR (2003). Endothelial cell signaling during conducted vasomotor responses. *Am J Physiol Heart Circ Physiol* 285**:** H119-126.

Dora KA, Hinton JM, Walker SD, Garland CJ (2000). An indirect influence of phenylephrine on the release of endothelium-derived vasodilators in rat small mesenteric artery. *Br J Pharmacol* 129**:** 381-387.

Dora KA, Gallagher NT, McNeish A, Garland CJ (2008). Modulation of endothelial cell $K_{Ca}3.1$ channels during endothelium-derived hyperpolarizing factor signaling in mesenteric resistance arteries. *Circ Res* 102**:** 1247-1255.

Duling BR, Berne RM (1970). Propagated vasodilation in the microcirculation of the hamster cheek pouch. *Circ Res* 26**:** 163-170.

Duling BR, Rivers RJ (1986). Isolation, cannulation, and perfusion of microvessels. In: Baker CH, Nastuk WG (eds). *Microcirculatory Technology*, edn. Orlando: Academic Press. p^pp 265-280.

Duling BR, Gore RW, Dacey RG, Jr., Damon DN (1981). Methods for isolation, cannulation, and in vitro study of single microvessels. *Am J Physiol* 241**:** H108-116.

Duza T, Sarelius IH (2004). Localized transient increases in endothelial cell Ca^{2+} in arterioles in situ: implications for coordination of vascular function. *Am J Physiol Heart Circ Physiol* 286**:** H2322-2331.

Edwards G, Dora KA, Gardener MJ, Garland CJ, Weston AH (1998). K^+ is an endothelium-derived hyperpolarizing factor in rat arteries. *Nature* 396**:** 269-272.

Emerson GG, Segal SS (2000a). Electrical coupling between endothelial cells and smooth muscle cells in hamster feed arteries: role in vasomotor control. *Circ Res* 87**:** 474-479.

Emerson GG, Segal SS (2000b). Endothelial cell pathway for conduction of hyperpolarization and vasodilation along hamster feed artery. *Circ Res* 86**:** 94-100.

Esfandiarei M, Fameli N, Choi YY, Tehrani AY, Hoskins JG, van Breemen C (2013). Waves of calcium depletion in the sarcoplasmic reticulum of vascular smooth muscle cells: an inside view of spatiotemporal Ca^{2+} regulation. *PLoS One* 8**:** e55333.

Eskelinen EL, Schmidt CK, Neu S, Willenborg M, Fuertes G, Salvador N*, et al.* (2004). Disturbed cholesterol traffic but normal proteolytic function in LAMP-1/LAMP-2 double-deficient fibroblasts. *Mol Biol Cell* 15**:** 3132-3145.

Esposito B, Gambara G, Lewis AM, Palombi F, D'Alessio A, Taylor LX*, et al.* (2011). NAADP links histamine H1 receptors to secretion of von Willebrand factor in human endothelial cells. *Blood* 117**:** 4968-4977.

Felix R, Sandoval A, Sánchez D, Gómora JC, Vega-Beltrán JLDl, Treviño CL*, et al.* (2003). ZD7288 inhibits low-threshold Ca^{2+} channel activity and regulates sperm function. *Biochem Biophys Res Commun* 311**:** 187-192.

Fenger-Gron J, Mulvany MJ, Christensen KL (1995). Mesenteric blood pressure profile of conscious, freely moving rats. *J Physiol* 488 (Pt 3)**:** 753-760.

Figueroa XF, Poblete I, Fernandez R, Pedemonte C, Cortes V, Huidobro-Toro JP (2009). NO production and eNOS phosphorylation induced by epinephrine through the activation of β-adrenoceptors. *Am J Physiol Heart Circ Physiol* 297**:** H134-143.

Flower RJ (2006). Prostaglandins, bioassay and inflammation. *Br J Pharmacol* 147 Suppl 1**:** S182-192.

Fox K, Ford I, Steg PG, Tendera M, Ferrari R, Investigators B (2008). Ivabradine for patients with stable coronary artery disease and left-ventricular systolic dysfunction (BEAUTIFUL): a randomised, double-blind, placebo-controlled trial. *Lancet* 372**:** 807-816.

Frishman WH (2013). β-Adrenergic blockade in cardiovascular disease. *J Cardiovasc Pharmacol Ther* 18**:** 310-319.

Furchgott RF (1983). Role of endothelium in responses of vascular smooth muscle. *Circ Res* 53**:** 557-573.

Furchgott RF, Zawadzki JV (1980). The obligatory role of endothelial cells in the relaxation of arterial smooth muscle by acetylcholine. *Nature* 288**:** 373-376.

Galvez A, Gimenez-Gallego G, Reuben JP, Roy-Contancin L, Feigenbaum P, Kaczorowski GJ*, et al.* (1990). Purification and characterization of a unique, potent, peptidyl probe for the high conductance calcium-activated potassium channel from venom of the scorpion *Buthus tamulus*. *J Biol Chem* 265**:** 11083-11090.

Ganitkevich V, Isenberg G (1990). Isolated guinea pig coronary smooth muscle cells. Acetylcholine induces hyperpolarization due to sarcoplasmic reticulum calcium release activating potassium channels. *Circ Res* 67**:** 525-528.

Garland CJ, McPherson GA (1992). Evidence that nitric oxide does not mediate the hyperpolarization and relaxation to acetylcholine in the rat small mesenteric artery. *Br J Pharmacol* 105**:** 429-435.

Garland CJ, Hiley CR, Dora KA (2011a). EDHF: spreading the influence of the endothelium. *Br J Pharmacol* 164**:** 839-852.

Garland CJ, Yarova PL, Jiménez-Altayó F, Dora KA (2011b). Vascular hyperpolarization to β-adrenoceptor agonists evokes spreading dilatation in rat isolated mesenteric arteries. *Br J Pharmacol* 164.

Genazzani AA, Galione A (1996). Nicotinic acid-adenine dinucleotide phosphate mobilizes Ca^{2+} from a thapsigargin-insensitive pool. *Biochem J* 315 (Pt 3)**:** 721-725.

Genazzani AA, Empson RM, Galione A (1996). Unique inactivation properties of NAADP-sensitive Ca^{2+} release. *J Biol Chem* 271**:** 11599-11602.

Gerasimenko JV, Maruyama Y, Yano K, Dolman NJ, Tepikin AV, Petersen OH*, et al.* (2003). NAADP mobilizes Ca^{2+} from a thapsigargin-sensitive store in the nuclear envelope by activating ryanodine receptors. *J Cell Biol* 163**:** 271-282.

Gordienko DV, Greenwood IA, Bolton TB (2001). Direct visualization of sarcoplasmic reticulum regions discharging Ca^{2+} sparks in vascular myocytes. *Cell Calcium* 29**:** 13-28.

Green ME, Edwards G, Kirkup AJ, Miller M, Weston AH (1996). Pharmacological characterization of the inwardly-rectifying current in the smooth muscle cells of the rat bladder. *Br J Pharmacol* 119**:** 1509-1518.

Greene D, Kang S, Kosenko A, Hoshi N (2012). Adrenergic regulation of HCN4 channel requires protein association with β_2-adrenergic receptor. *J Biol Chem* 287**:** 23690-23697.

Greenwood IA, Prestwich SA (2002). Characteristics of hyperpolarization-activated cation currents in portal vein smooth muscle cells. *Am J Physiol Cell Physiol* 282**:** C744-753.

Guimaraes S, Moura D (2001). Vascular adrenoceptors: an update. *Pharmacol Rev* 53**:** 319-356.

Guse AH (2013). N-terminal tagging of two-pore channels interferes with NAADP action. *The Biochemical journal* 453**:** e1-2.

Haller T, Dietl P, Deetjen P, Völkl H (1996). The lysosomal compartment as intracellular calcium store in MDCK cells: a possible involvement in $InsP_3$-mediated Ca^{2+} release. *Cell Calcium* 19**:** 157-165.

Hamill OP, Marty A, Neher E, Sakmann B, Sigworth FJ (1981). Improved patch-clamp techniques for high-resolution current recording from cells and cell-free membrane patches. *Pflugers Arch* 391**:** 85-100.

Herrmann S, Layh B, Ludwig A (2011). Novel insights into the distribution of cardiac HCN channels: an expression study in the mouse heart. *J Mol Cell Cardiol* 51**:** 997-1006.

Hill MA, Trippe KM, Li QX, Meininger GA (1992). Arteriolar arcades and pressure distribution in cremaster muscle microcirculation. *Microvasc Res* 44**:** 117-124.

Hilton SM (1959). A peripheral arterial conducting mechanism underlying dilatation of the femoral artery and concerned in functional vasodilatation in skeletal muscle. *J Physiol* 149**:** 93-111.

Hodgkin AL, Huxley AF, Katz B (1952). Measurement of current-voltage relations in the membrane of the giant axon of *Loligo*. *J Physiol* 116**:** 424-448.

Ignarro LJ, Byrns RE, Buga GM, Wood KS (1987). Endothelium-derived relaxing factor from pulmonary artery and vein possesses pharmacologic and chemical properties identical to those of nitric oxide radical. *Circ Res* 61**:** 866-879.

Isakson BE, Ramos SI, Duling BR (2007). Ca^{2+} and inositol 1,4,5-trisphosphate-mediated signaling across the myoendothelial junction. *Circ Res* 100**:** 246-254.

Ishibashi K, Suzuki M, Imai M (2000). Molecular cloning of a novel form (two-repeat) protein related to voltage-gated sodium and calcium channels. *Biochem Biophys Res Commun* 270**:** 370-376.

Jain P, Slama JT, Perez-Haddock LA, Walseth TF (2010). Nicotinic acid adenine dinucleotide phosphate analogues containing substituted nicotinic acid: effect of modification on Ca^{2+} release. *J Med Chem* 53**:** 7599-7612.

Johns A, Lategan TW, Lodge NJ, Ryan US, Van Breemen C, Adams DJ (1987). Calcium entry through receptor-operated channels in bovine pulmonary artery endothelial cells. *Tissue Cell* 19**:** 733-745.

Kansui Y, Garland CJ, Dora KA (2008). Enhanced spontaneous Ca^{2+} events in endothelial cells reflect signalling through myoendothelial gap junctions in pressurized mesenteric arteries. *Cell Calcium* 44**:** 135-146.

Kilpatrick BS, Eden ER, Schapira AH, Futter CE, Patel S (2013). Direct mobilisation of lysosomal Ca^{2+} triggers complex Ca^{2+} signals. *J Cell Sci* 126**:** 60-66.

Kinnear NP, Boittin FX, Thomas JM, Galione A, Evans AM (2004). Lysosome-sarcoplasmic reticulum junctions. A trigger zone for calcium signaling by nicotinic acid adenine dinucleotide phosphate and endothelin-1. *J Biol Chem* 279**:** 54319-54326.

Kinnear NP, Wyatt CN, Clark JH, Calcraft PJ, Fleischer S, Jeyakumar LH*, et al.* (2008). Lysosomes co-localize with ryanodine receptor subtype 3 to form a trigger zone for calcium signalling by NAADP in rat pulmonary arterial smooth muscle. *Cell Calcium* 44**:** 190-201.

Koch KW, Kaupp UB (1985). Cyclic GMP directly regulates a cation conductance in membranes of bovine rods by a cooperative mechanism. *J Biol Chem* 260**:** 6788-6800.

Kotecha N, Hill MA (2005). Myogenic contraction in rat skeletal muscle arterioles: smooth muscle membrane potential and Ca^{2+} signaling. *Am J Physiol Heart Circ Physiol* 289**:** H1326-1334.

Kuo IY, Wolfle SE, Hill CE (2011). T-type calcium channels and vascular function: the new kid on the block? *J Physiol* 589**:** 783-795.

Kuriyama H, Suzuki H (1978). The effects of acetylcholine on the membrane and contractile properties of smooth muscle cells of the rabbit superior mesenteric artery. *Br J Pharmacol* 64**:** 493-501.

Lamboley M, Pittet P, Koenigsberger M, Sauser R, Bény JL, Meister JJ (2005). Evidence for signaling via gap junctions from smooth muscle to endothelial cells in rat mesenteric arteries: possible implication of a second messenger. *Cell Calcium* 37**:** 311-320.

Lands AM, Luduena FP, Buzzo HJ (1967a). Differentiation of receptors responsive to isoproterenol. *Life Sci* 6**:** 2241-2249.

Lands AM, Arnold A, McAuliff JP, Luduena FP, Brown TG, Jr. (1967b). Differentiation of receptor systems activated by sympathomimetic amines. *Nature* 214**:** 597-598.

Langheinrich U, Mederos y Schnitzler M, Daut J (1998). Ca^{2+}-transients induced by K^+ channel openers in isolated coronary capillaries. *Pflugers Arch* 435**:** 435-438.

Ledoux J, Taylor MS, Bonev AD, Hannah RM, Solodushko V, Shui B*, et al.* (2008). Functional architecture of inositol 1,4,5-trisphosphate signaling in restricted spaces of myoendothelial projections. *Proc Natl Acad Sci U S A* 105**:** 9627-9632.

Lee HC (1997). Mechanisms of calcium signaling by cyclic ADP-ribose and NAADP. *Physiol Rev* 77**:** 1133-1164.

Lee HC, Aarhus R (1995). A derivative of NADP mobilizes calcium stores insensitive to inositol trisphosphate and cyclic ADP-ribose. *J Biol Chem* 270**:** 2152-2157.

Lew MJ, Rivers RJ, Duling BR (1989). Arteriolar smooth muscle responses are modulated by an intramural diffusion barrier. *Am J Physiol* 257**:** H10-16.

Lewis AM, Aley PK, Roomi A, Thomas JM, Masgrau R, Garnham C*, et al.* (2012). β-Adrenergic receptor signaling increases NAADP and cADPR levels in the heart. *Biochem Biophys Res Commun* 427**:** 326-329.

Li G, Cheung DW (1999). Effects of paxilline on K^+ channels in rat mesenteric arterial cells. *Eur J Pharmacol* 372**:** 103-107.

Lin-Moshier Y, Walseth TF, Churamani D, Davidson SM, Slama JT, Hooper R*, et al.* (2012). Photoaffinity labeling of nicotinic acid adenine dinucleotide phosphate (NAADP) targets in mammalian cells. *J Biol Chem* 287**:** 2296-2307.

Little TL, Xia J, Duling BR (1995). Dye tracers define differential endothelial and smooth muscle coupling patterns within the arteriolar wall. *Circ Res* 76**:** 498-504.

Liu J, Dobrzynski H, Yanni J, Boyett MR, Lei M (2007). Organisation of the mouse sinoatrial node: structure and expression of HCN channels. *Cardiovasc Res* 73**:** 729-738.

Looft-Wilson RC, Payne GW, Segal SS (2004). Connexin expression and conducted vasodilation along arteriolar endothelium in mouse skeletal muscle. *J Appl Physiol* 97**:** 1152-1158.

López-Sanjurjo CI, Tovey SC, Prole DL, Taylor CW (2013). Lysosomes shape Ins(1,4,5)P_3-evoked Ca^{2+} signals by selectively sequestering Ca^{2+} released from the endoplasmic reticulum. *J Cell Sci* 126**:** 289-300.

Lückhoff A, Busse R (1990). Calcium influx into endothelial cells and formation of endothelium-derived relaxing factor is controlled by the membrane potential. *Pflugers Arch* 416**:** 305-311.

Macgregor A, Yamasaki M, Rakovic S, Sanders L, Parkesh R, Churchill GC*, et al.* (2007). NAADP controls cross-talk between distinct Ca^{2+} stores in the heart. *J Biol Chem* 282**:** 15302-15311.

Marshall PW, Rouse W, Briggs I, Hargreaves RB, Mills SD, McLoughlin BJ (1993). ICI D7288, a novel sinoatrial node modulator. *J Cardiovasc Pharmacol* 21**:** 902-906.

Mauban JR, Zacharia J, Zhang J, Wier WG (2013). Vascular tone and Ca^{2+} signaling in murine cremaster muscle arterioles *in vivo*. *Microcirculation* 20**:** 269-277.

McNeish AJ, Altayo FJ, Garland CJ (2010). Evidence both L-type and non-L-type voltage-dependent calcium channels contribute to cerebral artery vasospasm following loss of NO in the rat. *Vascul Pharmacol* 53**:** 151-159.

McSherry IN, Spitaler MM, Takano H, Dora KA (2005). Endothelial cell Ca^{2+} increases are independent of membrane potential in pressurized rat mesenteric arteries. *Cell Calcium* 38**:** 23-33.

McSherry IN, Sandow SL, Campbell WB, Falck JR, Hill MA, Dora KA (2006). A role for heterocellular coupling and EETs in dilation of rat cremaster arteries. *Microcirculation* 13**:** 119-130.

Michels G, Er F, Khan I, Südkamp M, Herzig S, Hoppe UC (2005). Single-channel properties support a potential contribution of hyperpolarization-activated cyclic nucleotide-gated channels and I_f to cardiac arrhythmias. *Circulation* 111**:** 399-404.

Michels G, Brandt MC, Zagidullin N, Khan IF, Larbig R, van Aaken S*, et al.* (2008). Direct evidence for calcium conductance of hyperpolarization-activated cyclic nucleotide-gated channels and human native I_f at physiological calcium concentrations. *Cardiovasc Res* 78**:** 466-475.

Miriel VA, Mauban JR, Blaustein MP, Wier WG (1999). Local and cellular Ca^{2+} transients in smooth muscle of pressurized rat resistance arteries during myogenic and agonist stimulation. *J Physiol* 518 (Pt 3)**:** 815-824.

Molleman A (2002). *Patch clamping: an introductory guide to patch clamp electrophysiology*. edn.

Moncada S, Gryglewski RJ, Bunting S, Vane JR (1976). A lipid peroxide inhibits the enzyme in blood vessel microsomes that generates from prostaglandin endoperoxides the substance (prostaglandin X) which prevents platelet aggregation. *Prostaglandins* 12**:** 715-737.

Moore DH, Ruska H (1957). The fine structure of capillaries and small arteries. *J Biophys Biochem Cytol* 3**:** 457-462.

Morgan AJ, Davis LC, Wagner SK, Lewis AM, Parrington J, Churchill GC*, et al.* (2013). Bidirectional Ca^{2+} signaling occurs between the endoplasmic reticulum and acidic organelles. *J Cell Biol* 200**:** 789-805.

Mulvany MJ, Halpern W (1977). Contractile properties of small arterial resistance vessels in spontaneously hypertensive and normotensive rats. *Circ Res* 41**:** 19-26.

Nakashima M, Vanhoutte PM (1995). Isoproterenol causes hyperpolarization through opening of ATP-sensitive potassium channels in vascular smooth muscle of the canine saphenous vein. *J Pharmacol Exp Ther* 272**:** 379-384.

Nausch LW, Bonev AD, Heppner TJ, Tallini Y, Kotlikoff MI, Nelson MT (2012). Sympathetic nerve stimulation induces local endothelial Ca^{2+} signals to oppose vasoconstriction of mouse mesenteric arteries. *Am J Physiol Heart Circ Physiol* 302**:** H594-602.

Naylor E, Arredouani A, Vasudevan SR, Lewis AM, Parkesh R, Mizote A*, et al.* (2009). Identification of a chemical probe for NAADP by virtual screening. *Nat Chem Biol* 5**:** 220-226.

Neher E, Sakmann B (1976). Single-channel currents recorded from membrane of denervated frog muscle fibres. *Nature* 260**:** 799-802.

Nelson MT, Quayle JM (1995). Physiological roles and properties of potassium channels in arterial smooth muscle. *Am J Physiol Cell Physiol* 268**:** C799-822.

Nelson MT, Cheng H, Rubart M, Santana LF, Bonev AD, Knot HJ*, et al.* (1995). Relaxation of arterial smooth muscle by calcium sparks. *Science* 270**:** 633-637.

Nof E, Luria D, Brass D, Marek D, Lahat H, Reznik-Wolf H*, et al.* (2007). Point mutation in the HCN4 cardiac ion channel pore affecting synthesis, trafficking, and functional expression is associated with familial asymptomatic sinus bradycardia. *Circulation* 116**:** 463-470.

Patel S, Docampo R (2010). Acidic calcium stores open for business: expanding the potential for intracellular Ca^{2+} signaling. *Trends Cell Biol* 20**:** 277-286.

Patel S, Muallem S (2011). Acidic Ca^{2+} stores come to the fore. *Cell Calcium* 50**:** 109-112.

Pérez GJ, Bonev AD, Patlak JB, Nelson MT (1999). Functional coupling of ryanodine receptors to K_{Ca} channels in smooth muscle cells from rat cerebral arteries. *J Gen Physiol* 113**:** 229-238.

Pian P, Bucchi A, Decostanzo A, Robinson RB, Siegelbaum SA (2007). Modulation of cyclic nucleotide-regulated HCN channels by PIP_2 and receptors coupled to phospholipase C. *Pflugers Arch* 455**:** 125-145.

Pitt SJ, Lam AK, Rietdorf K, Galione A, Sitsapesan R (2014). Reconstituted human TPC1 is a proton-permeable ion channel and is activated by NAADP or Ca^{2+}. *Sci Signal* 7**:** ra46.

Pitt SJ, Funnell TM, Sitsapesan M, Venturi E, Rietdorf K, Ruas M*, et al.* (2010). TPC2 is a novel NAADP-sensitive Ca^{2+} release channel, operating as a dual sensor of luminal pH and Ca^{2+}. *J Biol Chem* 285**:** 35039-35046.

Postea O, Biel M (2011). Exploring HCN channels as novel drug targets. *Nat Rev Drug Discov* 10**:** 903-914.

Purves GI, Kamishima T, Davies LM, Quayle JM, Dart C (2009). Exchange protein activated by cAMP (Epac) mediates cAMP-dependent but protein kinase A-insensitive modulation of vascular ATP-sensitive potassium channels. *J Physiol* 587**:** 3639-3650.

Rhodin JA (1967). The ultrastructure of mammalian arterioles and precapillary sphincters. *J Ultrastruct Res* 18**:** 181-223.

Ringer S (1883). A further contribution regarding the influence of the different constituents of the blood on the contraction of the heart. *J Physiol* 4**:** 29-42 23.

Roberts OL, Kamishima T, Barrett-Jolley R, Quayle JM, Dart C (2013). Exchange protein activated by cAMP (Epac) induces vascular relaxation by activating Ca^{2+}-sensitive K^+ channels in rat mesenteric artery. *J Physiol* 591**:** 5107-5123.

Rosen D, Lewis AM, Mizote A, Thomas JM, Aley PK, Vasudevan SR*, et al.* (2009). Analogues of the nicotinic acid adenine dinucleotide phosphate (NAADP) antagonist Ned-19 indicate two binding sites on the NAADP receptor. *J Biol Chem* 284**:** 34930-34934.

Roubille F, Tardif JC (2013). New therapeutic targets in cardiology: heart failure and arrhythmia: HCN channels. *Circulation* 127**:** 1986-1996.

Sanchez M, McManus OB (1996). Paxilline inhibition of the alpha-subunit of the high-conductance calcium-activated potassium channel. *Neuropharmacology* 35**:** 963-968.

Sánchez-Alonso JL, Halliwell JV, Colino A (2008). ZD 7288 inhibits T-type calcium current in rat hippocampal pyramidal cells. *Neurosci Lett* 439**:** 275-280.

Sandow SL, Hill CE (2000). Incidence of myoendothelial gap junctions in the proximal and distal mesenteric arteries of the rat is suggestive of a role in endothelium-derived hyperpolarizing factor-mediated responses. *Circ Res* 86**:** 341-346.

Sandow SL, Neylon CB, Chen MX, Garland CJ (2006). Spatial separation of endothelial small- and intermediate-conductance calcium-activated potassium channels (K_{Ca}) and connexins: possible relationship to vasodilator function? *J Anat* 209**:** 689-698.

Sandow SL, Tare M, Coleman HA, Hill CE, Parkington HC (2002). Involvement of myoendothelial gap junctions in the actions of endothelium-derived hyperpolarizing factor. *Circ Res* 90**:** 1108-1113.

Schieder M, Rötzer K, Brüggemann A, Biel M, Wahl-Schott CA (2010). Characterization of two-pore channel 2 (TPCN2)-mediated Ca^{2+} currents in isolated lysosomes. *J Biol Chem* 285**:** 21219-21222.

Schwake M, Schröder B, Saftig P (2013). Lysosomal membrane proteins and their central role in physiology. *Traffic* 14**:** 739-748.

Seamon KB, Padgett W, Daly JW (1981). Forskolin: unique diterpene activator of adenylate cyclase in membranes and in intact cells. *Proc Natl Acad Sci U S A* 78**:** 3363-3367.

Segal SS, Duling BR (1986). Flow control among microvessels coordinated by intercellular conduction. *Science* 234**:** 868-870.

Shaw L, O'Neill S, Jones CJ, Austin C, Taggart MJ (2004). Comparison of U46619-, endothelin-1- or phenylephrine-induced changes in cellular Ca^{2+} profiles and Ca^{2+} sensitisation of constriction of pressurised rat resistance arteries. *Br J Pharmacol* 141**:** 678-688.

Shen B, Cheng KT, Leung YK, Kwok YC, Kwan HY, Wong CO*, et al.* (2008). Epinephrine-induced Ca^{2+} influx in vascular endothelial cells is mediated by CNGA2 channels. *J Mol Cell Cardiol* 45**:** 437-445.

Shigaki T, Hirschi KD (2006). Diverse functions and molecular properties emerging for CAX cation/H^+ exchangers in plants. *Plant Biol* 8**:** 419-429.

Shimokawa H, Yasutake H, Fujii K, Owada MK, Nakaike R, Fukumoto Y*, et al.* (1996). The importance of the hyperpolarizing mechanism increases as the vessel size decreases in endothelium-dependent relaxations in rat mesenteric circulation. *J Cardiovasc Pharmacol* 28**:** 703-711.

Smirnov SV, Aaronson PI (1992). Ca^{2+}-activated and voltage-gated K^+ currents in smooth muscle cells isolated from human mesenteric arteries. *J Physiol* 457**:** 431-454.

Socha MJ, Hakim CH, Jackson WF, Segal SS (2011). Temperature effects on morphological integrity and Ca^{2+} signaling in freshly isolated murine feed artery endothelial cell tubes. *Am J Physiol Heart Circ Physiol* 301**:** H773-783.

Sonkusare SK, Bonev AD, Ledoux J, Liedtke W, Kotlikoff MI, Heppner TJ*, et al.* (2012). Elementary Ca^{2+} signals through endothelial TRPV4 channels regulate vascular function. *Science* 336**:** 597-601.

Steinberg SF, Brunton LL (2001). Compartmentation of G protein-coupled signaling pathways in cardiac myocytes. *Annu Rev Pharmacol Toxicol* 41**:** 751-773.

Stenmark KR, Yeager ME, El Kasmi KC, Nozik-Grayck E, Gerasimovskaya EV, Li M*, et al.* (2013). The adventitia: essential regulator of vascular wall structure and function. *Annu Rev Physiol* 75**:** 23-47.

Stieber J, Stöckl G, Herrmann S, Hassfurth B, Hofmann F (2005). Functional expression of the human HCN3 channel. *J Biol Chem* 280**:** 34635-34643.

Stieber J, Herrmann S, Feil S, Löster J, Feil R, Biel M*, et al.* (2003). The hyperpolarization-activated channel HCN4 is required for the generation of pacemaker action potentials in the embryonic heart. *Proc Natl Acad Sci U S A* 100**:** 15235-15240.

Straub AC, Zeigler AC, Isakson BE (2014). The myoendothelial junction: connections that deliver the message. *Physiology* 29**:** 242-249.

Straub AC, Lohman AW, Billaud M, Johnstone SR, Dwyer ST, Lee MY*, et al.* (2012). Endothelial cell expression of haemoglobin α regulates nitric oxide signalling. *Nature* 491**:** 473-477.

Streb H, Irvine RF, Berridge MJ, Schulz I (1983). Release of Ca^{2+} from a non-mitochondrial intracellular store in pancreatic acinar cells by inositol-1,4,5-trisphosphate. *Nature* 306**:** 67-69.

Strøbæk D, Teuber L, Jørgensen TD, Ahring PK, Kjær K, Hansen RS*, et al.* (2004). Activation of human IK and SK Ca^{2+}-activated K^+ channels by NS309 (6,7-dichloro-1H-indole-2,3-dione 3-oxime). *Biochim Biophys Acta* 1665**:** 1-5.

Swedberg K, Komajda M, Bohm M, Borer JS, Ford I, Dubost-Brama A*, et al.* (2010). Ivabradine and outcomes in chronic heart failure (SHIFT): a randomised placebo-controlled study. *Lancet* 376**:** 875-885.

Takano H, Dora KA, Spitaler MM, Garland CJ (2004). Spreading dilatation in rat mesenteric arteries associated with calcium-independent endothelial cell hyperpolarization. *J Physiol* 556**:** 887-903.

Tallini YN, Brekke JF, Shui B, Doran R, Hwang SM, Nakai J*, et al.* (2007). Propagated endothelial Ca^{2+} waves and arteriolar dilation in vivo: measurements in Cx40 BAC GCaMP2 transgenic mice. *Circ Res* 101**:** 1300-1309.

Tanabe K, Tucker SJ, Matsuo M, Proks P, Ashcroft FM, Seino S*, et al.* (1999). Direct photoaffinity labeling of the Kir6.2 subunit of the ATP-sensitive K^+ channel by 8-azido-ATP. *J Biol Chem* 274**:** 3931-3933.

Tanaka Y, Guhde G, Suter A, Eskelinen EL, Hartmann D, Lüllmann-Rauch R*, et al.* (2000). Accumulation of autophagic vacuoles and cardiomyopathy in LAMP-2-deficient mice. *Nature* 406**:** 902-906.

Thollon C, Cambarrat C, Vian J, Prost JF, Peglion JL, Vilaine JP (1994). Electrophysiological effects of S 16257, a novel sino-atrial node modulator, on rabbit and guinea-pig cardiac preparations: comparison with UL-FS 49. *Br J Pharmacol* 112**:** 37-42.

Tracey WR, Peach MJ (1992). Differential muscarinic receptor mRNA expression by freshly isolated and cultured bovine aortic endothelial cells. *Circ Res* 70**:** 234-240.

Tran CH, Taylor MS, Plane F, Nagaraja S, Tsoukias NM, Solodushko V*, et al.* (2012). Endothelial Ca^{2+} wavelets and the induction of myoendothelial feedback. *Am J Physiol Cell Physiol* 302**:** C1226-1242.

Tsien RY (1980). New calcium indicators and buffers with high selectivity against magnesium and protons: design, synthesis, and properties of prototype structures. *Biochemistry* 19**:** 2396-2404.

van Breemen C, Chen Q, Laher I (1995). Superficial buffer barrier function of smooth muscle sarcoplasmic reticulum. *Trends Pharmacol Sci* 16**:** 98-105.

van Breemen C, Fameli N, Evans AM (2013). Pan-junctional sarcoplasmic reticulum in vascular smooth muscle: nanospace Ca^{2+} transport for site- and function-specific Ca^{2+} signalling. *J Physiol* 591**:** 2043-2054.

Wahl-Schott C, Biel M (2009). HCN channels: structure, cellular regulation and physiological function. *Cell Mol Life Sci* 66**:** 470-494.

Wainger BJ, DeGennaro M, Santoro B, Siegelbaum SA, Tibbs GR (2001). Molecular mechanism of cAMP modulation of HCN pacemaker channels. *Nature* 411**:** 805-810.

Waldron GJ, Garland CJ (1994). Effect of potassium channel blockers on L-NAME insensitive relaxations in rat small mesenteric artery. *Can J Physiol Pharmacol* 72 (Suppl. 1).

Walseth TF, Lin-Moshier Y, Jain P, Ruas M, Parrington J, Galione A*, et al.* (2012). Photoaffinity labeling of high affinity nicotinic acid adenine dinucleotide phosphate (NAADP)-binding proteins in sea urchin egg. *J Biol Chem* 287**:** 2308-2315.

Wang X, Zhang X, Dong XP, Samie M, Li X, Cheng X*, et al.* (2012). TPC proteins are phosphoinositide-activated sodium-selective ion channels in endosomes and lysosomes. *Cell* 151**:** 372-383.

Webb RC (2003). Smooth muscle contraction and relaxation. *Adv Physiol Educ* 27**:** 201-206.

Weber A (1959). On the role of calcium in the activity of adenosine 5'-triphosphate hydrolysis by actomyosin. *J Biol Chem* 234**:** 2764-2769.

White R, Hiley CR (2000). Hyperpolarisation of rat mesenteric endothelial cells by ATP-sensitive K^+ channel openers. *Eur J Pharmacol* 397**:** 279-290.

Winter P, Dora KA (2007). Spreading dilatation to luminal perfusion of ATP and UTP in rat isolated small mesenteric arteries. *J Physiol* 582**:** 335-347.

Wray S, Burdyga T, Noble K (2005). Calcium signalling in smooth muscle. *Cell Calcium* 38**:** 397-407.

Yamaguchi S, Jha A, Li Q, Soyombo AA, Dickinson GD, Churamani D*, et al.* (2011). Transient receptor potential mucolipin 1 (TRPML1) and two-pore channels are functionally independent organellar ion channels. *J Biol Chem* 286**:** 22934-22942.

Yao X, Garland CJ (2005). Recent developments in vascular endothelial cell transient receptor potential channels. *Circ Res* 97**:** 853-863.

Yarova PL, Smirnov SV, Dora KA, Garland CJ (2013). β_1-Adrenoceptor stimulation suppresses endothelial IK_{Ca}-channel hyperpolarization and associated dilatation in resistance arteries. *Br J Pharmacol* 169**:** 875-886.

Yeh HI, Rothery S, Dupont E, Coppen SR, Severs NJ (1998). Individual gap junction plaques contain multiple connexins in arterial endothelium. *Circ Res* 83**:** 1248-1263.

Yu X, Duan KL, Shang CF, Yu HG, Zhou Z (2004). Calcium influx through hyperpolarization-activated cation channels (I_h channels) contributes to activity-evoked neuronal secretion. *Proc Natl Acad Sci U S A* 101**:** 1051-1056.

Yu X, Chen XW, Zhou P, Yao L, Liu T, Zhang B*, et al.* (2007). Calcium influx through I_f channels in rat ventricular myocytes. *Am J Physiol Cell Physiol* 292**:** C1147-1155.

Zagotta WN, Olivier NB, Black KD, Young EC, Olson R, Gouaux E (2003). Structural basis for modulation and agonist specificity of HCN pacemaker channels. *Nature* 425**:** 200-205.

Zhang F, Li PL (2007). Reconstitution and characterization of a nicotinic acid adenine dinucleotide phosphate (NAADP)-sensitive Ca^{2+} release channel from liver lysosomes of rats. *J Biol Chem* 282**:** 25259-25269.

Zhang F, Xia M, Li PL (2010). Lysosome-dependent Ca^{2+} release response to Fas activation in coronary arterial myocytes through NAADP: evidence from CD38 gene knockouts. *Am J Physiol Cell Physiol* 298**:** C1209-1216.

Zhang F, Jin S, Yi F, Li PL (2009). TRP-ML1 functions as a lysosomal NAADP-sensitive Ca^{2+} release channel in coronary arterial myocytes. *J Cell Mol Med* 13**:** 3174-3185.

Zhang F, Xu M, Han WQ, Li PL (2011). Reconstitution of lysosomal NAADP-TRP-ML1 signaling pathway and its function in TRP-$ML1^{-/-}$ cells. *Am J Physiol Cell Physiol* 301**:** C421-430.

Zhang F, Zhang G, Zhang AY, Koeberl MJ, Wallander E, Li PL (2006). Production of NAADP and its role in Ca^{2+} mobilization associated with lysosomes in coronary arterial myocytes. *Am J Physiol Heart Circ Physiol* 291**:** H274-282.

Zhang Y, Gao YJ, Zuo J, Lee RM, Janssen LJ (2005). Alteration of arterial smooth muscle potassium channel composition and BK_{Ca} current modulation in hypertension. *Eur J Pharmacol* 514**:** 111-119.

Zong X, Schieder M, Cuny H, Fenske S, Gruner C, Rotzer K*, et al.* (2009). The two-pore channel TPCN2 mediates NAADP-dependent Ca^{2+}-release from lysosomal stores. *Pflugers Arch* 458**:** 891-899.

Zygmunt PM, Högestätt ED (1996). Role of potassium channels in endothelium-dependent relaxation resistant to nitroarginine in the rat hepatic artery. *Br J Pharmacol* 117**:** 1600-1606.